THE CHARACTERISATION OF PARTICULATE POLLUTION IN AN AIRPORT ENVIRONMENT: MANCHESTER INTERNATIONAL AIRPORT, UK, A CASE STUDY

S J JONES

PhD   2017

THE CHARACTERISATION OF PARTICULATE POLLUTION IN AN AIRPORT ENVIRONMENT: MANCHESTER INTERNATIONAL AIRPORT, UK, A CASE STUDY

SUSAN JANE JONES

A thesis submitted in partial fulfilment of the
requirements of the
Manchester Metropolitan University for the degree
of Doctor of Philosophy

Department of Science and the Environment:
Faculty of Science and Engineering,
Manchester Metropolitan University
2017

To my beloved husband John and my precious daughters Lucy and Sophie. Thank you for your never-ending faith, love and support.

"Your wings already exist, all you have to do is fly"

Author unknown

Table of Contents

List of Figures

SIRM = saturation isothermal remanent magnetisation;
$(B_0)_{CR}$ = coercivity of remanence

List of Tables

List of Abbreviations

ACRP	Airport Cooperative Research Programme
APU	Auxiliary Power Unit
ARM	Anhysteretic Remanent Magnetisation
BA	British Airways PLC
C/C	Carbon carbon
EDS	Energy dispersive X-ray spectroscopy
EDX	Energy dispersive X-ray
DEFRA	Department of the Environment, Food and Rural Affairs
EEA	European Environment Agency
EC	Elemental Carbon
EPA	United States Environment Protection Agency
ESR	Electron Spin Resonance
GSE	Ground support equipment
IPCC	Intergovernmental Panel on Climate Change
ICAO	International Civil Aviation Organization
LGW	London Gatwick Airport (UK)
LAX	Los Angeles International Airport
LHR	London Heathrow Airport (UK)
LTO	Landing and take off
MAN	Manchester International Airport (UK)
MD	Multidomain
PAH	Polycyclic aromatic hydrocarbon
PM	Particulate matter
PSD	Pseudo-single domain
SEM	Scanning Electron Microscopy
SIRM	Saturation Isothermal Remanent Magnetisation
SSD	Stable single domain
SPP	Superparamagnetic
TEM	Transmission electron microscopy

UFP	Ultrafine particulate matter
UHC	Unburned hydrocarbons
WHO	World Health Organization
XRF	X-ray fluorescence

Acknowledgements

Abstract

During the last fifty years there has been a significant increase in global air travel. This growth coupled with a better understanding of aircraft emission characteristics and their potential impact on health and the environment has become a cause of concern. Particulate matter (PM) is a major component of these emissions. However, PM emissions within the airport environment may originate from a range of sources. Studies relating to the identification of individual airport PM sources is limited and is now recognised as a research need for the aviation industry. The main aim of this research was to identify characteristic 'fingerprints' of primary particulates derived from key sources in an airport environment. This was undertaken using multiple methods incorporating magnetic measurements, geochemical analysis, SEM/EDX and ESR. The resulting 'fingerprints' have been used to investigate the characteristics and spatial distribution of particulates deposited within the 'airside' environment at Manchester International Airport, UK (MAN). PM dust samples collected from aircraft engine, brake and tyre sources display differing magnetic, chemical, morphological and ESR characteristics enabling them to be used as distinctive aircraft source 'fingerprints'. These sources were used to assist in the interpretation of the origin of PM material within the 'airside' environment. PM from grasses, surface soils, runways, taxiways, apron and adjacent areas were sampled. PM from different runway surface zones (e.g. take-off and landing) show contrasting characteristics which can be related to aircraft PM sources and are suggestive of distinctive emissions from the take-off and landing cycle. Samples collected from the runway take-off zone suggest an accumulation of particulates associated with aircraft emissions. Conversely, samples collected from the landing zone are more consistent with brake and tyre dust sources. Grasses and soils were found to be less suited as sinks for the determination of PM pollution. Samples collected from the taxiway and apron areas are indicative of mixed inputs. The results demonstrate the effectiveness of a multiple analytical approach for monitoring PM in the 'airside' airport environment.

Chapter 1

Introduction, aims and objectives

During the last fifty years the global demand for air travel has increased exponentially. In 2014, over 3.3 billion air passengers were carried worldwide (IATA, 2015) and based on a predicted average annual growth rate of 3.8%, this figure is expected to reach 6.4 billion by 2030 (ICAO, 2014). The increased demand for air travel, alongside the predicted expansion to meet future needs, has been accompanied by concerns regarding the potential impact on the environment and society from the local through to the regional and global scale (Webb *et al.*, 2008; Lobo *et al.*, 2012).

Aircraft emissions have been shown to have a significant impact on the global climate (IPCC, 1999; Lee *et al.*, 2009). During routine flight operations aircraft emit carbon dioxide (CO_2) thus contributing to the radiative forcing of the climate whilst indirect effects on the climate result from the catalytic production of ozone (O_3) resulting from nitrogen oxide (NO_x) emissions. Radiative effects on the climate may also result from emissions of soot and sulphate particles (Lee, 2004; Daley, 2010; Lee *et al.*, 2010). The black carbon emissions emitted by aircraft are thought to be an important factor in the development of contrails and contrail induced cirrus clouds (Liou *et al.*, 2013). Furthermore, it is thought that contrails and contrail induced cirrus clouds have a significant impact on the climate as a result of positive radiative forcing (Kinsey et al. 2011) although this remains inconclusive (Lee, 2004, Kinsey *et al.*, 2010; Tesche *et al.*, 2016). A range of environmental impacts are associated with airport-related activities at the local scale. Aircraft noise is one such impact which is recognised as being of key concern and is closely monitored by airports (Heathrow Airport, 2016; Manchester Airport, 2016). Excessive aircraft noise can be particularly problematic for those working and residing in close proximity to flight paths. It has been shown to pose a detrimental threat to health (Stansfield and Matheson, 2003; Correia *et al.*, 2013; Hansell *et al.*, 2013) and has also been reported to

have a negative impact on house prices within the airport vicinity (Pope, 2008; Mense and Kholodilin 2014). Airport activities have also been recognised to contribute to a range of other local environmental impacts including increased waste production, land contamination, water pollution and the modification and destruction of habitats (Daley, 2010; ICAO 2011).

The impact of particulate matter on health and the environment in the airport context is a cause of concern (Press-Kristensen, 2012; Masiol and Harrison, 2014). There is currently limited information regarding airport-derived particulate emissions. However, recent studies have included the development of a comprehensive emissions inventory for aircraft main engines, APU's and handling equipment based on a study at Copenhagen Airport, Denmark (Winther et al., 2015) and investigations into black carbon, size-resolved and total particle number concentrations within the vicinity of Schipol Airport, Netherlands (Keuken et al., 2015). Growing importance has been placed on the investigation of the potential impacts associated with PM emissions derived from aircraft and airport related activities (Press-Kristensen, 2012). Without such information it is likely that airports will encounter increased resistance to airport development whilst airline operators may face opposition to the addition and expansion of new and existing flight routes. In order to fully investigate the potential impact of airport derived particulates on airport employees, passengers and nearby communities it is important to ascertain the individual emission sources. Furthermore, the identification of the individual sources of particulates derived from within the airport environment, has been established as a key research priority for the aviation industry (Webb et al., 2008). The main focus of the current research in this area has been on aircraft engine emissions (e.g. Yu et al., 2017., Abegglen et al., 2016., Herndon et al., 2008; Kinsey et al., 2010; Lobo et al., 2012). A limited number of studies have investigated other sources of airport particulate emissions, including tyre smoke (Bennett et al., 2011). The identification and characterisation of individual sources, however, remains challenging.

1.1 Particulate matter

Particulate matter (PM) is comprised of a complex mixture of solid particles and liquid droplets suspended in air (Webb *et al.*, 2008). The term 'aerosol' is also used to describe the suspension of both solids and liquid droplets in air (Van Loon and Duffy, 2011). In general, the solid particles make up the non-volatile fraction whilst the liquid component comprises the volatile fraction. PM may be characterised, for example, by size, number or composition. PM within the atmosphere can be classified as either primary or secondary and may occur as a result of both natural and anthropogenic processes.

Primary PM emissions are those which originate from, or form in close proximity to the source as a result of physical and/or chemical processes. Primary PM is derived from a wide range of both natural and anthropogenic sources. Particles arising from anthropogenic related sources include those which are emitted directly into the atmosphere as a result of fossil fuel combustion processes. Examples of such emissions, resulting from the incomplete combustion of fossil fuel, include those derived from diesel engines; cooking; biomass burning and coal used for domestic and industrial purposes (Buzcu *et al.*, 2006; Lin *et al.*, 2016). Primary PM may also result from mechanical processes associated with anthropogenic activities including agricultural harvesting, cement manufacturing and quarrying. Major natural sources of primary PM within the atmosphere include sea spray; volcanic ash; pollen; mould spores; dust; sand and soil.

Secondary particles are formed within the atmosphere through the transformation of previously emitted precursor gases (Fuzzi *et al.*, 2015). A series of complex chemical reactions may result in the production of new particles or additions to those which are already present in the atmosphere (Webb *et al.*, 2008). Secondary PM is comprised of both inorganic and organic compounds. Secondary inorganic particles include those which are derived from the oxidation of sulphur and nitrogen oxides. The resultant compounds of sulphuric acid (H_2SO_4) and nitric acid (HNO_3) may further react to form ammonium salts

including ammonium sulphate $(NH_4)_2SO_4$ and ammonium nitrate $(NH_4)(NO_3)$. Secondary organic particles (volatile organic compounds) may also be formed through the reaction of biogenically produced particles (Perrino, 2010).

PM is conventionally also classified according to particle size with the diameter of particles in the ambient atmosphere ranging from <1 µm to ≥100 µm. Particle size is critical as smaller particles, with a diameter of 10 µm or less, and referred to as PM_{10} are known to pose the most serious threat to human health due to their potential for entering into the human respiratory system (Spassov *et al.*, 2004; Nelin et al., 2012). The residence time and dispersion of PM is largely determined by particle size, which is principally determined by the source (Tsiouri *et al.*, 2015). Particles derived from natural sources such as wind-blown dust and sea spray are characteristically >1 µm whereas particles produced as a result of anthropogenic combustion processes are often <1 µm. The terms coarse, fine and ultrafine are commonly used to further categorise and describe PM_{10}. Particles which fall within the size range of 2.5 µm to 10 µm in diameter are described as 'coarse' and those within the range of 0.1 µm to 2.5 µm referred to as 'fine'. The term ultrafine is used to describe particles with a diameter of 0.1 µm or less. The 'fine' and 'ultrafine' particle fraction (≤ 2.5 µm) of PM is most commonly termed $PM_{2.5}$. These relatively arbitrary classifications of size range are used as a short-hand for the potential anthropogenic impact of PM throughout the environmental health and pollution sciences and so are also employed in this study.

1.2 Particulate matter and health

Over recent years concerns regarding the impact of poor air quality on human health have been well documented (EEA, 2016; EPA, 2016; WHO, 2016). There is now increasing medical evidence to suggest that both long and short-term exposure to PM may be associated with a wide range of adverse health related issues (e.g. Pope *et al.*, 2004; Zanobetti *et al.*, 2008; Barrett *et al.*, *2010*; Pascal *et al.*, 2014; Shaughnessy *et al.*, 2015) resulting in rising hospital admissions and

increased morbidity and mortality rates (Burnett *et al.*, 2014; Carugno *et al.*, 2016).

It is widely established that particle size is critical in terms of the potential impact on the human body. Most particles exceeding 10 µm in diameter are effectively filtered out by the human respiratory system (Kim *et al.*, 2015), however, there is increasing medical evidence to suggest that increased exposure to smaller particles within the PM<10 µm (PM_{10}) diameter range may be responsible for a range of serious health issues (Barrett *et al.*, 2010). This is attributable to particles within the PM_{10} size range having the ability to enter into the human respiratory system. Such particles have the potential for penetrating more deeply into the fine alveoli of the lungs and consequently may subsequently enter into the bloodstream (Spassov *et al.*, 2004; Nelin *et al.*, 2012).

In addition to particle size, the chemical composition of PM is a further and significant contributory factor with regard to the detrimental impact of PM on the human respiratory and cardiovascular systems (DEFRA, 2005). PM has been found to contain a diverse range of chemical components, as a result of originating from a wide range of sources including industrial combustion processes; coal and biomass burning and vehicles (Tsiouri *et al.*, 2015; Lin *et al.*, 2016). The toxicity of PM has been shown to vary in relation to chemical composition. Particles enriched with soluble trace metals and endotoxins have been shown to pose a potential threat to human health (DEFRA, 2005; Mitchell *et al.*, 2015). A US study based on data collected from 187 counties between 2000 and 2005 identified increased hospital admissions for patients with cardiovascular and respiratory conditions in seasons and counties with elevated levels of $PM_{2.5}$ containing Nickel (Ni); Vanadium (V) or Elemental Carbon (EC). Furthermore, higher mortality rates were associated with higher levels of $PM_{2.5}$ containing Ni (Bell, 2012).

Polycyclic aromatic hydrocarbons (PAHs) in $PM_{2.5}$ have also been shown to pose a significant risk to human health. PAHs are organic compounds which are commonly comprised of a mixture of two or more organic compounds such as soot (sometimes referred to as black carbon). They are formed when organic

substances are exposed to high temperatures or pressures, for example, through the incomplete combustion of fossil fuels and organic materials (Abdel-Shafy and Mansour, 2016). They may also be emitted from natural sources such as volcanoes and forest fires (Wang *et al.*, 2014). PAHs are classified as being carcinogenic (Wang *et al.*, 2014) and are also known to have toxic and mutagenic properties (Rengarajan *et al.*, 2015).

There is now an abundance of medical evidence to associate long and short term exposure to particles in the fine and ultrafine range ($PM_{2.5}$) with a range of serious health issues most notably in association with cardiovascular and respiratory diseases (Pascal *et al.*, 2014). In recent years there has been substantial medical research to link long term exposure to $PM_{2.5}$ with cardiovascular disease resulting in conditions such as ischaemic heart disease; heart failure; cardiac arrest (Pope *et al.*, 2004; Burnett *et al.*, 2014) and ischaemic strokes (Lin *et al.*, 2016). Other studies have linked increased exposure to $PM_{2.5}$ with a rise in the number of people developing respiratory conditions including asthma, bronchitis and chronic obstructive pulmonary disease (COPD) (Zanobetti *et al.*, 2008; Burnett *et al.*, 2014). Numerous studies have also established links between the long term exposure to $PM_{2.5}$ and elevated incidences of cancer including lung cancer (Andreau *et al.*, 2012; Whiteman *et al.*, 2013; Yun *et al.*, 2015; Wong *et al.*, 2016) and colon cancer (Buggiano *et al.*, 2015). There is currently much less medical evidence to link serious health effects with exposure to particles in the coarse size range (DEFRA, 2005). There is, however, now increasing medical evidence to associate increased exposure to coarse PM with higher incidences of patients requiring hospital treatment for asthma (Malig *et al.*, 2013).

The impact of PM on the health of the population has been investigated from a local to global scale. It is currently estimated that in excess of three million premature deaths worldwide each year may be directly attributable to increased PM emissions (WHO, 2016). A regional study, which focused on data collected from eighteen of the most highly polluted and densely populated areas of Lombardy in northern Italy between 2003 and 2006, found that short-term exposure to PM_{10}, was a significant contributory factor in the increased numbers

of people suffering from respiratory conditions. Increased hospital admissions and respiratory mortality was particularly prevalent amongst those in the older age categories (Carugno *et al.*, 2016). In a further study conducted in Beijing, China between 2000 and 2011, it was concluded that approximately 4000 premature deaths per year were directly attributable to long-term exposure to $PM_{2.5}$ (Meng *et al.*, 2016).

1.3 Particulate matter in the airport environment

The growing demand for air travel during recent years has generated concerns regarding the potential impacts associated with increased emissions of airport derived PM (Webb *et al.*, 2008; Press Kristensen, 2012). Potential sources of PM emissions within the airport environment are extensive and the list of sources identified in the following section is not exhaustive. The section, however, aims to highlight the main aircraft and airport-derived PM, which are relevant to this research.

The airport environment constitutes a wide range of potential sources of PM including aircraft; ground service equipment (GSE); vehicles and buildings (Agrawal *et al.*, 2008; Webb *et al.*, 2008; Lobo *et al.*, 2011). Airport derived PM has been shown to make a significant contribution to increased levels of PM in nearby communities (Westerdahl *et al.*, 2008; Zhu *et al.*, 2011; Hsu *et al.*, 2013).

1.3.1 Aircraft derived particulate matter

Aircraft derived particulate emissions constitute a major source of PM in the airport environment. A significant proportion of these emissions are derived from aircraft engines (Herndon et al., 2005; Rogers et al., 2005; Lobo et al., 2011) and thus aircraft engine emissions remain the dominant focus of most of the current research in this area (e.g. Kinsey et al., 2010; Lobo et al., 2012; Liati et al., 2014). However, there are a number of other key sources of non-engine aircraft PM

emissions including Auxiliary Power Units (APU) and brake and tyre-wear emissions. At present, however, research relating to these sources remains limited, though contributions of brake and tyre wear debris have been found to be significant particularly in relation to ground level PM_{10} aircraft emissions. At London Gatwick Airport, UK (LGW), for example, ~69% by mass of such emissions were attributed to brake and tyre wear (Morris, 2006).

1.3.1.1 Aircraft engine emissions

Aircraft engine emissions are generated during routine aircraft operations including idling; taxiing; take-off and landing (Herndon *et al.*, 2005; ICAO, 2011; Masiol and Harrison, 2014). The volume and characteristics of such emissions are, however, dependent on a number of factors including the number of aircraft operations; aircraft engine type; fuel type and length of flight (ICAO, 2011). Mazaheri *et al.* (2011) found that significantly higher PM emissions were associated with aircraft departure manoeuvres as opposed to aircraft arrival operations as a result of increased engine emissions during take-off and the initial climb.

Aircraft main engines are primarily classified as gas turbine engines or internal combustion piston engines. Gas turbine engines can be further categorised as turbofan and turboprop engine types (ICAO, 2011). Gas turbine engine combustion is largely controlled by onboard computers and as such there is a strong link between the power produced by the engine and the resultant emissions (Yacovitch *et al.*, 2016). Most modern day civil and general aviation aircraft are, however, fitted with turbofan jet engines. Turbofan engines are most commonly fuelled by the kerosene-type jet fuels Jet A and Jet A-1 with Jet A fuel being the most frequently used aviation fuel worldwide (Wayson *et al.*, 2009; ICAO, 2011; Masiol and Harrison, 2014). In a turbofan jet engine the energy for thrust is generated by a large fan and a turbojet, with most of the thrust being generated by the fan. The turbojet section comprises an inlet compressor and a fuel combustion section into which fuel is added and ignited. The compressor is driven by energy generated by the exhaust gas and thrust generated by the

exhaust nozzle as the exhaust gas is accelerated from the back of the engine (Masiol and Harrison, 2014).

Particulates emitted as a result of jet engine combustion are comprised of both primary and secondary PM emissions (Wayson *et al.*, 2009). The predominant particle size of such emissions has been found to be within the >100 nm mean diameter size range (e.g. Herndon *et al.*, 2008; Kinsey *et al.*, 2010). Soot, which is formed through the incomplete combustion of fossil fuel (Herndon *et al.*, 2008; Dodson *et al.*, 2009) is the most dominant primary PM emitted from the combustion chamber of a jet engine, though other constituents such as dust, metal and ceramic particles may also be present (Mazaheri *et al.*, 2013). Jet exhaust emissions have been shown to comprise a significant proportion of PAHs, which are formed through the incomplete combustion of fuel (Spicer *et al.*,1992) and are likely to be a component of the soot.

Various gas phase species including CO_2; H_2O; CO; NO_x, SO_x and unburned hydrocarbons (UHC) are also formed through the combustion process. Secondary particulates including nitrates, sulphates and organic compounds result from a series of reaction stages including nucleation, condensation and coagulation as volatile gas phase species enter the atmosphere via the engine exhaust system. During this phase aerosols may form as a result of homogenous nucleation and condensation of the emitted gases, or through heterogeneous nucleation where newly formed gases condense onto existing particles (Robinson *et al.*, 2010; Fuzzi *et al.*, 2015). For example, in excess of 90% of the sulphur in Jet A fuel is oxidised to sulphur dioxide followed by conversion to other secondary sulphate compounds (Wayson *et al.*, 2009).

Turboprop engines though less common than turbofan engines are used in some smaller and regional aircraft. In the UK, airlines operating such aircraft include Flybe and Ryanair. Turboprop engines, like turbofan engines, are most often fuelled with Jet A and Jet A-1 fuel and comprise a turbine engine core which is fitted with a reduction gear to power the propellers. Smaller (light) aircraft, are commonly fitted with piston engines, which are fuelled with aviation gasoline (avgas) and work on a similar principle to spark ignition car engines (Masiol and

Harrison, 2014). The operation of piston engines is controlled by the pilot through the use of levers such as the throttle and mixer. In this engine type the combustion of fuel is intermittent rather than the continuous combustion which occurs in jet engines. In contrast to gas turbine engines, the rate of emissions from different piston engines is significantly variable (Yacovitch *et al.*, 2016). Helicopters, though less numerous than jet and light aircraft provide a further source of PM in the airport environment. They are equipped with turboshaft engines, which are similar in operation to a turbojet but designed to generate shaft power rather than jet thrust (Masiol and Harrison, 2014).

1.3.1.2 Auxiliary power unit (APU)

In addition to the main engine most large modern aircraft are fitted with an APU. The APU is a small gas turbine engine, which is most commonly housed in the tail cone of the aircraft. It is used to provide electrical energy to the aircraft when on-site ground power is unavailable. It is also used for the production of compressed air during main engine start up (Schäfer *et al.*, 2003) and as a source of power during emergency situations. The APU operates as a mini jet engine and is fuelled by kerosene, which is fed from the main fuel tanks. APU emissions have been shown to be very similar in operation to larger aircraft jet engines due to their similarity in design and functionality (Lobo *et al.*, 2013).

1.3.1.3 Tyre wear debris

Aircraft tyre wear debris (tyre dust) has been identified as a major source of PM in the airport environment (Morris, 2006) and moreover has been shown to contribute significantly to pollution in the urban environment, particularly as a source of zinc (Adachi and Tainosho 2004). Tyre dust is generated during normal tyre wear as a result of mechanical abrasion and thermal degradation (Bennett *et al.*, 2011). Tyre abrasion also occurs during nose wheel retraction as a result of the spin brake function which is associated with specific aircraft types including the Boeing 747-436 and Boeing 767-336. The resultant tyre debris accumulates on ledges and gullies in the nose landing gear wheel well (BA Engineering, pers. comm., 2012).

The emission of tyre particulates is clearly visible during aircraft landing operations and is identifiable as a puff of smoke (Lobo *et al.*, 2013) as the tyres of the landing gear touch down onto the runway and are rapidly brought from rest to aircraft landing ground speed. Morris (2006) has estimated on the simple basis of average weight loss that a B747 could lose as much as ~1kg of rubber per landing (Morris, 2006). However, it is important to note that PM emissions from aircraft tyres are reliant on numerous factors including aircraft weight; number of wheels; meteorological conditions; length of runway; taxiway design and airline operating procedures (Morris 2006; Bennett *et al.*, 2011).

Coarser particles are generated through aircraft tyre wear and the re-suspension of particles resulting from the turbulence created during aircraft movements (BAA, 2006) particularly during take-off and landing (Mazaheri *et al.*, 2013). Tyre-wear is largely comprised of particles in the coarse particle size fraction (Morris, 2006; Bennett *et al.*, 2011). Sub-micron (ultrafine) PM may be generated, however through the thermal degradation of tyre polymer and the volatilization of extender oils (Bennett *et al.*, 2011). In addition to tyre wear debris, tyre dust may also comprise brake dust; mineral and asphalt material from the runway as well as debris resulting from the erosion of runway and taxiway markings (Adachi and Tainosho 2004). The turbulence in the boundary layer near the runway created by aircraft movements' results in such materials becoming re-suspended thus providing a further and significant contribution to PM in the airport environment (Curran, 2006).

1.3.1.4 Brake wear debris

There is currently an abundance of literature relating to road vehicle brake wear (e.g. Abu-Allaban *et al.*, 2003; Grigoratos and Martini 2015) but at present research relating specifically to aircraft brake wear remains limited. The operation of aircraft brakes is intermittent and intense whereas the operation of road vehicle brakes is characterised as being smoother and more frequent. Owing to the differences in operation it is unfeasible to make a direct comparison between the two in terms of the rate of brake wear (Curran, 2006).

Modern aircraft brakes are of carbon-carbon (C/C) composition (Fan *et al.*, 2017). However, additives are frequently added to the brakes to modify the friction

properties, temperature characteristics and mechanical properties of the brakes or to act as antioxidants during braking operations (Blau, 2001).   Brake lining wear occurs most commonly during landing and less significantly during taxiing operations as a result of frictional heat generation. The resultant debris forms a friction film of abraded wear debris that may often adhere to the wear surfaces of the C/C composite brakes. The resultant wear debris is subsequently released as airborne PM (Hutton *et al.*, 1999, Curran, 2006). However, Lobo *et al.* (2013), found that it was not possible to identify distinctive emission signatures from landing aircraft during the braking phase.

1.3.2 Non-aircraft particulate matter emissions

A further and significant source of airport related PM emissions arises from the operation of ground handling equipment used to service aircraft for maintenance purposes and during operational turnaround. Ground handling services typically comprise emissions from ground support equipment (GSE); airside traffic and aircraft refuelling and de-icing activities (ICAO 2011). Examples of airport GSE include aircraft tugs; ground power units (GPU) (used for the provision of power in addition to or as an alternative to the APU); baggage tugs; conveyor belts; passenger stairs and cargo loaders. In addition to GSE, numerous airside traffic vehicles are in operation to support airport ground handling services and include catering vehicles; fuel and water trucks; passenger buses and airport operations vehicles (Webb *et al.*, 2008; ICAO 2011; Masiol and Harrison 2014).

The vehicle-derived emissions resulting from the use of GSE equipment and airport vehicles may be comprised of both exhaust and non-exhaust particulates. PM exhaust emissions are produced through the incomplete combustion of fossil fuel (Hunt *et al.*, 1984, Grigoratos and Martini 2015). The sources of non-exhaust vehicle particles are varied and include tyre, brake and clutch wear debris. Non-exhaust particulates may also comprise previously deposited environmental material, which has become re-suspended due to the turbulence created by moving traffic (Grigoratos and Martini 2015).

Other sources of airport PM may also include emissions from heating facilities; kitchens; restaurants; airport and aircraft maintenance facilities as well as those

derived from airport fire services and construction activities. Another important contribution to PM emissions within the airport environment arises from the transportation of people and goods to and from the airport including those from road and rail networks (Dodson *et al.*, 2009).

It is important to acknowledge that PM emissions within the airport and the immediate vicinity may be comprised of a complex mixture of particulates. As well as the wide variety of aircraft and airport related sources there may be regional PM emissions arising from natural, urban and industrial sources. This complex mixture of particulates may subsequently become re-suspended by the movement of aircraft and vehicles or by the wind (Abu-Allaban *et al.*, 2003).

1.4 Previous studies/research relating to particulate matter in the airport environment

Over recent years, the continued rapid growth in air travel amidst concerns regarding the potential environmental and health impacts of airport derived PM has led to increased research in this area. It is now widely acknowledged that aircraft-derived engine emissions constitute a significant source of PM in the airport environment (e.g. Masiol and Harrison 2014; Lobo *et al.*, 2015). This has led to increasing research interest in this area and at present, aircraft engine emissions remain the dominant focus of most of the current research in relation to aircraft and airport PM studies. In acknowledgement of the need to develop a much greater understanding of the quantity and potential impact of aircraft engine emissions on air quality and climate change, Wayson *et al.* (2009), developed the currently used, first order approximation 3.0 methodology (FOA3), for the estimation of aircraft engine emissions from certified commercial aircraft. In an attempt to further understand and quantify the environmental impacts of airport operations in the UK, a more detailed inventory incorporating emissions from LTO activities; APUs and GSE vehicles was also developed (Stettler *et al.*, 2011). However, in the past decade or so black smoke from aircraft engines has significantly reduced as a consequence of new technology which has resulted in a reduction of particle size but not number.

The need for the characterisation of PM emissions within the airport environment was identified as a research priority for the aviation industry in the Airport Cooperative Research Programme (ACRP) report by Webb *et al.* (2008). Prior to and since this time, researchers have used a variety of approaches and techniques in an attempt to investigate the physical and chemical characteristics of aircraft engine PM and gaseous emissions. Plume capture and analysis is a commonly used technique. It has been used to investigate various aspects of both primary and secondary aircraft engine PM including mass, concentration, particle size and composition (e.g. Herndon *et al.*, 2008; Kinsey *et al.*, 2010; Lobo *et al.*, 2012) and more specifically the differences observed between different aircraft operations including idle and take-off (Herndon *et al.*, 2005); taxiing (Johnson *et al.*, 2008) and during all stages of the LTO cycle (Mazaheri *et al.*, 2011; Mazaheri *et al.*, 2013). A number of other methods have also been used for the characterisation of aircraft engine derived PM including electron microscopy (Liati *et al.*, 2014), real time instruments (Rogers *et al.*, 2005), high volume air sampling and particle size analysis (Agrawal *et al.*, 2008) and LIDAR (Eberhard *et al.*, 2005). In addition to aircraft engine PM a number of characterisation studies relating to other aircraft sources have also been conducted. These have included studies to investigate the composition of smoke from landing aircraft (Bennett *et al.*, 2011) and aircraft engine lubrication oil emissions (Yu *et al.*, 2012).

A growing number of researchers have investigated the air quality impacts associated with aircraft emissions on both the airport environment and on the neighbourhoods within close proximity to them. A variety of techniques have been used to investigate this issue alongside air quality data collected from mobile air monitoring platforms (Westerdahl *et al.*, 2008; Hu *et al.*, 2009; Hudda *et al.*, 2014), stationary monitoring sites (Yu *et al.*, 2004; Zhu *et al.*, 2011; Hsu *et al.*, 2012; Hsu *et al.*, 2013) and databanks (Elbir, 2008). In a Turkish based study, the emissions from aircraft engine exhausts at various stages of the LTO cycle were estimated using real flight data and emissions factor data from the ICAO engine exhaust emissions databank. Longer taxiing times were shown to be an important factor in increased emissions of both CO and NO_x as well as HC emissions (Elbir, 2008).

The mounting medical evidence to associate increased exposure to $PM_{2.5}$ with adverse health effects has resulted on increasing emphasis being placed on the health of airport workers and nearby communities. Therefore, details of the level and nature of airport related PM emissions has become of increasing significance. Yim *et al.* (2015) used a multi-scale modelling approach to assess the impact of aircraft engine emissions on air quality and human health from the local to global scale. They concluded that aviation related emissions resulted in ~16000 premature deaths per year, of which, 25% were attributable to emissions resulting from LTO operations. A growing number of researchers have conducted investigations relating to the 'ultrafine' (UFP) PM fraction. A report based on a detailed study of PM emissions from various sources at Copenhagen Airport provided evidence to suggest that 90% of ultrafine PM originated from airport derived sources (Press-Kristensen, 2012). A number of previous researchers have focused on the serious health issues associated with increased exposure to ultrafine diesel particulates. There has been limited research, however, relating to the toxicity of UFP particulates from aircraft engine exhausts (Tesseraux, 2004; Lai *et al.*, 2016). Consequently, the Copenhagen study highlights the urgent need for research into the nature of airport derived PM in order to assess the health implications for airport employees and in particular those working in close proximity to aircraft sources of ultrafine PM such as aircraft engine and diesel vehicle exhausts (Press-Kristensen, 2012).

A number of other researchers have used a variety of techniques to investigate UFP concentrations in and around airports. Regression modelling has been applied to various combinations of high resolution monitoring, flight operations and meteorological data to enable quantification of the contribution of LTO activities in comparison to other sources. Significant contributions from LTO events have been observed particularly during aircraft departure activities (Hsu *et al.*, 2012) and have been shown to contribute significantly to UFP concentrations in close proximity to departure runways (Hsu *et al.*, 2013). A number of other studies have used regression modelling to investigate UFP concentrations downwind of airports. Elevated UFP concentrations, which were largely associated with aircraft departure and take-off activities were observed up to 660m downwind of Santa Monica Airport, USA (SMA) (Hu *et al.*, 2009), and

600m of LAX (Westerdahl *et al.*, 2008; Zhu *et al.*, 2011). More recently, the air quality impacts associated with aircraft and airport related activities at a much greater distance from an airport have also been investigated. In a study at LAX, increased particle number (PN) concentrations were shown to extend up to 16 km downwind of the airport. Furthermore, it was concluded that the air quality impacts of airport activities downwind of Los Angeles International Airport, USA (LAX) were significant and had previously been considerably underestimated (Hudda *et al.*, 2014). The air quality impacts associated with secondary PM and PM_{10} have also been investigated through the use of non-parametric regression. An assessment of the air quality impacts on neighbourhoods within the vicinity of large urban airports have further been investigated through the use of non-parametric regression. Secondary PM and PM_{10} data was used to investigate the impacts on communities within the neighbouring communities of two large international airports including LAX and Hong Kong International Airport, CN (HKIA). The study concluded that airport vehicle derived emissions were the dominant source of PM within the locality of LAX and aircraft derived PM emissions at HKIA (Yu *et al.*, 2004).

In other airport related PM studies a number of techniques have been used for the investigation of primary PM within the airport environment. Electron microscopy and spectroscopy techniques including transmission electron microscopy (TEM), Raman and Auger electron spectroscopy (AES) have been used to examine the morphological and chemical characteristics of soot derived from a gas turbine aircraft engine (Popovitcheva *et al.*, 2000). More recently Abegglen *et al.* (2016) investigated the chemical composition of aircraft engine PM emissions using single particle time-of-flight mass spectrometry whilst Yu *et al.* (2017) used a range of instruments including an AVL particle counter, engine exhaust particle sizer and soot particle aerosol mass spectrometer to measure and characterise PM emissions from two commercial gas turbine aircraft engines.

Magnetic measurements techniques have also been used effectively to characterise and differentiate between different pollutant emission sources in agricultural and industrial areas. In a soil study conducted in southern France, three dominant pollutant emission sources were identified across an area extending ~$500km^2$ including those originating from the airport, road traffic and

the steel industry (Lecoanet *et al.*, 2003). In a further study the concentration and chemical composition of $\leq PM_{10}$ at El Prat, Barcelona, ES (BCN) were investigated to discriminate between particles originating from different sources including industrial/road traffic; crustal; sea salt; secondary inorganic aerosols and potassium (K). The researchers concluded that ambient air PM_{10} levels within the vicinity of BCN were not directly as a result of aircraft operations. However, the research does suggest that microflakes of aluminous alloys identified within the ambient PM_{10} filters are likely to be attributable to aircraft activities (Amato *et al.*, 2010).

Much of the current focus of research relating to aircraft and airport derived PM remains on aircraft engine exhaust emissions. Many of these studies have focused primarily on secondary PM, however, there are currently few airport related studies, which focus entirely on primary PM emissions. Therefore, the focus of this research is entirely on primary PM.

1.5 Aims and Objectives

The principal aim of this PhD study is to employ a methodology that enables the identification of distinctive and characteristic 'fingerprints' of primary particulates derived from sources within the airport environment. This method will be used to assess the presence and distribution of different emission sources within this environment. To achieve this aim, the following primary objectives have been identified:

1. To analyse particulates from different airport derived sources (aircraft engines, brakes and tyres) using multiple analytical techniques including magnetic, geochemical, SEM/EDX and ESR analyses, to determine characteristics that could be used to identify environmental 'fingerprints' of particulate sources.

2. To use these 'fingerprints' and analytical methods to characterise particulate sinks such as runway and operational surfaces including taxiway, apron and adjacent grasses, and determine their suitability for enabling the monitoring of particulate pollution within the airport environment.

1.6 Thesis Overview

Chapter 1 provides a general introduction to PM and a summary of the potential health related issues associated with such emissions. The chapter includes an overview of the sources of the potential sources of PM in the airport environment and includes a review of the associated literature and includes the aims and objectives associated with this research study.

Chapter 2 presents a literature review incorporating previous approaches to the characterisation of primary PM.

Chapter 3 presents the methodologies associated with this research including the field and laboratory techniques and statistical analyses employed in this research.

Chapters 4 to 7 incorporate the results of each of the methods used within this study:

- Chapter 4 – Magnetic measurements
- Chapter 5 – Chemical analysis
- Chapter 6 – Scanning electron microscopy and energy dispersive x-ray (SEM/EDX).
- Chapter 7 – Electron spin resonance (ESR)

Chapter 8 provides a discussion of the results sections.

Chapter 9 presents the research findings, concluding remarks and recommendations for further work.

Chapter 2

Literature Review:
Previous approaches to the characterisation of primary PM

In order to fully investigate the potential health and environmental impacts associated with airport derived PM emissions on airport employees, passengers and nearby communities, it is important to determine the individual emission sources. As stated in Chapter 1 (§ 1.5), the key aim of this research is to be able to identify characteristic 'fingerprints', which would facilitate source attribution. This chapter provides a review of techniques which have been used in previous studies to investigate the characterisation of primary PM in the environment.

2.1 Environmental magnetism

Environmental magnetism measurements comprise a combination of sensitive, non-destructive, inexpensive and relatively rapid techniques, which involves the application of artificially induced magnetic fields to a wide range of natural and anthropogenically derived environmental materials including atmospheric dusts; soils, rocks and sediments (Walden *et al.,* 1999). These techniques, described in more detail under Methodologies, Chapter 3, enable information to be gained regarding the mineralogy, grain size, morphology and concentration of magnetic minerals within the material of investigation. Magnetic minerals are produced and transformed by a range of environmental and anthropogenic processes (Oldfield, 1999). The strong variability of Fe mineral phases in particulates provides a basis for their characterisation and identification of and distinguishing between, different sources (Shu *et al.*, 2001).

In previous studies, environmental magnetism has been used as an effective technique for investigation into the sources and spatial and temporal dispersal patterns of PM. In such studies, a range of fixed and mobile monitoring platforms have been used for the collection of PM samples including high volume air samplers (e.g. Hunt *et al.*, 1984; Spassov *et al.*, 2004); air monitoring stations (e.g. Muxworthy *et al.*, 2003; Sagnotti *et al.*, 2006); dust sweepings (e.g. Lyons

et al., 2012); surface soils (e.g. Lecoanet *et al*., 2001; Lecoanet *et al*., 2003; Wang *et al*., 2014) and vegetation samples (e.g. Matzka and Maher 1999; Sadeghian, 2012; Muñoz *et al*., 2017).

Several studies have used magnetic measurements techniques for the identification of characteristic particulate 'fingerprints' thus enabling the discrimination of different emission types and PM sources in urban and industrial environments (Hunt *et al*., 1984; Sagnotti *et al*., 2006). Different natural processes such as weathering, soil erosion and volcanic activity (Oldfield *et al*., 1985; Walden *et al*., 1991; Lyons *et al*., 2012) and those associated with anthropogenic combustion give rise to particulate emissions with distinctive magnetic characteristics or 'fingerprints'. Hunt *et al.* (1984) identified distinctive magnetic contrasts between vehicle-derived particulates and fly-ash particulates originating from an electricity generating power station. The vehicle emissions were dominated by ferrimagnetic (i.e. magnetite-type) minerals whilst the fly-ash samples, derived from solid fuel (coal) combustion, showed a different magnetic behaviour consistent with a significant antiferromagnetic (i.e. haematite-type) content. The different combustion processes and fossil fuels give rise to particulate emissions of contrasting magnetic mineralogy and grain size.

In other studies, magnetic concentration and grain size parameters have been used to characterise atmospheric dust samples and to identify and distinguish between particulates arising from natural and anthropogenic sources. Significant differences have been observed in the magnetic characteristics of particulates derived from fossil fuel combustion and other industrial processes with those resulting from soil erosion (Oldfield *et al*., 1985; Hunt, 1986) and also between vehicular and aeolian dusts (Sagnotti *et al*., 2006) and dusts originating north and south of the Sahara/Sahel transition (Lyons *et al*., 2012). Grain size parameters have also been used to further differentiate between vehicular derived particulates. Vehicle exhaust emissions were characterised by fine superparamagnetic (SPP) grain sizes whilst the abraded metallic particles were associated with coarser multidomain (MD) magnetic grain sizes (Sagnotti *et al*., 2006). Magnetic concentration parameters including magnetic susceptibility (χ) and saturation isothermal remanent magnetisation (SIRM) have been used effectively in monitoring the concentration and spatial patterns of urban pollution.

In studies conducted by Spassov *et al.* (2004) and Muxworthy *et al.* (2003), magnetic concentration parameters were used to identify traffic emissions as being the dominant pollution source in sites exposed to different pollution sources across Switzerland and Germany.

Magnetic 'enhancement' of soil refers to the generally higher concentrations of magnetic minerals within the surface soil. Surface enhancement, caused by the formation of maghaemite and magnetite, may occur for various reasons including burning, natural pedogenic processes, the biological activity of micro-organisms and atmospheric deposition. The accumulation of anthropogenically-derived particulates, originating from high temperature fossil fuel combustion can result in the significant magnetic enhancement of surface soils (Zong *et al.*, 2017), especially where other enhancement processes are less significant. The magnetic properties of surface soils have been shown to be useful in the identification of contemporary emissions from both local and regional pollution sources (Sharma and Tripathi 2008). In other studies magnetic measurement techniques have been applied to surface soils, to enable identification and differentiation between particulates deposited from different pollution sources. Lecoanet *et al.* (2001) applied the determination of concentration and grain size parameters to salt marsh soils to discriminate between metallurgical dusts and those resulting from natural pedogenesis. Environmental magnetism techniques have been used effectively to identify and differentiate between particulates resulting from road traffic, airport and steelwork emissions (Lecoanet *et al.,* 2003) and to distinguish between emissions arising from industrial/ vehicular sources with those resulting from domestic pollution (Wang *et al.,* 2014). However, the interpretation of such data can be complicated by the *in situ* formation of magnetic minerals through weathering and pedogenic processes (Hanesch *et al.,* 2007).

Increasingly magnetic measurements have been applied to investigating vegetation, as a sink of atmospheric particulates, to obtain quantification of particulate sources and urban pollution. Vegetation has been shown be an effective receptor and biomonitor of particulate pollution as vegetation surfaces provide a large surface area for PM deposition and collection, whilst constantly interacting with the surrounding environment. An increasing number of researchers have used magnetic biomonitoring, incorporating the use of tree

leaves, as an efficient and cost effective method for monitoring PM pollution (e.g. Matzka and Maher, 1999; Szonyi *et al.,* 2008; Hansard *et al.,* 2011; Sadeghian, 2012; Muñoz *et al.,* 2017). Magnetic biomonitoring has been used to investigate both the spatial and temporal patterns of vehicular pollution within urban areas (Matzka and Maher, 1999; Szonyi *et al.,* 2008; Sadeghian, 2012; Muñoz *et al.,* 2017) and to identify differences in the magnetic characteristics of particulates derived from industrial and vehicular sources (Hansard *et al.,* 2011). Leaves from a wide range of different tree species have been used in such investigations including Silver Birch (*Betula pendula*) (Matzka and Maher, 1999); Elm (*Ulmus carpinifolia*) (Sadeghian, 2012); Oak (*Quercus Ilex*) (Szonyi *et al.*, 2008) and Sycamore *(Acer negundo)*, Plane (*Platanus orientalis*) and Black Locust (*Robinia pseudoacacia*) (Muñoz *et al.*, 2017). However, the ability of leaves to capture PM, has been found to be significantly variable dependent on the tree species (Cao *et al.,* 2015; Muñoz *et al.,* 2017). Furthermore, rainfall and wind can result in decreased leaf magnetic loadings due to particulates being washed and eroded away (Matzka and Maher, 1999; Sadeghian, 2012; Norouzi *et al.*, 2016).

2.1.1 Electron Spin Resonance (ESR)

Electron Spin Resonance (ESR) also referred to as Electron Paramagnetic Resonance (EPR) spectroscopy is a highly sensitive technique which is used to investigate the immediate magnetic and chemical environment of the intrinsic magnetic moments within atoms, molecules, minerals and materials (§ 3.8).

ESR facilitates the analysis of electronic structures of materials containing unpaired electrons (Mabbs, 1993) i.e. electron states that give rise to paramagnetism and cooperative ferrimagnetism, ferromagnetism and antiferromagnetism (Crook *et al.*, 2002).

This sensitive technique has been shown to be highly effective in the analysis of weakly magnetic environmental samples where it is difficult to use conventional magnetic measurements and for samples where diamagnetic components predominate (Crook *et al.*, 2002). The technique has previously been applied in a diverse range of applications e.g. to determine and monitor heavy metal pollution in seawater (Virmani and Zeller, 1974) and natural water systems

(Angino *et al.*, 1971) and to investigate the behaviour of paramagnetic species in river (Boughriet *et al.*, 1992); estuarine (Ouddane *et al.*, 2001); coastal/marine (Wakeman and Carpenter, 1974; Crook *et al.*, 2002; Algarasamy & Hoon 2017) and anoxic (Billon *et al.*, 2003) sediments and systems. The potential for ESR to assist in 'fingerprinting' and source apportionment has been demonstrated in studies of environmental sediments (Crook *et al.*, 2002; Algarasamy and Hoon 2017). To date, however, the use of ESR in studies of environmental magnetism remains limited and has not previously been applied to land based sediments.

2.2 Geochemical analysis

In studies of environmental pollution, inorganic chemical analysis has been used as an effective technique for investigating the source and concentration of pollutants in urban environments. Chemical analyses techniques have been applied to air filters (Amato *et al.*, 2009; Onat *et al.*, 2013); house dusts (Deschamps *et al.*, 2014); surface soils (Al-Fatlawi and Al-Alwani, 2012) and mosses and lichens (Aničić *et al.*, 2009; Adamo *et al.*, 2007) to enable discrimination between different pollution sources. In a study conducted at El Prat airport, Barcelona (Spain), chemical analysis of PM_{10} samples collected on filter papers identified crustal PM as being the main source of particulates. However, dust samples collected from the airport runway revealed unusually high concentrations of Ba, Zn and Mo, which were thought to be attributed to the smoke and debris released from aircraft tyres upon landing (Amato *et al.*, 2010). In other studies of urban pollution, chemical analysis has been used to investigate the spatial variations in road dusts originating from different sources. Amato *et al.* (2009) identified increased levels of crustal components including Ca, Li, Sc, Sr, Rb and As, in areas within close proximity to demolition/construction sites. Similarly, Onat *et al.* (2013) identified distinctive chemical 'fingerprints' in $PM_{2.5}$ samples collected on filter papers collected from an urban area of Istanbul (Turkey). Crustal materials were characterised by the presence of Mg, Al, Ba and Si and those originating from the more dominant anthropogenic sources, by high concentrations of S, Cr, Zn, Cu and K (Onat *et al.*, 2013).

The presence of certain heavy metals can often be indicative of more specific anthropogenic sources. Al-Fatlawi and Al-Alwani, (2012) investigated the

concentrations of Pb, Zn, Ni, Cr, Co and Cd in roadside surface soil samples from Hilla City, (Iraq). The high levels of Pb, Zn, Ni and Co which were observed in the samples were attributed to emissions from traffic related sources. In a similar study, Onder *et al.* (2007) applied geochemical analysis techniques to surface soil and grass samples taken from green areas within Konya, (Turkey). The results indicated that heavy metal pollution levels and most notably, those of Pb, Cu, Cr and Cd, were highest in areas adjacent to busy roads and industrial areas.

Aničić *et al.* (2009) used moss bags to investigate the atmospheric deposition of heavy metals in Belgrade (Serbia). Anthropogenic related emissions sources were attributed to the high concentrations of V, Cu, As and Ni observed within the study area. Sun *et al.* (2009) also used moss bags to investigate the deposition of heavy metals including Hg, Cu, Pb, Zn and Ni in Chongqing (China). The results showed that heavy metal levels were particularly high in the site adjacent to the main industrial area which was thought to be related to the discharge of waste gas. Adamo *et al.* (2007) used lichens and mosses to assess the suitability of different vegetation species for the assessment of the deposition of particulate matter. Elemental concentrations, particularly for Fe and Zn were shown to be higher in mosses rather than lichens, possibly due to differences in their external surface features influencing the accumulation rate of particulates.

2.3 Scanning Electron Microscopy and Energy Dispersive X-Ray (EDX)

In some studies SEM and energy dispersive X-Ray (EDX) analyses have been used alongside magnetic measurements to investigate the morphology, grain size distribution and chemical composition of magnetic particles. (Energy dispersive X-ray spectroscopy is also referred to as EDS, but the acronym EDX will be used throughout this thesis). The techniques have been used to characterise and differentiate magnetic particles derived from both anthropogenic (Blaha *et al.*, 2008; Kim *et al.*, 2009; Jordanova *et al.*, 2012; Górka-Kostrubiec 2015) and natural sources (Jordanova *et al.*, 2012). Magnetic analyses have shown magnetite to be the predominant magnetic mineral in particulates arising from anthropogenic sources (Jordanova *et al.*, 2012; Górka-Kostrubiec 2015)

and, furthermore, magnetic particle concentrations have been found to increase with decreasing granulometric size (Górka-Kostrubiec 2015).

A combination of magnetic measurements techniques and SEM/EDX techniques has further been used to enable the differentiation between emission sources. Lehndorff *et al.* (2006) found significant variability between six sites with diverse emission backgrounds in a study in Cologne, (Germany). In several studies, SEM observations together with EDX analyses have been conducted on magnetic particulates extracted from bulk dust samples. SEM analysis has revealed that magnetic particulates resulting from high temperature combustion processes, such as the burning of fossil fuels are dominated by spherule shaped particulates (Blaha *et al.*, 2008; Kim *et al.*, 2009; Jordanova *et al.*, 2012). The surface morphologies of such spherules have been shown to be extremely diverse e.g. orange peel and thread like (Górka-Kostrubiec 2015). In contrast to this, the magnetic particulates associated with vehicular derived sources displayed more irregular morphologies (Kim *et al.*, 2009; Górka-Kostrubiec 2015). SEM analysis also revealed that both spherical and irregular shaped anthropogenic magnetic particulates are predominantly within the fine grain size range i.e. < ~ 60 µm. (Blaha *et al.*, 2008; Kim *et al.*, 2009).

EDX has been used to examine the elemental composition of magnetic particulates derived from fly ash samples (Blaha *et al.*, 2008); road dusts (Kim *et al.*, 2009) and house dusts (Górka-Kostrubiec 2015). Differences in the chemical composition of particulates enables their discrimination between different sources. In an urban road dust study in Seoul (South Korea), the spherical magnetic particulates were found to be predominantly associated with Fe, O and C together with minor elements including Al, Ca, Mg and Si. The chemical composition of these spherules indicated that they were most likely to be derived from fossil fuel combustion. The chemical composition of the irregular shaped particulates were found to be far more diverse and moreover individual particulates were seen to display various chemical combinations. Particulates resulting from vehicle brake wear were associated with Fe and iron oxides and Al, Ca, K, Mg and Si, whilst aggregates of Fe oxides together with C and S, were

identified as being characteristic of particulates derived from vehicle engine exhaust emissions (Kim *et al.*, 2009).

2.4 Integrated Approaches

In other investigations of urban or industrial pollution an integrated approach involving various combinations of magnetic measurements, geochemical analysis and SEM/EDX has been used.

2.4.1 Magnetic measurements and geochemical analysis

A number of researchers have focused on the use of magnetic measurements and geochemical analysis. Heavy metal contamination is a key concern, particularly in urban areas, due to the potential threat which it poses to human health (e.g. DEFRA 2005; Arteaga *et al.*, 2015). Heavy metals are naturally occurring elements which are found throughout the lithosphere (Tchounwou *et al.*, 2012). However, within the urban environment, such pollutants occur largely as a result of anthropogenic activities and may be derived from a wide range of emission sources including industrial; vehicular; fossil fuel combustion and waste disposal. Heavy metals are commonly associated with magnetic particulates and previous studies have identified a significant correlation between magnetic measurements and heavy metal concentrations (e.g. Xie *et al.,* 2001; Zhu *et al.,* 2013). As such, magnetic measurements alongside geochemical techniques have increasingly been used, as a method for investigating urban pollution.

Road dusts act as an important sink of particulates within the urban environment and are comprised of a complex mixture of particulates derived from a wide range of natural and anthropogenic sources including soil material, plant and leaf litter, construction material, vehicular emissions and fossil fuel combustion emissions (Robertson *et al.*, 2003; Wang *et al.*, 2012). Various novel methods have been employed for the collection of road dust samples (e.g. vacuum cleaners (Szczepaniak-Wnuk and Górka-Kostrubiec 2016). Researchers have routinely sampled road and footpath surfaces, however, using a dustpan and brush method due to the relative ease and speed of sample collection (e.g. Xie *et al.*, 1999; Robertson *et al.*, 2003; Yang *et al.*, 2010; Wang *et al.*, 2012). The use of

a combined magnetic/geochemical approach has been shown to be effective in determining the source, type and concentration of heavy metals in such dusts (e.g. Xie *et al.*, 1999; Robertson *et al.*, 2003; Wang *et al.*, 2012).

In a number of studies, magnetic concentration parameters alongside heavy metal analyses have been used for the identification of different pollution sources. High concentrations of ferrimagnetic minerals and heavy metals have been identified as being indicative of inputs resulting from anthropogenic activities including those resulting from industrial emissions (Wang *et al.*, 2012) and vehicular traffic (e.g. Robertson *et al.*, 2003; Lu *et al.*, 2005; Yang *et al.*, 2010). Wang *et al.* (2012) investigated the pollution levels in several residential, commercial and industrial districts within the industrial city of Lanzhou, China. Significant correlations were identified between magnetic mineral concentrations and Fe, As, Cu, Mn, Ni, P and Zn, which were consistent with the heavy metal pollution within the study area, being largely related to combustion derived PM emissions.

Yang *et al.* (2010) found that Pb was associated with smaller magnetic grain sizes (e.g. single domain (SD)) which were considered to be from industrially derived emissions, whilst Cu, Ni and Fe were associated with coarser magnetic grain size fractions (e.g. multi-domain (MD), which were thought to be from vehicular traffic emissions. The techniques have further been used to characterise emissions from specific vehicular derived sources, for example, a strong correlation between χ; ARM and SIRM and Cu and Sb is suggestive of brake wear emissions rather than those derived from vehicle exhausts (Revuelta *et al.*, 2014).

In other road dust studies strong correlations between magnetic concentration parameters (χ, ARM; SIRM) and the concentration of heavy metals has identified the potential for magnetic measurements to be an effective proxy of heavy metal pollution (Lu *et al.*, 2005; Yang *et al.*, 2010). Yang *et al.* (2010) also use magnetic ratios such as ARM/χ, as an effective proxy measurement for Cu, Fe, and Ni emissions resulting from vehicular traffic (Yang *et al.*, 2010) . These studies highlight the potential of the use of a combined magnetic and geochemical approach for the assessment of source apportionment in urban areas (Wang *et al.*, 2012).

Urban soil contamination is a major environmental issue, owing to the potential for soils to act as a sink for environmental pollutants. The magnetic fraction of topsoils can also become highly enriched in heavy metals as a result of the deposition of particulates from anthropogenic activities such as those related to industry and vehicle exhaust emissions (Hu *et al.*, 2007; Xia *et al.*, 2014). Significant correlations between heavy metals and magnetic measurements of surface soils indicate that magnetic measurement techniques can be used effectively in monitoring soil pollution (Hu *et al.*, 2007). As such, an increasing number of researchers have focused their investigations on the magnetic and heavy metal pollution associated with surface soils (e.g. Hay *et al.*, 1997; Lu *et al.*, 2007; Sharma and Tripathi, 2008; Blundell *et al.*, 2009; Jiang *et al.*, 2012; Xia *et al.*, 2014; Wang *et al.*, 2015). In a study of the spatial pattern of urban pollution, Blundell *et al.* (2009) completed magnetic measurements and geochemical analyses on surface soils from a large number of sites across England and Wales, to enable the identification of sites dominated by pollution derived particulates. A positive correlation between magnetic concentration and heavy metals associated with anthropogenic activities were evident in sites within close proximity to urban conurbations.

A combined magnetic and geochemical approach has also been used effectively to distinguish between different pollution sources in the urban environment (e.g. Gautam *et al.*, 2005; Lu and Bai 2006; Wang *et al.*, 2015). Specific heavy metals are associated with different sources. Heavy metals such as, Cr, Cu, Pb and Zn (Blundell *et al.*, 2009; Xia *et al.*, 2014) and Cd, Cu, Pb and Zn (Lu and Bai 2006) have been found to be indicative of anthropogenically derived heavy metals resulting from industrial activities, fossil fuel combustion and vehicular emissions. In a further study, surface soil samples with high concentrations of Zn, Cr, Mn, Cu, Pb, Cd and Fe were observed in industrial and roadside locations (Jiang *et al.*, 2012). In these studies, the significant correlations which have been established between heavy metals and magnetic properties assist in establishing that magnetic minerals and heavy metals have common sources (Xia *et al.*, 2014).

In a study conducted in Shanghai, (China), the differences in the magnetic and geochemical properties of surface soils from urban and agricultural areas of the city were examined. The magnetic fraction of the urban surface soil samples were found to be highly enriched with heavy metals. Therefore, it was concluded that the magnetic minerals within the urban surface soil samples, arose primarily as a result of anthropogenic activities, rather than originating from soil parent materials and pedogenic processes, as in the agricultural soils (Hu *et al.*, 2007).

Wang *et al.* (2015), investigated surface soil samples from three rapidly developing industrial cities in north west China. Different correlations were observed between magnetic concentrations and heavy metals in the three cities thus indicating significant differences between the pollution sources in the different cities. In another study the combined techniques were used to investigate pollution levels and sources in different areas of land use in Yinchuan city, northwest China (Xia *et al.*, 2014). Residential and university campus areas were found to be largely dominated by crustal material and were characterised by low concentrations of magnetic minerals and heavy metals. Conversely, the industrial areas were found to display high concentrations of coarse magnetite and heavy metals associated with anthropogenic activities i.e. Cr, Pb and Zn.

The use of biomonitoring techniques for monitoring atmospheric pollution has previously been outlined (§ 2.1). An increasing number of researchers have applied a combined magnetic and geochemical approach to tree leaves to investigate the levels and patterns of pollution in the urban environment. Tree leaves are routinely used due to their efficiency as a biogenic receptor of PM.

Tree leaves from a variety of species were used in a comprehensive study to investigate particle pollution in different locations across various cities in northern Portugal. Significant positive correlations between magnetic concentration parameters (χ and SIRM) and Cu and Fe were revealed, thus highlighting the efficiency of using such magnetic parameters as a proxy for the assessment of Cu and Fe contamination in atmospheric dusts deposited on Oleander (*Nerium oleander)* tree leaves (Sant'Ovaia *et al.*, 2012). Similarly, Oriental Thuja

(*Platycladus orientalis)* tree leaves were used to investigate contamination levels within the heavily polluted city of Linfen, north east China. Analyses revealed a significant correlation between magnetic susceptibility and Fe, Cr, Ni, Cu and Pb levels in heavily polluted industrial areas (Cao *et al.*, 2015). These findings are also reinforced by the work of Norouzi *et al.* (2016), who found strong correlations between magnetic susceptibility and heavy metal concentrations for leaf samples from Plane (*Platanus orientalis*) trees collected in Isfahan, Iran.

These studies, once again, demonstrate the applicability of χ as a proxy method for heavy metal contamination and in particular with those originating from anthropogenic and vehicular related sources (Norouzi *et al.*, 2016). Furthermore, a combined magnetic/geochemical approach has been shown to be effective in discriminating particulates derived from different sources. Sant'Ovaia *et al.* (2012) were able to differentiate between urban and rural areas through the application of combined analyses to Lime (*Tilia spp.*) tree leaves.

2.4.2 Magnetic Measurements and SEM/EDX

In other investigations of urban and industrial pollution, a combined fully integrated approach incorporating magnetic measurements, geochemical analysis, SEM and EDX has been used to provide a comprehensive assessment of the magnetic, chemical and morphological characteristics of environmental pollutants at a local and regional scale. A range of different media have been used as particle sinks including road dusts (Kim *et al.*, 2007; Crosby *et al.*, 2014); tree leaves (Urbat *et al.*, 2004; Maher *et al.*, 2008); surface soils (Zong *et al.*, 2017) and snow, moss and lichens (Bucko, 2012).

Kim *et al.* (2007) used magnetic concentration and grain size parameters to identify temporal variations in road dust samples collected from various high traffic and industrial locations within Seoul, Korea. Distinctive seasonal variations were observed between samples collected in the summer and winter months. Lower concentrations of fine grained (e.g. SD, PSD) magnetic minerals were observed within samples collected during the summer months and a high concentration of coarser grained (e.g. MD) magnetic minerals were predominant

in samples collected during the winter months. The variations were attributed to the seasonal influx variations of anthropogenic magnetic minerals e.g. high rainfall events (resulting in the wash-out of magnetic minerals) and a much lower demand for domestic heating systems during the summer months. The transportation of anthropogenic particulates into the area, from heavily industrialised areas in western Seoul, occurs due to the strong prevailing north westerly winds, which are a common feature during winter months. Further analysis using SEM/EDX also enabled information to be gleaned regarding the morphological and elemental composition of magnetic particles extracted from the bulk road dust samples. Three distinctive categories of magnetic particles were identified, i.e. spherules; angular and aggregates. The most commonly occurring particles were spherules of iron oxide (30 – 250 μm), determined to be derived from fossil fuel combustion processes originating from power stations, industrial processes and domestic heating sources. Aggregates of iron oxides and Fe, C and S were thought to be associated with vehicle exhaust emissions whilst aggregates of pure Fe and Al, Ca, Fe, K, Mg and Si were associated with the abrasion of vehicle braking systems. Angular iron oxides and silicates were thought to be derived from natural sources.

Zong *et al.* (2017) used the combined techniques on surface soil samples to characterise and determine the sources of heavy metal pollution in Anshan, (China), an industrial city dominated by the steel industry. Magnetic and geochemical analyses of the surface soil samples revealed the dominant magnetic minerals to be magnetite, haematite and metallic iron. Magnetic mineral grains, found to be largely in the (PSD/MD) size range were identified as being the main contributor to the magnetic enhancement of surface soils. SEM observations revealed the presence of both spherule and irregular shaped magnetic particles indicating the presence of industrial and vehicular emissions in the surface soils. The association of magnetic minerals with specific heavy metals enables discrimination between different sources. The presence of magnetic minerals alongside Fe, Pb, Zn and Cu are indicative of contaminants resulting from steel production, coal combustion and vehicular emissions whilst the presence of magnetic minerals and the metals Cd and Cr are likely to result from a mixed source of industrial activities and soil parent materials. Statistical

analyses revealed a significant correlation between magnetic concentrations, heavy metals and the Tomlinson Pollution Load Index (PLI) thus identifying that low field magnetic susceptibility (χlf) and SIRM could be used effectively as a proxy method for the determination of heavy metal pollution in urban surface soils. Spatial distribution analysis indicated that the pollution hotspots were associated with emissions from the steel industry.

In a further study Bucko, (2012) applied the techniques to a range of different media (surface soils; snow; moss and lichens) to assess the spatio-temporal distribution of traffic related roadside pollution. Magnetic concentrations were found to be the greatest in samples located closest to the edge of roads and were significantly higher in roadside locations with the greatest traffic densities. Geochemical analyses revealed high concentrations of heavy metals associated with both exhaust and non-exhaust vehicular emissions. SEM/EDX revealed that the road dusts contained angular/aggregate particles (1 – 300 μm) associated with non-exhaust emissions and Fe spherules (1-100 μm) resulting from high temperature combustion processes associated with nearby power stations and vehicle exhaust emissions. The combined analyses revealed the predominance of vehicular derived traffic emissions within the study area.

Maher *et al.* (2008) also applied the combined technique to Birch tree (*Betula pendula)* leaf samples to investigate the spatial and temporal pattern of vehicle derived pollutants in Norwich, UK. Significant correlations were identified between leaf magnetic concentrations and Fe and Pb. SEM/EDX analyses identified the presence of fine (<1 μm) lead and iron rich spherules. The study concluded that the main source of lead, iron and magnetic loadings on the sampled roadside birch tree leaves were associated with vehicle exhaust emissions rather than those originating from other sources such as vehicle tyre and brake wear and natural sources.

Magnetic measurements alongside SEM/EDX have also been used to investigate the spatial and temporal distribution of particulate pollution using biomonitoring

techniques (Lehndorff *et al.*, 2006; Mitchell and Maher, 2009) and passive air sampling methods (Cao *et al.*, 2015).

In a study to investigate the levels of vehicular derived PM emissions in Lancaster, UK, SIRM analysis of tree leaf and air filter samples revealed an increase in SIRM values within samples with higher traffic densities i.e. in close proximity to roads (Mitchell and Maher 2009). Moreover, morphological and chemical analysis revealed the dominance of spherical iron rich particulates within the fine particle size range $\sim 0.1 - 1$ µm, identified as being characteristic of anthropogenically derived emissions.

Cao *et al.* (2015) investigated the use of an artificial passive sampling method for the investigation into industrial derived PM emissions across different sampling sites in Linfen, China. Significant differences were observed in the spatial variation of χ across the different sampling sites but not between the artificial sampler and leaf samples, thereby demonstrating the efficiency of an artificial sampling method as an alternative to the more traditional biomonitoring methods which had previously been used. The different magnetic, morphological and chemical characteristics of particulates from different sampling sites within close proximity to various industrial sources further demonstrates the potential of a combined approach to enable differentiation between different industrial sources e.g. power, steel, cement and coking plants (Cao *et al.* 2015).

Chapter 3

Methodologies

Chapter 3 outlines the methodological procedures incorporated within this study including sample collection, laboratory methods and statistical analyses. The laboratory work was completed at several UK based universities including Manchester Metropolitan University; Edge Hill University; Liverpool University and Manchester University due to the requirement for access to specialist equipment.

3.1 Sample Collection

Sample collection took place at two main study sites. The aircraft source sampling took place at the British Airways (BA) engineering facility London Heathrow Airport, UK (LHR) between 17th August 2010 and 1st August 2013, and the environmental sampling at Manchester International Airport, UK (MAN) between 31st January 2011 and 2nd July 2014 (Figure 3.1). The research required extensive access to security controlled areas within each airfield and its associated buildings. Therefore, it was essential to identify airports and airlines which were both willing and able to accommodate the labour intensive support required to satisfy the safety and security implications associated with conducting fieldwork within a 24 operational airfield. Permissions were initially sought and granted by Dr Tim Walmsley, Head of Environment at MAN and Jennifer O'Brien, Former Air Quality and Noise Manager, BA Environment Department, LHR.

3.2 Aircraft source sampling

Aircraft source samples (engine, brake and tyre dusts) were collected from a range of different BA jet aircraft at the BA engineering facility at LHR. Although these dusts are derived from individual aircraft it is acknowledged that they may also contain particulates from multiple mechanical, atmospheric and environmental sources subjected to the high (and potentially differing) engine

operating temperatures. LHR is located 15 miles west of London (Figure 3.1) and is the main hub airport for BA, the flag-carrying airline of the UK. BA is the largest UK based airline in terms of fleet size, carrying a total of 39.6 million passengers in 2014 (IATA, 2016).

BA has three main maintenance hangars at LHR. Access to aircraft was restricted to the Technical Block J (TBJ) and the Fleet Support Unit (FSU) due to operational and maintenance considerations. TBJ is used for long haul aircraft requiring significant maintenance/repairs whilst the FSU accommodates short haul aircraft requiring minor maintenance.

Prior to sampling, discussions were held with key BA engineering and environmental specialists based at LHR, in order to ascertain the areas of the aircraft from which aircraft source samples of engine, brake and tyre dust could best be obtained. The aircraft sampled included Boeing 747-436; 767-336; 777-236 and Airbus A319-131 and A320-232 (Table 3.1). Individual dust samples were collected using a clean wooden spatula and/or small paint brush and immediately transferred to clean, self-sealed polythene bags to avoid contamination.

3.2.2 Engine Dust Sampling

Samples of engine dust (n = 13; sample mass: 0.6 - 1.4 g) were collected from aircraft based in the maintenance hangars during the time of visit. Samples from several turbofan engines (Table 3.1) were collected from the mixer shroud which surrounds the turbine blades (Figure 3.2). The mixer shroud facilitates efficient mixing of the hot air from the turbines with slower and cooler bypass air which results in increased engine efficiency and noise reduction. Particulates emitted through jet engine combustion processes (as outlined in Chapter 1, section 1.3.1.1), directly impact onto the mixer shroud during routine engine function, leading to a slight accumulation over time (BA Engineering, 2010, pers.comm).
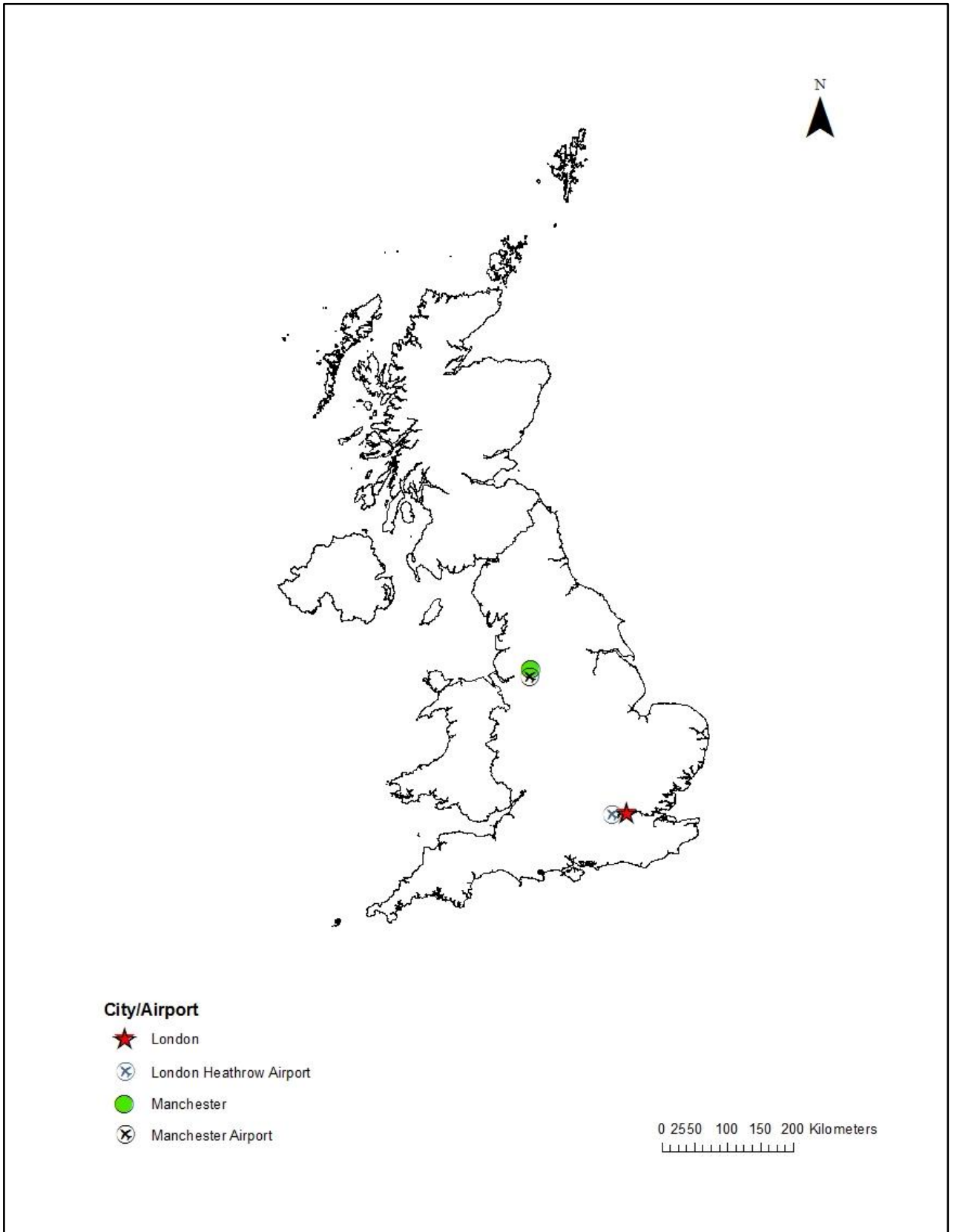
Figure 3.1: Map showing the locations of Manchester International Airport and London Heathrow Airport within the UK (map created in ArcGIS using UK Border data from the UK Data service, 2017).

Table 3.1: Aircraft manufacturer, type and engine used for aircraft source sampling including number and mass (g).

Manufacturer	Type	Engine	Number ($n =$)	Mass (g)
Airbus	A319-131	V2522-A5	1	0.53
Airbus	A320-232	V2527-A5	1	0.91
Boeing	747-436	RB211-524G2-T-19	3	Range: 0.90 – 1.20
Boeing	767-336	RB211-524H-36	6	Range: 0.58 – 1.39
Boeing	777-236	RB211 Trent 895-A	2	Range: 1.08 – 1.23

Figure 3.2: Engine dust sampling. Image shows samples being collected from the mixer shroud.

3.2.3 Brake Dust Sampling

Brake dust samples (n = 16; sample mass: 0.75 - 3.5 g) were extracted from the wheel hubs of various aircraft (Table 3.1). Brake lining wear occurs most commonly during landing and less significantly during taxiing operations as a result of frictional heat generation (Curran, 2006) which results in the production of brake dust. Bennett *et al.* (2011), suggest that samples derived from the undercarriage and wheel hub areas are likely to contain PM derived from a range of sources including tyres, brakes, runways and taxiways. However, following discussions with BA engineers (BA Engineering, 2011, pers. comm.) it was decided that brake dust sampling would focus on the wheel hub area (Figure 3.3) as this would largely restrict the sample to brake-derived material.

Figure 3.3: Brake dust sampling. Image shows samples being extracted from the wheel hub of a 777-236 aircraft.

3.2.4 Tyre Dust Sampling

Tyre dust samples (n = 4; sample mass: 1.9 – 5.0 g) were extracted from the nose landing gear wheel well of a Boeing 747-436 and a Boeing 767-336 aircraft (Figure 3.4). Tyre dust accumulates on ledges and gullies within this area, as a result of tyre abrasion, which occurs during nose wheel retraction through the action of the spin brake function associated with these aircraft types (BA Engineering, 2011, pers. comm.).

Figure 3.4: Tyre dust sampling. Image on left shows the nose landing gear of a BA Boeing 747 aircraft. Image on right indicates the ledges within the front wheel from which tyre debris was collected.

3.3 Environmental Field Sampling

Environmental sampling has been used effectively in previous studies as a method for monitoring particulate pollution (§ 2.1 to 2.4) (e.g. Matzka and Maher, 1999; Lecoanet *et al.* 2003; Lu and Bai, 2006; Onder *et al.* 2007).

Environmental samples including surface soil, grass and runway dust were collected during an extensive programme of sampling which was conducted at MAN between 31st January 2011 and 2nd July 2014.

Samples of grass, soil and runway dust were collected from pre-defined areas located within the perimeter of the airfield (Figures 3.5 and 3.6).

Apron Areas

Section

▢	Section B/2
▢	Section B/4
▢	Section B/5
▢	Section B/6

0   0.25   0.5   1 Kilometres

Figure 3.5: Satellite image of MAN displaying the Apron sampling areas (Google Earth, 2017). Final map created in ArcGIS (v. 10.4.1).

Runway & Taxiway Areas

- Runway 23L/05R – Zone A
- Runway 23L/05R – Zone B
- Alongside runway 23L/05R
- Critical Area
- Taxiway T1
- Taxiway VA1
- Taxiway C
- Taxiway D

Figure 3.6: Satellite image of MAN displaying the main runway 23L/05R; Critical Area and Taxiway sampling areas described within the text (Google Earth, 2017). Final map created in ArcGIS (v.10.4.1).

The areas were selected following consultation with MAN airport operations staff. Previous studies have shown that rainfall and wind can have a significant impact on particulate accumulation in relation to vegetation (e.g. Matzka and Maher 1999; Norouzi *et al.* 2016) and road dusts (Kim *et al.* 2007). Therefore, a minimum of five days dry weather preceded each sampling visit to diminish the wash-out effect as described in Kim *et al.* (2007). The sampling took place in two distinct phases due to access limitations associated with conducting fieldwork within a 24 hour operational airfield. The first phase was conducted between 31st January 2011 and 11th July 2013 and focused on runway 23L/05R and the adjacent areas of grass and soil (Figure 3.7). The second phase took place on 1st and 2nd July 2014 to incorporate runway 23R/05L and the adjacent apron, taxiway and grassland areas (Figure 3.7). An airport operations staff member was assigned to accompany the researcher and accompanying fieldwork assistants during each field visit. Temporary security passes were applied for in advance of each visit. Access to the airfield on each visit was subject to the scrutiny of airport security. Permission to access specific areas of the airfield was subject to air traffic control authorisation. For all environmental sampling methods, individual samples were transferred to clean, clearly labelled self-sealed polythene bags.

3.3.1 Site Location

MAN is located 17km south west of Manchester in the north west of England and is the third largest airport in the UK (Figures 3.1 and 3.8). MAN was selected as the most appropriate site for conducting environmental sampling owing to its convenient location for the research and also since it is the largest regional airport in the UK, handling over 163,657 passenger flights in 2014/15 and serving in excess of 25.6 million passengers in 2016 (Manchester Airport, 2017).

The airport is accessible via an extensive communication network including road, rail and metro links. The airport is directly accessible from the east and west via junction 5 of the M56 motorway which provides access to the wider national motorway network. The airport has its own railway station providing access to major cities throughout the UK via the national rail network (Manchester Airport, 2016).
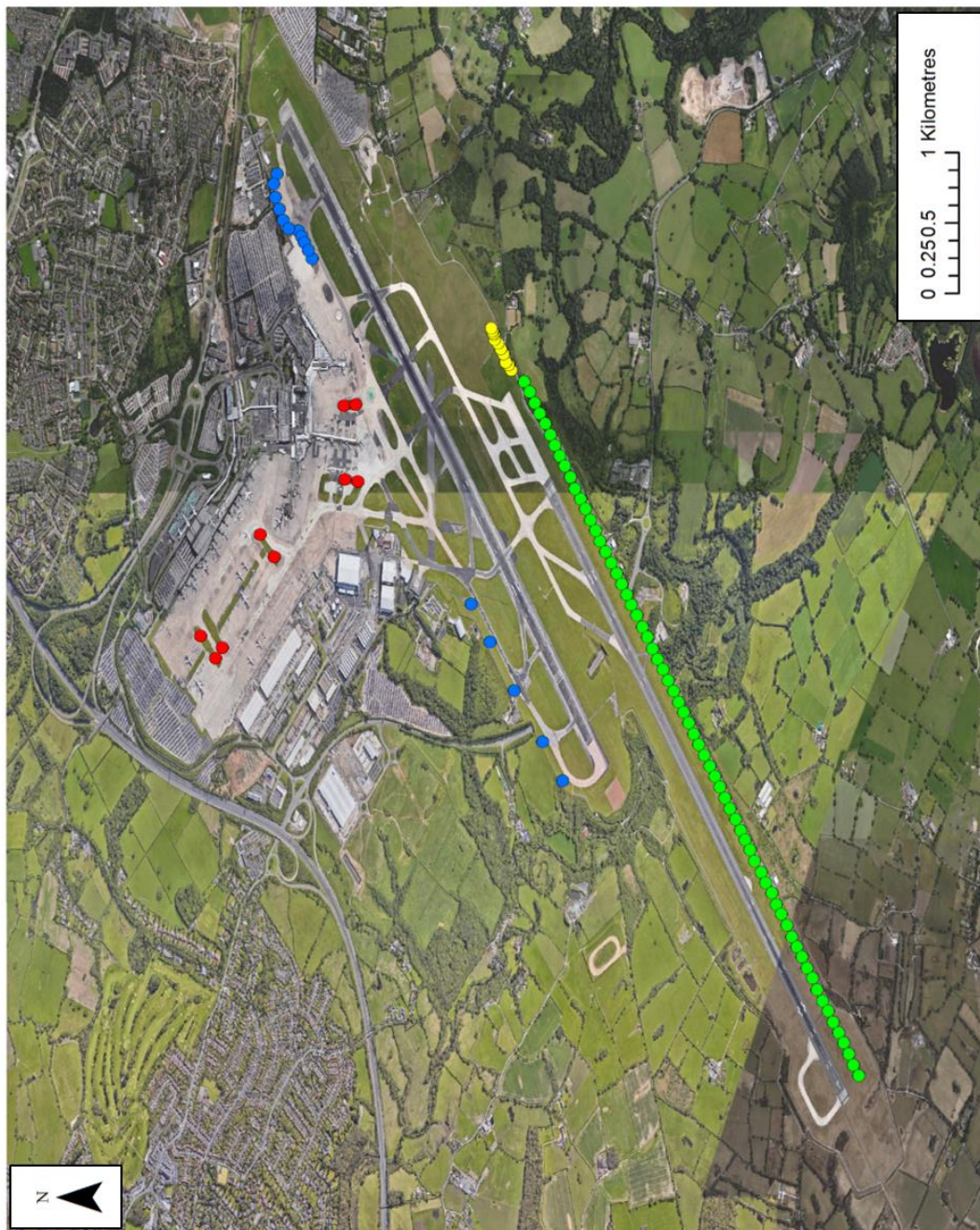
Figure 3.7: Satellite image of MAN displaying the grass and soil sampling locations (Google Earth, 2017). Final map created in ArcGIS (v.10.4.1).
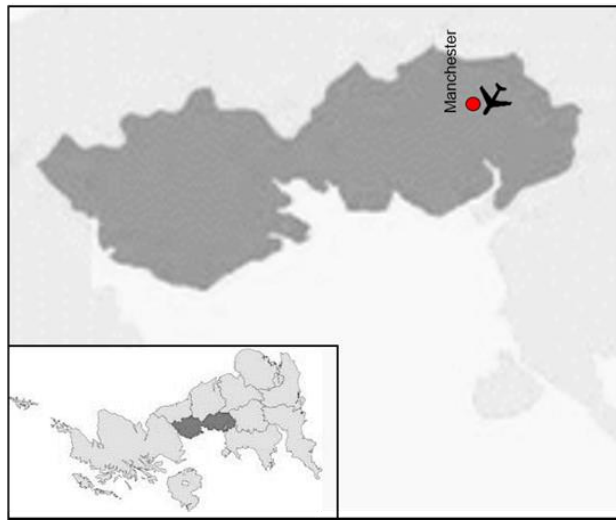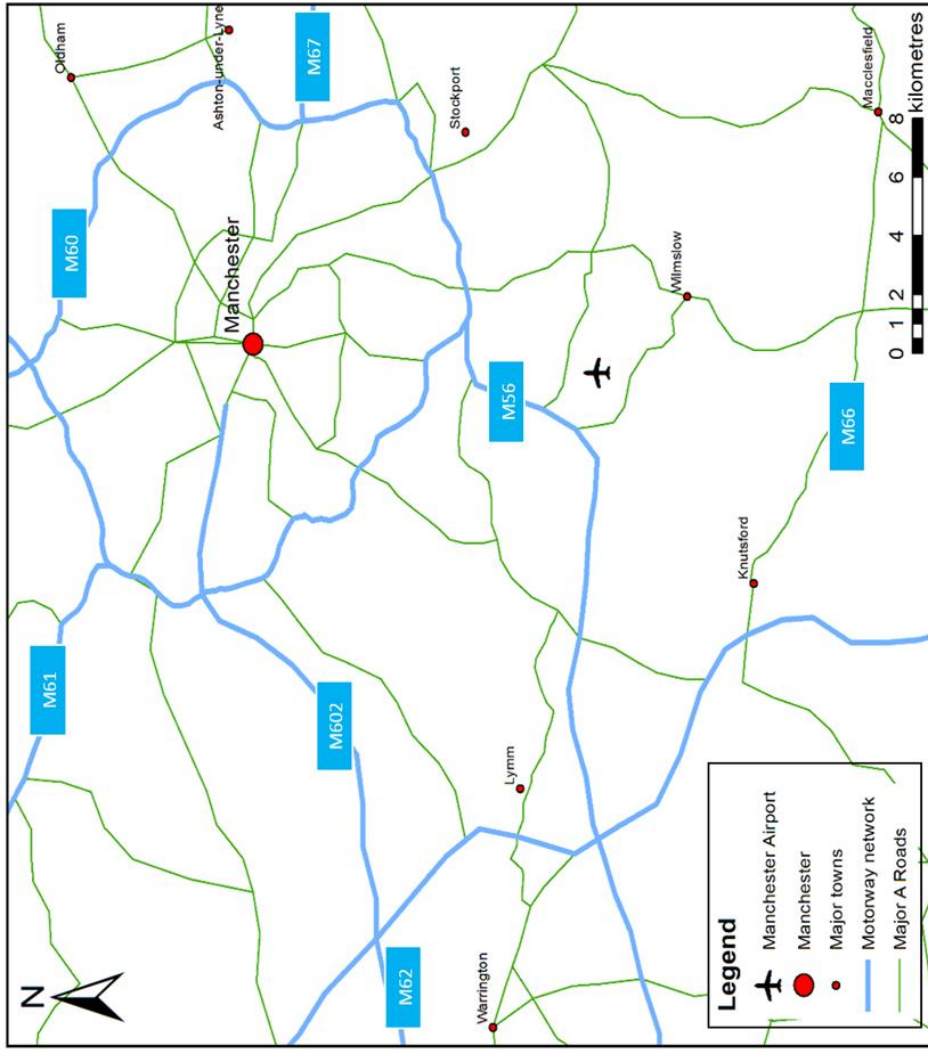
Figure 3.8: The map on the left shows the location of Manchester International Airport within the north west of England, UK. The map on the right shows the location of the airport in relation to Manchester city centre and major towns, the motorway network and major A roads within its proximity (maps created in ArcGIS using UK Border data from the UK Data service, 2017 and Ordnance Survey Data from Edina Digimap, 2017).

The Metrolink service to the airport which opened in November 2014 also provides direct access to the airport through the Greater Manchester tram network (Metrolink, 2016).

MAN has two runways 23R/05L (Runway 1) and 23L/05R (Runway 2). The runways are used in tandem throughout the week for a maximum period of up to eight hours per day. The nature of the operations is dependent on the prevailing wind direction. When westerly wind directions prevail departures take place on runway 23L and landings on 23R. There are no landings on 23L, apart from in exceptional circumstances, due to the absence of an Instrument Landing System (ILS) on this runway. When the wind is from an easterly direction 05R is used for arrivals, and 05L for departures. Outside these periods single runway operations are maintained with 23R/05L operating as the main runway (Crompton, 2010, pers., comm.).

3.3.2 Grass Sampling

Phase 1: 31st January 2011 - 11th July 2013

For grass sampling, a minimum of five days dry weather preceded each sampling visit to allow for a build-up of particulates on vegetation (grass) surfaces much of which would otherwise be washed off by rainfall (§ 2.1). Grass was selected as the vegetation medium due to it being the most abundant vegetation type. Samples were obtained using stainless steel cutting sheers. The upper 20cm of grass was sampled at each location and individual samples transferred to clean self-sealed polythene bags. A 50m tape measure was used to measure the distance between each sampling location and a hand held Global Positioning System (GPS) used to record the GPS co-ordinate of each sampling site.

Samples of grass were collected at 50m intervals alongside runway 23L/05R (Runway length: 3048m), along a transect line located 1m from the edge of the runway (Figure 3.7). The transect was extended 200m beyond the eastern end of the runway, adjacent to the Instrument Landing System (ILS) critical area of 05R. Additional samples were collected from within the critical area preceding the

start of runway 23L. Sampling within the critical area commenced at 5m from the edge of runway 23L**.**

Samples were collected along the extended centre line at 25m intervals up to 155m, followed by samples at 170m, 180m, 190m and 200m (the initial systematic sampling interval was interrupted by the presence of the ILS equipment).

Phase 2: 1st July 2014 - 2nd July 2014

Samples of grass ($n = 25$)   were collected from a number of pre-defined zones (B, C and D) which were located within the apron and taxiway areas and alongside runway 23R/05L (Figures 3.5 and 3.6).   Access to most of runway 23R/05L was prohibited due to the safety restrictions imposed as a result of the 24 hour operational procedures which take place on this runway. Limited access, however, was granted to section D (Figure 3.6).   In addition to this, the outstanding grass sampling from phase 1 was also completed.   Samples were collected from alongside runway 23L/05R following the sampling procedure described in phase 1.   Sampling commenced at 2675m and continued at 50m intervals to the end of the runway (3048m).

3.3.3 Soil Sampling

Soil sampling was conducted alongside the grass sampling. Each sampling point was identified using the procedure previously outlined in section 3.2.3. At each sampling point ($n = 25$), the upper 5cm of surface soil (approximately 500 cm^3) was extracted using a stainless steel bulb planter.

3.3.4 Runway Dust Sampling

Runway dust sampling took place between 31st January 2011 and 11th July 2013. A minimum of five days dry weather preceded each sampling visit to enable particle accumulation (§ 3.3). Several methods of dust collection have previously

been used by other researchers e.g. domestic vacuum cleaners (Lai *et al.* 2016; Szczepaniak-Wnuk and Górka-Kostrubiec 2016); custom built dust samplers with filters (Amato et al. 2009; Pant et al. 2015) and sweeping with a polyethylene dustpan and brush (Xie et al. 1999; Robertson et al. 2003; Yang et al. 2010; Wang et al. 2012). The dustpan and brush method was selected for use in this study, due to the rapid and relative ease of sample collection. Runway dust sampling was completed along runway 23L/05R.
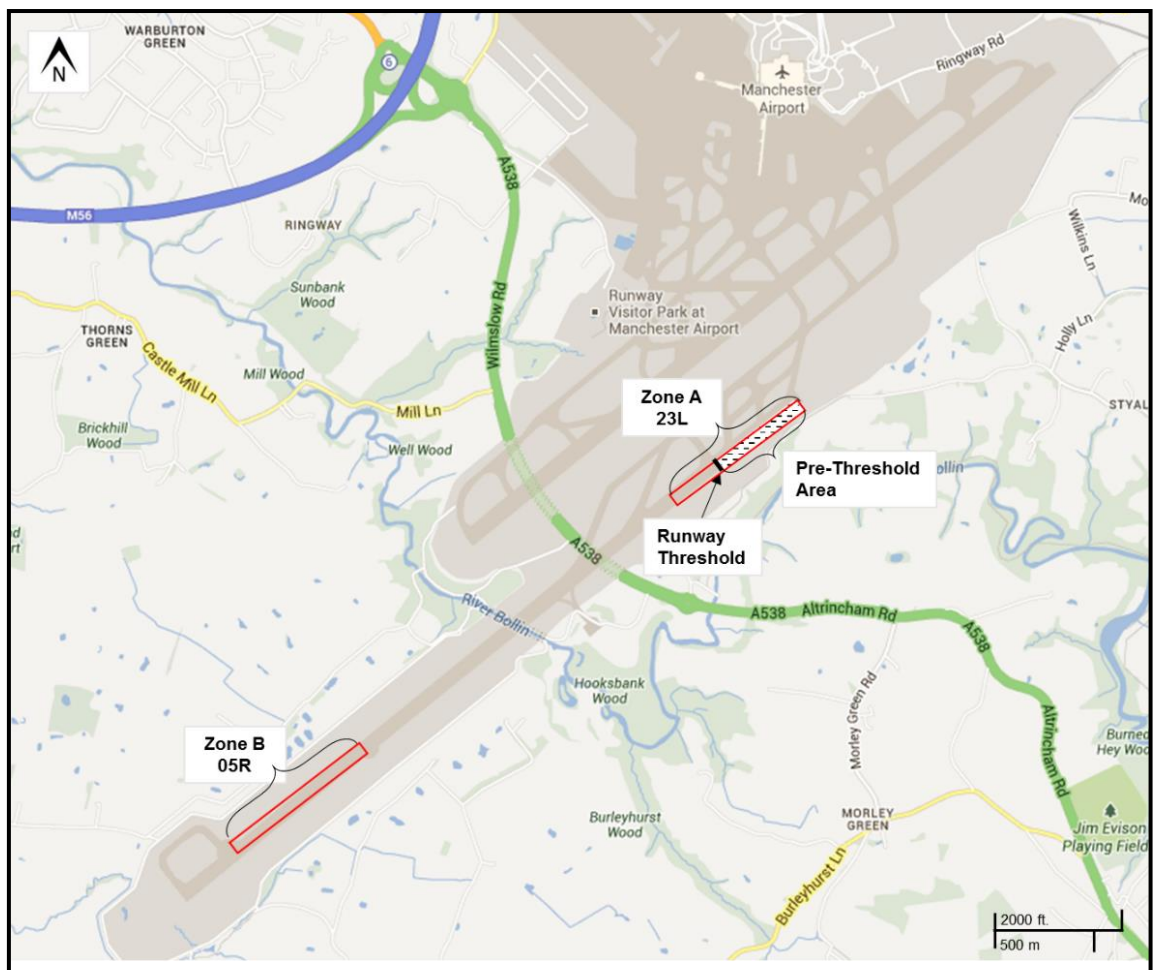
Figure 3.9: Location of runway dust sampling sites, runways 23L and 05R, MAN. Zone A (0 - 725m) represents a section of the runway which would include the initial stages of the take-off cycle on runway 23L. Zone B (2300 - 3000m) represents the main landing zone on runway 05R (Map adapted from Google Maps, 2014).

Figure 3.10: Satellite image of MAN displaying the Taxiway and Apron dust sampling areas (Google Earth, 2017). Final map created in ArcGIS (v. 10.4.1).

Sampling was attempted at 100 m intervals and at intervening sections where there was a clear accumulation of dust. Sampling commenced from the start of the runway pre-threshold area of runway 23L and continued along the entire length of the runway (3048 m). However, at most locations only very low sample masses were obtained (<0.2 g). Significant accumulations of runway dust (0.6 – 0.8 g) were obtained from a number of locations along the runway (i.e. at 400 m; 500 m; 575 m; 600 m; 700 m; 725 m; 2375 m; 2500 m; 2600 m; 2700m; 2800 m; 2900 m; 3000 m) (Figure 3.9). The specific sampling locations are detailed in Appendix 1.

3.3.5 Apron and Taxiway Dust Sampling

Sampling sites were identified following discussions with the airport operations team due to safety and security considerations associated with active aircraft movements. Samples of apron and taxiway dust were collected from pre identified zones (B, C and D) (Figures 3.5 and 3.6). However, specific sampling points within each zone could only be identified at the time of the visit due to air traffic control restrictions and aircraft movements. A total of 19 samples were collected from each zone as follows (B: $n = 11$; C: $n = 2$; D: $n = 2$; T1: $n = 2$; VA1: $n = 2$) (Figures 3.5, 3.6 and 3.10). The specific site numbers are identified in Appendix 1. Samples were collected using a clean dustpan and brush as previously identified in section 3.3.4.

3.4 Laboratory methods

The following section outlines each of the laboratory techniques employed in this study.

3.4.1 Sample preparation (general)

The soil and grass samples were dried at room temperature and all samples together with the engine, brake, tyre, runway, apron and taxiway dust samples screened to remove any visible traces of foreign matter including plastic brush

bristles, hair and animal matter. All soil and dust samples were sieved to remove the >2 mm size fraction.

3.5 Environmental magnetism

Environmental magnetic measurements focus on the non-directional magnetic properties of natural materials. The measurements involve the application of artificially induced magnetic fields to natural samples in order to determine the concentration and type/grain size of magnetic minerals. Variations in the data often relate to transformations of magnetic iron oxides due to environmental processes.

The results are used to make inferences about source or process. The following sections provide an introduction to the physical basis of the magnetic behaviour of natural materials and the magnetic parameters used in this study.

3.5.1 Types of Magnetic Behaviour

All minerals display some form of magnetic behaviour occurring as a result of electron and orbital spins within the atoms of the constituent elements. In the absence of any unpaired electrons and cooperative coupling between them, all elements and materials are diamagnetic, a weak magnetic effect. The four most important types of magnetic behaviour in environmental magnetism are ferrimagnetism, antiferromagnetism, paramagnetism and diamagnetism.

A guide to the different forms of magnetic behaviour can be found in Appendix 2.

3.5.2 Magnetic Grain Size

The detailed magnetic behaviour of ferrimagnetic and antiferromagnetic minerals is largely determined by magnetic grain size. Magnetic grain size and sediment particle size are not fully independent, though coarse mineral particles may be characterised by fine magnetic grains whose magnetic properties reflect the size of magnetic grains not particle size.

Magnetic grains are composed of domains, the number of which is related to the size of the grain. Large crystals are usually subdivided into many compartments or domains (multidomain) that act as separate entities responding differently to external fields and also towards each other to achieve a state of lowest energy following alignment in a strong magnetic field. When multidomain grains are removed from a saturating field they display a decline in remanent magnetisation over time, which is known as 'viscous loss of remanence'.

Stable single domain grains are characteristic of smaller magnetic grain sizes. As magnetic grain size decreases it becomes less energetically advantageous for division into separate domains, therefore, each grain forms its own magnetic domain. Stable single domain grains do not display any significant viscous loss of remanence.

In between the stable single domain and multidomain grain sizes is an intermediate band of pseudo-single domain grains, which display transitional characteristics.

Grains smaller than the stable single domain grain size are too small to retain a magnetic remanence at room temperature. The magnetic moment induced by a strong magnetic field is lost by thermal randomisation; such grains are referred to as superparamagnetic.

The small size range of grains at the stable single domain and superparamagnetic border are referred to as fine viscous grains. Fine viscous grains exhibit a delayed response to changes in magnetic fields. Whilst fine viscous grains do show some loss of remanence, they also display a unique property: when magnetised in a low field at high frequency some superparamagnetic grains behave like stable single domain grains with lower magnetic susceptibility (Walden et al, 1999). Grain size changes largely relate to ferrimagnetic minerals, as most antiferromagnetic minerals are stable single domain.

3.5.3 Sample preparation for mineral magnetic measurements

Individual samples of grass, soil, engine, brake, tyre, runway, apron and taxiway dust were gently disaggregated before being packed tightly into pre weighed 10 ml plastic containers. Each sample was reweighed after packing so as to be able to calculate the mass specific values. All weights were recorded to two decimal places (mg) using a pre-calibrated balance. A range of standard magnetic measurements were completed on all samples (§ 3.5.3) at Edge Hill University, Ormskirk, L39 4QP, (UK).

3.5.4 Mineral magnetic parameters and their measurements

3.5.4.1 Magnetic Susceptibility (χ)

Magnetic susceptibility (χ) is the ratio between the magnetisation induced in a sample and the strength of the magnetising field. Each sample was subjected to a weak magnetic field (0.1_{mT}) by means of a Bartington Instruments MS2B magnetic susceptibility sensor and the resultant induced magnetisation measured on a Bartington Instruments magnetic susceptibility meter. Higher susceptibility readings are recorded in samples which contain a greater amount of ferrimagnetic minerals and therefore χ can be used to determine the concentration of ferrimagnetic minerals within a sample. Where ferrimagnetic minerals are absent or sparse, non-spin cooperative (weaker) paramagnetic forms of magnetic minerals, may provide a significant contribution to susceptibility which may be diagnostic of individual environmental sources (§ 3.8).

3.5.4.2 Anhysteretic Remanent Magnetisation (ARM)

An ARM was induced within each sample using a Molspin shielded alternating field demagnetiser (Bartington Instruments, Witney, Oxon., OX28 4GE, UK) with a peak alternating field (AF) of 100 $_{mT}$ and a direct current (DC) biasing field of 0.04 $_{mT}$. A Molspin magnetometer was used to record the increase/decrease in remanent moments for each sample and was recorded as the ARM. The ARM

data is presented within this thesis as susceptibility of ARM (χARM) through normalisation of the ARM for the DC biasing field used (0.04mT; 31.84 Am^{-1}). ARM is used as a measure of the concentration of magnetic minerals within a sample but is also used to distinguish the finer grain sizes. Assemblages containing greater proportions of stable single domain (SSD) grains display a relatively higher ARM.

3.5.4.3 Saturation Isothermal Remanent Magnetisation (SIRM)

SIRM is the magnetisation retained by a sample after it has been subject to intense magnetisation e.g. a saturating magnetic field. SIRM was measured on a Molspin magnetometer after magnetisation at 1 Tesla (1T) using a Molspin pulse magnetiser. It is assumed that the IRM acquired in the initial forward field of 1T is equivalent to the Saturation Isothermal Remanent Magnetisation (SIRM). Although it is affected by the magnetic grain size and mineralogy of a sample, SIRM also increases with the concentration of magnetic minerals in a sample.

3.5.4.4 Demagnetisation Parameters

These parameters use SIRM as the starting point and involve progressively placing the sample in reverse fields (backfields) of increasing strength. At each stage or backfield, the new remanence (IRM) is measured and plotted as a ratio of the original SIRM. The measurements can be used to produce a coercivity curve (Figure 3.11). The coercivity of SIRM ((Bo)$_{CR}$) is the reverse field required to reduce the SIRM to zero. The coercivity is not routinely determined for all samples due to the time required. Consequently in this study only a small number of discriminating reverse fields (backfields) have been employed. Reverse field ratios were determined by placing a previously saturated sample successively in reverse fields of increasing strength (-20mT; -100mT; -300mT) and measuring the isothermal remanence at each stage. The data are expressed as a ratio IRM$_{-xmT}$/SIRM. More negative reverse field ratios are indicative of 'soft' magnetic behaviour exhibited by ferrimagnetic mineral assemblages of coarse grain size (i.e. multidomain). 'Hard' magnetic behaviour is evidenced by more positive

ratios, and shows the presence in a sample of fine-grained ferrimagnetic material (stable single domain) and antiferromagnetic minerals.

3.5.4.5 Interparametric Ratios

A number of the measured magnetic parameters may be combined in ratios to provide further insight into variations in ferrimagnetic mineral grain size. These are referred to as interparametric ratios. The ones used in this study are:

3.5.4.5.1 $\chi ARM/\chi$

Where there is little variation in magnetic mineral type, the ratio of χARM divided by χ can be diagnostic of magnetic mineral grain size, with larger ratios indicative of finer ferrimagnetic mineral grain sizes (King *et al.*, 1982).
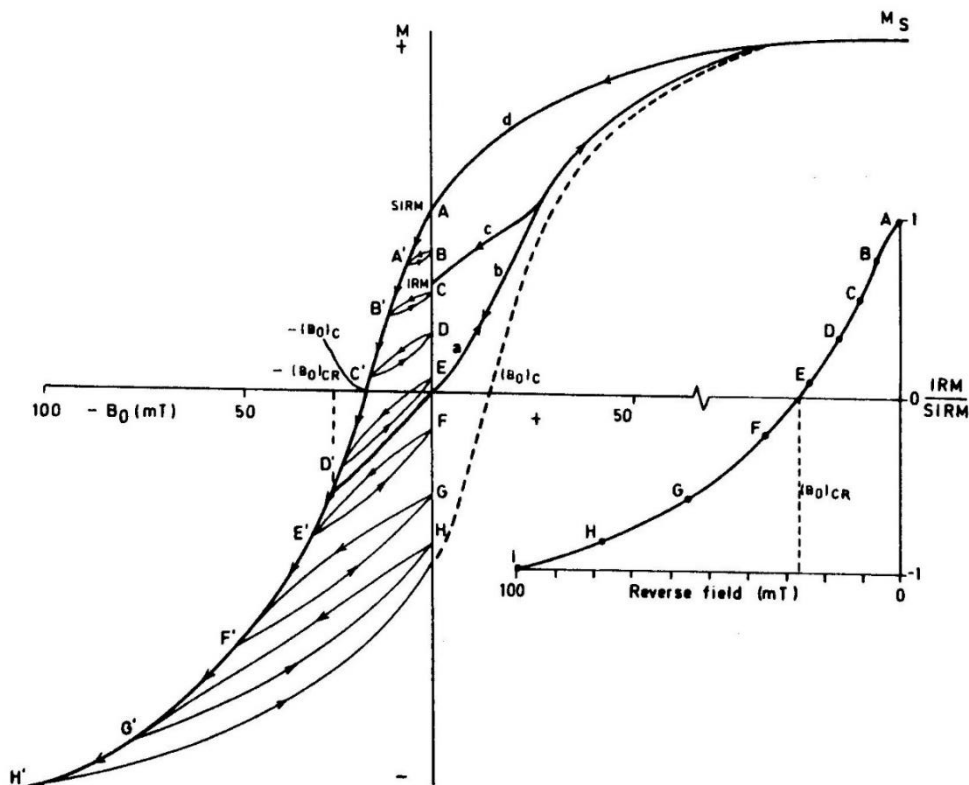
Figure 3.11: The hysteresis loop: Inset: the coercivity of remanence curve produced from the reverse field ratios A – I. (Abbreviations: M = induced magnetisation; B_0 = applied magnetic field; M_s = saturation magnetisation; SIRM = saturation isothermal remanent magnetisation; $(B_0)_{CR}$ = coercivity of remanence) (Thompson and Oldfield, 1986).

55

3.5.4.5.2 χARM/SIRM

The ratio of χARM to SIRM is diagnostic of variations in magnetic mineral grain size in samples where the magnetic mineral type remains relatively constant and is particularly sensitive to SSD grain sizes. Larger ratios, i.e. >200 are representative of finer ferrimagnetic mineral grain sizes (Maher, 1988).

In samples where there is minimal variation in magnetic mineral type, variations in ferrimagnetic mineral grain size can be useful/are important in discriminating between different sources.

3.6 Chemical analysis

Chemical analysis of the bulk samples was completed using X-Ray Fluorescence spectrometry (XRF). XRF is a widely used, rapid and non-destructive technique for the chemical analysis of environmental samples and requires minimal sample preparation (Boyle, 2000; Onat *et al.*, 2013; Deschamps *et al.*, 2014). The technique is based on the photoelectric fluorescence of characteristic secondary X-rays after the given sample has been bombarded with a stream of primary X-rays and provides quantitative data for a wide range of elements (Boyle, 2000). Whilst there are a range of other techniques which can be used for the chemical analysis of environmental samples e.g. Atomic Absorption Spectroscopy (AAS) and Inductively Coupled Plasma Mass Spectrometry (ICP–MS) these methods often require chemical digestion of the sample prior to analysis. Therefore, XRF was chosen in this study due to the non-destructive sample preparation and the need to complete other analyses on the samples.

3.6.1 XRF Sample preparation and analysis

All individual aircraft source and environmental samples of runway, apron and taxiway dusts and soils, which had previously been disaggregated for magnetic measurements, were placed directly into XRF sample pots. However, due to the very low small sample weights of the grass samples, samples from specific areas were bulked together. Grass samples of 10 g mass were combined and homogenised from the following areas (B; C; D and at 500 m intervals adjacent

to runway 23L/05R). The samples were ground to a fine powder using a coffee grinder before being packed into individual XRF sample holders.   Three subsamples from each homogenised bulk sample were measured. Prior to XRF analysis, each sample was gently compacted to a maximum depth of 4 – 5 mm using a brass plunger.   Sample measurements including all aircraft source samples (i.e. engine, brake and tyre dusts); runway dusts; taxiway and apron dusts were completed using a Bruker S_2 Ranger energy dispersive XRF analyser located within the Department of Geography and Planning at the University of Liverpool, Liverpool, L69 3BX (UK).   Prior to measurements, the instrument was calibrated using a range of reference materials, which contained certified levels of element concentrations (Appendix 3a). Due to the unavailability of the Bruker S_2 Ranger during the latter 12 months of this research due to technical reasons, chemical analysis of the remaining samples (i.e. grass and soil) was completed using an Oxford Instruments X-MET 7500 Series portable XRF analyser within the Department of Geography at Edge Hill University, Ormskirk, L39 4QP (UK). Calibration between the two instruments was completed by remeasuring a number of samples ($n = 10$) that had previously been measured using the Bruker S_2 Ranger and that covered a wide range of element concentrations. For each metal of interest, the data showed a strong linear relationship between the concentrations from each XRF analyser, and therefore a linear regression was used to derive 'Bruker equivalent' values from the EHU analyser data (Appendix 3b).

3.7 Scanning Electron Microscopy and Energy Dispersive X-Ray Spectroscopy Analysis

Scanning electron microscopy (SEM) alongside energy dispersive X-Ray spectroscopy (EDX) is an effective technique used to investigate the morphological characteristics and elemental composition of particulates derived from a wide range of environmental samples e.g., (Kim *et al.*, 2007; Saragnese *et al.*, 2011; Cao *et al.*, 2015; Zong *et al.*, 2017). Previous studies have focused on the analysis of magnetic particles extracted from a range of environmental samples (Kim *et al.*, 2007; Blaha *et al.*, 2008; Bucko, 2012; Górka-Kostrubiec, 2015). This was attempted on the aircraft source samples (i.e. engine, brake and

tyre dusts) using a hand magnet method as described by Kim et al., (2007). However, due to small sample sizes and the low concentrations of magnetic minerals within individual samples, the extraction of magnetic extracts proved unsuccessful and nothing of significance could be obtained for analysis.

3.7.1 SEM/EDX Sample preparation and analysis

Individual aircaft source and environmental samples were mounted onto 12.5 mm carbon stubs in preparation for SEM/EDX analyses. Analyses were completed on a total of 25 samples (engine $n = 5$; brake $n = 5$; tyre $n = 3$; apron $n = 3$; taxiway $n = 4$; runway $n = 5$). SEM/EDX analyses was not completed on the grass and soil samples due to the very low contamination levels within the grass samples and the complexity and variability of the inorganic and organic components within the surface soil samples. Such differences may result, for example, from the weathering of the parent material and pedogenic processes (Hanesch *et al.,* 2007) and inputs of anthropogenically derived partiuclates from local and regional pollution sources (Sharma and Tripathi, 2008; Zong *et al.*, 2017).

Sample mounts were analysed using a Zeiss Supra 40VP SEM system equipped with an EDAX energy dispersive spectrometry (EDX) at Manchester Metropolitan University, Manchester, M1 5GD (UK).   The samples were observed in partial vacuum conditions using backscattered electron imaging. For SEM analysis, the typical beam of current was 1.0 kV and the working distance 5 mm. SEM observations were typically carried out at magnifications of 4 - 10 K.   The chemical composition of specific areas and individual particles of interest within each sample was determined using EDX.

Direct observations of bulk dust samples and individual particles for each sample set were conducted (i.e. engine; brake; tyre; runway; taxiway and apron). SEM/EDX was used to investigate the morphological; chemical and particle size characteristics of selected areas within each stub and individual particles for each dust group (engine: $n = 30$; brake: $n = 27$; tyre: $n = 23$; runway: $n = 29$; taxiway and apron: $n = 35$). A standard sedimentary geology 'roundness chart' (Pettijohn *et al.,* 1987)   was used to determine the shape of individual particles and soil

structure classification chart (USDA, 2017) for the textural descriptions described in Chapter 6 (§ 6.1.1 and 6.2.1 and 6.2.2).

3.8 Electron Spin Resonance

Electron spin resonance (ESR), also referred to as electron paramagnetic resonance (EPR) spectroscopy is a highly sensitive magnetic resonance technique for the investigation of magnetic materials (Wertz and Bolton, 1986). ESR facilitates the analysis of electronic structures of materials containing unpaired electrons (Mabbs, 1993) i.e. electron states that give rise to paramagnetism and cooperative ferrimagnetism, ferromagnetism and antiferromagnetism (Crook *et al.*, 2002). This potential is due to the sensitivity of ESR to the immediate magnetic and chemical environment of the intrinsic magnetic moments within atoms, molecules, minerals and materials.

When magnetic spins (atomic, molecular or particulate magnetic moments) are immersed in a DC field they precess around the applied field at the Larmor Frequency. The frequency is determined by the magnitude of the magnetic spin and the local field magnitude, therefore, ESR is sensitive to the local spin and magnetic moment environment.

The free electron is paramagnetic and has a fundamental quantum spin of ½. This results in a so called quantum mechanical g-factor which is very close to 2.00. In a dilute (low concentration spin system) a narrow ESR absorption line is produced. When these spins couple, ferri, ferro-, anti- ferro- magnetic ordering occurs which alters, and tends to broaden, the shape of the ESR absorption spectrum. Diamagnetic materials with an even number of electrons have no 'free' or unpaired spins and are therefore ESR silent. This means that ESR probes the magnetic moments that also give rise to the properties measured in conventional environmental magnetism, but at very high sensitivity. Only a few mg of sample are needed for ESR in comparison to the higher mass (~ >5 g) for Environmental Magnetism.

Experimentally the Larmor precession is detected by also immersing samples in a microwave field. Absorption occurs when the frequencies of the microwave field

and Larmor precession become equal. Quantum mechanically this is equivalent to the spins undergoing transitions between the Zeeman Energy levels caused by the application of the DC field, lifting quantum mechanical spin degeneracy. That is, in the absence of a magnetic field free electrons have equal energies in all directions, their energies are said to be degenerate.

The technique has been shown to be highly effective in the analysis of weakly magnetic environmental samples where it is difficult to use conventional magnetic measurements and for samples where diamagnetic components predominate (Crook *et al.*, 2002). To date, however, the use of ESR in studies of environmental magnetism remains limited (§ 2.1.1).

As part of a supplementary study ESR has been applied to airport derived aircraft source and environmental samples to compliment and extend the other techniques described within this thesis.

3.8.1 ESR Sample preparation and analysis

A supplementary study was conducted on a small suite of aircraft source and environmental samples (engine $n = 3$; brake $n = 3$; tyre $n = 3$; taxiway $n = 1$; runway $n = 2$; soil $n = 2$; grass $n = 2$; runway marking debris (yellow paint) $n = 1$. The ESR analysis was completed at the Photon Science Institute at The University of Manchester, Manchester, M13 9PL (UK). ESR spectra were recorded at X-band (9.6 GHz) using a Bruker ESP300E spectrometer. A simplified diagram of the ESR equipment is shown in Figure 3.12. To ensure that all ESR absorption conditions are sampled the experimental field is scanned. Individual samples were placed inside a resonant microwave positioned within a scanning DC field. The microwave frequency which is applied to the high-Q cavity (typically Q > 5000, when Q is a measure of the quality of the cavity and its effective gain) is adjusted to ensure that the cavity is operating at resonance. This fine tuning results in the gain of the cavity being extremely high and thus also the sensitivity of the ESR technique.

ESR absorption appropriate to magnetic materials has been modelled by Hoon using an electromagnetic model (Appendix 4). This has been applied to the analysis of environmental sediments (Crook *et al* ., 2002; Alagarsamy and Hoon

2017) and has further been applied within this preliminary study, which focuses on a small number of samples that are representative of the various airport derived aircraft source and environmental samples which are the focus of this research.
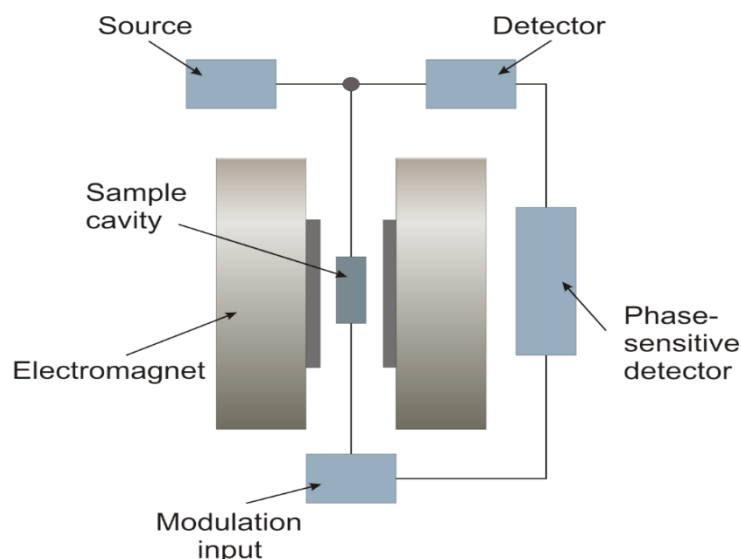
Figure 3.12: Simplified block diagram of a typical X-band ESR spectrometer (Alagarsamy and Hoon, 2015).

3.9 Statistical Analysis

The descriptive statistics described within Chapters 4 to 6 have been calculated using the statistical software package Minitab version 17 which has also been used for the Cluster Analysis described in § 3.9.3.

3.9.2 Multivariate Statistics

To investigate the relationship between the main metallic elements and the direct and environmental sources, principal components analysis (PCA) was performed using the statistical software package PAST version 3.16.

PCA enables data reduction by extracting a small number of independent factors (principal components) for the analysis of relationships amongst observed variables (Lu *et al.*, 2010). PCA is used widely in urban pollution studies to assist

in the differentiation and identification of pollution sources and furthermore to investigate source attribution (Lu *et al.*, 2010; Wang *et al.*2012).

In this study PCA has been applied to the geochemical data for the aircraft source samples to assist in the elemental classification and characterisation of the aircraft engine, brake and tyre dusts. PCA was also applied to the runway, taxiway and apron dust samples to investigate the elemental associations within each of the different areas.

3.9.3 Cluster Analysis

Cluster analysis (CA) is an established technique which is used widely in environmental studies (e.g. Adachi and Tainosho, 2004; Lu *et al.*, 2010; Xia *et al.*, 2014). The technique, which is applied to a combination of internal variables, enables the classification of a set of observations into two or more mutually exclusive groups. Within this study CA has been applied to the magnetic parameters associated with the aircraft source samples to classify the source samples into groups based on the magnetic characteristics of the individual samples.

Chapter 4

Results: Magnetic measurements

Chapter 4, sections 4.1 to 4.4 comprises a description of the magnetic measurements results together with an initial interpretation of this data focusing on the magnetic mineralogy and grain size characteristics of all aircraft source and environmental samples. The mean value (± 1SD) for each variable is presented within Tables 4.1 to 4.7 and Figures 4.1 to 4.16 and provides information on the magnetic mineralogy, concentration and grain size of the magnetic assemblages within each sample set.

For the depositional environments (e.g. runway, apron, taxiway, soils and grass) concentration parameters may provide an insight into varying deposition patterns if it can be assumed that there is no change in the nature of the magnetic material.

4.1 Aircraft Source Samples

4.1.1 Engine, Brake and Tyre Dusts

i)   *Magnetic Description*

Table 4.1 summarises the results of the magnetic analyses which were completed on the aircraft source samples (i.e. aircraft brake, engine and tyre dusts). The variables presented within the table provide information on the magnetic mineralogy and grain size of the magnetic assemblages within each sample set rather than concentration related variables.

Figure 4.1a displays the χARM/χ data for each of the aircraft source samples. χARM/χ values for brake dusts have a mean of 19.72 Am^{-1} ± 5.2 (range: 9.90 Am^{-1} to 29.73 Am^{-1}) in comparison to the engine dusts which have a mean value of 53.42 Am^{-1} ± 9.53 (range: 36.02 Am^{-1} to 68.77 Am^{-1}) and the tyre dusts with a mean value of 21.55 Am^{-1} ± 6.09 (range: 15.76 Am^{-1} to 27.90 Am^{-1}). The χARM/SIRM values (Figure 4.1b) for the brake dusts have a mean value of 122.57 (10^{-6}) ± 17.44 (range: 87.92 (10^{-6}) to 152.16 (10^{-6})) whereas the engine dusts have a mean value of 260.80 (10^{-6}) ± 50.10 (range: 166.7 (10^{-6}) to 331.8

(10^{-6})) and the tyre dusts a mean value of 164.23 (10^{-6}) ± 12.89 (range: 150.50 (10^{-6}) to 176.06 (10^{-6})).

Figure 4.2a shows the lower reverse field ratio ($IRM_{-20mT}/SIRM$) data for the aircraft source samples. The brake dusts have a mean value of 0.58 ± 0.05 (range:0.48 to 0.65), whereas the engine dust samples display a mean value of 0.70 ± 0.06 (range: 0.60 to 0.80) and the tyre dusts 0.71 ± 0.01 (range: 0.69 to 0.72). The $IRM_{-100mT}/SIRM$ ratio (Figure 4.2b) for the brake dust samples has a mean value of -0.64 ± 0.04 (range: -0.71 to -0.59), whereas the engine dusts have a mean value of -0.51 ± 0.09 (range: -0.65 to -0.37) and the tyre dusts a mean of -0.55 ± -0.01 (range: -0.56 to -0.54). The higher reverse field ratio ($IRM_{-300mT}/SIRM$) (Figure 4.2c) for the brake dusts has a mean of -0.97 ± 0.01(range:-0.98 to -0.95), whilst the engine dusts have a mean value of -0.90 ± 0.02 (range: -0.93 to -0.88) and the tyre dusts -0.94 ± 0.00 (range: -0.95 to -0.94).

ii) *Magnetic interpretation*

The lower $\chi ARM/\chi$ and $\chi ARM/SIRM$ ratios exhibited by the brake and tyre dust samples are indicative of coarser ferrimagnetic mineral grain sizes. Conversely, the engine dusts display higher $\chi ARM/\chi$ and $\chi ARM/SIRM$ ratios which suggest finer ferrimagnetic mineral grain sizes.

The more positive $IRM_{-20mT}/SIRM$ ratios for the engine dusts suggest that these samples are dominated by finer ferrimagnetic mineral grain sizes in contrast to the brake dusts which feature less positive ratios that are indicative of coarser ferrimagnetic mineral grain sizes.

The less negative higher reverse field ratios ($IRM_{-100mT}/SIRM$ and $IRM_{-300mT}/SIRM$) for the engine dusts suggest the presence of a significant antiferromagnetic component within this sample set. The initial forward SIRM would be reverse saturated (i.e. $IRM_{-300mT}/SIRM$ = -1.0) if the sample was dominated by ferrimagnetic minerals. For the brake dust samples, the more negative $IRM_{-100mT}/SIRM$ ratios and $IRM_{-300mT}/SIRM$ ratios that are almost reverse saturated indicate a predominantly coarser ferrimagnetic mineral content. The tyre dust samples are situated midway between the engine and brake dusts for

the $IRM_{-100mT}/SIRM$ and $IRM_{-300mT}/SIRM$ ratios which suggests intermediate characteristics.
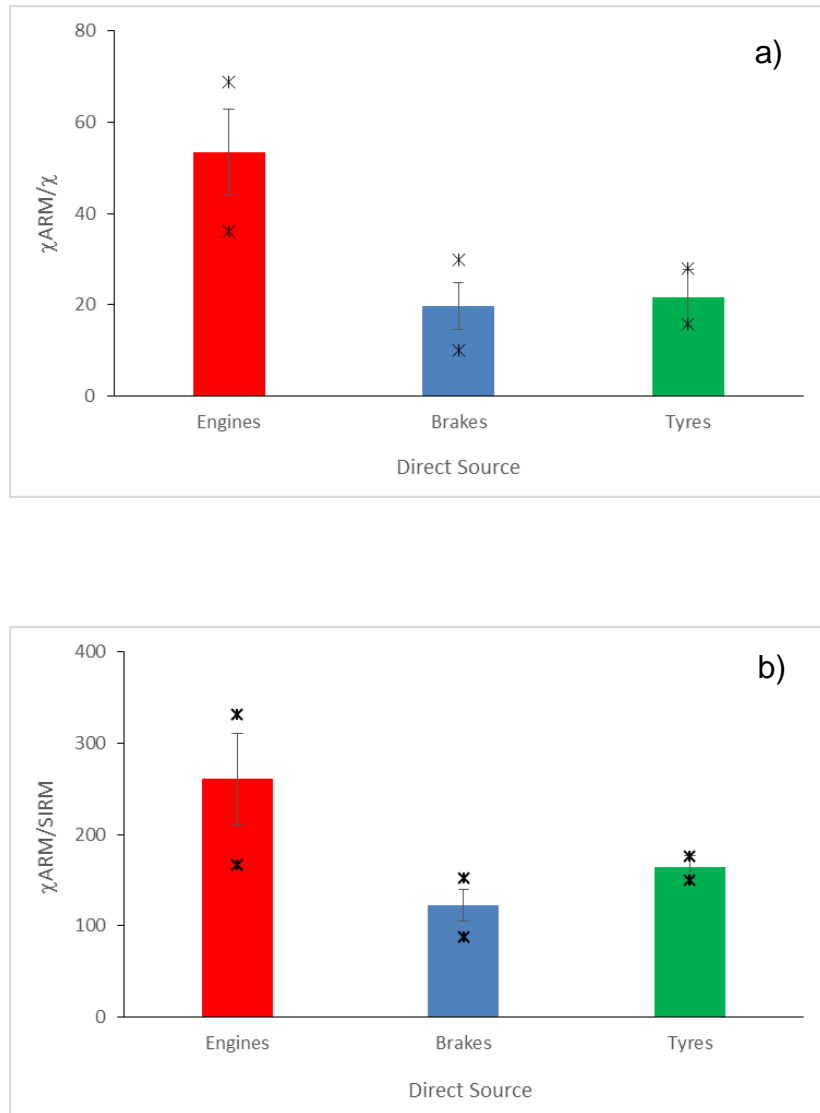
Figure 4.1: (a) $\chi ARM/\chi$ and (b) $\chi ARM/SIRM$ for the aircraft source samples (i.e. aircraft engine ($n = 13$), brake ($n = 16$) and tyre dusts ($n = 4$)). Mean values are displayed with bars showing ± 1 standard deviation. The minimum and maximum values are indicated by the markers (✱).
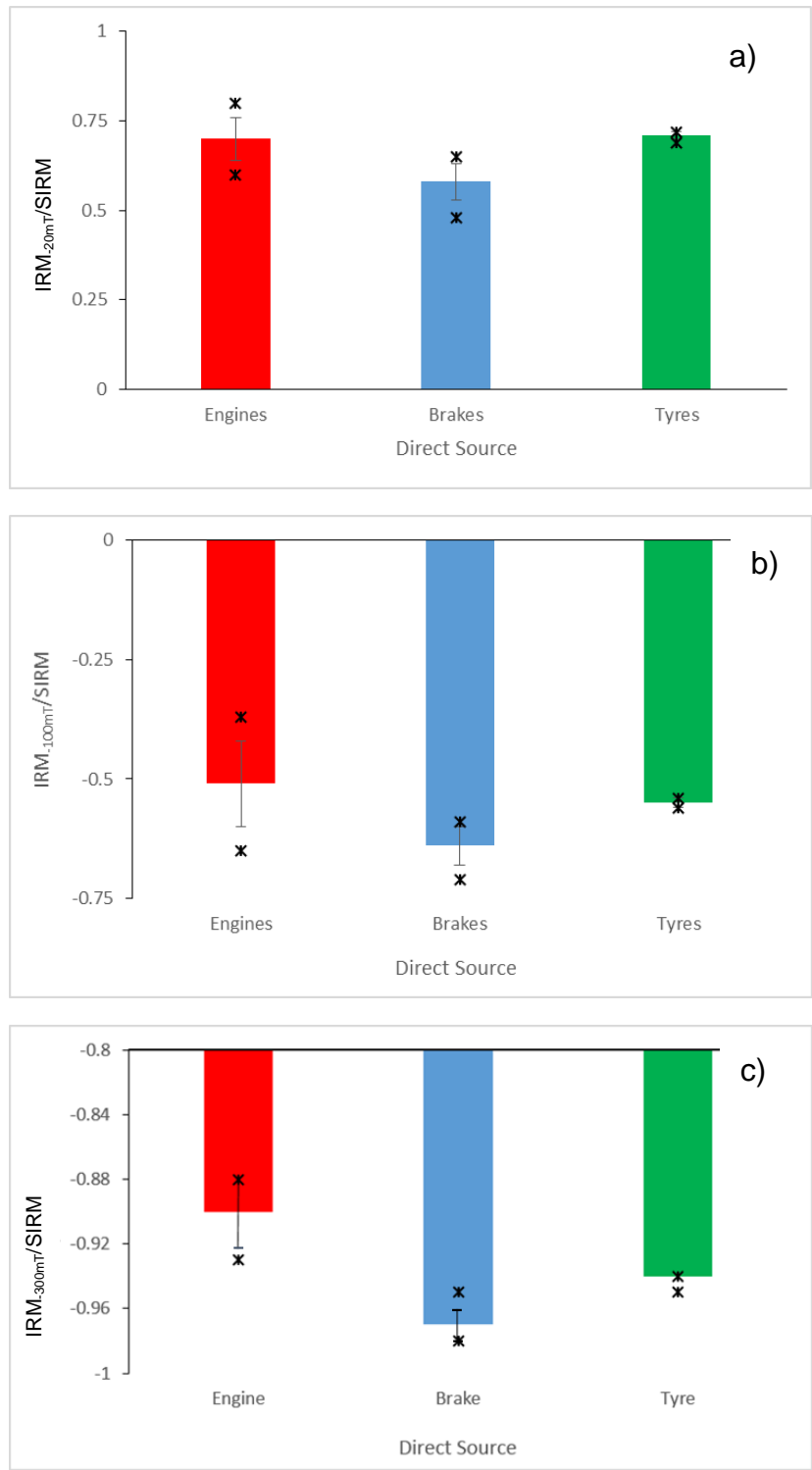
Figure 4.2: (a) IRM$_{-20mT}$ /SIRM; (b) IRM$_{-100mT}$ /SIRM (c) IRM$_{-300mT}$ /SIRM for the aircraft source samples (i.e. aircraft engine (n = 13), brake (n = 16) and tyre dusts (n = 4)).   Mean values are displayed with standard deviation (± 1SD) bars. The minimum and maximum values are indicated by the markers (✳).

Table 4.1: Summary of magnetic parameters for the aircraft engine, brake and tyre dusts.

Magnetic parameters		Brake ($n = 16$)	Engine ($n = 13$)	Tyre ($n = 4$)
$\chi ARM/\chi$ Am^{-1}	Range	9.90 – 29.73	36.02 – 68.77	15.76 -27.9
	Mean ± 1SD	19.72 ± 5.20	53.42 ± 9.53	21.55 ± 6.09
$\chi ARM/SIRM$ (10^{-6})	Range	87.92 – 152.16	166.70 – 331.8	150.5 – 176.06
	Mean ± 1SD	122.57 ± 17.44	260.8 ± 50.1	164.23 ± 12.89
IRM$_{-20mT}$ /SIRM	Range	0.48 – 0.65	0.60 – 0.80	0.69 – 0.72
	Mean ± 1SD	0.58 ± 0.05	0.70 ± 0.06	0.71 ± 0.01
IRM$_{-100mT}$ /SIRM	Range	-0.71 - -0.59	-0.65 - -0.37	-0.56 - -0.54
	Mean ± 1SD	-0.64 ± 0.04	-0.51 ± 0.09	-0.55 ± -0.01
IRM$_{-300mT}$ /SIRM	Range	-0.98 - -0.95	-0.93 - -0.88	-0.95 - -0.94
	Mean ± 1SD	-0.97 ± 0.01	-0.90 ± 0.02	-0.94 ± 0.00

Table 4.2: Summary of magnetic parameters for the runway dusts.

Magnetic parameters		Zone A (Take-off) ($n = 6$)	Zone B (Landing) ($n = 7$)
SIRM 10^{-6}Am^{2}kg^{-1}	Range	6137.38 – 11159.02	6948.38 – 33683.80
	Mean ± SD	7862.38 ± 1768.03	18233.96 ± 9327.42
IRM$_{-20mT}$ /SIRM	Range	0.62 – 0.79	0.66 – 0.73
	Mean ± SD	0.71 ± 0.06	0.70 ± 0.03
IRM$_{-100mT}$ /SIRM	Range	-0.42 - -0.30	-0.54 - -0.50
	Mean ±SD	-0.36 ± 0.05	-0.52 ± 0.02
IRM$_{-300mT}$ /SIRM	Range	-0.90 - -0.83	-0.97 - -0.94
	Mean ± SD	-0.87 ± 0.03	-0.96 ± 0.01

4.2 Environmental Dust Samples

4.2.1 Runway Dusts

i) *Magnetic Description*

Figure 4.3 displays the SIRM values for the runway dust samples collected along runway 23L/05R (§ 3.3.4). There is a clear distinction in SIRM values between the two Zones with Zone A displaying generally lower SIRM values than Zone B. In Zone A, there is little variation in the SIRM values which range from the lowest value of 6137.38 $10^{-6}Am^2kg^{-1}$ at 700 m to the highest value of 11159.02 $10^{-6}Am^2kg^{-1}$ at 400 m. In contrast to this the SIRM values in Zone B are generally higher but display greater variability. Within this Zone, SIRM values begin to increase from 13011.04 $10^{-6}Am^2kg^{-1}$ at 2375 m to the highest value of 33683.80 $10^{-6}Am^2kg^{-1}$ at 2700 m. SIRM values then decrease markedly to 13647.71 $10^{-6}Am^2kg^{-1}$ at 2800 m with a further decrease to the lowest SIRM value in Zone B of 6948.38 $10^{-6}Am^2kg^{-1}$ at 3000 m.

Table 4.2 summarises the magnetic analyses completed on the runway dust samples. The lower reverse field ratios (IRM_{-20mT}/SIRM) for the runway dusts in Zone A display a mean value of 0.71 ± 0.06 (range:0.62 to 0.79) and the samples in Zone B a mean value of 0.70 ± 0.03 (range: 0.66 to 0.73). IRM_{-100mT}/SIRM ratios for the samples in Zone A have a mean value of -0.36 ± 0.05 (range: -0.42 to -0.30), whereas the samples from Zone B have a mean value of -0.52 ± 0.02 (range: -0.54 to -0.50). The IRM_{-300mT}/SIRM ratios for the runway dust samples display a mean value of -0.87 ± 0.03 (range:-0.90 to -0.83), whilst the dust samples in Zone B have a mean value of -0.96 ± 0.01 (range: -0.97 to -0.94).

Interparametric ratios ($\chi ARM/\chi$ and χARM/SIRM) are not available for the runway dust samples due to low sample mass and low magnetic mineral concentrations preventing the accurate measurement of χ and ARM.
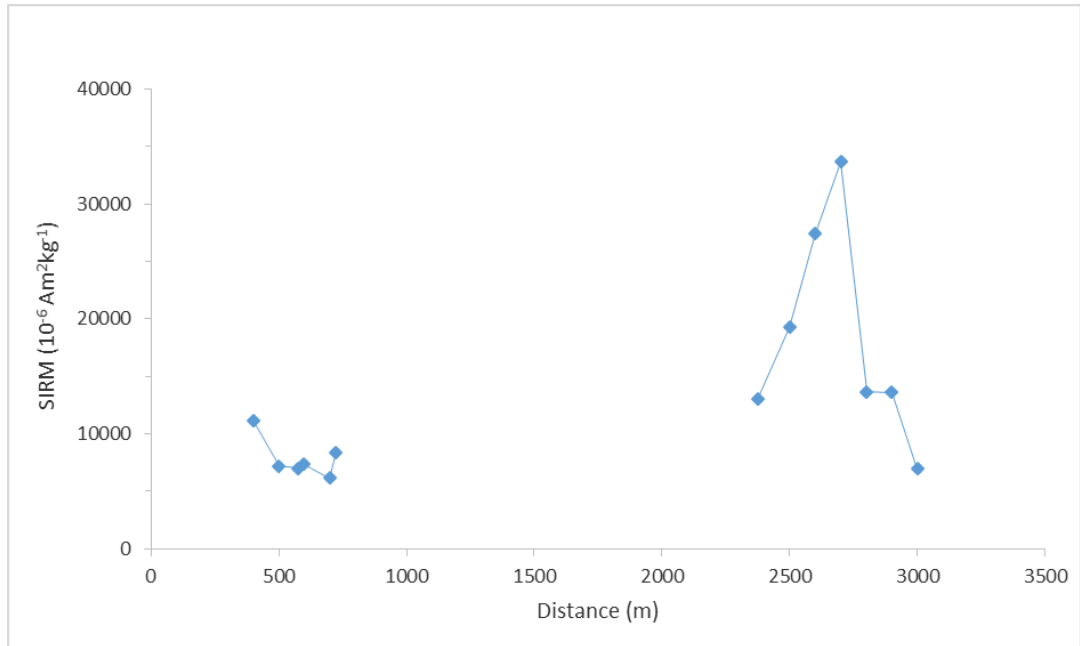
Figure 4.3: SIRM of the runway dusts with distance along
runway 23L/05R (Zone A = 0-725 m; Zone B = 2300 – 3000 m).
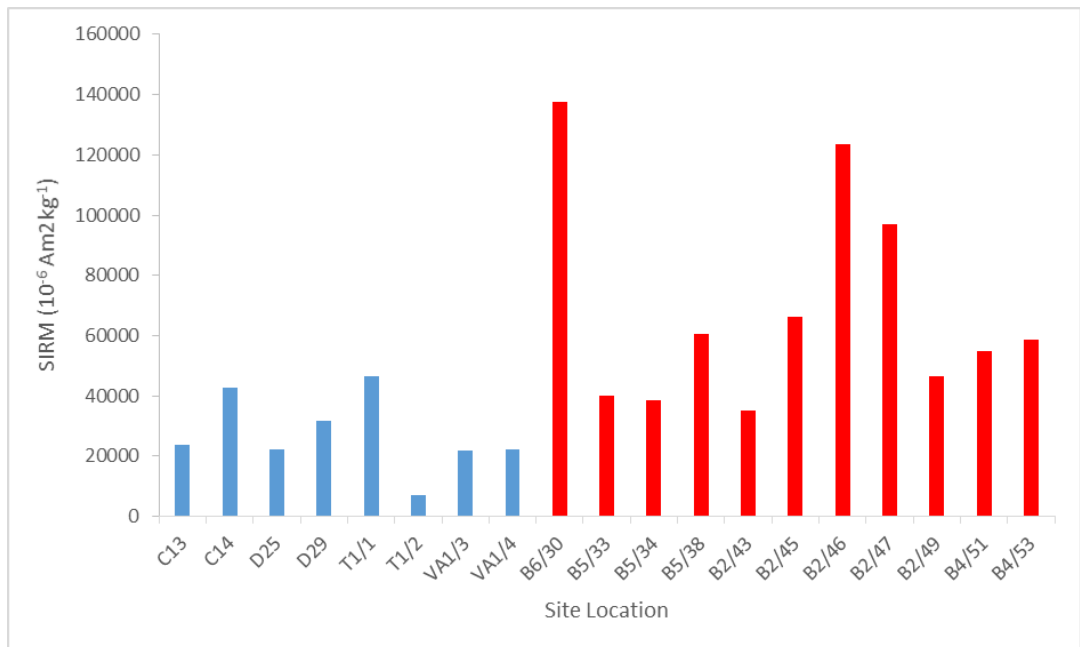
Figure 4.4: SIRM of the dust samples collected from the taxiway
and apron areas by site location.

ii)   *Magnetic interpretation*

Figure 4.3 identifies two distinct phases. In Zone A (Figure 3.9), magnetic mineral concentrations are low and remain fairly constant. In Zone B magnetic mineral concentrations, as indicated by SIRM, are generally higher than those in Zone B. High magnetic mineral concentrations are evident at 2375 m.

Concentrations then continue to increase markedly with distance along the runway with the highest magnetic mineral concentration being displayed at 2700 m. Magnetic mineral concentrations remain high but there is a marked decline in concentration at 2800 m and a notable change to low magnetic mineral concentrations at 3000 m.

The samples are not differentiated strongly on the lower reverse field ratio (IRM-$_{20mT}$/SIRM) but separate in relation to the higher reverse field ratios. The less negative IRM-$_{100mT}$/SIRM and IRM-$_{300mT}$/SIRM ratios shown in the samples in Zone A suggest that these dusts contain a significant antiferromagentic component. The more negative higher reverse field ratios displayed in the Zone B dusts indicate a predominantly ferrimagnetic assemblage.

4.2.2 Taxiway and Apron Dusts

i)   *Magnetic description*

A summary of the magnetic analyses which were completed on the taxiway and apron dusts is presented in Table 4.3. Figure 4.4 displays the SIRM values for the taxiway and apron dusts in relation to the individual site numbers (Appendix 1). The SIRM values displayed in the taxiway dust samples are extremely variable ranging from a low value of 7012.43 10^{-6}Am^{2}kg^{-1} at T1.2 to a high value of 4516.32 10^{-6}Am^{2}kg^{-1} at T1.1. However, with the exception of the lowest value at T1.2, SIRM values for the taxiway dust samples are high. The apron dusts also show wide variability in the SIRM values between samples. Overall, however, the SIRM values for the apron dusts are higher than those of the taxiway dust samples. Values range from an SIRM value of 35248.95 10^{-6}Am^{2}kg^{-1} at B2/43 to the highest SIRM value of 137733.27 10^{-6}Am^{2}kg^{-1} at B6/30.

The χARM/χ values for the taxiway and apron dusts are displayed in Figure 4.5 There is some variability between low and high ratios within each of the sample sets. Within the taxiway dusts, however, ratios are generally low <40 Am^{-1} at most site locations with the exception of sites C13 and C14 which display higher ratios of 43.75 Am^{-1} and 54.29 Am^{-1} respectively. The range of values within the apron dusts is also variable. However, once again, ratios are predominantly low with the exception of higher values of 47.12 Am^{-1} at B6/30 and 46.93 Am^{-1} at B4/51.

χARM/SIRM values are shown in Figure 4.6. The χARM/SIRM ratios also show variations within the sample sets. Predominantly however, the taxiway dust samples have lower values <200 (10^{-6}) with the exception of C14 which has a higher value of 218.67 (10^{-6}). Much greater variability between high and low ratios is displayed in the apron dust samples with higher ratios >200 (10^{-6}) being evident at locations B2/43; B2/46; B2/47 and B4/51.

The lower reverse field ratio (IRM$_{-20mT}$/SIRM) for the taxiway dusts has a mean value of 0.52 ± 0.12 (range: 0.41 to 0.70) and for the apron dusts the mean value is 0.50 ± 0.13 (range: 0.20 to 0.65). The IRM$_{-100mT}$/SIRM ratio for the taxiway dusts has a mean value of -0.60 ± -0.11 (range: -0.84 to -0.49) and the apron dusts a mean value of -0.61 ± 0.20 (range: -0.81 to -0.07). The higher reverse field ratio (IRM$_{-300mT}$/SIRM) for the taxiway dusts has a mean value of -0.90 ± 0.06 (range: -1.00 to -0.82) and the apron dusts a mean value of -0.95 ± 0.03 (range: -1.00 to -0.91).

ii) *Magnetic Interpretation*

Throughout both the taxiway and apron areas magnetic mineral concentrations are high with the exception of a lower magnetic mineral concentration within the taxiway dusts at T1.2 (Figure 4.4).

Figure 4.5: χARM/χ of the dust samples collected from the taxiway and apron areas by site location.
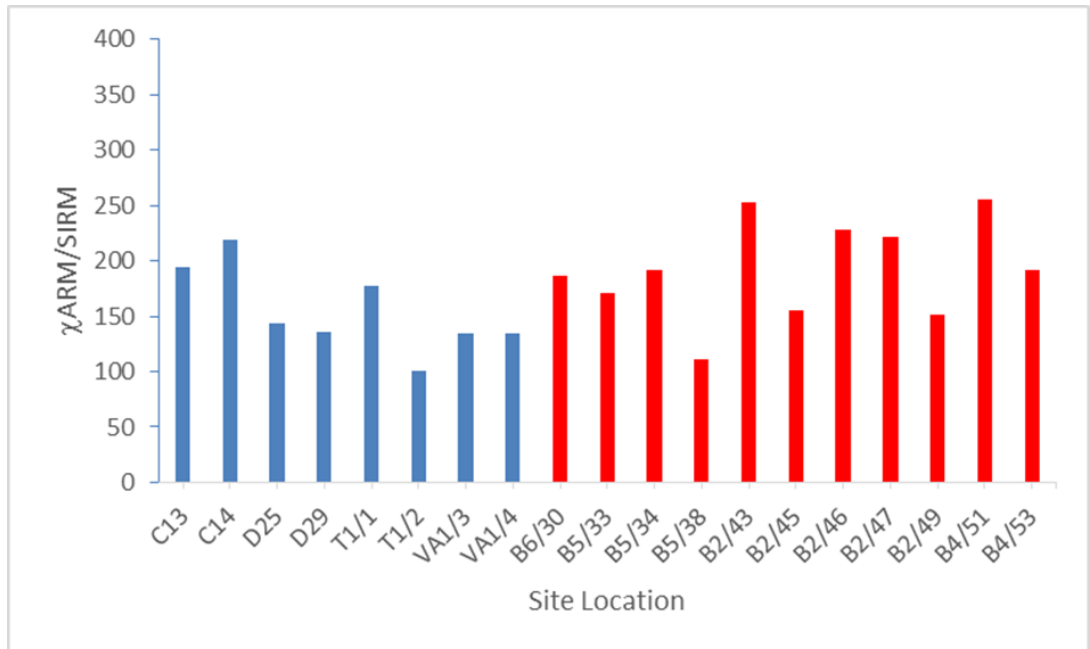
Figure 4.6: χARM/SIRM of the dust samples collected from the taxiway and apron areas by site location.

The variablitly within the χARM/χ and χARM/SIRM ratios indicates that there is some variability between coarser and finer ferrimagnetic mineral grain sizes within each of the sample sets. Both ratios indicate finer ferrimagnetic grain sizes which are particularly evident within the χARM/SIRM ratio in the taxiway sample collected at C14 and within the apron dusts at B2/43; B2/46; B2/47 and B4/51. Overall, however, values are in the lower range which indicates that both the taxiway and apron dusts are dominstaed by coarser ferrimagnetic mineral grain sizes.

The lower reverse field ratio (IRM$_{-20mT}$/SIRM) ranges from more positive to less positive ratios which indicate the presence of both fine and coarse grained ferrimagnetic mineral grain sizes within both sample sets . The less negative mean values displayed in the higher reverse field ratios (IRM$_{-100mT}$/SIRM and IRM$_{-300mT}$/SIRM) for both the taxiway and apron dusts suggests that both sample sets contain a significant antiferromagetic component. However, in relation to each sample set the range of IRM$_{-300mT}$/SIRM values extends to a more negative maximum value of -1.0 which indicates that the intial forward SIRM within these samples is completely reverse saturated (i.e. IRM$_{-300mT}$/SIRM = -1.0) and that both the taxiway and apron dusts also contain samples which are dominated by ferrimagnetic minerals. The wide range of values displayed in each sample set indicates that both the taxiway and apron dusts contain mixed assemblages containing both antiferromagnetic and ferrimagnetic minerals.

4.3 Environmental Grass Samples

4.3.1 Runway 23L/05R Grass Samples

i) Magnetic Description

A summary of the magnetic analyses which were completed on the grass samples collected alongside runway 23L/05R are presented in Table 4.4. Figure 4.7 displays the SIRM values for the runway grass samples. Three distinct phases are clearly illustrated. The first of these extends from the critical area to 475 m. Within this phase SIRM values can be seen to rise markedly within the

Critical Area (-200 m to 0 m) from 250.36 10^{-6}Am^{2}kg^{-1} at -190 m to 966.17 10^{-6}Am^{2}kg^{-1} at -5 m.

Table 4.3 Magnetic parameters for all taxiway and apron dusts

Magnetic parameters		Dusts: Taxiway ($n = 8$)	Dusts: Apron ($n = 11$)
SIRM 10^{-6}Am^{2}kg^{-1}	Range	7012.43 – 46516.32	35248.95 – 137733.27
	Mean ± 1SD	27225.00 ± 12723.00	68984.00 ± 34995.00
χARM/χ Am^{-1}	Range	22.97 to 54.29	21.75 to 47.12
	Mean ± 1SD	32.48 ± 11.28	34.31 ± 8.50
χARM/SIRM (10^{-6})	Range	101.00 to 218.70	111.70 to 255.70
	Mean ± 1SD	155.20 ± 38.40	192.60 ± 44.70
IRM$_{-20mT}$/SIRM	Range	0.41 to 0.70	0.20 to 0.65
	Mean ± 1SD	0.52 ± 0.12	0.50 ± 0.13
IRM$_{-100mT}$/SIRM	Range	-0.84 to -0.49	-0.81 to -0.07
	Mean ± 1SD	-0.60 ± -0.11	-0.61 ± 0.20
IRM$_{-300mT}$/SIRM	Range	-1.00 to -0.82	-1.00 to -0.91
	Mean ± 1SD	-0.90 ± 0.06	-0.95 ± 0.03

Between the runway threshold (0 m) and 475 m SIRM values remain relatively high but display an overall downward trend with SIRM values fluctuating between the lowest value of 414.00 10^{-6}Am^{2}kg^{-1} at 400 m and 867.41 10^{-6}Am^{2}kg^{-1} at 150 m. From 475 m SIRM values show a marked decrease to a minimum value of 112.21 10^{-6}Am^{2}kg^{-1} at 675 m. The second phase extends from 675 m to 1625 m with values fluctuating between the minimum value at 675 m to a maximum value of 286.12 10^{-6}Am^{2}kg^{-1}.at 1325 m. The third distinct phase, in which values remain relatively low, extends from 1925 m to the end of the transect with the exception of a slight increase to 190.25 10^{-6}Am^{2}kg^{-1} at 2575 m.

Figure 4.8 displays the reverse field ratio data for the grass samples. Within the Critical Area (-200 m to 0 m), the IRM$_{-20mT}$/SIRM and IRM$_{-100mT}$/SIRM ratios become increasingly positive with increasing distance towards the beginning of the runway threshold. From the start of the runway threshold up to 975 m the reverse field ratios show slight fluctuations from more positive to more negative values particularly in relation to the IRM$_{-20mT}$/SIRM ratios which range from a minimum of 0.74 at 300 m to 0.80 at 450 m and 525 m. From 575 m to 975 m the reverse field ratios remain relatively constant. From 975 m to the end of the transect ratios gradually become more negative. There are, however, occaional fluctuations to more positive values, particularly in the lowest reverse field ratio (IRM$_{-20mT}$/SIRM). Throughout the length of the transect the IRM$_{-300mT}$ ratio shows only slight variation and remains close to a ratio of 1.0 with ratios ranging from a minimum of -0.93 at -200 m to a maximum of -1.0 at -55 m; 400 m; 2025 m; 2725 m; 3025 m and 3075 m.

Interparametric ratios (χARM/χ and χARM/SIRM) are not available for the grass samples due to low sample mass and low magnetic mineral concentrations precluding the accurate measurement of χ and ARM.

Table 4.4: Summary of magnetic parameters for the grass samples collected alongside runway 23L/05R.

Magnetic parameters		Runway 23L/05R
SIRM $10^{-6}Am^2kg^{-1}$	Range	27.41 – 966.17
	Mean ± SD	255.85 ± 225.12
IRM$_{-20mT}$ /SIRM	Range	0.74 – 0.80
	Mean ± SD	0.77 ± 0.05
IRM$_{-100mT}$ /SIRM	Range	-0.63 – -0.40
	Mean ±SD	-0.54 ± 0.07
IRM$_{-300mT}$ /SIRM	Range	-1.00 - -0.93
	Mean ± SD	-0.97 ± 0.02
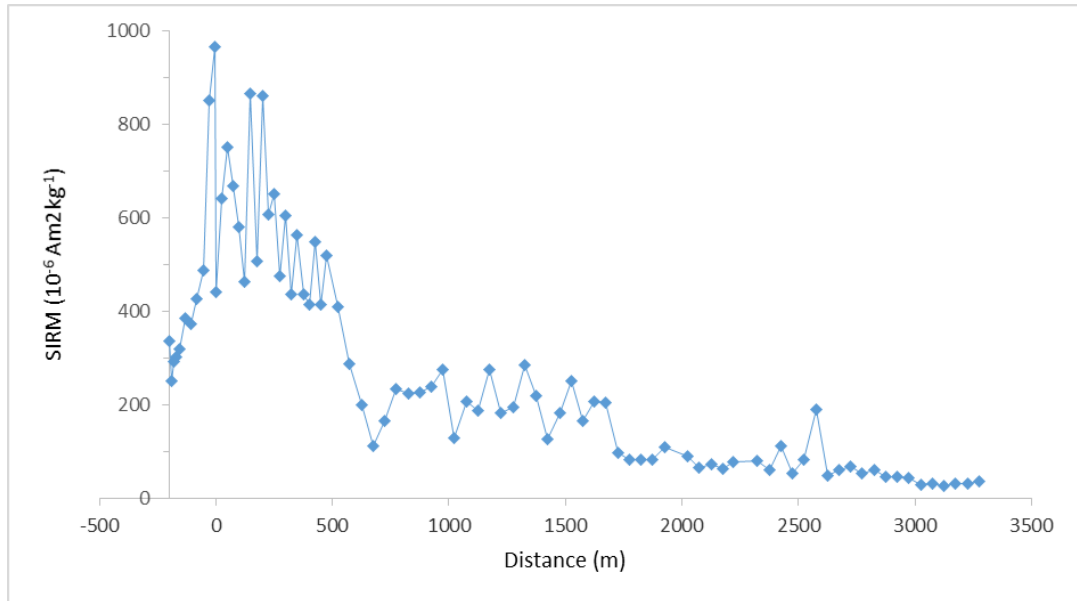
Figure 4.7: SIRM of the grass samples with distance along runway 23L/05R.
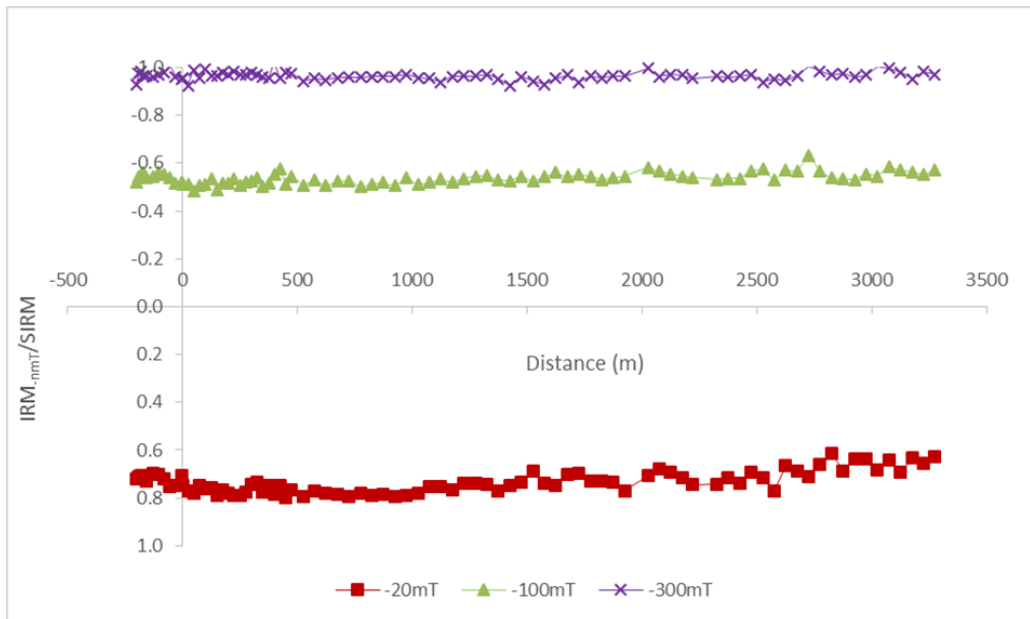
Figure 4.8: Reverse field ratios of the grass samples with distance along runway 23L/05R.

ii) *Magnetic interpretation*

The SIRM data display three distinctive phases (Figure 4.7). In the first of these phases which extends from the critical area to 475 m, magnetic mineral concentrations are high, rising to an exceptionally high level at the start of the runway threshold. From 475 m magnetic mineral concentrations decline abruptly to a zone of low concentrations between 675 m and 1625 m, and even lower concentrations from 1625 m to the end of the transect.

The fluctuations in the lower reverse field ratios, particularly in relation to the IRM$_{-20mT}$/SIRM reflect variations in ferrimagnetic mineral grain size. More positive ratios indicate finer ferrimagnetic mineral grain sizes and more negative ratios imply coarser ferrimagnetic mineral grain sizes. These results indicate that throughout the critical area and up to the start of the runway threshold (-200 m to 0 m) ferrimagnetic grain sizes become increasingly fine. The more positive ratios which extend from the runway threshold to 975 m are also indicative of finer grain sizes, although there are some fluctuations, to more negative ratios between 0 m and 975 m indicating a shift to coarser ferrimagnetic mineral grain sizes at these points. At 975 m to the end of the transect there is a gradual shift to generally coarser ferrimagnetic minerals although the occasional fluctuations to more positive ratios, suggest finer ferrimagnetic mineral grain sizes. The higher reverse field ratios (IRM$_{-100mT}$ and IRM$_{-300mT}$/SIRM remains close to a ratio of -1.0 throughout the entire transect and suggests that the magnetic record is dominated by ferrimagnetic minerals.

4.3.2 Apron and Taxiway Grass Samples

i)   *Magnetic description*

A summary of the magnetic analyses which were completed on the apron and taxiway grass samples is shown in Table 4.5. Figure 4.9 displays the SIRM values for the taxiway and apron grass areas in relation to the individual site numbers (Appendix 1). SIRM values for the grass samples collected in the areas adjacent to the taxiways are low and extremely variable ranging from the lowest value of 61.73 10^{-6}Am^{2}kg^{-1} at C8 to a maximum value of 730.51 10^{-6}Am^{2}kg^{-1} at D28. However, there is a notable increase to higher SIRM values of 327.40 10^{-}

$^6Am^2kg^{-1}$ at C4 and 380.92 $10^{-6}Am^2kg^{-1}$ at C3 respectively. Two significant peaks in SIRM are evident at C1 which displays a value of 713.60 $10^{-6}Am^2kg^{-1}$ and at D28 which has a value of 730.51 $10^{-6}Am^2kg^{-1}$.

The SIRM values for the grass samples in the apron areas are also low and there is much less variability between the samples which have a mean value of 106.50 $10^{-6}Am^2kg^{-1}$ ± 52.00 (range: 42.30 $10^{-6}Am^2kg^{-1}$ to 193.32 $10^{-6}Am^2kg^{-1}$). However, SIRM values are generally much lower than the values displayed in the taxiway grass samples. SIRM values range from the lowest value of 42.30 $10^{-6}Am^2kg^{-1}$ at B2/41 to the highest value of 193.32 $10^{-6}Am^2kg^{-1}$ at B.37. A slight increase in magnetic mineral concentratons is evident at B36 to 172.96 $10^{-6}Am^2kg^{-1}$ and at B37 to 193.32 $10^{-6}Am^2kg^{-1}$.

Table 4.5 displays the reverse field ratio data for the taxiway and apron grass samples. The IRM$_{-20mT}$/SIRM values for the taxiway grass samples have a mean of 0.68 ± 0.05 (range: 0.62 to 0.77) whilst the apron grass samples have a mean value of 0.60 ± 0.12 (range: 0.32 to 0.71). The IRM$_{-100mT}$/SIRM values for the taxiway samples display a mean value of -0.55 ± 0.06 (range: -0.60 to -0.39) and the apron grass samples a mean of -0.60 ± 0.04 (range: -0.70 to -0.56). The IRM$_{-300mT}$/SIRM values for the taxiway grass samples have a mean value of -0.93 ± 0.04 (range: -1.00 to -0.83) whilst the apron grass samples have a mean value of -0.97 ± 0.02 (range: -1.00 to -0.95).

ii)   Magnetic Interpretation

SIRM is indicative of the magnetic mineral concentration within a sample. Magnetic mineral concentrations within the grass samples collected from both the taxiway and apron are low. However, there is some variation between the two sample sets. Magnetic mineral concentrations within the taxiway areas are generally greater than those collected from the apron areas. An increase in magnetic mineral concentrations is apparent at C4 and C3. A further increase to much higher concentrations of magnetic minerals is evident at site numbers C1 and D28. There is much less variability in the concentration of magnetic minerals within the apron grass areas which remain low and constant throughout with the exception of a slight increase in magnetic mineral concentrations at locations B36 and B37.

The range of the lower reverse field ratio (IRM$_{-20mT}$/SIRM) fluctuates between more positive and more negative ratios which indicates the presence of both fine and coarse ferrimagnetic mineral grains sizes within the taxiway and apron grass samples. The less negative mean values shown in the higher reverse field ratios (IRM$_{-100mT}$/SIRM and IRM$_{-300mT}$/SIRM) indicates the presence of a significant antiferromagetic component. However, the range of values displayed within both sample sets also indicates that there is a presence of ferrimagnetic minerals within the sample sets. Moreover, the higher reverse field ratio (IRM$_{-300mT}$/SIRM) extends to a more negative maximum value of -1.0 which indicates that the intial forward SIRM within these samples is completely reverse saturated (i.e. IRM$_{-300mT}$/SIRM = -1.0) and therefore indicating that the taxiway and apron grass samples contain samples which are dominated by ferrimagnetic minerals. The wide range of values displayed in each sample set indicates that both the taxiway and apron grass samples contain mixed assemblages comprising a mixed assemblage of both antiferromagnetic and ferrimagnetic minerals. However, the taxiway grass samples display more less negative minimum values than the apron grass samples which suggests that the antiferromagnetic component is greatest within the taxiway samples.

Table 4.5: Summary of magnetic parameters
for the taxiway and apron grass samples.

Magnetic parameters		Taxiway ($n = 16$)	Apron ($n = 9$)
SIRM 10^{-6}Am^{2}kg^{-1}	Range	61.73 – 730.51	42.30 – 193.32
	Mean ± SD	219.60 ± 215.40	106.50 ± 52.00
IRM$_{-20mT}$ /SIRM	Range	0.62 – 0.77	0.32 – 0.71
	Mean ± SD	0.68 ± 0.05	0.60 ± 0.12
IRM$_{-100mT}$ /SIRM	Range	-0.60 to -0.39	-0.70 - -0.56
	Mean ±SD	-0.55 ± 0.06	-0.60 ± 0.04
IRM$_{-300mT}$ /SIRM	Range	-1.00 - -0.83	-1.00 - -0.95
	Mean ± SD	-0.93 ± 0.04	-0.97 ± 0.02
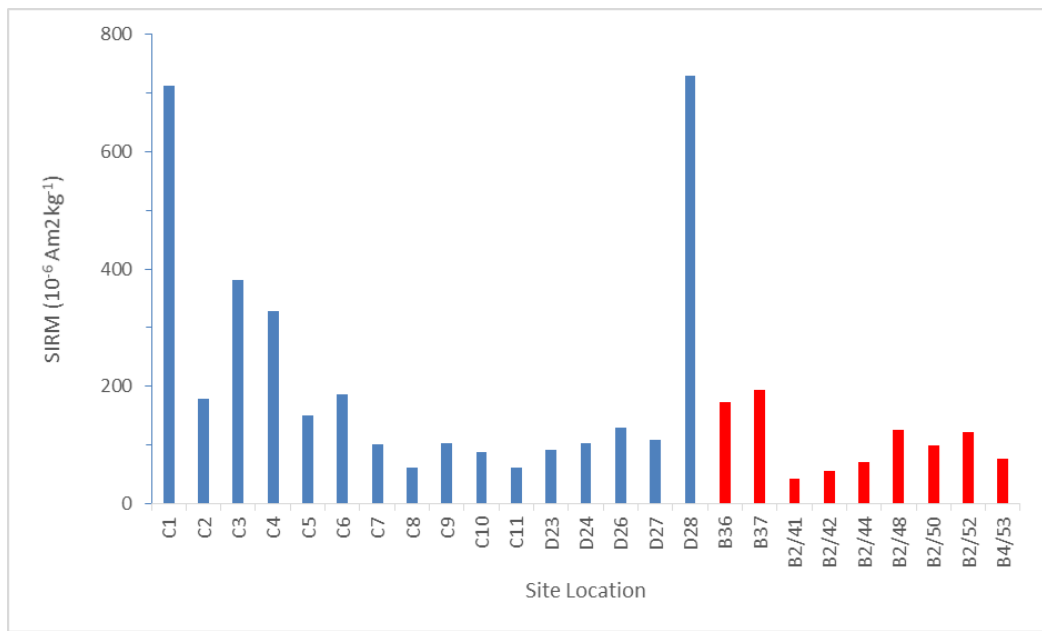
Figure 4.9: SIRM of the grass samples collected from the taxiway and apron areas by site location.
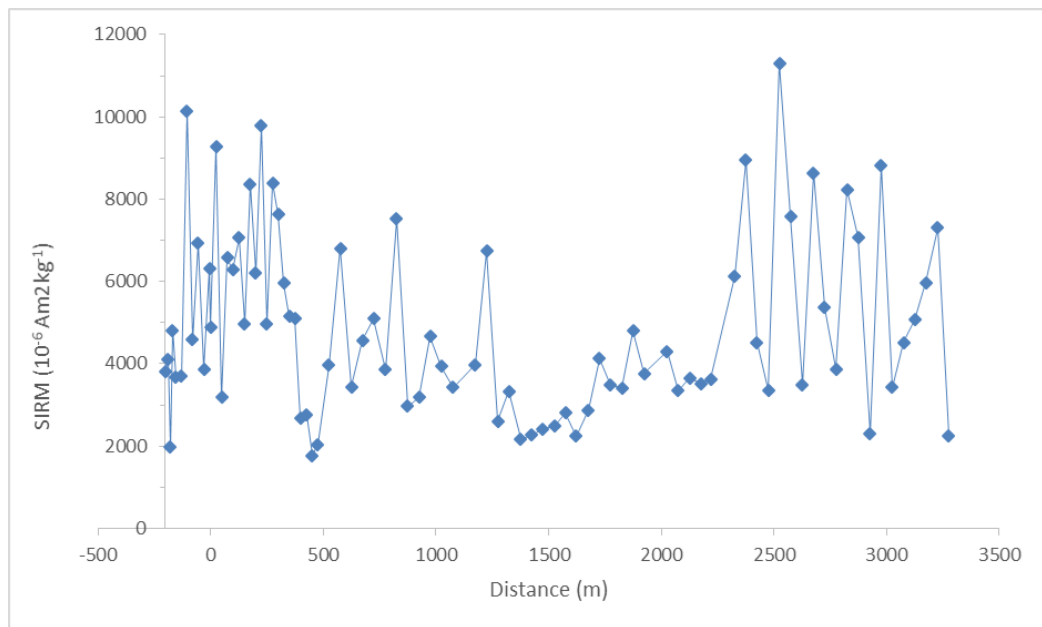
Figure 4.10: SIRM of the soil samples with distance along runway 23L/05R.

4.4 Environmental Soil Samples

4.4.1 Runway 23L/05R Soil Samples

i) Magnetic Description

A summary of the magnetic analyses completed on the soil samples collected alongside runway 23L/05R is presented in Table 4.6. Figure 4.10 displays the SIRM values for these samples. SIRM values within the critical area at -200 m to -105 m, display an upward trend with values ranging from a minimum of 1969.71 $10^{-6}Am^2kg^{-1}$ at -180 m to a maximum of 10142.70 $10^{-6}Am^2kg^{-1}$ at -105 m. SIRM values remain high within the remainder of the critical area and from the runway threshold up to 275m. Whilst there are some fluctuations in the values, the overall trend is an increase in SIRM. At 275 m values show a marked decrease to 1768.59 $10^{-6}Am^2kg^{-1}$ at 450 m. Between 450 m and 1225 m SIRM values fluctuate between lower values of 2032.85 $10^{-6}Am^2kg^{-1}$ at 475 m to higher values of 7522.91 $10^{-6}Am^2kg^{-1}$ at 825 m. SIRM values then decrease markedly to a very low value of 2174.41 $10^{-6}Am^2kg^{-1}$ at 1375 m. Between 1375 m and 2175 m SIRM values fluctuate but remain relatively low. There is, however, an overall but slight increase in SIRM to a maximum of 4793.78 $10^{-6}Am^2kg^{-1}$ at 1875 m. SIRM values begin to increase markedly at 2175 m to reach 8942.33 $10^{-6}Am^2kg^{-1}$ at 2375 m. Values appear extremely variable throughout the remainder of the transect and range from a minimum value of 2236.73 $10^{-6}Am^2kg^{-1}$ at 3275 m to a maximum value of 11309.28 $10^{-6}Am^2kg^{-1}$ at 2525 m.

Figure 4.11 displays the reverse field ratios for the soil samples. The lower reverse field ratio (IRM_{-20mT}/SIRM) gradually becomes more positive between -200 m and 625 m. Between 625 m and 2325 m, the ratios fluctuate, from sample to sample, between more positive and more negative ratios but overall there is little change. From 2325 m the ratios gradually become more negative. However, there is some distinct fluctuation between more positive and more negative ratios, especially between 2325 m and 2625 m.

In contrast, the higher reverse field ratios (-100$_{mT}$/SIRM and -300$_{mT}$/SIRM) become more negative between -200 m and 275 m, before a more positive shift between 275 m and 575 m.

Between 575 m and 2625 m, ratios fluctuate between more positive and more negative values, although this seems to be sample-to-sample variability rather than an obvious trend in the data. From 2625 m until the end of the transect, reverse field ratios are significantly more negative although fluctuations are still evident.

Table 4.6: Summary of the magnetic parameters for the soil samples collected alongside runway 23L/05R.

Magnetic parameters		Runway 23L/05R
SIRM 10^{-6}Am^{2}kg^{-1}	Range	1768.59 – 11309.28
	Mean ± SD	4886.05 ± 2190.43
χARM/χ Am^{-1}	Range	38.23 – 74.28
	Mean ± SD	51.27 ± 6.85
χARM/SIRM (10^{-6})	Range	152.30 – 395.86
	Mean ± SD	257.97± 47.81
IRM$_{-20mT}$ /SIRM	Range	0.41 – 0.74
	Mean ± SD	0.65 ± 0.06
IRM$_{-100mT}$ /SIRM	Range	-0.77 - -0.36
	Mean ±SD	-0.53 ± 0.07
IRM$_{-300mT}$ /SIRM	Range	-0.97 - -0.71
	Mean ± SD	-0.84 ± 0.05
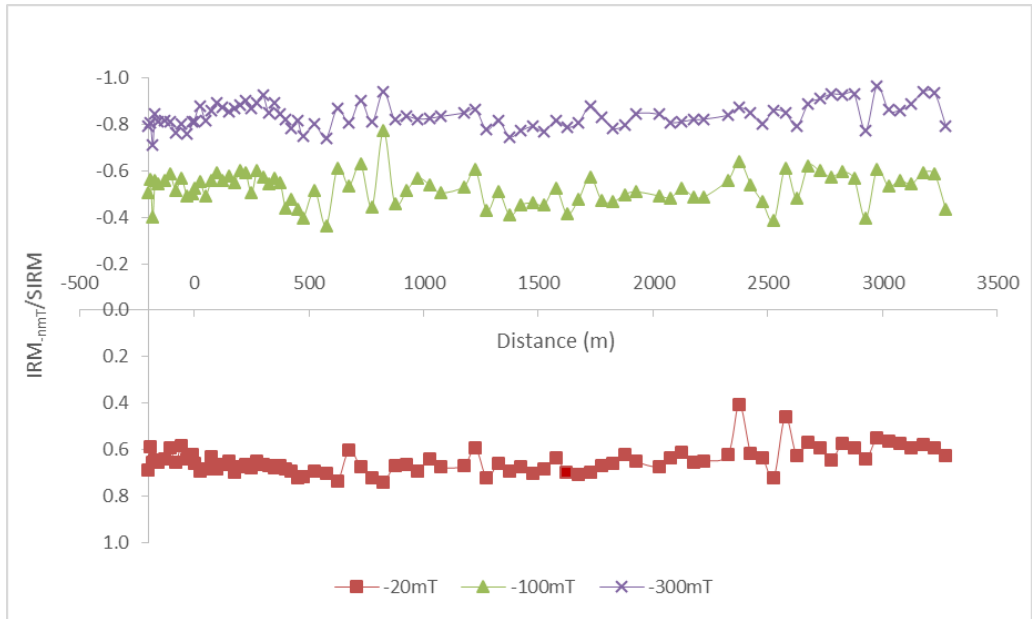
Figure 4.11: Reverse field ratios for the soil samples with distance along runway 23L/05R.
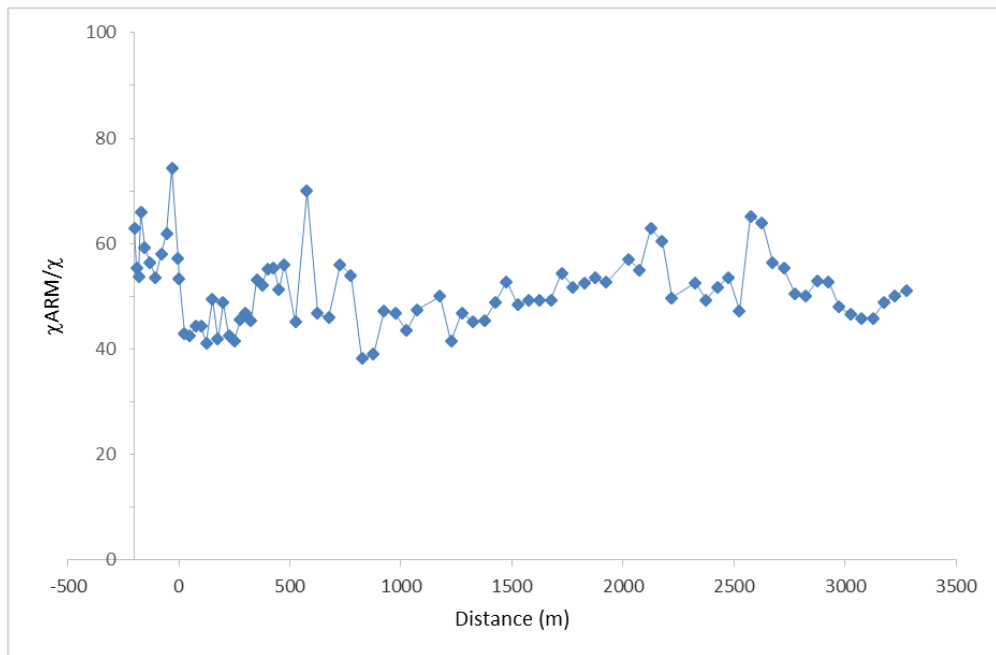
Figure 4.12: χARM/χ for the soil samples with distance along runway 23L/05R.

χARM/χ (Figure 4.12) and χARM/SIRM (Figure 4.13) ratios are generally high in the critical area (-200 m – 0 m) >53.56 Am^{-1} and 229.10 (10^{-6}) respectively but decrease significantly to a phase of predominantly low ratios which are particularly evident in the χARM/SIRM values from the start of the runway threshold and up to 250 m. The ratios then fluctuate between higher and lower values before they gradually increase up to higher values of 62.84 Am^{-1} and 326.33 (10^{-6}) at 2125 m. The overall trend between 275 m and 2125 m is however, towards higher values.   Between 2125 m and 2475 m the ratios continue to remain high before a change to a lower value which is particularly notable within the χARM/SIRM ratio which decreases to 152.30 (10^{-6}) at 2525 m. At 2575 m and 2625 m there is a significant shift towards high χARM/χ and χARM/SIRM ratios once again.   From 2675 m to the end of the transect values remain high but display an overall decline although there is some fluctuation between higher and lower values, which is particularly evident in the low χARM/SIRM value of 181.43 (10^{-6}) displayed at 2975 m.

ii)   Magnetic Interpretation

Magnetic mineral concentrations increase within the critical area, and remain high throughout this area and from the runway threshold up to 275 m. Between 275 m and 450 m there is a marked decrease in magnetic mineral concentration. Between 450 m and 1225 m magnetic mineral concentrations fluctuate between lower concentrations at 450 m and higher concentrations at 825 m. Concentrations remain relatively low between 1375 m and 2175 m but display a gradual increase towards 2175 m. Concentrations increase markedly between 2175 m and 2375 m however, concentrations throughout the remainder of the profile are very variable ranging from low concentrations at 3275 m to very high concentrations at 2525 m.

The variations within the lower reverse field ratio (IRM$_{-20mT}$/SIRM) between -200 m and 625 m; 625 m and 2325 m and 2325 m and 2625 m are indicative of shifts between finer and coarser ferrimagnetic grain sizes.   The results indicate that magnetic grain sizes become increasingly fine throughout the critical area (-200 m – 0 m) and from the runway threshold to 625 m. The fluctuation between more

positive and negative ratios between 625 m and 2325 m is indicative of variations between finer and coarser ferrimagnetic mineral grain sizes. At 2325 m the increasingly negative ratios indicate coarser grained ferrimagnetic grain sizes although there are some fluctuations to finer ferrimagnetic grain sizes and in particular between 2325 m and 2625 m.

The more negative IRM-$_{100mT}$ and IRM-$_{300mT}$/SIRM ratios within the critical area (-200 m – 0 m) and from the start of the runway threshold to 275 m indicate that the samples contain predominantly ferrimagnetic minerals together with a significant antiferromagnetic component. The more positive shift towards a -1.0 ratio between 275 m and 575 m suggests that the magnetic record between these points is dominated by ferrimagnetic minerals. Beyond this point and up to 2625 m a shift between samples dominated by ferrimagnetic minerals and those which contain a significant antiferromagnetic component occurs as evidenced by the fluctuation between more positive and more negative ratios. From 2625 m to the end of the transect the more negative ratios indicate that there is a significant antiferromagnetic component within the samples.

The high χARM/χ and χARM /SIRM ratios which are displayed within the critical area are indicative of finer ferrimagnetic mineral grain sizes. From the start of the runway threshold and up to 250 m there is a shift to predominantly coarser grained ferrimagnetic mineral grain sizes. Between 275 m and 2125 m ferrimagnetic mineral grain sizes become increasingly fine. There is a further shift to coarser ferrimagnetic grain sizes at 2525 m before a change to predominantly finer ferrimagnetic mineral grain sizes between 2675 m and the end of the transect with the exception of a shift to coarser ferrimagnetic mineral grain size at 2975 m.
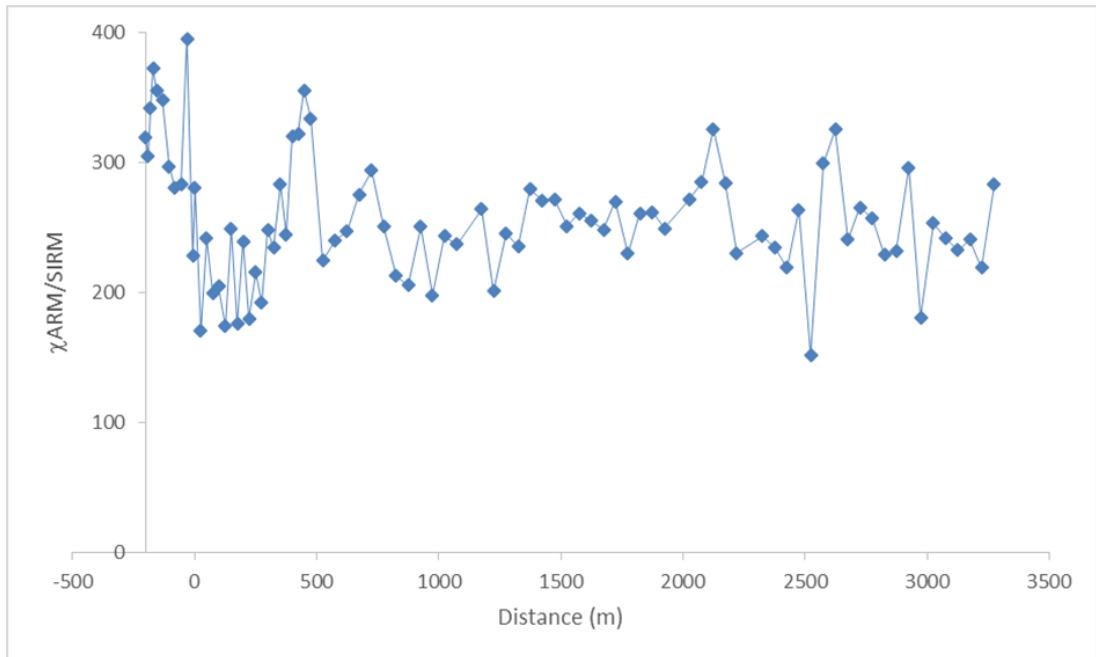
Figure 4.13: χARM/SIRM for the soil samples with distance along runway 23L/05R.
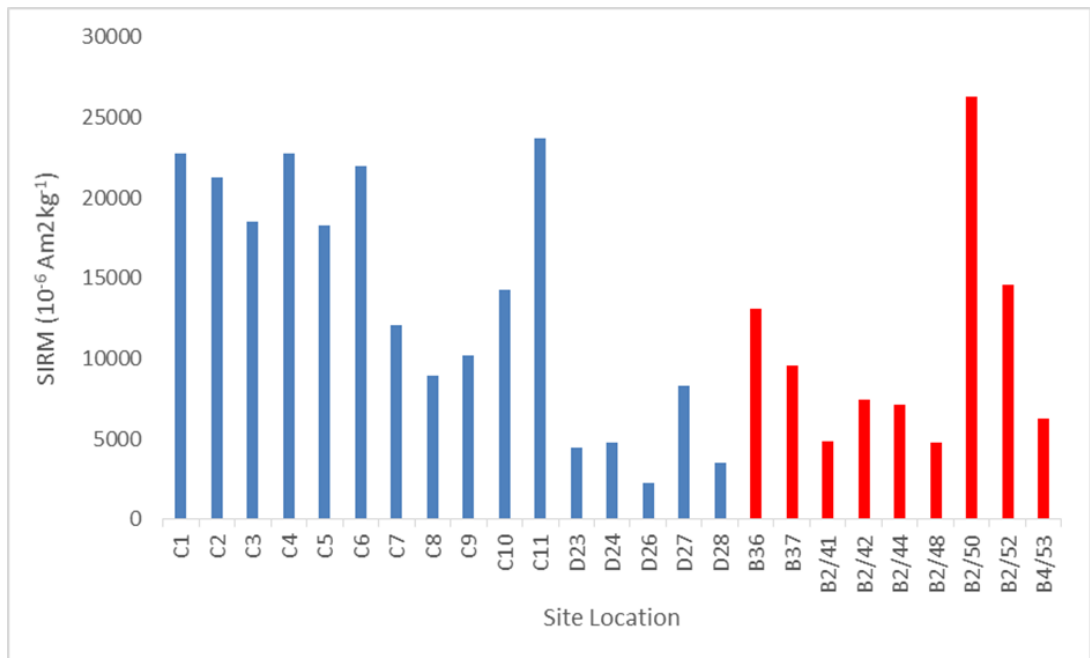
Figure 4.14: SIRM of the soil samples collected from the taxiway and apron areas by site location.

4.4.2 Apron and Taxiway Soil Samples

i)   *Magnetic Description*

Figure 4.14 displays the SIRM values for the taxiway and apron soil samples in relation to the individual site numbers (Appendix 1). SIRM values for the soil samples within both the taxiway and apron areas are extremely variable. SIRM values for the taxiway soil samples collected from Zone D are lower than those collected from Zone C. In Zone D values range from the lowest value of 2265.34 $10^{-6}Am^2kg^{-1}$ at D26 to the highest value of 8277.61 $10^{-6}Am^2kg^{-1}$ at D27. SIRM values within Zone C are higher ranging from 8918.73 $10^{-6}Am^2kg^{-1}$ at C8 to a very high value of 23726.71 $10^{-6}Am^2kg^{-1}$ at C11. The SIRM values of the soil samples collected within the apron areas are highly variable. The lowest value of 4873.58 $10^{-6}Am^2kg^{-1}$ is displayed at B2/41. There is a slight increase to higher SIRM values of 13063.37 $10^{-6}Am^2kg^{-1}$ at B36 and 14576.73 $10^{-6}Am^2kg^{-1}$ at B2.52. There is a significant increase in SIRM value to the highest value of 26274.02 $10^{-6}Am^2kg^{-1}$ at B2/50.

The $\chi ARM/\chi$ (Figure 4.15) and $\chi ARM/SIRM$ (Figure 4.16) ratios are generally very high for the soil samples collected from both the taxiway and apron areas. However, within each of the sample sets a small number of low $\chi ARM/\chi$ and $\chi ARM/SIRM$ ratios are also evident which are particularly prominent for the $\chi ARM/SIRM$ ratios. Within the taxiway samples low $\chi ARM/SIRM$ ratios are evident at sites C1, C2, D24 and D27. The low values within this area range from 158.54 (10^{-6}) at D27 to 193.43 (10^{-6}) at D24. The $\chi ARM/SIRM$ ratios for all other taxiway sites are high i.e. >200 (10^{-6}) with the highest ratio of 367.44 (10^{-6}) displayed at D26. Similarly, the majority of $\chi ARM/SIRM$ ratios for the apron dusts are also high. However, some low values occur at B2/52, B36 and B37. The low values within the apron samples range from 153.00 (10^{-6}) at B2/52 to 186.97 (10^{-6}) at B37. All other values are high >200 (10^{-6}) with very high values of 307.37 (10^{-6}) and 331.51 (10^{-6}) recorded at sites B4/53 and B2/42 respectively.

Table 4.5 summarises all of the results of the magnetic analyses completed on the soil samples collected from the taxiway and apron areas. The lower reverse

field ratios (IRM$_{-20mT}$/SIRM) for the taxiway soils display a mean value of 0.64 ± 0.06 (range: 0.56 to 0.74) and the apron soils a mean value of 0.60 ± 0.04 (range: 0.53 to 0.67). IRM$_{-100mT}$/SIRM ratios for the taxiway soil samples display a mean value of -0.63 ± 0.19 (range: -0.83 to -0.23), whereas the samples from Zone B have a mean value of -0.55 ± 0.05 (range: -0.66 to -0.49). The IRM$_{-300mT}$/SIRM ratios for the runway dust samples display a mean value of -0.86 ± 0.09 (range: -0.94 to -0.62), whilst the dust samples in Zone B have a mean value of -0.84 ± 0.05 (range: -0.90 to -0.76).

ii) Magnetic Interpretation

SIRM is indicative of the magnetic mineral concentration within a sample. Magnetic mineral concentrations within the soil samples collected from both the taxiway and apron areas are extremely variable. The soil samples collected from Zone D generally display much lower magnetic mineral concentrations than the samples collected from Zone C, with the exception of a marked increase in concentration at D27. Magnetic mineral concentrations within Zone C are high with the highest concentration being recorded at C11. The concentration of magnetic minerals within the soils collected from the apron areas, as for the taxiway areas, are also highly variable. Lower magnetic mineral concentrations are evident at B2/41. An increase in magnetic mineral concentration is shown in locations B36, B37 with a marked increase to very high magnetic mineral concentrations at B2/50.

The generally high χARM/χ and χARM /SIRM ratios exhibited by both the taxiway and apron soil samples indicate that each sample set is dominated by finer ferrimagnetic grain sizes which become increasingly fine within the taxiway samples at D26 and the apron samples at B4/53 and B2/42. The lower χARM /SIRM ratios which are evident in the taxiway samples at C1, C2, D24 and D27 and within the apron samples at B2/52, B36 and B37 are indicative of coarser ferrimagnetic mineral grain sizes at these points.

The more postitive IRM$_{-20mT}$/SIRM ratios displayed in both sample sets suggest the dominance of finer ferrimagnetic mineral grain sizes. However, the range of values also extends to less positive values which indicates that there is also a

presence of coarser ferrimagnetic mineral grain sizes within the sample sets and which further support the findings of the interparametric ratios (χARM/χ and χARM /SIRM) as described above.

The less negative higher reverse field ratios (IRM$_{-100mT}$/SIRM and IRM$_{-300mT}$/SIRM) displayed in both sample sets suggests that there is a significant antiferromagnetic component within both the taxiway and apron soil samples.

Table 4.7: Summary of magnetic parameters for the taxiway and apron soil samples.

Magnetic parameters		Taxiway ($n = 16$)	Apron ($n = 9$)
SIRM 10^{-6}Am^{2}kg^{-1}	Range	2265.34 - 23726.71	4873.58 - 26274.02
	Mean ± SD	13637 ± 7754	10429.71 ± 6860
χARM/χ Am^{-1}	Range	35.83 - 80.20	38.07 - 78.08
	Mean ± SD	57.34 ± 11.67	52.28 ± 14.64
χARM/SIRM (10^{-6})	Range	158.54 - 367.44	153.00 - 331.51
	Mean ± SD	240.99 ± 52.10	229.75 ± 60.50
IRM$_{-20mT}$ /SIRM	Range	0.56 - 0.74	0.53 - 0.67
	Mean ± SD	0.64 ± 0.06	0.60 ± 0.04
IRM$_{-100mT}$ /SIRM	Range	-0.83 - -0.23	-0.66 - -0.49
	Mean ±SD	-0.63 ± 0.19	-0.55 ± 0.05
IRM$_{-300mT}$ /SIRM	Range	-0.94 - -0.62	-0.90 - -0.76
	Mean ± SD	-0.86 ± 0.09	-0.84 ± 0.05
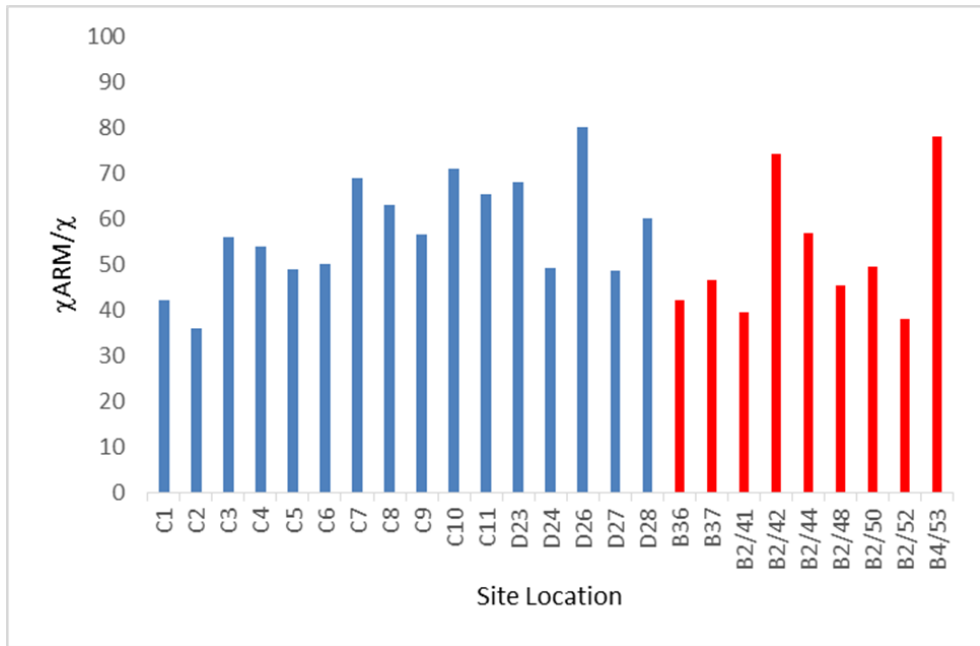
Figure 4.15: χARM/χ of the soil samples collected from the taxiway and apron areas by site location.
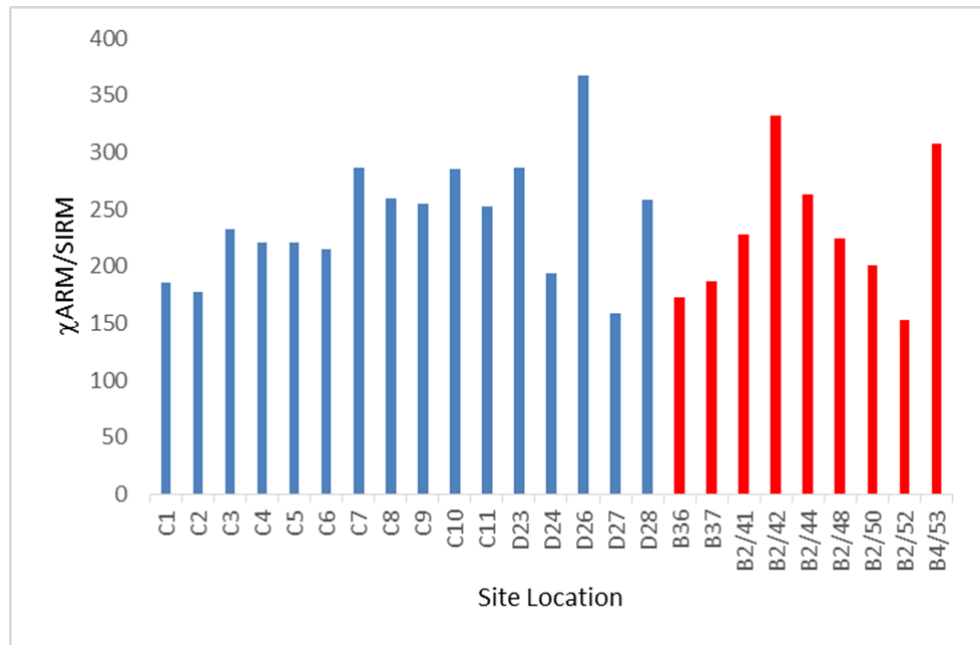
Figure 4.16: χARM/SIRM of the soil samples collected from the taxiway and apron areas by site location.

Chapter 5

Results: Chemical Analysis

Chapter 5, sections 5.1 to 5.4 includes a description of the chemical analysis results for the aircraft source and environmental samples.   The main elemental metallic composition of each of the aircraft source (i.e. engines, brakes and tyres), environmental dust samples (i.e. runway, taxiway and apron) and grass and soil samples is presented.   The remaining weight is made up principally of Carbon with other trace metals (§ 6.1).

5.1 Aircraft Source Samples

The chemical analysis results for the aircraft source dust samples (i.e. engines; brakes and tyres) including the mean value (± 1SD) and range is presented in Table 5.1 and Figure 5.1.   The mean concentrations are referred to throughout this section.

Very similar concentrations of Ti are shown in both the brake and tyre dust samples of 10.91 (g kg^{-1}) and 10.13 (g kg^{-1}) respectively in contrast to the engine samples which display a much lower concentration of 2.38 (g kg^{-1}). The Cr content of 25.10 (g kg^{-1}) displayed in the engine dusts samples is notably higher than the lower concentrations <7.80 (g kg^{-1}) for the brake and tyre dusts. There is much greater variability in Fe concentrations between each sample set. The lowest value of 11.80 (g kg^{-1}) is seen in the engine dust samples whilst a higher concentration of 137.21 (g kg^{-1}) is displayed within the brake dusts. Low Ni concentrations are displayed in both the brake and tyre dust samples of 0.90 (g kg^{-1}) and 0.14 (g kg^{-1}) respectively in comparison to the engine dusts which show a higher value of 23.74 (g kg^{-1}). Cu content is very low for the engine dust samples (0.40 (g kg^{-1})). Cu concentrations increase to 3.36 (g kg^{-1}) for the brake dusts and 14.11 (g kg^{-1}) for the tyre dusts. Similarly, the Zn values are lowest in the engine dust samples (0.17 (g kg^{-1})) whilst the brake dust samples show a higher concentration of 17.85 (g kg^{-1}). However, the tyre dusts display the largest concentration of all the aircraft source samples of 65.21 (g kg^{-1}). Pb content in

each of the sample sets ranges from 0.86 (g kg^{-1}) in the engine dusts to a minima of 0.05 (g kg^{-1}) for the brake dusts. Similar Al values are shown in both the engine and brake dust samples of 12.98 (g kg^{-1}) and 14.46 (g kg^{-1}) respectively. An increase to a higher Al content of 22.00 (g kg^{-1}) is displayed in the tyre dust samples.
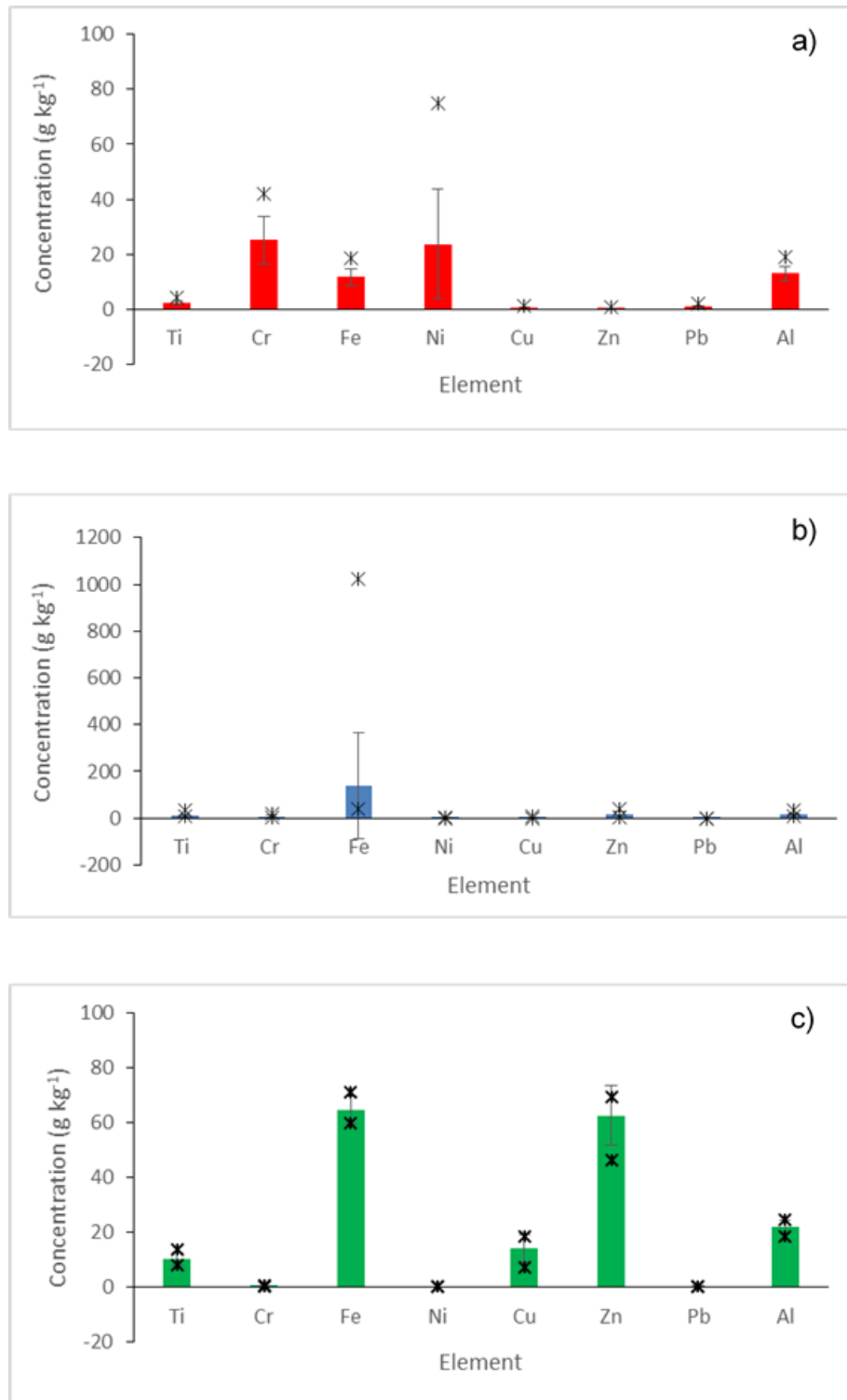
Figure 5.1: Mean elemental concentrations (g kg^{-1}) including error bars and minimum/ maximum data for the direct source dust samples: a) engine (n = 13), brake (n = 16), tyre dusts (n = 4).

Table 5.1: Summary of elemental concentrations (g kg^{-1}) for the aircraft source dust samples (i.e. engines, brakes and

Element		Brake (*n* = 16)	Engine (*n* = 13)	Tyre (*n* = 4)
Ti	Range	6.20 – 26.70	1.52 – 4.39	7.96 – 13.63
	Mean ± SD	10.91 ± 5.39	2.38 ± 0.77	10.13 ± 2.44
Cr	Range	1.12 – 17.58	10.49 – 42.17	0.06 – 0.07
	Mean ± SD	7.80 ± 6.11	25.10 ± 8.47	0.06 ± 0.01
Fe	Range	40.10 – 981.00	7.10 – 18.40	59.70 – 71.10
	Mean ±SD	137.21 ± 225.86	11.80 ± 3.00	64.63 ± 5.03
Ni	Range	0.38 – 2.15	6.35 – 75.09	0.10 – 0.18
	Mean ± SD	0.90 ± 0.55	23.74 ± 19.87	0.14 ± 0.04
Cu	Range	0.89 – 10.12	0.00 – 1.10	7.29 – 18.48
	Mean ± SD	3.36 ± 2.08	0.40 ± 0.43	14.11 ± 5.06
Zn	Range	5.07 – 31.94	0.0 – 0.62	46.36 – 69.29
	Mean ± SD	17.85 ± 8.88	0.17 ± 0.19	62.51 ± 10.85
Pb	Range	0.00 – 0.20	0.17 – 1.91	0.28 – 0.40
	Mean ± SD	0.05 ± 0.06	0.86 ± 0.50	0.33 ± 0.05
Al	Range	10.20 – 23.50	9.90 – 19.20	18.70 – 24.60
	Mean ± SD	14.46 ± 3.41	12.98 ± 2.48	22.00 ± 2.50

5.2 Environmental Dust Samples

5.2.1 Runway Dusts

The chemical analysis results for the environmental runway dust samples collected from runway 23L/05R (§ 3.3.4) are presented in Figures 5.2 a and 5.2b. The mean value (± 1SD) and range is presented in Table 5.2. There is a clear distinction between the Ti concentrations in each of the runway Zones (§ 3.3.4) (Figure 5.2 a). Ti content in Zone A remains fairly constant ranging from 1.93 (g kg^{-1}) at 600 m to 3.44 (g kg^{-1}) at 725 m. In contrast to this the Ti concentrations in Zone B are notably higher and show much greater variability. Lower Ti values of 4.22 (g kg^{-1}) and 3.77 (g kg^{-1}) are displayed at 2375 m and 2500 m respectively. Concentrations then increase significantly to higher values of 8.23 (g kg^{-1}) at 2600 m and 8.31 (g kg^{-1}) at 2700 m. There is a slight decrease to 5.68 (g kg^{-1}) at 2800 m. Ti content then remains fairly constant throughout the remainder of Zone B with the exception of a slight decrease to 4.82 (g kg^{-1}) at 3000 m.

A clear distinction is evident between the Cr content in Zone A and Zone B with Zone B displaying greater concentrations (Figure 5.2 a). Cr content within Zone A remains low and constant between 400 m and 700 m ranging from 0.07 (g kg^{-1}) at 575 m to 0.09 (g kg^{-1}) at 500 m. A slight increase in concentration is evident at 725 m to 0.17 (g kg^{-1}). Cr values within Zone B are higher and show much greater variability than those in Zone A. There is a slight decrease in concentration between 0.25 (g kg^{-1}) at 2375 m to 0.16 (g kg^{-1}) at 2500 m. Concentrations then increase to 0.47 (g kg^{-1}) at 2600 m. There is a slight fluctuation in Cr content between 2600 m and 2900 m, however, concentrations remain fairly constant throughout this section before decreasing to a lower value of 0.21 (g kg^{-1}) at 3000 m.

Fe content (Figure 5.2 a) in Zone A is lower than in Zone B. Within Zone A, Fe concentration decreases from 33.62 (g kg^{-1}) at 400 m to lower values <19.00 (g kg^{-1}) between 500 m and 700m with a minima of 13.70 (g kg^{-1}) at 575 m. Concentrations increase again to 32.50 (g kg^{-1}) at 725 m. At the beginning of Zone B, Fe content is similar to Zone A, however, at 2600 m there is an increase to the highest level in Zone B of 81.10 (g kg^{-1}) at 2600 m. Values then remain high to 2900 m before a slight decrease to 44.10 (g kg^{-1}) at 3000 m.

94
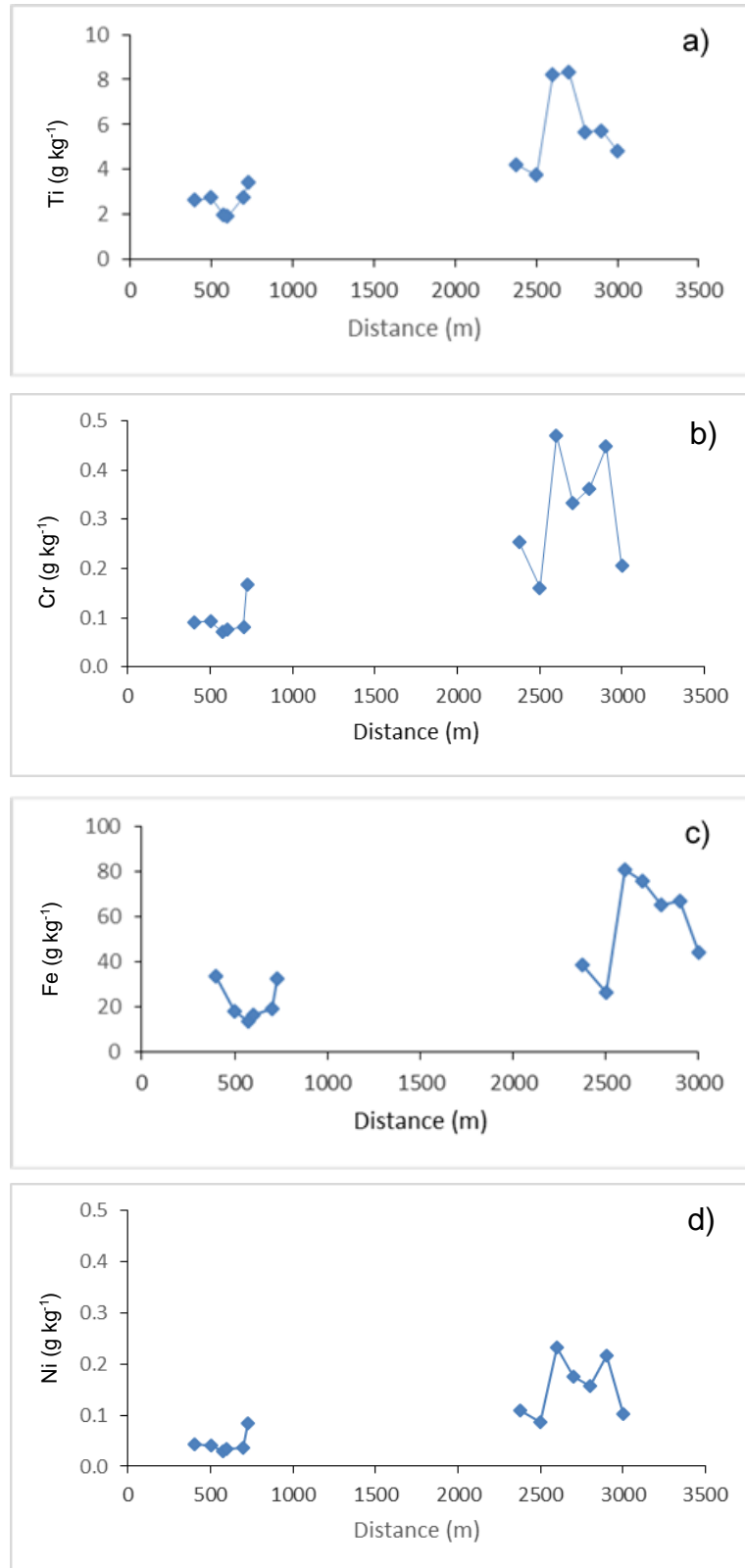
Figure 5.2a: Ti; Cr; Fe and Ni concentrations (g kg^{-1}) for the runway dusts with distance along runway 23L/05R a) Ti, b) Cr, c) Fe; d) Ni. Zone A: 400 m – 725 m; Zone B: 2375 m – 3000m.
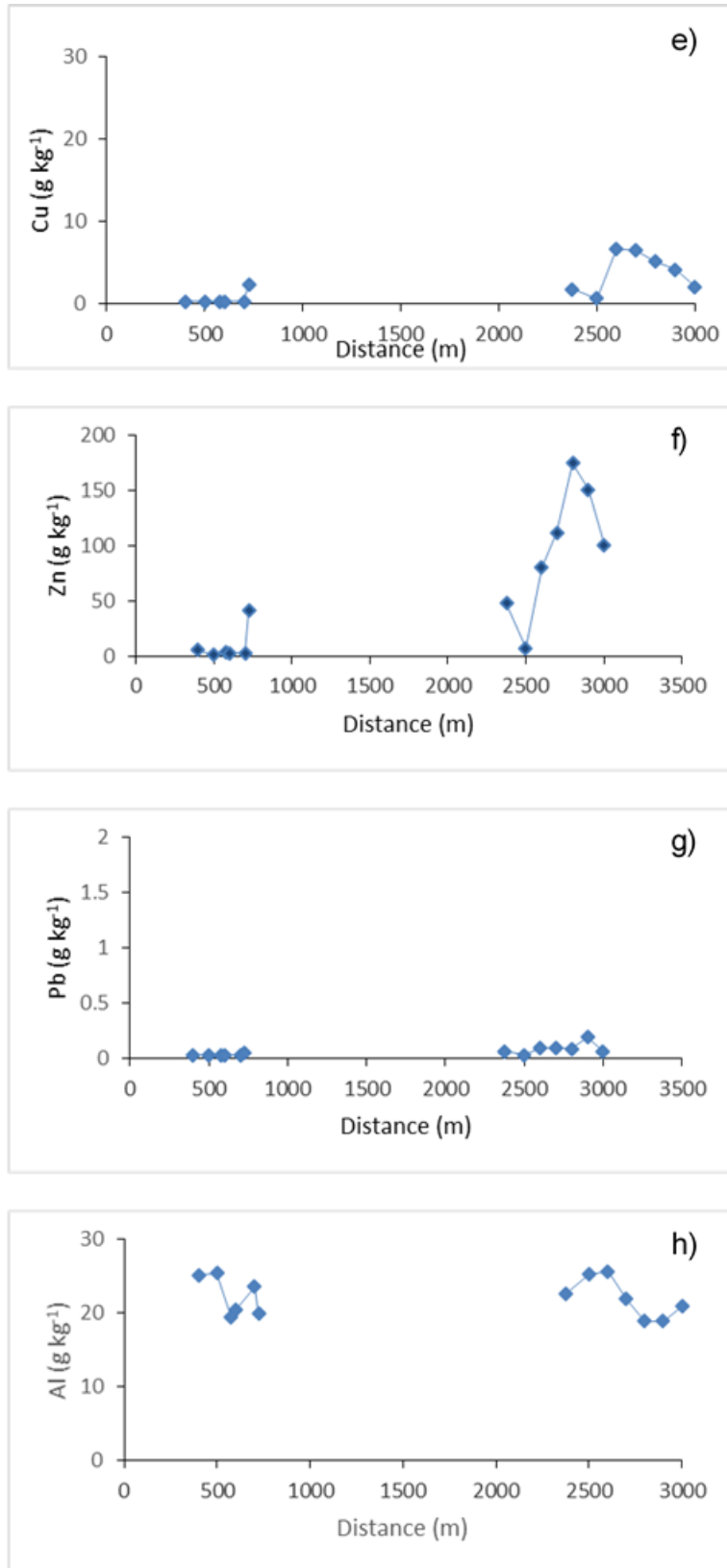
Figure 5.2b: Cu; Zn; Pb and Al concentrations (g kg^{-1}) for the runway dusts with distance along runway 23L/05R e) Cu; f) Zn; g) Pb; h) Al.

Table 5.2: Summary of elemental concentrations (g kg^{-1}) for the runway dusts with distance along runway 23L/05R (Zone A: 400 m – 725 m; Zone B: 2375 m – 3000m).

Element		Zone A (Take-off) (*n* = 6)	Zone B (Landing) (*n* = 7)
Ti	Range	1.93 – 3.44	3.77 – 8.31
	Mean ± SD	2.59 ± 0.56	5.83 ± 1.82
Cr	Range	0.07 – 0.17	0.16 – 0.47
	Mean ± SD	0.10 ± 0.04	0.32 ± 0.12
Fe	Range	13.70 – 33.62	26.60 – 81.10
	Mean ±SD	22.25 ± 8.57	57.01 ± 20.61
Ni	Range	0.03 – 0.09	0.09 – 0.23
	Mean ± SD	0.05 ± 0.02	0.15 ± 0.06
Cu	Range	0.31 – 2.36	0.68 – 6.72
	Mean ± SD	0.67 ± 0.83	3.87 ± 2.39
Zn	Range	1.68 – 41.43	7.38 – 175.12
	Mean ± SD	9.78 ± 15.56	64.64 ± 5.76
Pb	Range	0.03 – 0.05	0.03 – 0.19
	Mean ± SD	0.03 ± 0.01	0.09 ± 0.05
Al	Range	19.40 – 25.40	18.90 – 25.70
	Mean ± SD	22.34 ± 2.73	22.03 ± 2.75

Ni concentrations (Figure 5.2 a) within Zone A are low ranging from the lowest value of 0.03 (g kg^{-1}) at 575 m to 0.09 (g kg^{-1}) at 725 m. At the start of Zone B (2375 m to 2500 m), Ni content remains similar to the values displayed in Zone A, however, there is a slight increase in concentration to 0.23 (g kg^{-1}) at 2600 m. Ni content remains fairly constant between 2600 m and 2900 m though there is some variation between slightly lower and higher values before a decrease to 0.10 (g kg^{-1}) at 3000 m.

Overall, the Cu concentrations (Figure 5.2 b) in Zone A are lower than those in Zone B. A very low range of values is displayed between 400 m and 700 m in Zone A which range from 0.31 (g kg^{-1}) at 700 m to 0.35 (g kg^{-1}) at 575 m. There

is however, an increase in Cu concentration at 725 m to 2.36 (g kg^{-1}). Cu content within Zone B is generally higher than in Zone A, however, there is some variability. There is a decrease in Cu values between 2375 m and 2500 m from 1.77 (g kg^{-1}) to 0.68 (g kg^{-1}) before an increase to the highest concentration of Cu of 6.72 (g kg^{-1}) at 2600 m. Values remain higher within Zone B although there is a gradual decrease in concentration between 2600 m to 4.22 (g kg^{-1}) at 2900 m and a marked decrease to 2.12 (g kg-^{1}) at 3000 m.

For Zn (Figure 5.2 b) concentrations are considerably lower in Zone A in comparison to Zone B. Lower levels <5.81(g kg^{-1}) are observed in Zone A between 400 m and 700m. However, there is an increase to a higher concentration of 41.43 (g kg^{-1}) at 725 m. There is a further increase in Zn content at the start of Zone B to 48.30 (g kg^{-1}) at 2375 m before a notable decrease to 7.38 (g kg^{-1}) at 2500 m. Between 2600 m and 2800 m Zn there is a progressive increase in concentration from 80.60 (g kg^{-1}) to 175.12 (g kg^{-1}). Values remain high in comparison to Zone A but begin to decrease with distance along the runway to 100.77 (g kg^{-1}) at 3000 m.

There is much less variability in Pb concentration between Zones A and B (Figure 5.2 b) than is displayed by other elements. Overall however, concentrations in Zone A are lower than those in Zone B. Pb content is very low between 400 m and 725 m ranging from 0.03 (g kg^{-1}) at 575 m to 0.05 (g kg-^{1}) at 725 m. There is an overall increase in concentrations within Zone B from 0.07 (g kg^{-1}) at 2385 m to 0.19 (g kg^{-1}) at 2900 m. A decrease in concentration is evident to lower levels of 0.03 (g kg^{-1}) at 2500 m and 0.06 (g kg^{-1}) at 3000 m respectively.

Al concentration (Figure 5.2 b) within the two Zones display a very similar range, although the values within each Zone are extremely variable. In Zone A, Al content is higher at the beginning of the Zone with a value of 25.22 (g kg^{-1}) being displayed at 400 m. There is a very slight increase to 25.40 (g kg^{-1}) followed by a decrease to 19.40 (g kg^{-1}) at 575 m. Concentrations increase once again to 23.60 (g kg^{-1}) at 700m before decreasing to 19.90 (g kg^{-1}) at 725 m. In Zone B, Al content steadily increases between 2375 m and 2600 m from 22.60 (g kg^{-1}) to 25.70 (g kg^{-1}) respectively. Concentrations then decrease to 18.90 (g kg^{-1}) at 2900 m before a slight increase to 20.90 (g kg^{-1}) at 3000 m.

5.2.2 Taxiway and Apron Dusts

Elemental concentrations for the taxiway and apron dusts are displayed in Figures 5.3a and 5.3b. The mean value (± 1SD) and range is presented in Table 5.3. The Ti (g kg^{-1}) values are shown in Figure 5.3a. Ti content within the taxiway samples ranges from 3.19 (g kg^{-1}) at T1/2 to 6.36 (g kg^{-1}) at D29. There is little variability in the concentrations displayed within the samples in areas C; T1 and VA. An increase in Ti concentration is, however, evident in area D which displays an increase to 5.71 (g kg^{-1}) at D25 and a further increase to the highest value of 6.36 (g kg^{-1}) at D29. In contrast to this the apron dust samples generally display higher concentrations than the taxiway dusts. A lower value, similar to those seen in the taxiway dusts of 4.94 (g kg^{-1}) is displayed at B6/30. However, higher concentrations are displayed in all other apron dust samples which range from 5.63 (g kg^{-1}) at B2/47 to the highest level of 8.07 (g kg^{-1}) at B5/34.

Cr concentrations (Figure 5.3a) are lower in the taxiway dust samples. A very low Cr content of 0.06 (g kg^{-1}) is displayed at T1/2. A slight increase in concentration is evident in the samples collected at C14; T1/1; VA1/3 and D25 which increase to 0.24 (g kg^{-1}) at C14. There is an increase to 0.29 (g kg^{-1}) at C13 and a further increase to the highest level seen within the taxiway dust samples of 0.31 (g kg^{-1}) at D29. The apron dust samples display much higher concentrations which range from 0.23 (g kg^{-1}) at B2/46 to 0.44 (g kg^{-1}) at B6/30.

Fe concentration (Figure 5.3a) is high throughout the taxiway and apron dusts. Within the taxiway dust samples the lowest value of 20.80 (g kg^{-1}) is displayed at T1/2. A notable increase in Fe content occurs within Zone D to 46.10 (g kg^{-1}) at D25 and the highest concentration of 59.20 (g kg^{-1}) at D29. Overall, the apron dusts display much higher values which range from 61.30 (g kg^{-1}) to 96.20 (g kg^{-1}) at B5/34.

The Ni content (Figure 5.3a) within both sample sets is very low <0.24 (g kg^{-1}). Overall, however, the taxiway samples display the lowest concentrations which range from 0.04 (g kg^{-1}) at T1/2 to 0.13 (g kg^{-1}) at D29. Concentrations within the apron dust samples are generally higher and show much greater variability with

evident peaks in concentration at B4/53; B2/47 and B6/30 to 0.18 (g kg^{-1}); 0.21 (g kg^{-1}) and 0.24 (g kg^{-1}) respectively.
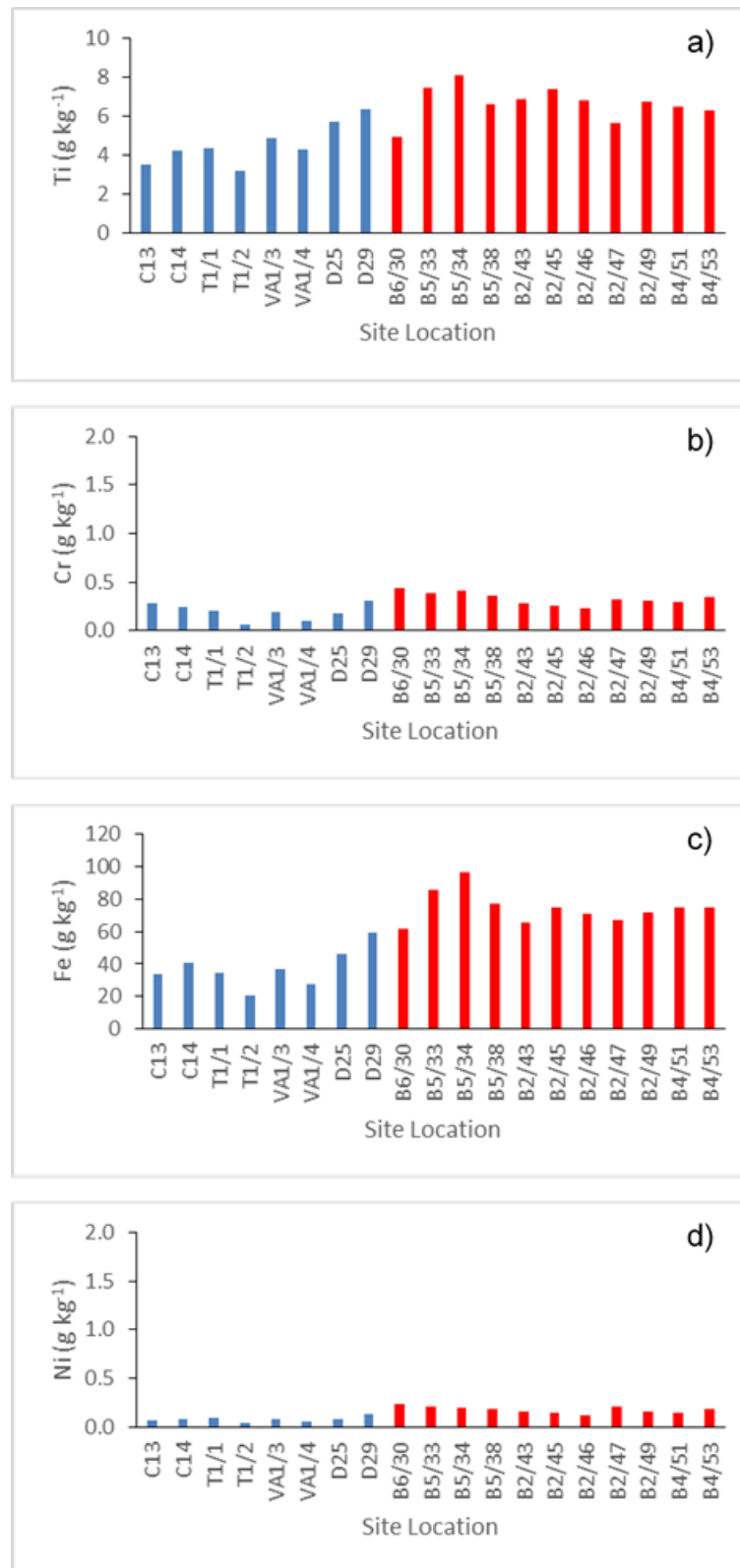
Figure 5.3a: Ti; Cr; Fe and Ni concentrations (g kg^{-1}) for the taxiway and apron dusts a) Ti; b) Cr; c) Fe; d) Ni.
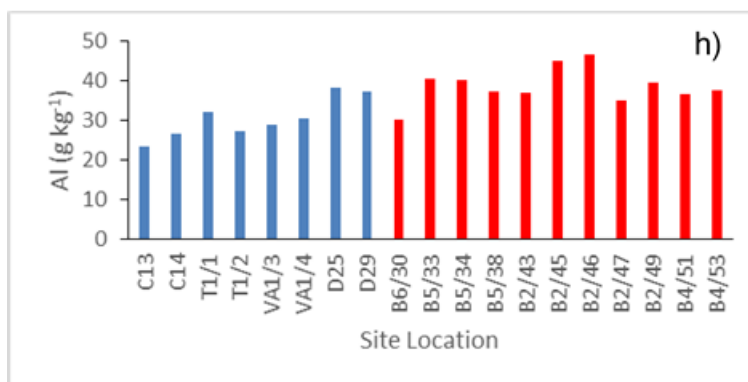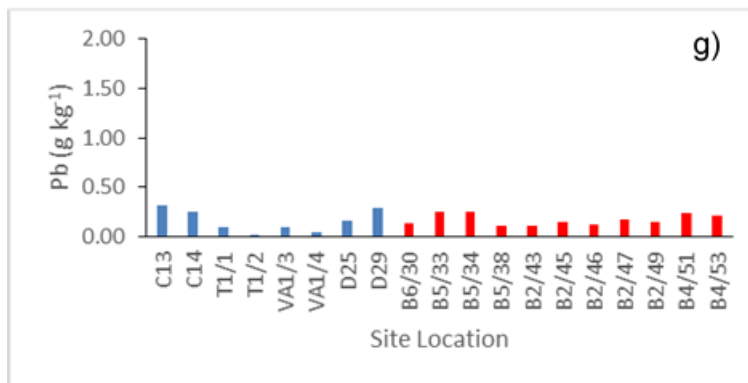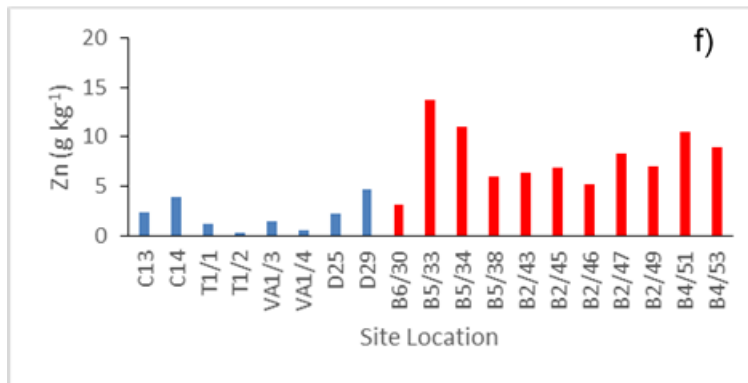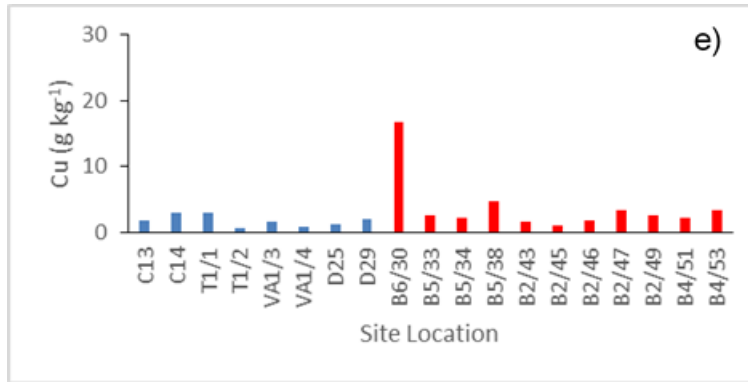
Table 5.3b: Cu; Zn; Pb and Al concentrations (g kg^{-1}) for the taxiway and apron dusts e) Cu, f) Zn, g) Pb, h) Al.

The Cu content (Figure 5.3b) is extremely variable. Within the taxiway dusts lower concentrations <1.00 (g kg^{-1}) are evident at T1/2 and VA1/4. However, there is an increase to 3.01 (g kg^{-1}) at C14 and to 3.05 (g kg^{-1}) at T1/1. Overall, however, Cu concentration is higher within the apron dusts although lower values of 1.09 (g kg^{-1}) and 1.67 (g kg^{-1}) are evident at B2/45 and B2/43 respectively. An increase to 4.67 (g kg^{-1}) is seen at B5/38 and a further increase to the highest concentration of 16.68 (g kg^{-1}) at B6/30.

Zn content (Figure 5.3b) within both the taxiway and apron sample sets is extremely variable. Much lower concentrations are evident within the taxiway dusts at T1/2 and VA1/4 of 0.32 (g kg^{-1}) and 0.57 (g kg^{-1}) respectively. However, there is an increase to a higher concentration of 2.36 (g kg^{-1}) at C13 and further increases at C14 and D29 to 3.95 (g kg^{-1}) and 4.62 (g kg^{-1}) respectively. The Zn concentrations are high throughout each of the apron dust locations. The lowest Zn concentration of 3.16 (g kg^{-1}) is displayed at B6/30. Notable increases in concentrations occur at B4/51 to 10.55 (g kg^{-1}) and to 11.04 (g kg^{-1}) at B5/34 and the highest value of 13.71 (g kg^{-1}) at B5/33.

Pb concentrations (Figure 5.3b) are very low throughout the taxiway and apron dusts. Extremely low values <0.05 (g kg^{-1}) are evident within the taxiway dusts at T1/2 and VA1/4. An increase to higher concentrations >0.20 (g kg^{-1}) can be seen at C14 and D29 and to 0.32 (g kg^{-1}) at C13. The Pb concentrations displayed within the apron dusts are similar to those seen within the taxiway dusts, however, there is much less variability between each site location. Pb content within this area ranges from 0.11 (g kg^{-1}) at B2/43 to 0.25 (g kg^{-1}) at B5/34.

The Al content (Figure 5.3b) within the taxiway and apron dusts is high. Concentrations within the taxiway samples range from the lowest value of 23.30 (g kg^{-1}) at C13 to 38.30 (g kg^{-1}) at D25. There is little variation in the concentrations displayed by the apron dusts although a slightly lower content of 30.10 (g kg^{-1}) is evident at B6/30 and there is a marked increase to 44.90 (g kg^{-1}) at B2/45 and 46.70 (g kg^{-1}) at B2/46.

102

Table 5.3: Summary of elemental concentrations (g kg^{-1}) for the taxiway and apron dusts.

Element		Taxiway ($n = 8$)	Apron ($n = 11$)
Ti	Range	3.19 – 6.36	4.94 – 8.07
	Mean ± SD	4.56 ± 1.59	6.65 ± 1.57
Cr	Range	0.06 – 0.31	0.23 – 0.44
	Mean ± SD	0.20 ± 0.12	0.33 ± 0.11
Fe	Range	20.80 – 59.20	61.30 – 96.20
	Mean ±SD	37.31 ± 19.26	74.65 ± 17.61
Ni	Range	0.04 – 0.13	0.12 – 0.24
	Mean ± SD	0.08 ± 0.04	0.18 ± 0.06
Cu	Range	0.57 – 3.05	1.09 – 16.68
	Mean ± SD	1.79 ± 1.24	3.84 ± 8.32
Zn	Range	0.32 – 4.62	3.16 – 13.71
	Mean ± SD	2.09 ± 2.17	7.92 ± 5.28
Pb	Range	0.03 – 0.32	0.11 – 0.25
	Mean ± SD	0.16 ± 0.14	0.17 ± 0.07
Al	Range	23.30 – 38.30	30.10 – 46.70
	Mean ± SD	30.58 ± 7.50	38.65 ± 8.30

5.3 Environmental Grass Samples

5.3.1 Runway 23L/05R Grass Samples

The main element concentrations for the grass samples collected alongside runway 23L/05R (§ 3.3.2) are displayed in Figure 5.4. The mean value (± 1SD) and range are presented in Table 5.4. Fe concentrations are high throughout the transect ranging from 24.19 (g kg^{-1}) at 3175 m to 27.39 (g kg^{-1}) at -200 m. Within the critical area, a decrease in concentration is evident between -200 m and -155 m from 27.39 (g kg^{-1}) to 24.83 (g kg^{-1}) before concentrations begin to increase again to 25.71 (g kg^{-1}) at -5 m. From the start of the runway (0 m) to the end of the transect there is very little variation in concentration which ranges from 24.19 (g kg^{-1}) at 3175 m to 25.36 (g kg^{-1}) at 250 m.

There is little variation in Cu concentration throughout the transect (Figure 5.4) with the exception of within the critical area between -200 m and -5m. Cu content shows an overall increase from the lowest value of 2.07 (g kg^{-1}) at -200 m to the highest value of 2.18 (g kg^{-1}) at -5 m. Concentrations remain fairly constant throughout the remainder of the transect ranging from 2.07 (g kg^{-1}) at 2325 m to 2.12 (g kg^{-1}) at 250 m.

There is very little variation in Zn concentration throughout the transect. Zn content remains fairly constant ranging from 2.95 (g kg^{-1}) at -200 m to 3.01 (g kg^{-1}) at -5 m. Pb concentrations (Figure 5.4) are exceptionally low < 0.04 (g kg^{-1}) with minimal variation along the entire transect.

5.3.2 Apron and Taxiway Grass Samples

The elemental concentrations for the taxiway and apron grass samples are shown in Figure 5.5. The mean value (± 1SD) and range is presented in Table 5.5. Slight variations are displayed in the concentrations of Fe; Cu; Zn and Pb between each of the sample sets. The most significant elemental concentrations are for Fe. There is little variability between the two sample sets with values ranging from the lowest value of 24.49 (g kg^{-1}) within the apron grass samples at B4/52 to 27.09 (g kg^{-1}) within the taxiway grass samples at C3. The number of samples (*n*) is small due to the samples being pooled (± 50 m) but the sites are distinct, C3 and C8 for example separated by 250 m. Metal concentrations are observed to be very uniform across all sites. Very similar Cu and Zn concentrations are shown in both the taxiway and apron grass samples. There is very little variation in Cu concentration throughout both sets of samples. The lowest value of 2.07 (g kg^{-1}) is displayed within the apron grass samples at B2/48 and the highest of 2.10 (g kg^{-1}) within the taxiway samples at D25. Similarly, there is very little variation in Zn concentrations between the different areas and site locations. Concentrations range from the lowest value of 2.97 (g kg^{-1}) at D25 to the highest value of 3.05 (g kg^{-1}) at B4/52. Concentrations of Pb (Figure 5.5) for all samples are very low and display negligible values of <0.04 (g kg^{-1}).
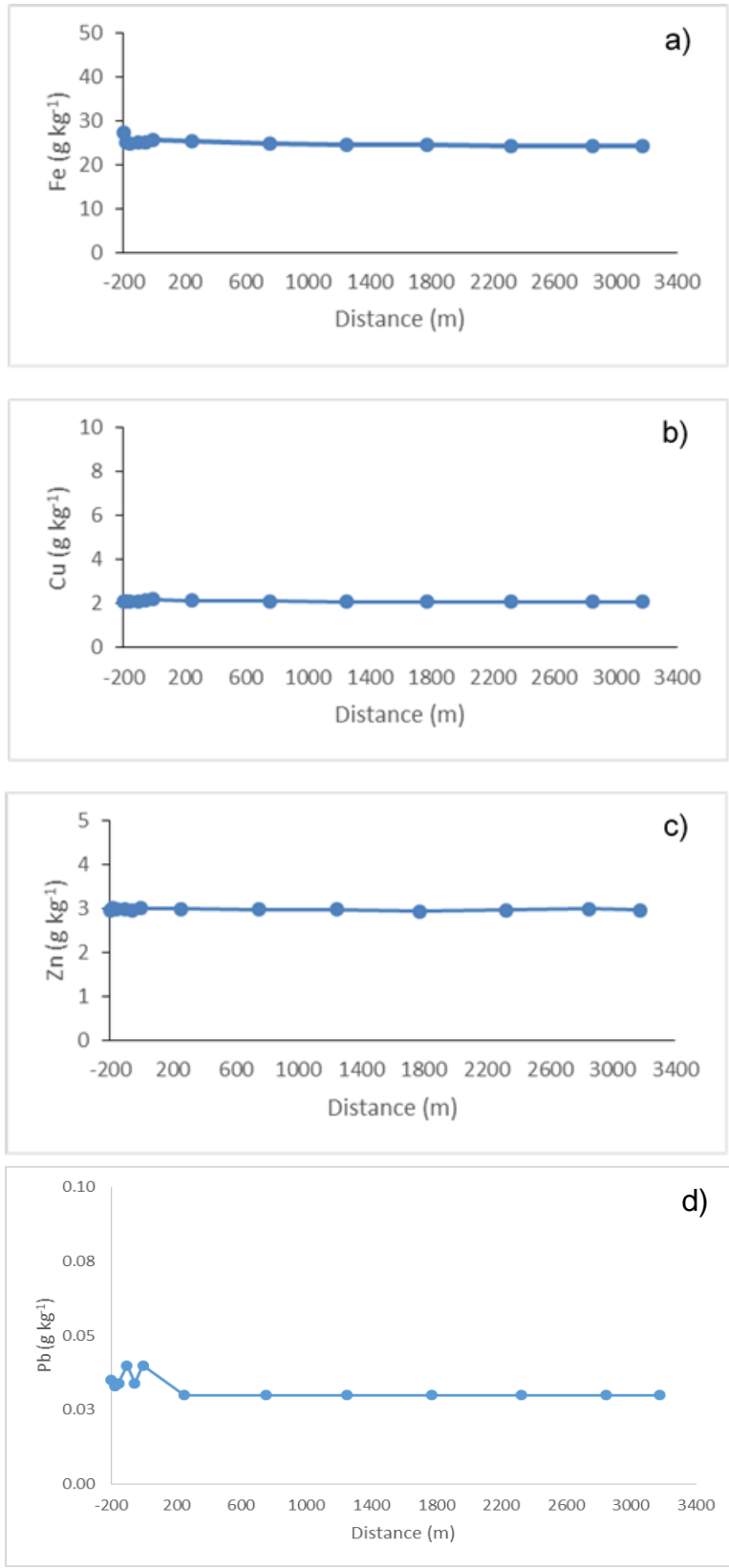
Figure 5.4: Fe; Cu; Zn and Pb concentrations (g kg^{-1}) for the runway grass samples with distance along runway 23L/05R a) Fe; b) Cu; c) Zn; d) Pb.
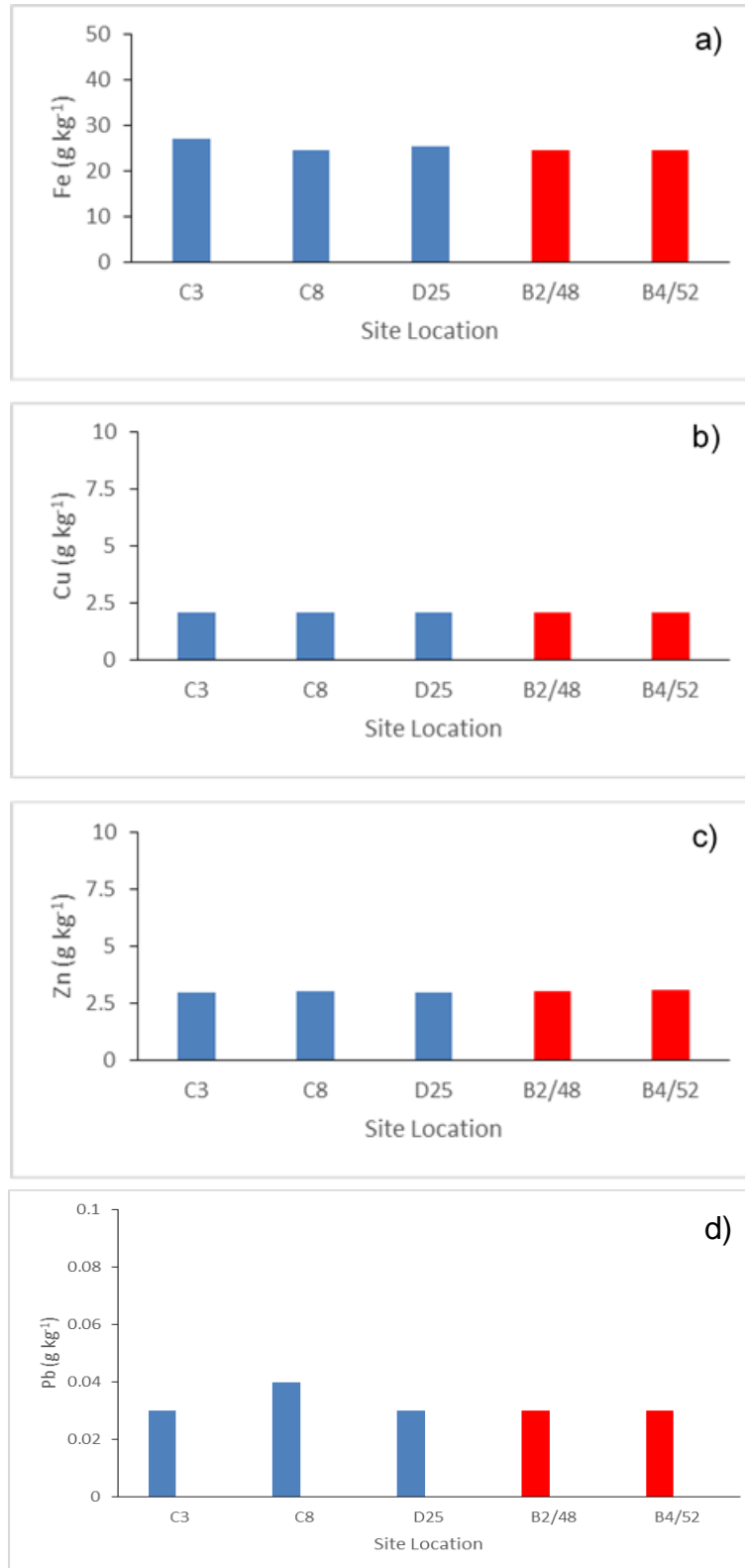
Figure 5.5: Fe; Cu; Zn and Pb concentrations (g kg^{-1}) for the taxiway and apron grass samples a) Fe; b) Cu; c) Zn; d) Pb.

Table 5.4: Summary of elemental concentrations (g kg^{-1}) for the runway 23L/05R grass samples.

Element concentration		Runway 23L/05R ($n = 13$)
Fe	Range	24.19 – 27.39
	Mean ±SD	25.04 ± 0.84
Cu	Range	2.07 – 2.18
	Mean ± SD	2.10 ± 0.03
Zn	Range	2.95 – 3.01
	Mean ± SD	2.98 ± 0.02
Pb	Range	0.03 – 0.04
	Mean ± SD	0.01 ± 0.00

Table 5.5: Summary of elemental concentrations for the taxiway and apron grass samples.

Element concentration		Taxiway ($n = 3$)	Apron ($n = 2$)
Fe	Range	24.53 – 27.09	24.49 – 24.51
	Mean ±SD	25.64 ± 1.31	24.50 ± 0.01
Cu	Range	2.07 – 2.10	2.07 – 2.09
	Mean ± SD	2.09 ± 0.01	2.08 ± 0.01
Zn	Range	2.97 – 3.01	2.97 – 3.05
	Mean ± SD	2.98 ± 0.02	3.03 ± 0.03
Pb	Range	0.03 – 0.04	0.03 – 0.03
	Mean ± SD	0.03 ± 0.04	0.03 ± 0.00

5.4 Environmental Soil Samples

5.4.1 Runway 23L/05R Soil Samples

The elemental concentrations for the soil samples collected alongside runway 23L/05R (§ 3.3.3) are displayed in Figures 5.6a and 5.6b. The mean value (± 1SD) and range is presented in Table 5.6. Ti concentrations (Figure 5.6a) are high throughout the transect >13.80 (g kg^{-1}) but there are fluctuations between higher and lower concentrations throughout. Within the critical area, between -200 m and -180 m, Ti concentration increases to 19.39 (g kg^{-1}) before decreasing to a lower value of 13.80 (g kg^{-1}) at -170 m. From this point there is an overall increase in concentration to 19.18 (g kg^{-1}) at 25 m. There is some slight variation in concentrations up to 625 m although values remain fairly constant. A decrease in concentration occurs at 725 m to 14.76 (g kg^{-1}) before increasing again to 18.98 (g kg^{-1}) at 825 m. Values then remain fairly constant up to 2220 m although some fluctuations between low and high values are evident between these points. There is a further decrease in values from 18.88 at 2220 m to 13.82 (g kg^{-1}) at 2425 before a subsequent increase to 18.84 (g kg^{-1}) at 2625 m. Values then remain fairly constant with the exception of a slight decrease to a lower value of 14.97 (g kg^{-1}) at 3225 m. Little variation is shown in Cr concentrations with distance along the runway. Cr content ranges from 2.16 (g kg^{-1}) at 1525 m to a maxima of 2.38 (g kg^{-1}) at 2675 m.

Very high Fe (g kg^{-1}) concentrations are evident within the soil samples throughout the transect (Figure 5.6a). Along with the high concentrations there is also extensive variability between each sampling point. At the start of the critical area values are elevated reaching 77.91 (g kg^{-1}) at -190 m. There is a subsequent decrease in concentration to 59.54 (g kg^{-1}) at -170 m. Concentrations then increase to 88.76 (g kg^{-1}) at 25 m. There is some variation between higher and lower values between this point and 575 m, however values remain high. At 575 m there is a further notable decrease to 64.02 (g kg^{-1}) at 725 m before another increase to 75.70 (g kg^{-1}) at 825 m. Between 825 m and 1725 m, there is an overall decrease in concentrations to 63.92 (g kg^{-1}). There are significant fluctuations between higher and lower values with distance along the

transect. However, significant increases are evident to 88.28 (g kg^{-1}) at 1925 m; 88.23 (g kg^{-1}) at 2525 m and a decrease to 54.32 (g kg^{-1}) at 3225 m.

There is very little change in Ni concentrations throughout the transect with values ranging from 0.24 (g kg^{-1}) at 775 m to 0.26 (g kg^{-1}) at 3025 m; 35225 m and 3275 m with the exception of a slight increase in concentration to 0.27 (g kg^{-1}) at 2575 m.

Figure 5.6a displays the Cu (g kg^{-1}) concentrations for the soil samples with distance along the transect. Cu concentrations are >2.11 (g kg^{-1}) and remain fairly constant with minimal variation along the transect with the exception of some slight increases in concentration within the critical area at -5 m and with distance along the transect at 225 m and 2125 m to 2.35 (g kg^{-1}); 2.33 (g kg^{-1}) and 2.57 (g kg^{-1}) respectively.

Zn content (Figure 5.6b) remains fairly constant throughout the critical area and up to 2175 m (<3.06 (g kg^{-1})) with the exception of a slight peak in concentration within the critical area to 3.40 (g kg^{-1}) at -105 m. However, from 2175 m there is an overall increase in concentrations from 3.06 (g kg^{-1}) to the highest value of 3.61 (g kg^{-1}) at 2825 m.
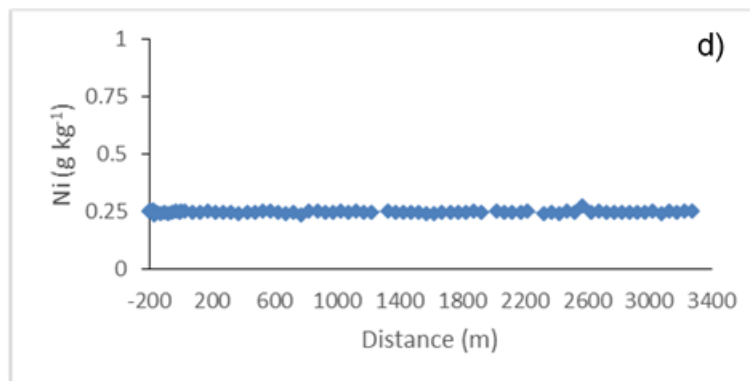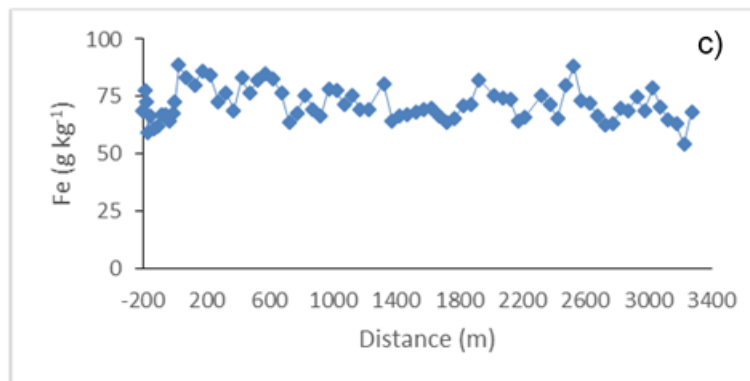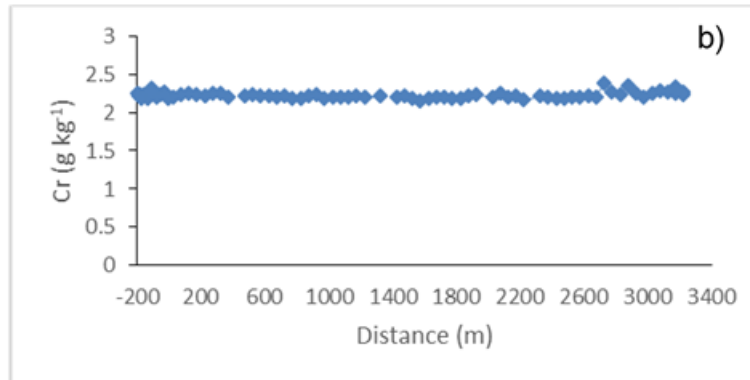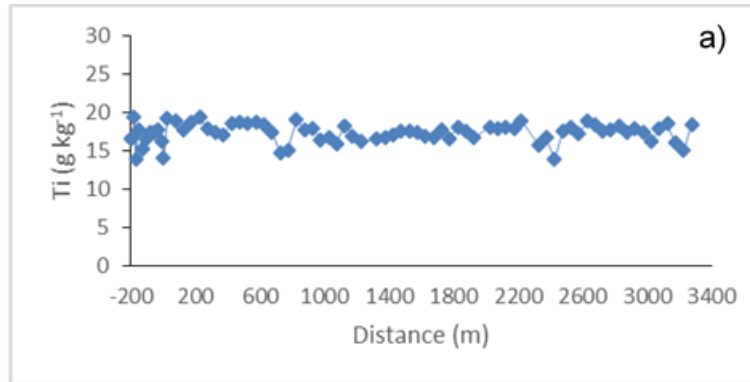
Figure 5.6a: Ti; Cr; Fe and Ni concentrations (g kg^{-1}) for the runway soil samples with distance along runway 23L/05R a) Ti; b) Cr; c) Fe; d) Ni.
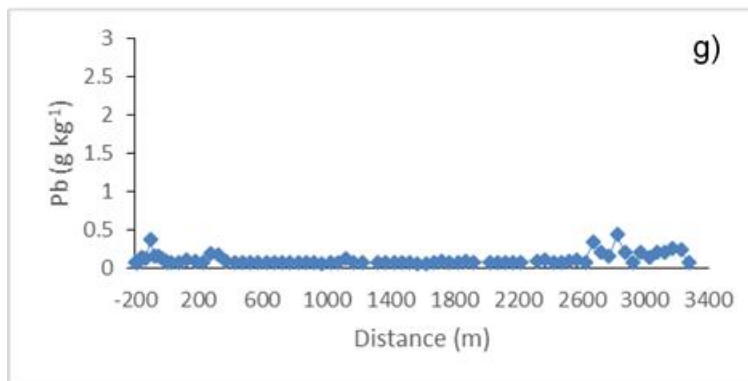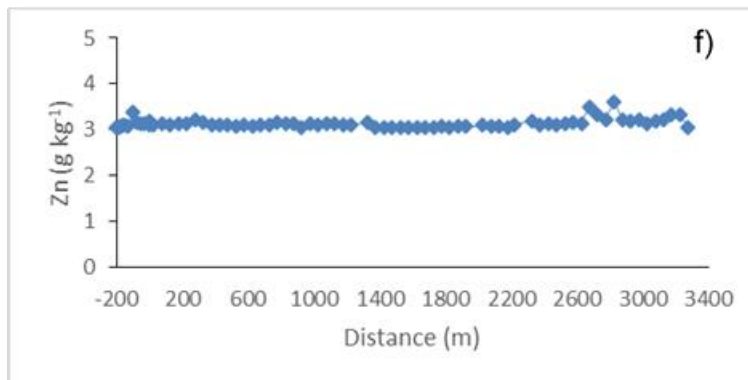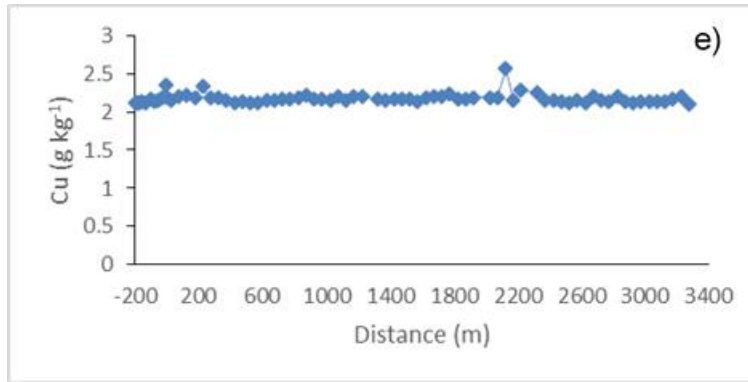
Figure 5.6b: Cu, Zn and Pb concentrations (g kg^{-1}) for the runway soil samples dusts with distance along runway 23L/05R e) Cu; f) Zn; g) Pb.

Table 5.6: Summary of elemental concentrations (g kg^{-1}) for the runway 23L/05R soil samples.

Element		Runway 23L/05R (n = 33)
Ti	Range	13.80 – 19.39
	Mean ± SD	17.28 ± 1.26
Cr	Range	2.16 – 2.38
	Mean ± SD	2.22 ± 0.04
Fe	Range	54.32 – 88.76
	Mean ±SD	71.82 ± 7.22
Ni	Range	0.24 – 0.27
	Mean ± SD	0.25 ± 0.00
Cu	Range	2.10 – 2.57
	Mean ± SD	2.10 ± 0.06
Zn	Range	3.04 – 3.61
	Mean ± SD	3.14 ± 0.10
Pb	Range	0.07 – 0.44
	Mean ± SD	0.12 ± 0.07

Very low Pb concentrations are evident throughout the transect <0.44 (g kg^{-1}) (Figure 5.6b) although there is some variation between lower and high values with distance alongside the runway. A slight increase in concentrations occurs within the critical area from 0.07 (g kg^{-1}) at -200 m to 0.37 (g kg^{-1}) at -105 m. A subsequent decrease in concentration occurs throughout the remainder of the critical area and the beginning of the runway to 0.08 (g kg^{-1}) at 25 m. There is little variability in concentrations from this point to 2625 m with the exception of a slight increase to 0.19 (g kg^{-1}) at 275 m and to 0.34 (g kg^{-1}) at 2675 m. Pb content peaks at 2825 m to 0.44 (g kg^{-1}) before decreasing to a lower concentration of 0.07 (g kg^{-1}) at 2925 m. A further increase in concentration is evident at 2975 m to 0.21 (g kg^{-1}) and with distance along the transect to 0.26 (g kg^{-1}) at 3175 m before decreasing to 0.08 at 3275 m.

5.4.2 Taxiway and Apron Soil Samples

The elemental concentrations for the taxiway and apron soil samples are shown in Figures 5.7a and 5.7b. The mean value (± 1 SD) and range is presented in Table 5.7. Ti values are high throughout both sample sets. However, there is some variability between sites and overall lower concentrations are displayed within the taxiway soils. Within the taxiway soils, lower values are evident within Area C (C1 to C6) which range from 10.83 (g kg^{-1}) at C3 to 13.14 (g kg^{-1}) at C2. An increase in concentration occurs within the remainder of soils collected from Area C (C8 to C11) and those collected within Zone D. The soil samples collected within these areas range from 14.48 (g kg^{-1}) at D23 to 18.00 (g kg^{-1}) at C11. Within the apron soil samples Ti concentrations are high and there is little variation between site locations with the exception of a slightly lower concentration of 13.12 (g kg^{-1}) at B4/53. All other values are >16.04 (g kg^{-1}) peaking at 19.18 (g kg^{-1}) at B2/48.

Cr concentrations remain constant throughout with minimal variation between the two sample sets and amongst the individual sites (Figure 5.7a). Values range from a minimum value of 2.17 (g kg^{-1}) at B2/52 to 2.25 (g kg^{-1}) at B2/41.

Fe content is high throughout both the taxiway and apron soil samples (Figure 5.7a). There is, however, some significant variation between the site locations. Within the taxiway areas Area C values show notable differences. Sites C3 and C10 display the lowest concentrations of 64.55 (g kg^{-1}) and 59.67 (g kg^{-1}) respectively.   An increase to higher values >77.80 (g kg^{-1}) is evident in sites C2; C5; C6 and C8 and a further increase to a higher value of 92.20 (g kg^{-1}) at C1. Values within Area D are very high ranging from 72.85 (g kg^{-1}) at D24 to 92.92 (g kg^{-1}) at D28. Concentrations within the apron soil samples are also extremely variable. The lowest concentration of 51.01 (g kg^{-1}) is displayed at B4/53. There are notable increases in concentration to >68.77 (g kg^{-1}) at sites B36; B37 and B2/52. A further increase in concentration is evident in sites B2/41 and B2/42 to B2/50 with the highest value of 104.59 (g kg^{-1}) being displayed at B2/41.

Ni concentrations (Figure 5.7a) are very low throughout and there is very little variation between the samples and the sample sets. Values range from 0.24 (g kg^{-1}) at B4/53 to 0.27 (g kg^{-1}) at D24.

113

Very similar Cu concentrations (Figure 5.7b) are seen throughout the samples which mostly range from 2.15 (g kg^{-1}) at C5 to 2.44 (g kg^{-1}) at D28, however, several increases to higher values are evident particularly within the apron soil samples. Increases can be seen within the taxiway samples to 2.96 (g kg^{-1}) at D24 and within the apron soils to 2.77 (g kg^{-1}); 2.70 (g kg^{-1}) and 3.12 (g kg^{-1}) at B37; B37 and B2/52 respectively.

Zn concentrations (Figure 5.7b) are very similar throughout both sample sets displaying very little deviation from the lowest value of 3.20 (g kg^{-1}) at D28 (taxiway). There are, however, 2 slight peaks in concentration within the apron dust samples to 3.93 (g kg^{-1}) at B36 and 3.87 (g kg^{-1}) at B2/52.

Pb (g kg^{-1}) values (Figure 5.7b) are generally very low <0.29 (g kg^{-1}), although there is some variability between the samples within both the taxiway and apron soils. Taxiway concentrations range from 0.07 (g kg^{-1}) at D26 to 0.29 (g kg^{-1}) at C11. There are some slight peaks in concentration to higher values >0.20 (g kg^{-1}) at C1 and C4 and a further increase to the highest value of 0.29 (g kg^{-1}) at C11. The apron soil samples show much less variability between the samples with concentrations ranging from 0.08 (g kg^{-1}) at B2/41 to the highest value of 0.15 (g kg^{-1}) at B36.
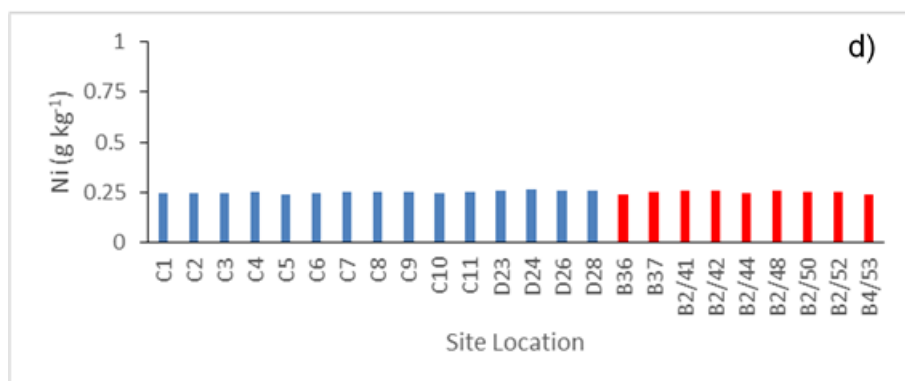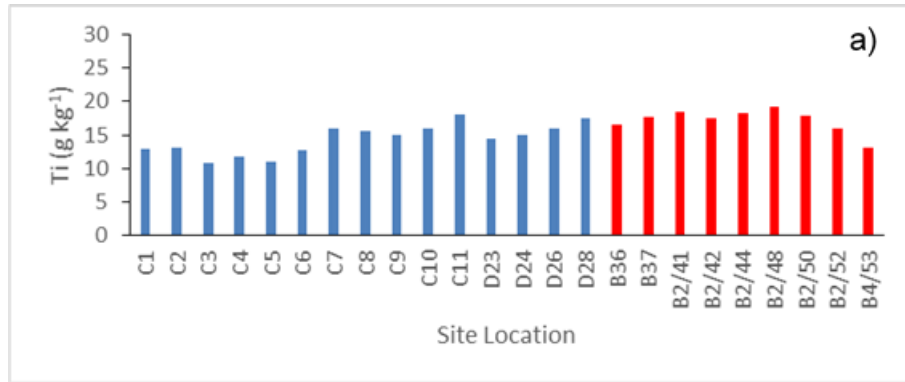
Figure 5.7a: Ti; Cr; Fe and Ni concentrations (g kg^{-1}) for the taxiway and apron soil samples a) Ti, b) Cr, c) Fe, d) Ni.

115
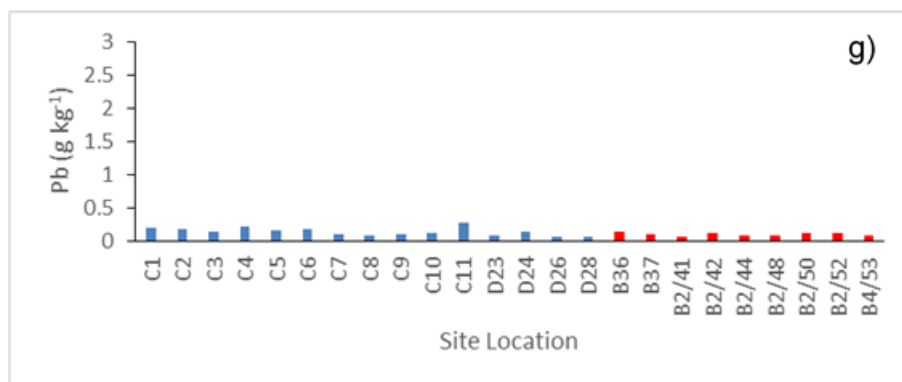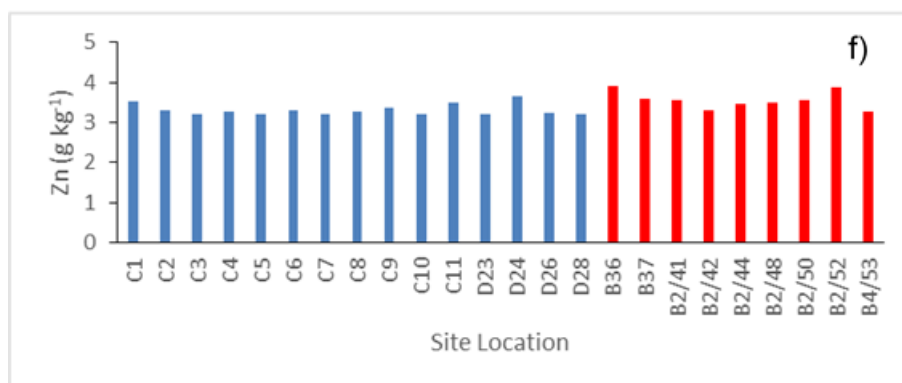
Figure 5.7b: Cu, Zn and Pb (g kg^{-1}) for the taxiway and apron soil samples e) Cu, f) Zn, g) Pb.

Table 5.7: Summary of elemental concentrations (g kg^{-1}) for the taxiway and apron soil samples.

Element		Taxiway ($n = 8$)	Apron ($n = 11$)
Ti	Range	10.83 – 18.00	13.12 – 19.18
	Mean ± SD	13.93 ± 3.60	16.92 ± 3.06
Cr	Range	2.17 – 2.25	2.17 – 2.25
	Mean ± SD	1.65 ± 1.16	1.84 ± 1.20
Fe	Range	59.67 – 92.20	51.01 – 104.59
	Mean ±SD	74.42 ± 16.28	81.75 ± 26.89
Ni	Range	0.24 – 0.26	0.24 – 0.27
	Mean ± SD	0.25 ± 0.01	0.25 ± 0.01
Cu	Range	2.15 – 2.27	2.17 – 3.12
	Mean ± SD	2.20 ± 0.06	2.47 ± 0.48
Zn	Range	3.20 – 3.53	3.20 – 3.93
	Mean ± SD	3.30 ± 0.17	3.51 ± 0.36
Pb	Range	0.10 – 0.29	0.07 – 0.16
	Mean ± SD	0.17± 0.10	0.11 ± 0.05

Chapter 6

Results: SEM/EDX

Chapter 6 sections 6.1 to 6.2 presents the SEM/EDX results completed on the aircraft source and environmental dust samples (i.e. runway, taxiway and apron dusts). The particle roundness and textural classifications are described in § 3.7.

6.1 Aircraft Source Samples

6.1.1 Engine, Brake and Tyre Dusts

i)   *Particle size (µm)*

The particle size diameter (µm) of the engine, brake and tyre dusts are displayed in Figure 6.1. The engine dusts contain a wide range of particle sizes (0-35 µm; 40-45 µm and 60+ µm). However, they are dominated by small particles, of which, 48.2% are within the 0-5 µm size range. There is little size variation within the brake dust samples with 87.0% of the particles displayed lying within the 0-15 µm range. Moreover, 69.6% of such particles are equally distributed between the 0-5 µm and 5-10 µm size categories.   The tyre dusts contain a wide range of particle sizes from 0-5 µm through to 55-60 µm with the exception of a gap between 35 and 55 µm. The distribution of particles is quite even between the various size ranges. However, a slightly higher percentage is seen within the 0-5 µm and 15-20 µm categories which each contain 20% of the particles.

ii)   *Particle roundness*

The particle roundness (frequency %) for each of the aircraft source samples (i.e. engine; brake and tyre dusts) is shown in Figure 6.2. The engine dust particles are distributed across each of the roundness categories. The particles are predominantly within the angular and sub-angular categories which contain 76.7% of the particles, with 20% within the rounded category. Brake dust particles are distributed across the rounded; sub rounded and sub angular categories. The

majority of brake dust particles (81.5%) are within the sub angular classification, with 14.8% within the rounded category.   The tyre dust particles are distributed across each of the roundness categories. The predominant category is rounded which contains 60.9% of the tyre dust particles.

iii)   SEM/EDX

The general SEM images show that the engine dusts display a 'crumb' like texture (Figure 6.3). The chemical composition of the areas identified in Figure 6.3 are predominantly comprised of O (44.6 – 62.2%); C (11.8 – 38.4%) and Si (10.4 – 19.6%) along with trace amounts of other elements (<3.0%) including S; Na; Al; Ni; Cr; Fe; P; K; Mg and Ca. Elemental analysis of individual particles (Figure 6.4) reveals that the angular and sub-angular particles (*a* and *e*) are largely comprised of C (17.5% - 75.1%) and O (17.5 – 61.6%). Trace amounts (<2.6%) of other elements are also common to these particles including S; Na; Cr; Al; P and Mg. The rounded and sub-rounded engine dust particles (Figure 6.4*b* to *d*) have distinctive 'spherical' and 'molten drop' (Xue and Lu, 2008 (§ 3.7.1)) morphologies and smooth surface textures (Figure 6.4). However, smaller particles can also be seen to be adhered to the particle surfaces and a hollow is evident within Figure 6.4c. The predominant chemical composition of these particles is O (56.4 – 63.5%); C (12.9 – 26.3%); and Si (6.4 – 17.4%). S (2.3 – 5.8%) was also found to be present within these particles along with other elements in smaller amounts (i.e. <1.9%) including Ni; Al; Na; Cr; P; Fe; Ti; Mg; K and Ca.

The general SEM images of the brake dusts reveal a largely blocky texture (Figure 6.5). The chemical composition of the areas identified in Figure 6.5 are dominated by C (87.4 – 91.9 %) with O (7.4 – 7.9%) also being present. Much smaller quantities of other elements are also evident (<2.2%) including Na; Mg; Al; Si; P; S; K; Ca and Fe.   All brake dust particles (Figure 6.6a and 6.6b) are comprised principally of C (>75.8 %) and O (>7.7 %) with trace amounts (<1.7%) of Si; Fe; Ca; Al and S.
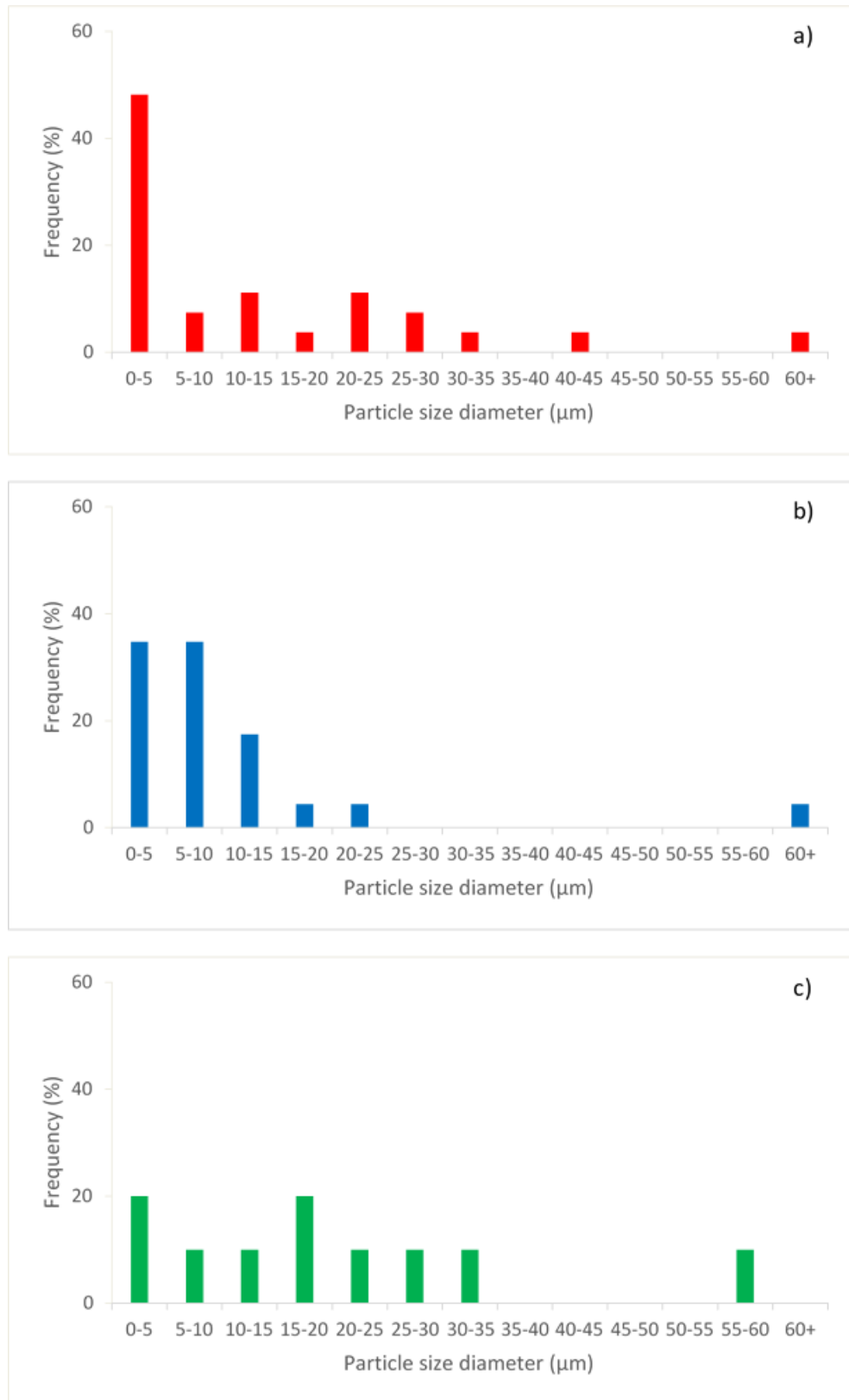
Figure 6.1: Particle size diameter (μm) for the aircraft source dust samples: a) engines, b) brakes, and c) tyres.
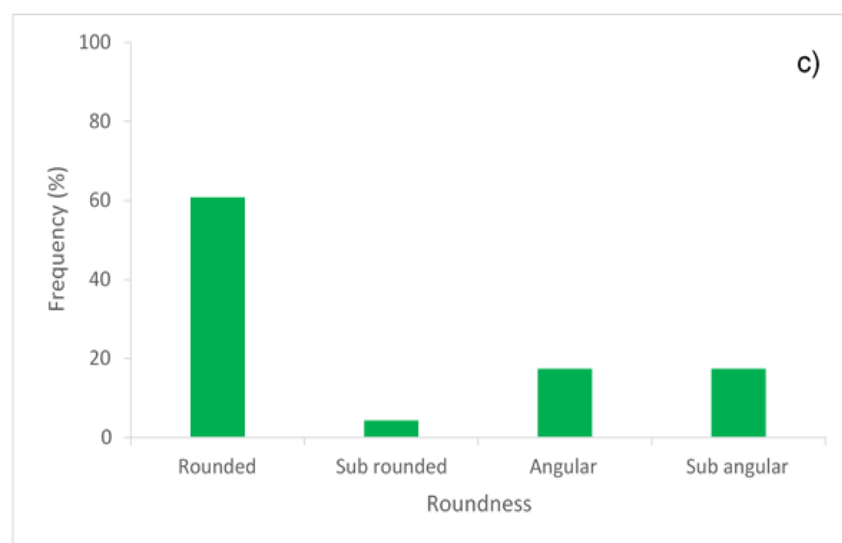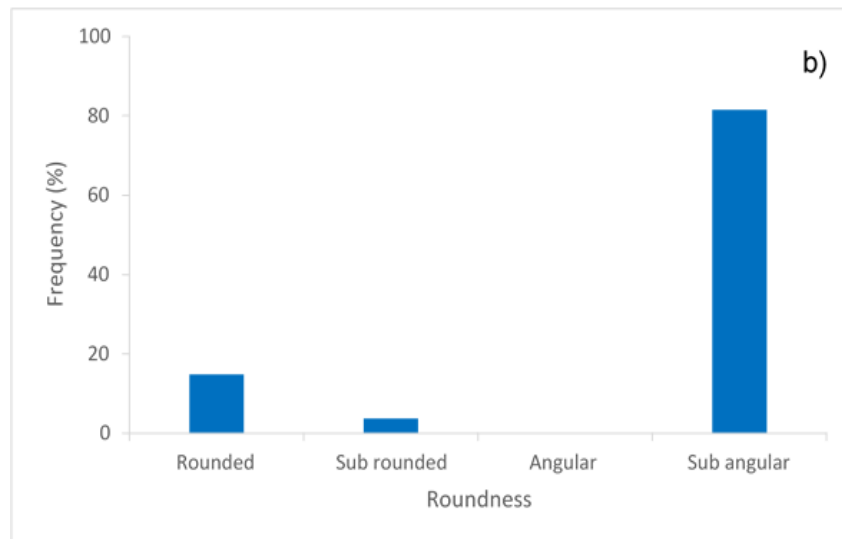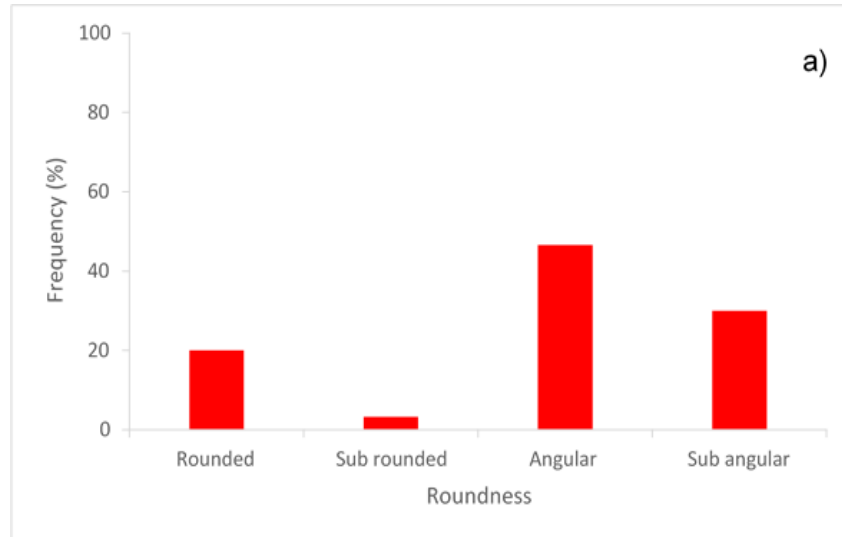
Figure 6.2: Particle roundness (frequency %) for the aircraft source dust samples: a) engines, b) brakes, and c) tyres.
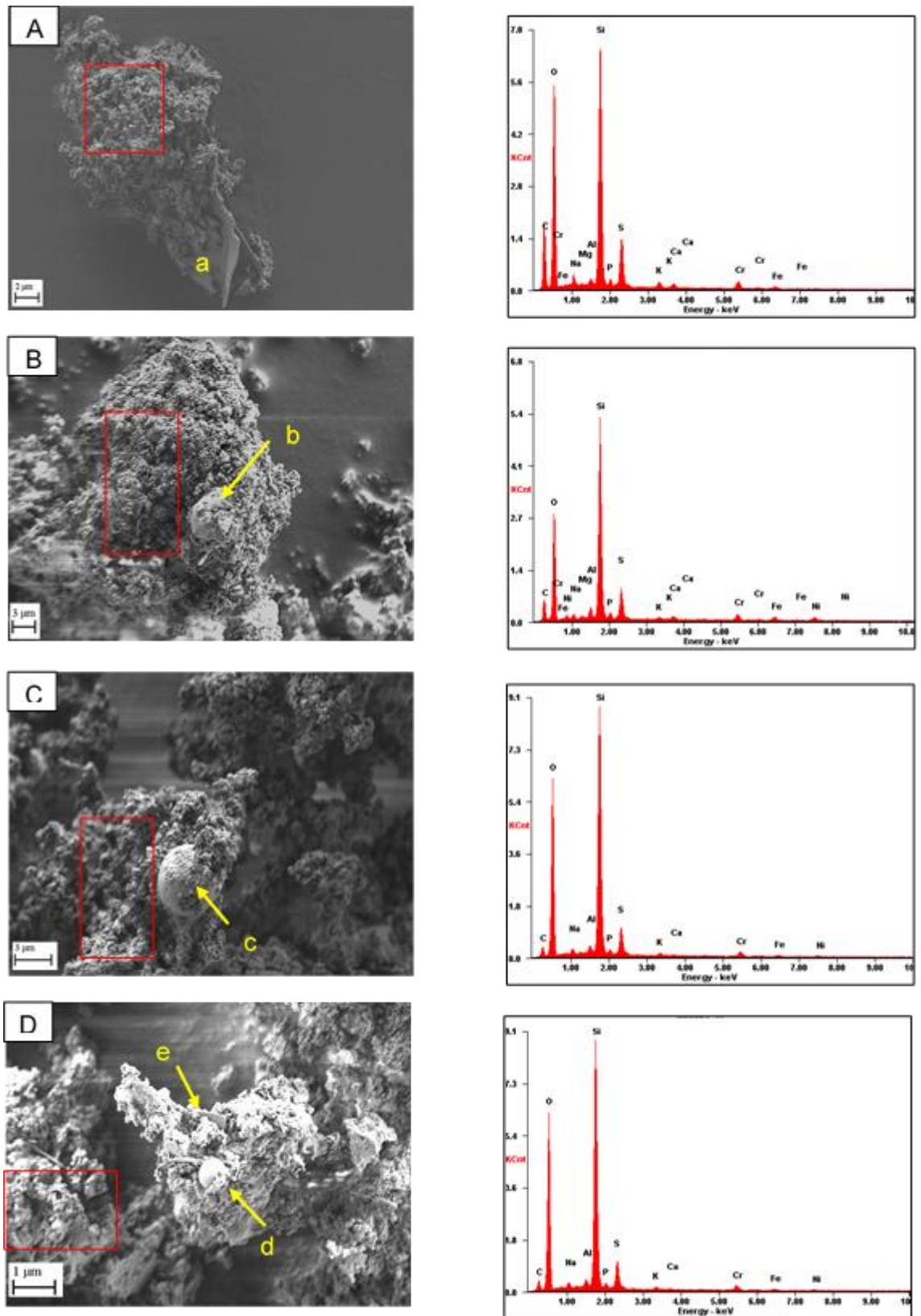
Figure 6.3: SEM images (A-D) showing the general morphological composition of the engine dust samples and individual particles (*a - e*). The EDX spectra for each image relates to the area within the red box. The EDX spectra of the individual particles are shown in Figure 6.4.
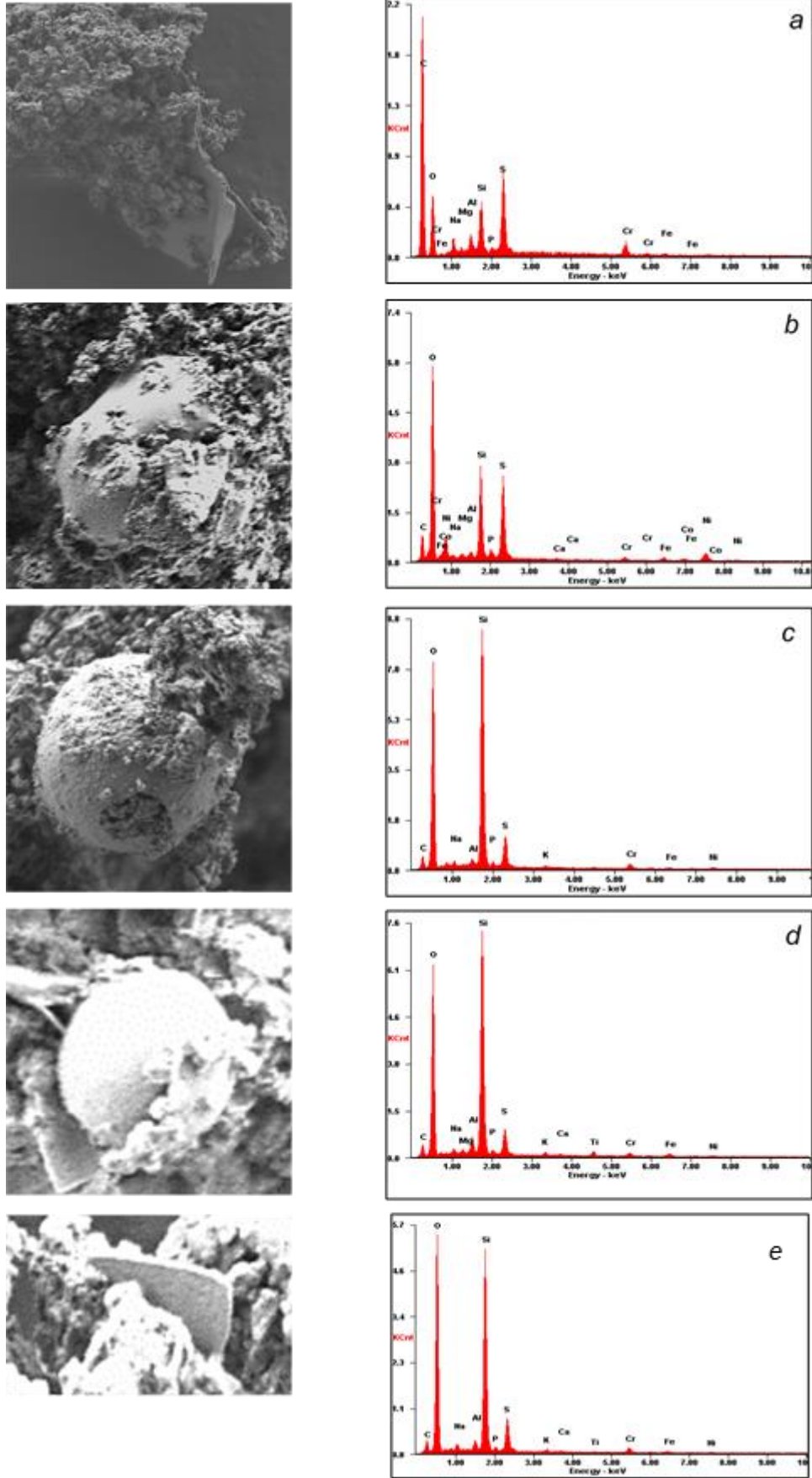
Figure 6.4: SEM images of Individual engine
dust particles and associated EDX spectra.
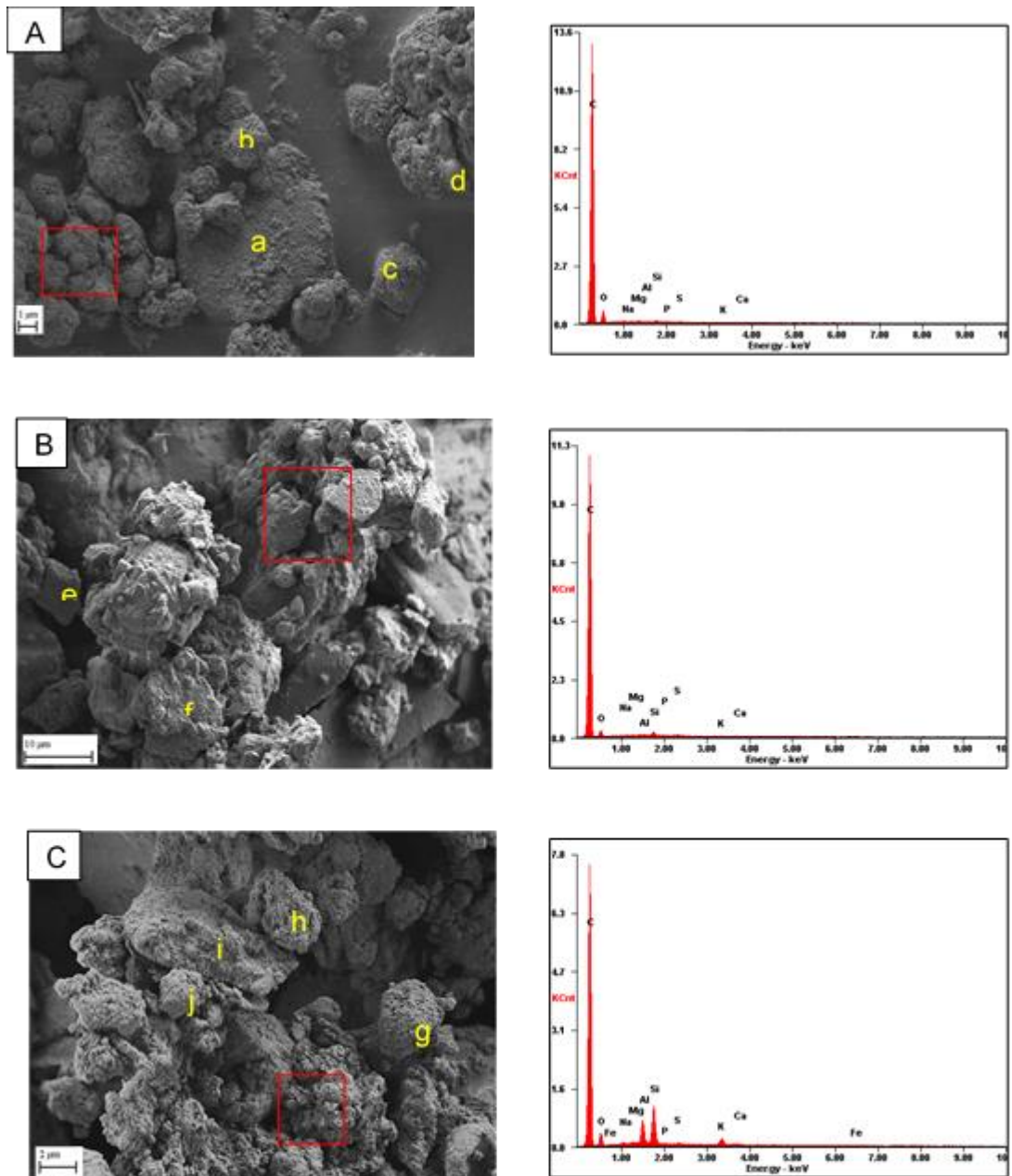
Figure 6.5: SEM images (A-C) showing the general morphological composition of the brake dust samples and individual particles (*a* - *j*). The EDX spectra for each image relates to the area within the red box. The EDX spectra of the individual particles are shown in Figures 6.6a and 6.6b.

Figure 6.6a: SEM images of Individual brake dust particles (*a* to *e*) and associated EDX spectra.

Figure 6.6b: SEM images of Individual brake dust particles (*f* to *j*) and associated EDX spectra.

Tyre dusts are composed largely of consolidated 'granular' like material (Figure 6.7). Chemical analysis of specific areas identified within each of the bulk images shows that they are dominated by C (67.3 – 77.5%) and O (16.7 – 23.4%). Si is also present in smaller quantities (1.9 – 7.2%) along with trace amounts (<3.7%) of Al; Ca; S; Zn; Fe; Mg; Na; K; Cu; Ti and P. The rounded and sub-rounded tyre dust particles (Figure 6.8) display distinctive microstructural characteristics i.e. 'spherical' (*a; b; d* and *e*) and 'molten-drop' (*c*) with 'smooth' (*b*) and 'orange-peel' (*a - e*) textures. Smaller particles appear to be adhered onto the surface area of particle *d.*

The tyre dust particles (Figure 6.8) are dominated by C (16.5 – 67.6%); O (14.7 – 51.7%); Si (3.6 – 18.7%) and Al (2.7 – 13.5%). Fe (0.4 – 7.5) is also present within each of the individual tyre dust particles along with trace amounts (i.e. <2.2%) of K; Mg and Na. Several other elements including Ca; Ti; Zn; S; P and Cu are evident in smaller amounts (<6.5%) within a significant number of particles.

6.2 Environmental Dust Samples

6.2.1 Runway Dusts

i)   *Particle size (µm)*

The particle size diameter (µm) of the runway dust samples is shown in Figure 6.9. All particles within the runway dust samples collected from the take-off zone (Zone A: 0 – 725 m) are ≤ 10 µm in size with 75% of these within the 0-5 µm category. The particles within the runway dusts from the landing zone (Zone B: 2300 – 3000 m) contain a wide range of particle sizes (i.e. 0-15 µm; 20-25 µm and 45-50 µm). However, 81.0% of these are within the 0-15 µm size range, of which 57.1% are distributed evenly between the 0-5 µm and 5-10 µm categories.

ii) *Particle roundness*

The runway dust samples (Figure 6.10) from the take-off zone (Zone A: 0 – 725 m) are comprised of rounded and angular particles with the majority of these particles (75%) within the angular category. Particle roundness within the landing zone dusts (Zone B: 2300 – 3000 m) is evenly distributed across the rounded (38.1%); sub-rounded (23.8%) and angular (38.1%) categories.

iii) **SEM/EDX**

Textural analysis of the runway dusts collected from the take-off zone (Zone A: 0 – 725 m) reveals that they are largely composed of consolidated 'granular' like material (Figure 6.11). The chemical composition of the general areas (Figure 6.11) is predominantly O (29.8 - 57.0%); C (10.7 – 59.5%) and Si (4.2 – 16.2%). Smaller amounts of Al (2.0 – 7.8%) and Na (0.4 – 5.3%) are also present along with trace amounts (<1.9%) of Mg; Fe; Ca and K. The rounded particle *'c'* (Figure 6.12) has an 'orange peel' texture. Elemental analysis shows that this particle is O (47.4%) and C (28.0%) rich but also comprises Si (11.1%) and Al (9.7%) and trace amounts (<1.1%) of Fe; K; Na; Mg; S and Ti. The angular particles (Figure 6.12a; *b* and *d*) are composed predominantly of O (49.4 – 62.5 %); C (6.4 – 27.1%) and Si (15.6 – 28.1%). Al is also present within these particles but in smaller quantities (i.e. 0.4 – 7.0%). A presence of Na (<8.4%) is evident within some particles along with trace amounts (<0.6%) of Mg and K.

The runway dusts collected from the landing zone (Zone B: 2300 – 3000 m) comprise a consolidated 'granular' like texture (Figure 6.13). The elemental composition of the specified areas (Figure 6.13) are predominantly composed of C (75.7% - 89.2%) and O (9.2 – 17.0%). Trace amounts (<1.0%) of Zn; Fe; S; Al; Ca; Mg; K; are also evident. The rounded individual particles within this zone have a distinctive 'orange peel' texture (Figure 6.14) and are C rich (>64.7%) with O (>10.0%). Other common elements which are present in low quantities (<0.7%) include Ca; S; Al and Zn. Trace amounts of P; Si; Cu; Mg and Fe (<0.7%) are also evident within some particles.
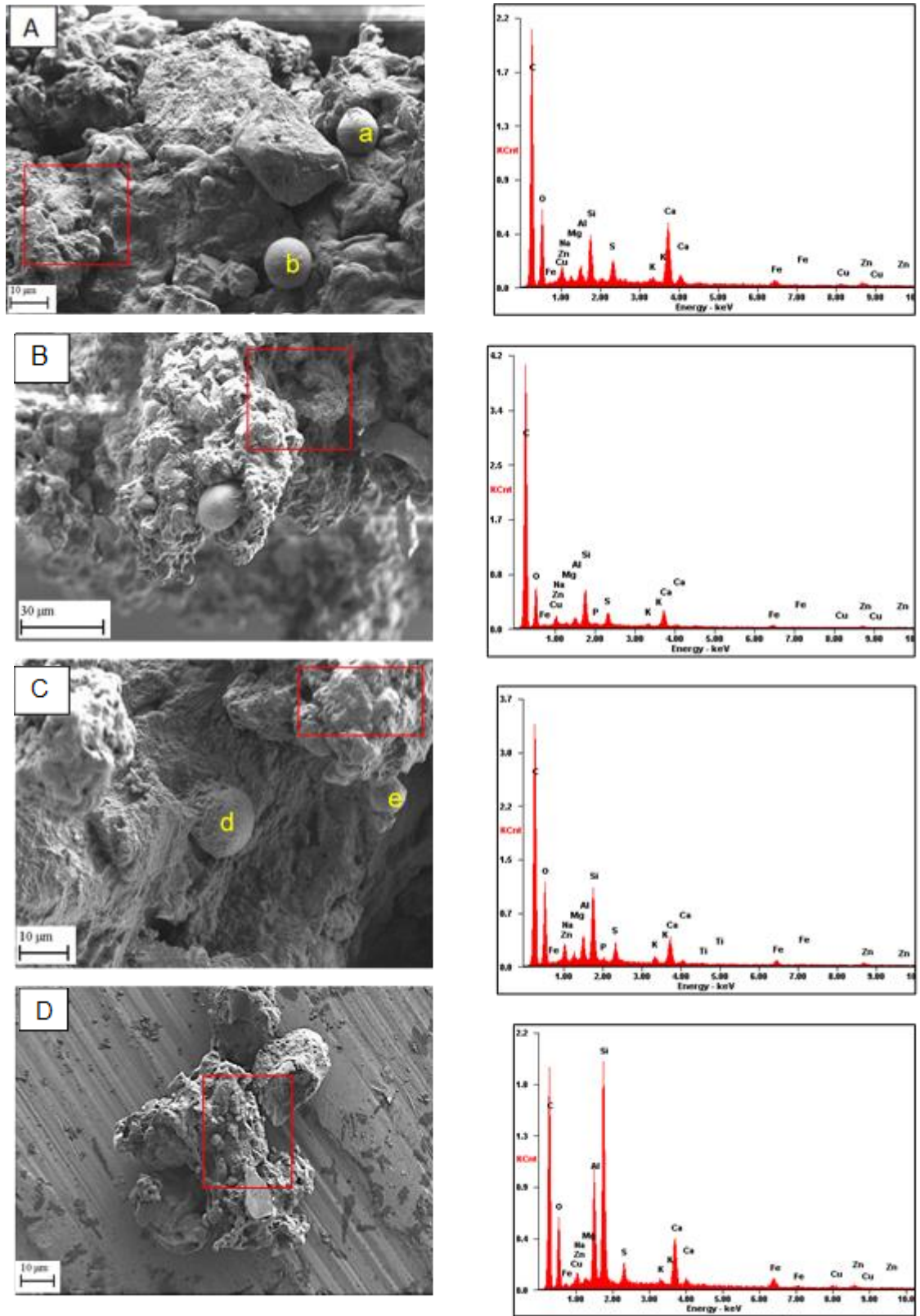
Figure 6.7: SEM images (A-D) showing the general morphological composition of the tyre dust samples and specific particles (*a - e*). The EDX spectra for each image relates to the area within the red box. The EDX spectra of the individual particles are shown in Figure 6.8).
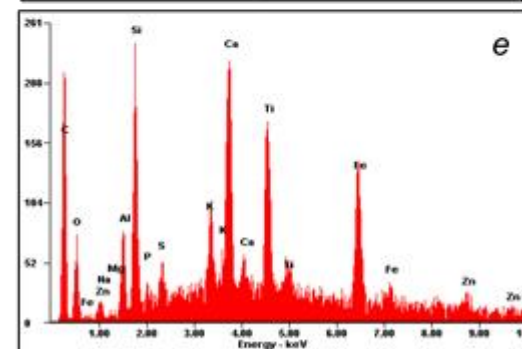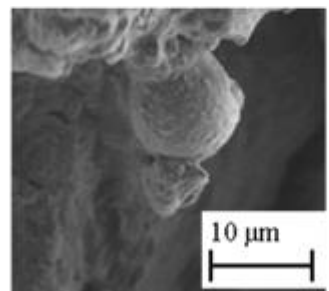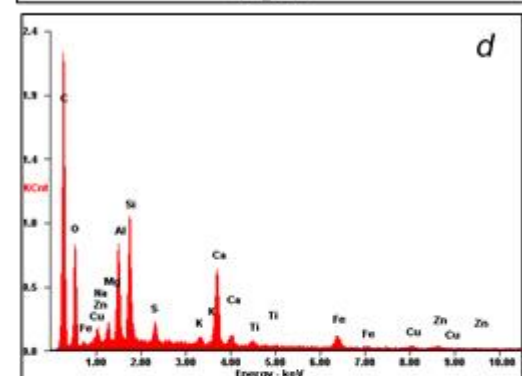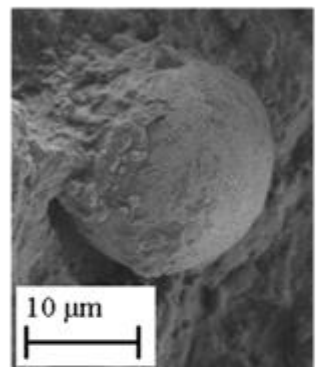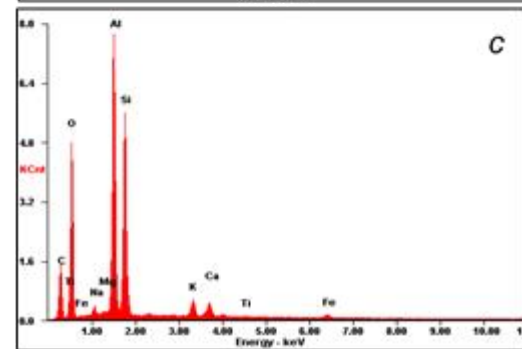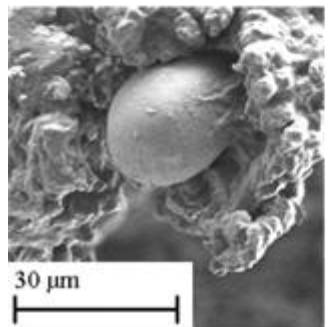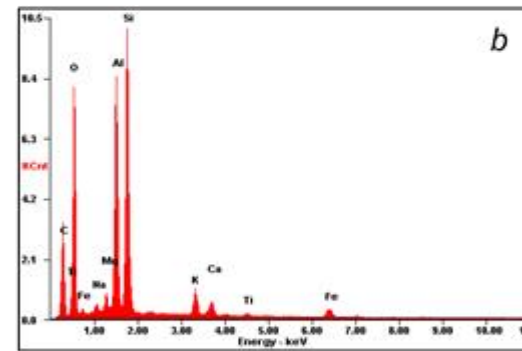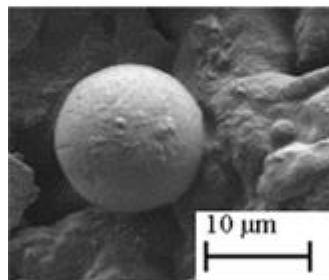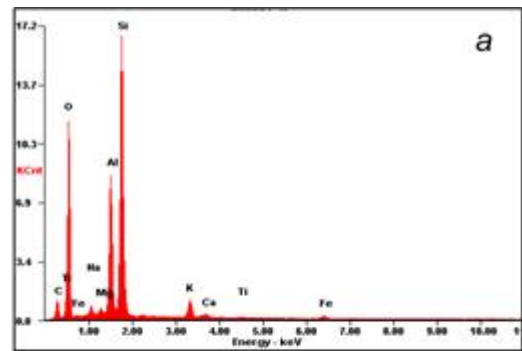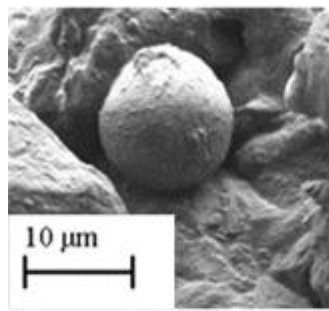
Figure 6.8: SEM images of Individual tyre dust particles and associated EDX spectra.
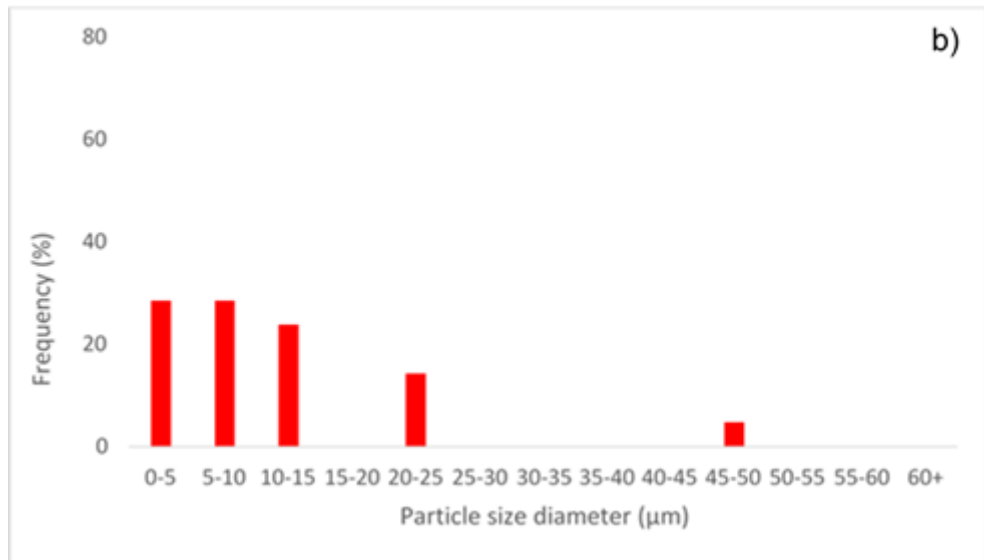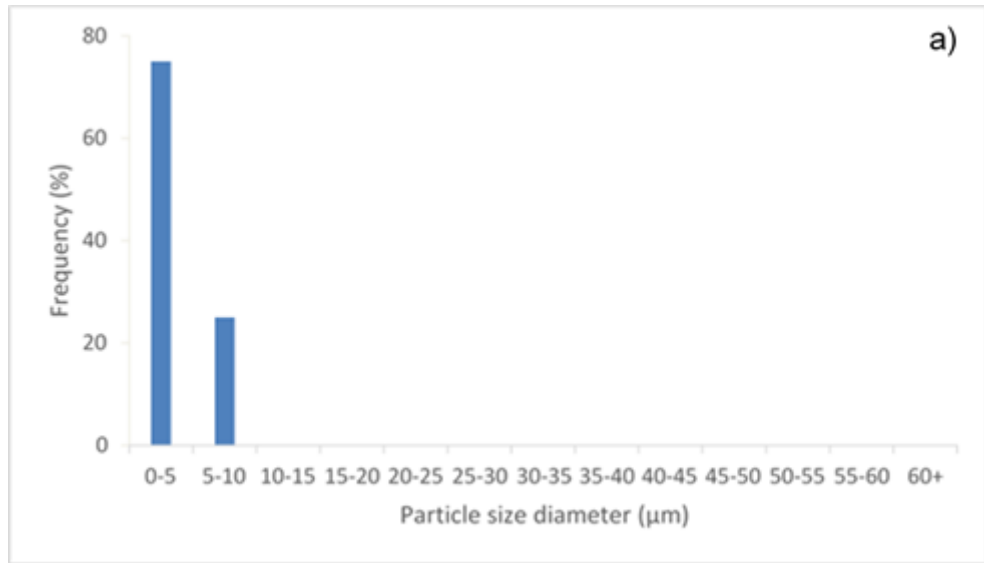
Figure 6.9: Particle size diameter (µm) for the runway dust samples: a) Zone A: 0 – 725 m b) Zone B: 2300 – 3000 m.
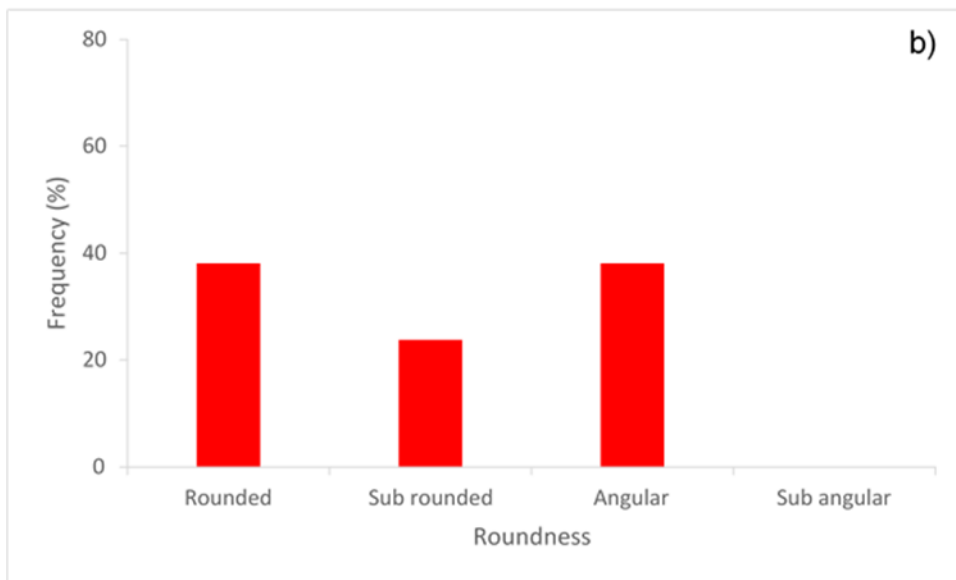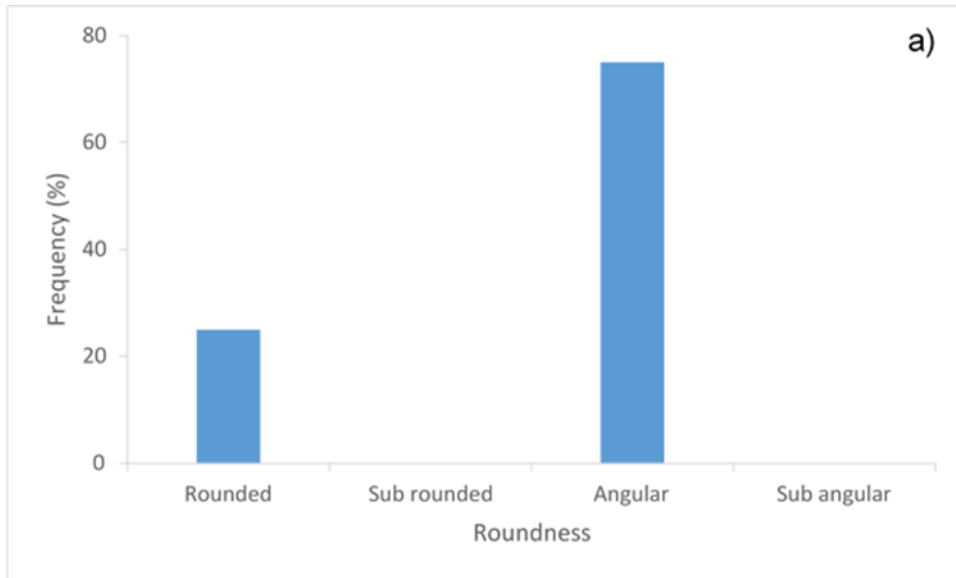
Figure 6.10: Particle roundness (frequency %) for the runway dust samples: a) Zone A: 0 – 725 m b) Zone B: 2300 - 3000.
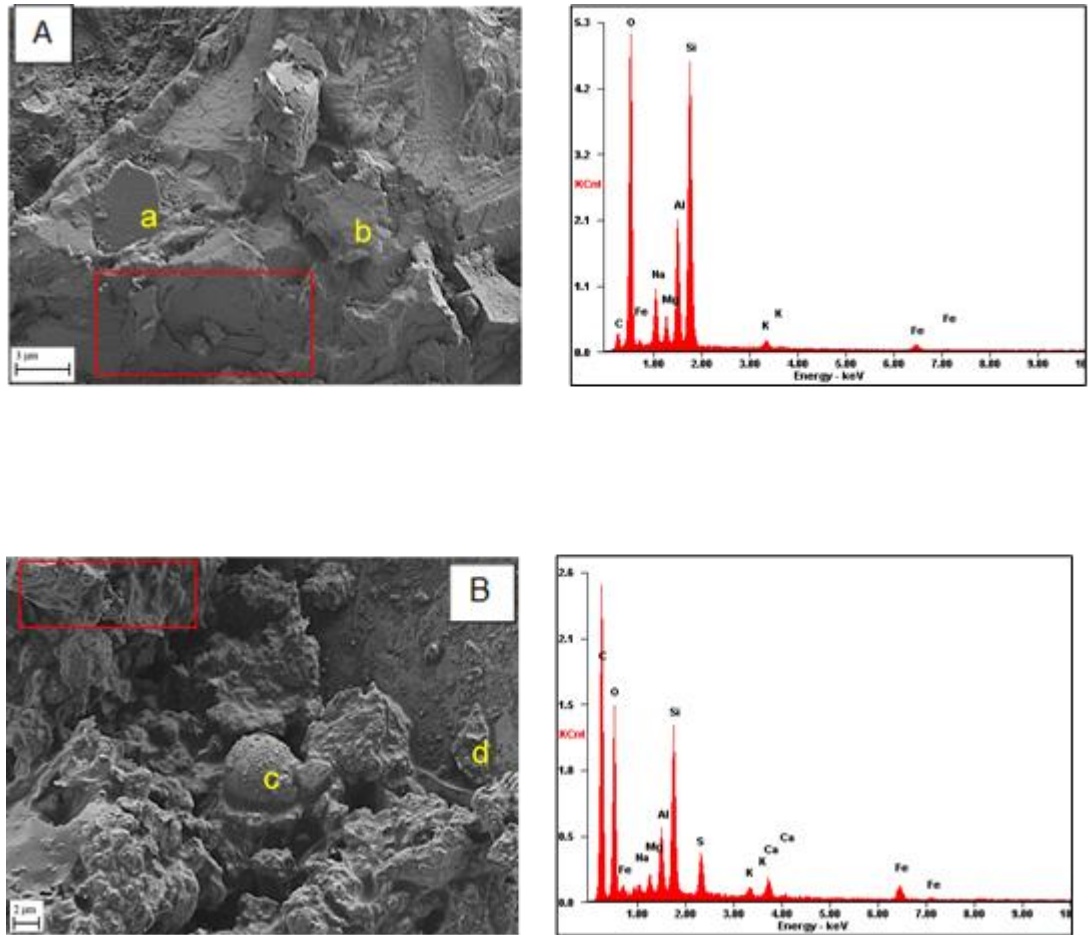
Figure 6.11: SEM images (A-B) showing the general morphological composition of the runway dusts (Zone A: 0 – 725 m) and individual particles (*a* - *d*). The EDX spectra for each image relates to the area within the red box. The EDX spectra of the particles are shown in Figure 6.12.
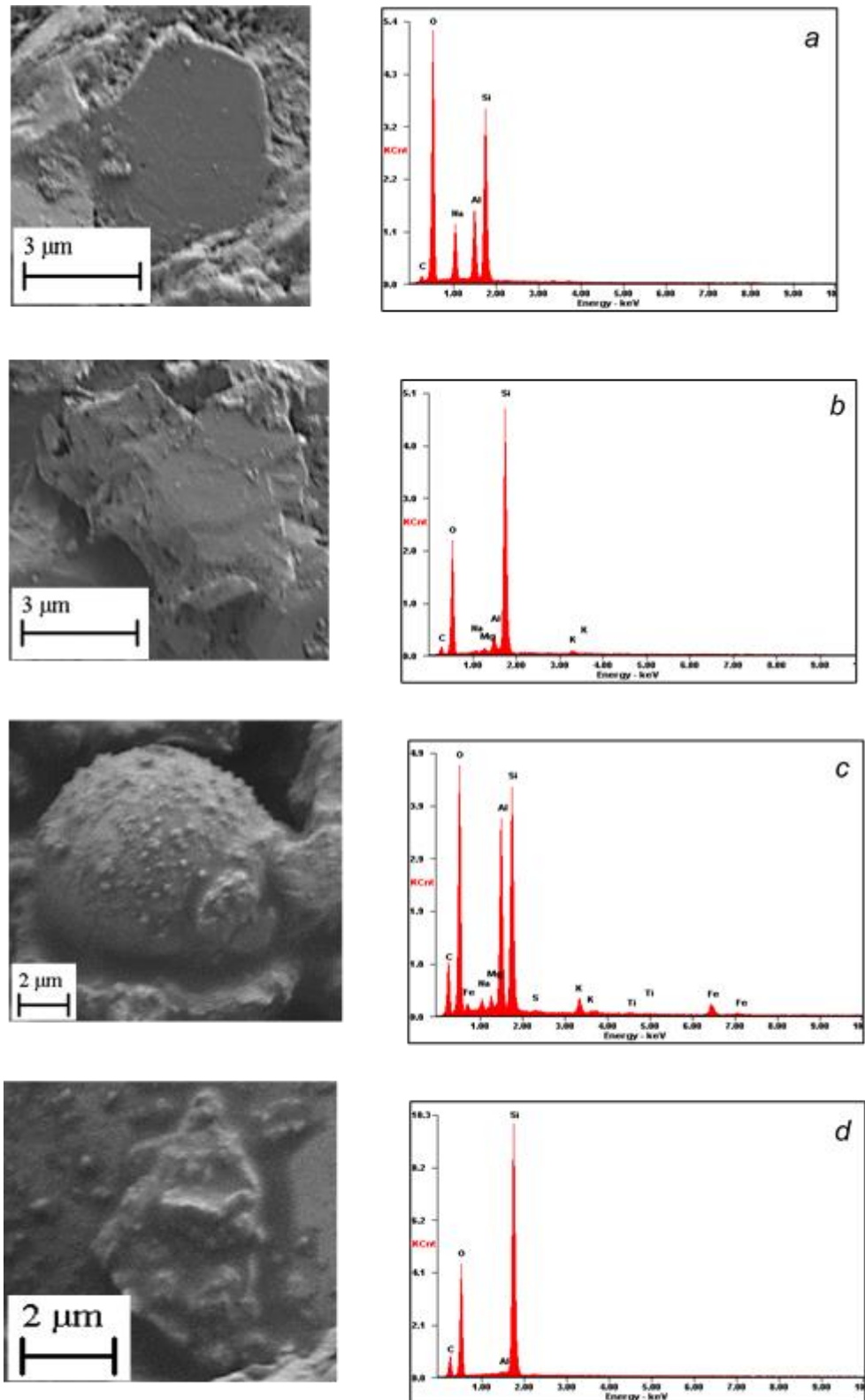
Figure 6.12: SEM images of Individual Zone A (0 – 725 m) dust particles and associated EDX spectra.
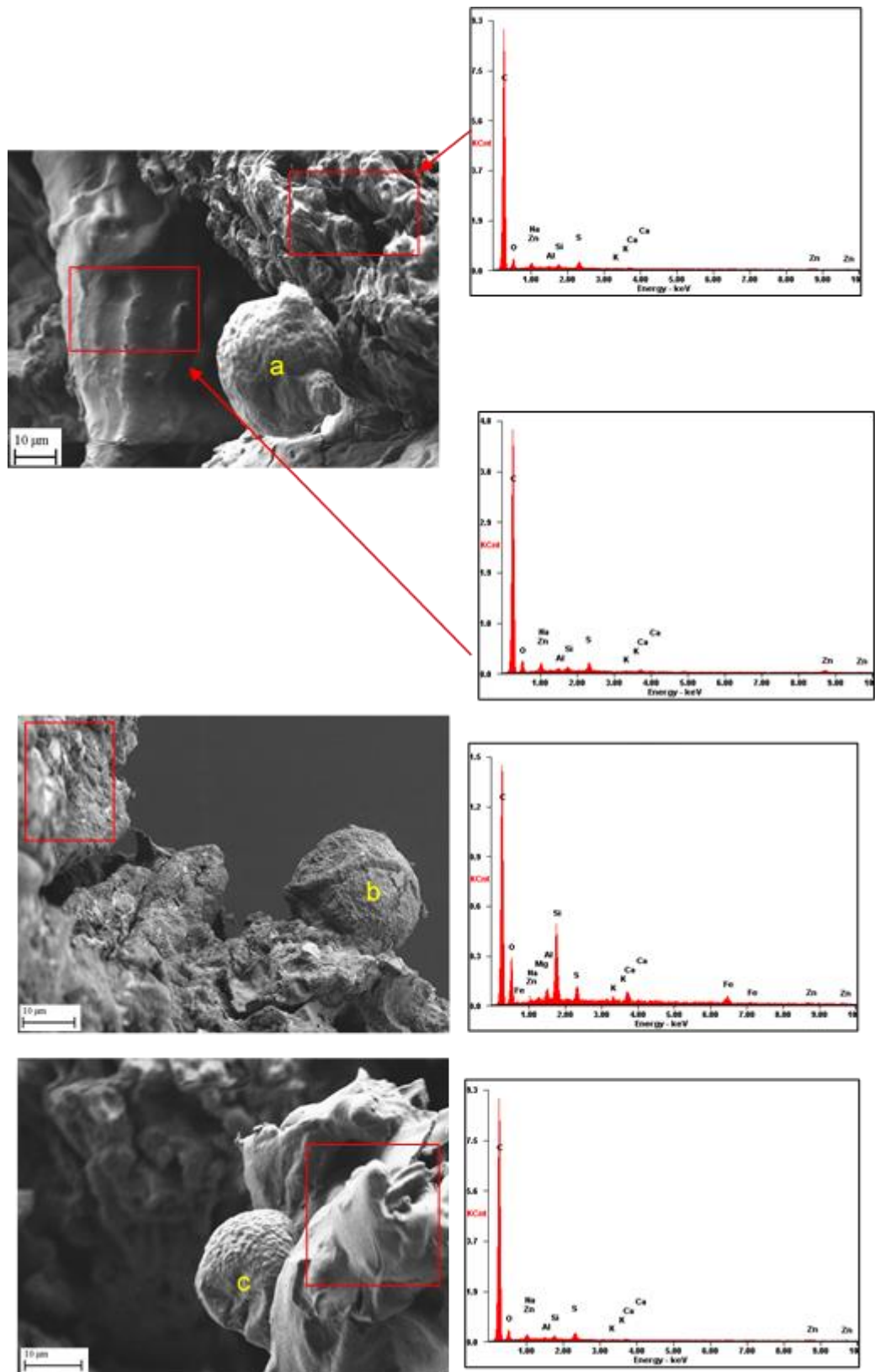
Figure 6.13: SEM images (A-C) showing the general morphological composition of the runway dusts (Zone B: 2300 – 3000 m) and individual particles (*a* - *c*). The EDX spectra for each image relates to the area within the red box. The EDX spectra of the specific particles are shown in Figure 6.14.
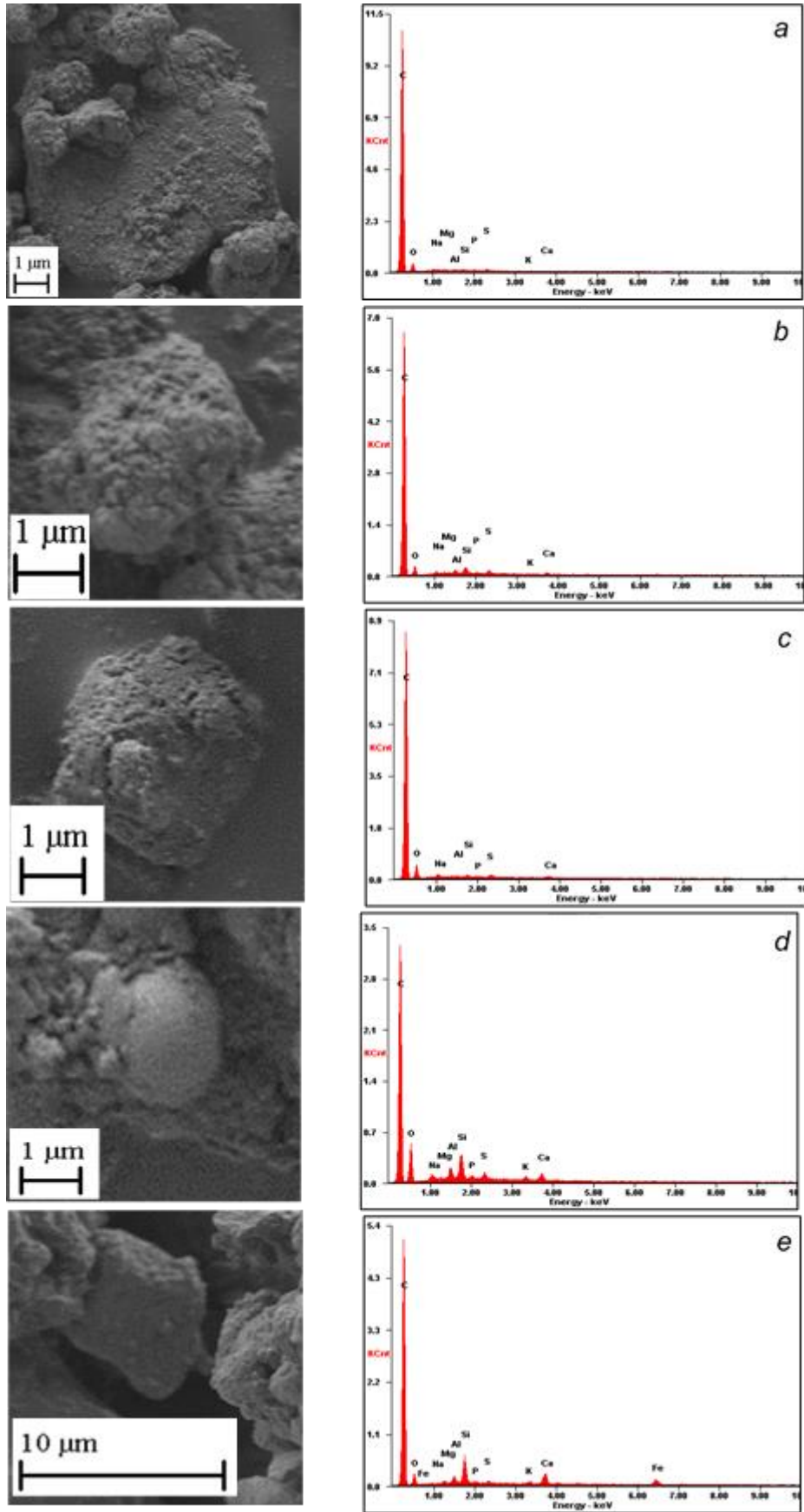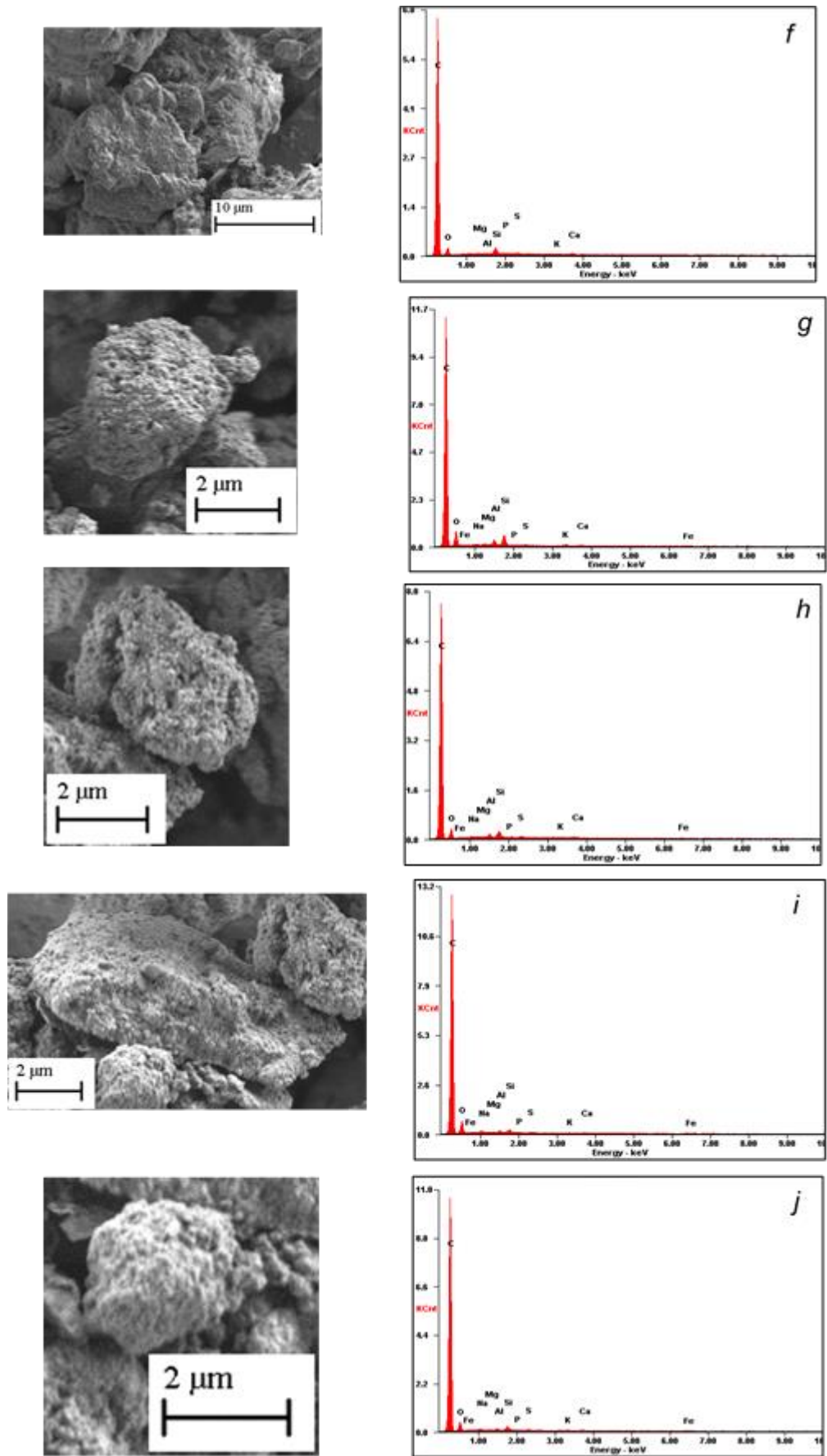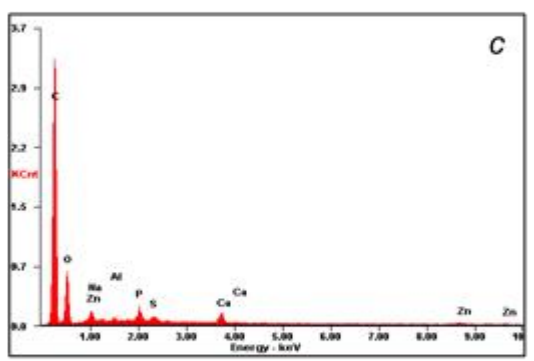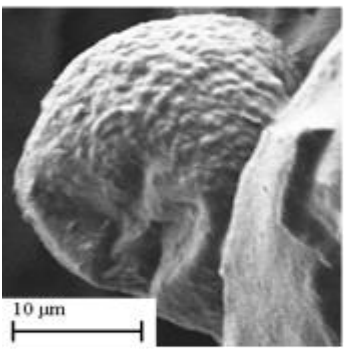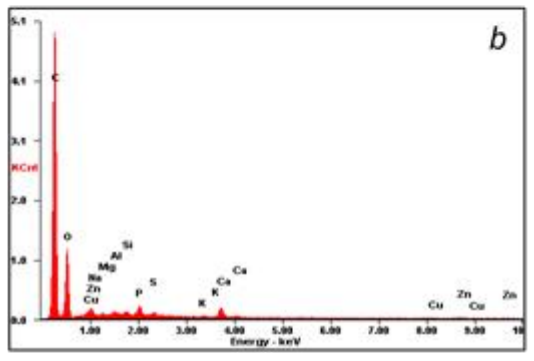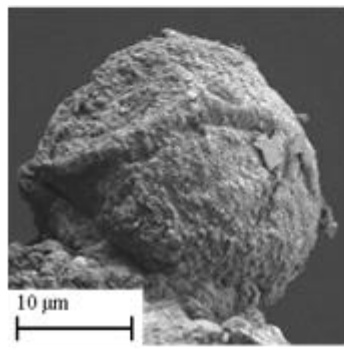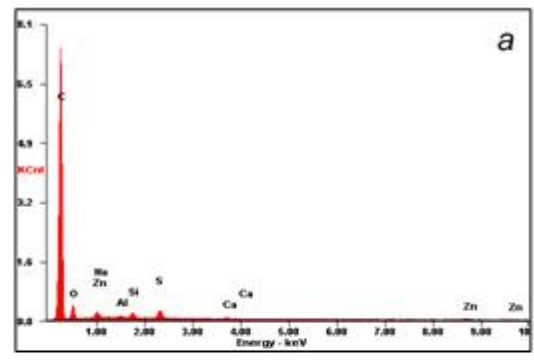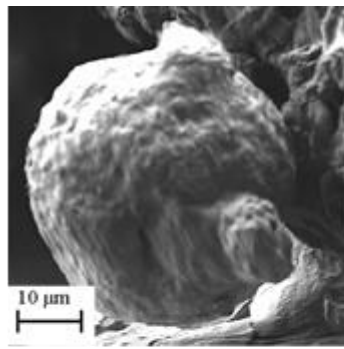
Figure 6.14: SEM images of individual runway dust particles (Zone B: 2300 – 3000 m) and associated EDX spectra.

6.2.2 Taxiway and Apron Dusts

i)   *Particle size (μm)*

The particle size diameter (μm) of the taxiway and apron dust samples (Figure 6.15) shows that the particles within the taxiway dust samples are distributed across a range of particle sizes within the ≤ 20 μm categories. The highest % of these particles (45%) are within the 0-5 μm size range.   The distribution of particles then decreases with size with 25%; 15% and 10% being displayed within the 5-10 μm; 10-15 μm and 15-20 μm categories respectively. Within the apron dust samples there is wide variation in particle size from 0 to 60+ μm. However, the majority of these particles fall within the 0-5 μm (23.1%) and 5-10 μm (38.5%) size categories.

ii)   *Particle roundness*

The particle roundness for the taxiway and apron dusts is shown in Figure 6.16. There is wide variation in particle roundness within the taxiway dusts which are distributed across the full range of categories, although, the rounded and angular categories contain the highest distribution (%) of 40.9% and 31.8% respectively. The apron dust particles are distributed across the rounded, sub-rounded and angular classifications with angular being the predominant category containing 61.5% of particles.

iii)   *SEM/EDX*

The taxiway dust samples display 'blocky' and consolidated 'granular' like textures (Figure 6.17). The chemical composition of the areas identified in Figure 6.17 are predominantly composed of C (27.0 – 55.9%) and O (39.1 – 52.1%) with smaller amounts of Si (1.6 – 11.3%) and Al (1.1 - 5.5%) also present. Smaller amounts (i.e. <2.2%) of other elements including Ca; Mg; Zn; Fe; K; S; P and Ti are also evident. The rounded and sub-rounded particles display smooth surface textures (Figure 6.18) with smaller particles adhered to these surfaces.   The main elements within the taxiway particles (Figure 6.18) are C (6.8 – 69.0%); O (26.9

– 59.0%); Si (0.3 – 16.3%); Al (0.3 – 14.8%) and Ca (0.1 – 10.2%). Other key elements that are present within all particles but in much smaller quantities (<4.7%) include Mg; Fe and K. In addition to this, low concentrations of other elements (<0.7%) are also evident within some particles including Zn; S; Na; Mn; Ti and P.

The apron dusts display consolidated 'granular'; 'blocky' and 'crumb' like textures (Figure 6.19). The elemental composition of the specific areas (Figure 6.19) are largely comprised of C (33.9 – 62.7%) and O (28.9 – 44.1%) with Si (1.6 – 8.5%); Ca (0.6 – 6.2%) and trace amounts (<3.5) of Al; Mg; Fe; K; S; Na; Ti and P. The main elements within the apron dust particles (Figure 6.20) include C (10.3 – 67.2%); O (25.7 – 64.9%); Si (0.6 – 24.8%); Al (0.5 – 7.0%) and Ca (0.3 – 12.1%). Other elements which are present in much smaller quantities (<1.8%) within some of the particles include Fe; Mg; S; K; P; Na; Zn; Ti and Cu.
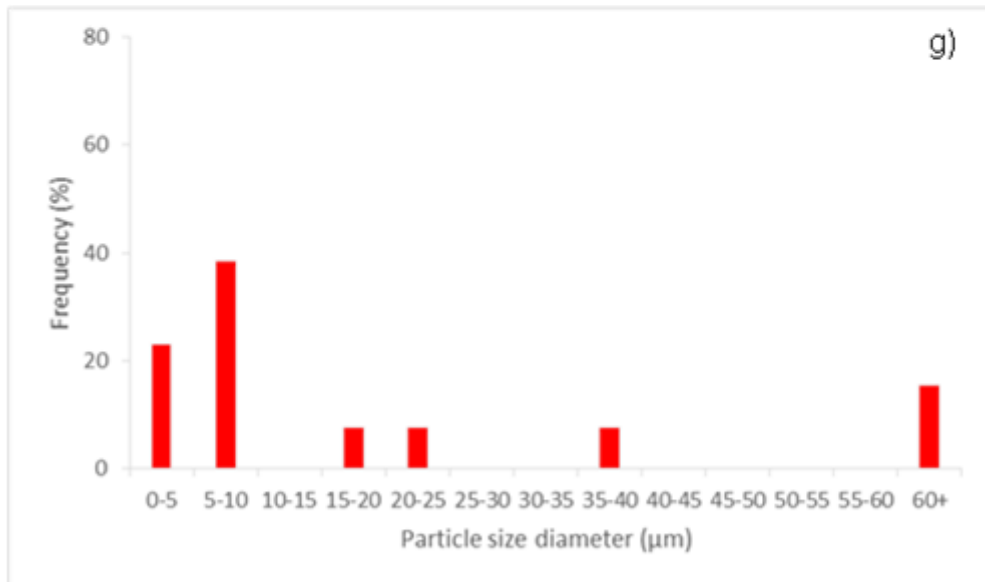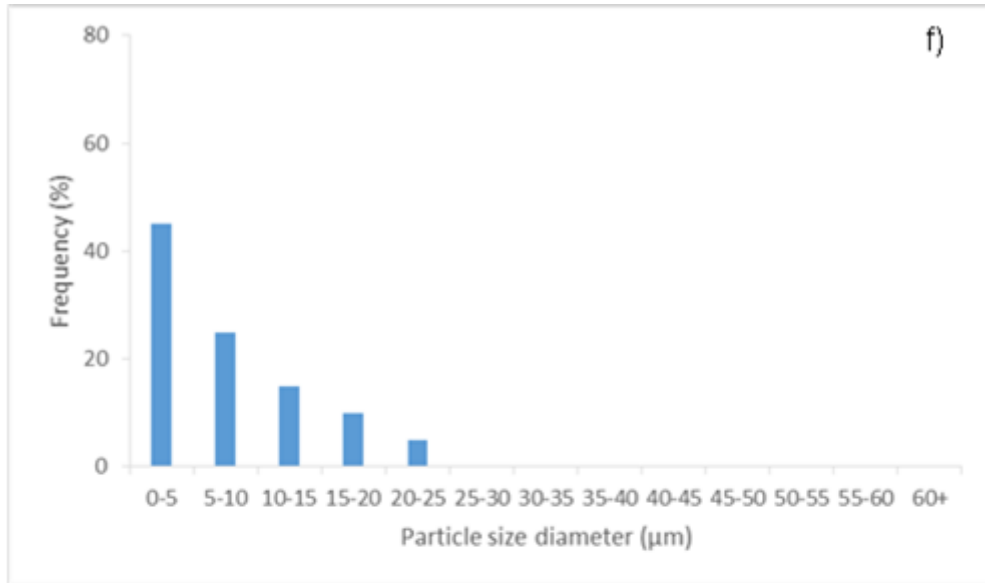
Figure 6.15: Particle size diameter (µm) for the taxiway and apron dust samples: a) Taxiway, b) Apron.
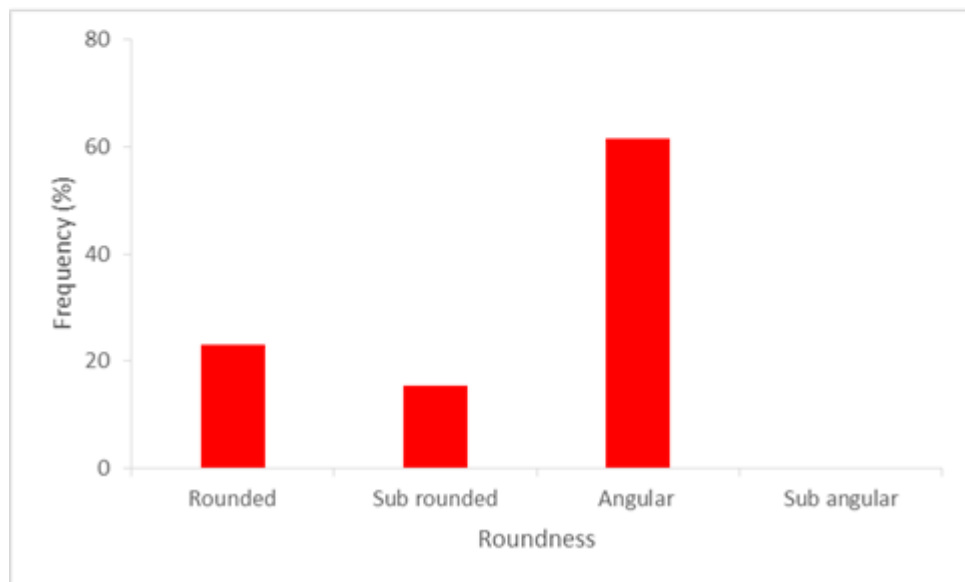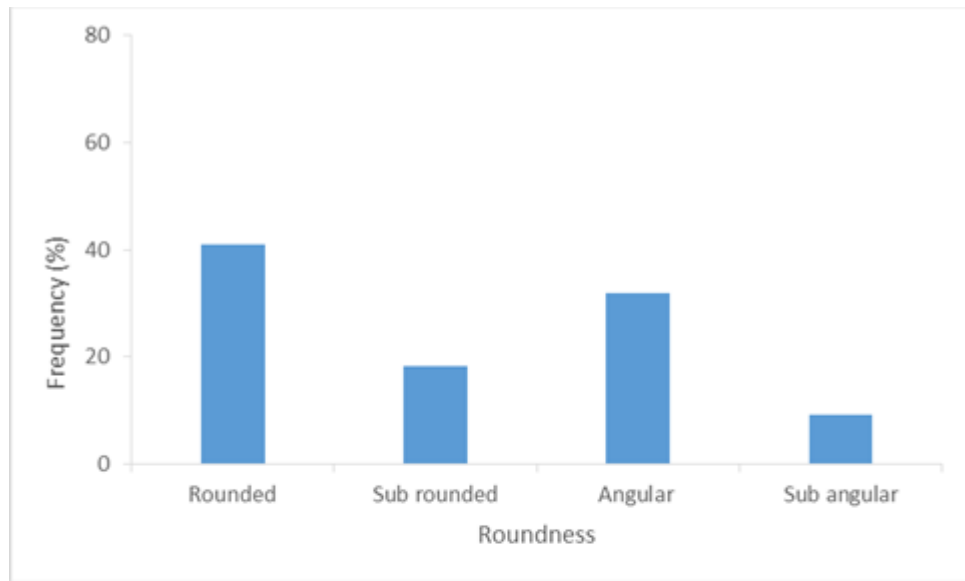
Figure 6.16: Particle roundness (frequency %) for the taxiway and apron dust samples: a) Taxiway, b) Apron.
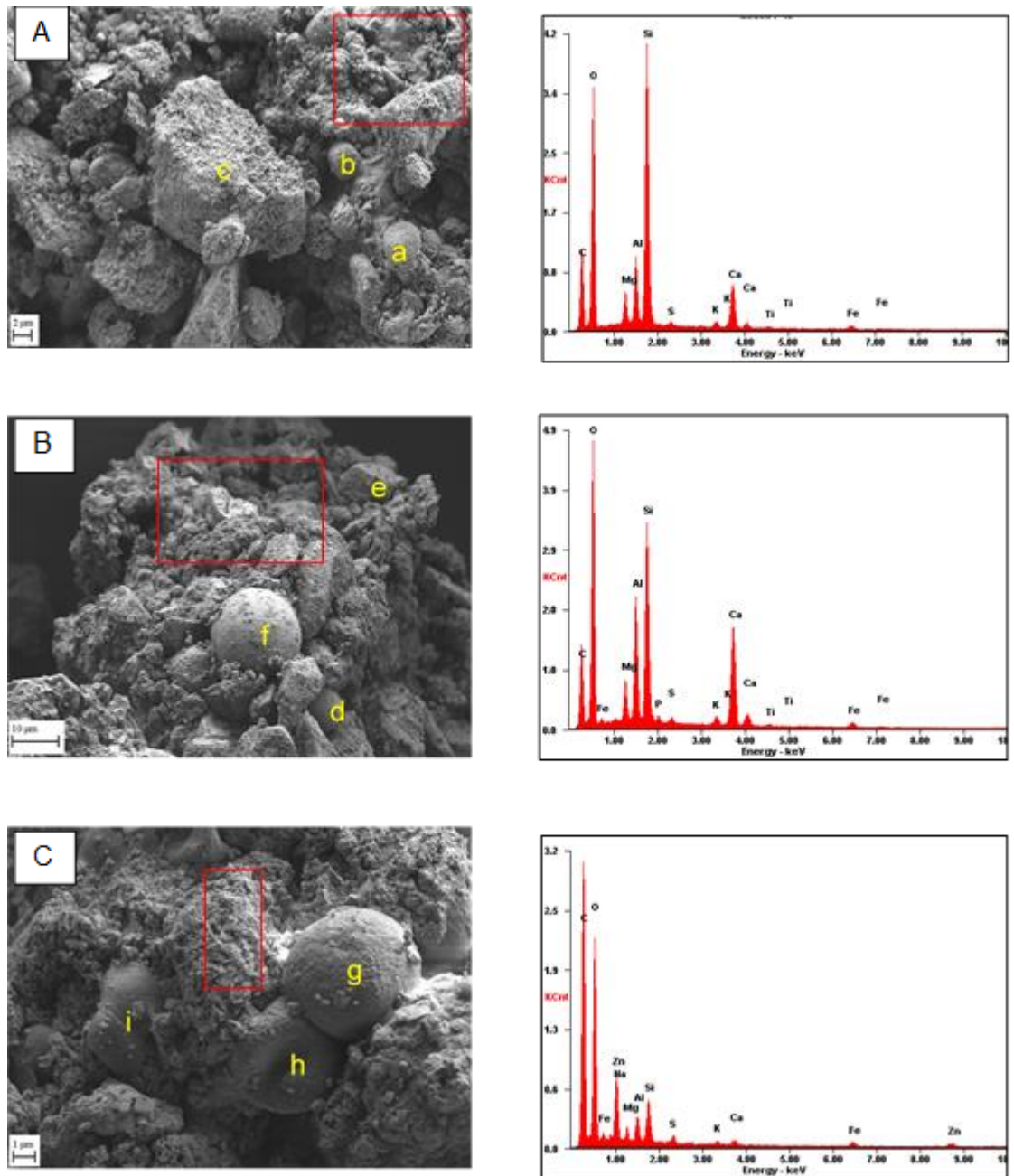
Figure 6.17: SEM images (A-C) showing the general morphological composition of the taxiway dust samples and individual particles (*a - i*). The EDX spectra for each image relates to the area within the red box. The EDX spectra of the specific particles are shown in Figures 6.18a and 6.18b.
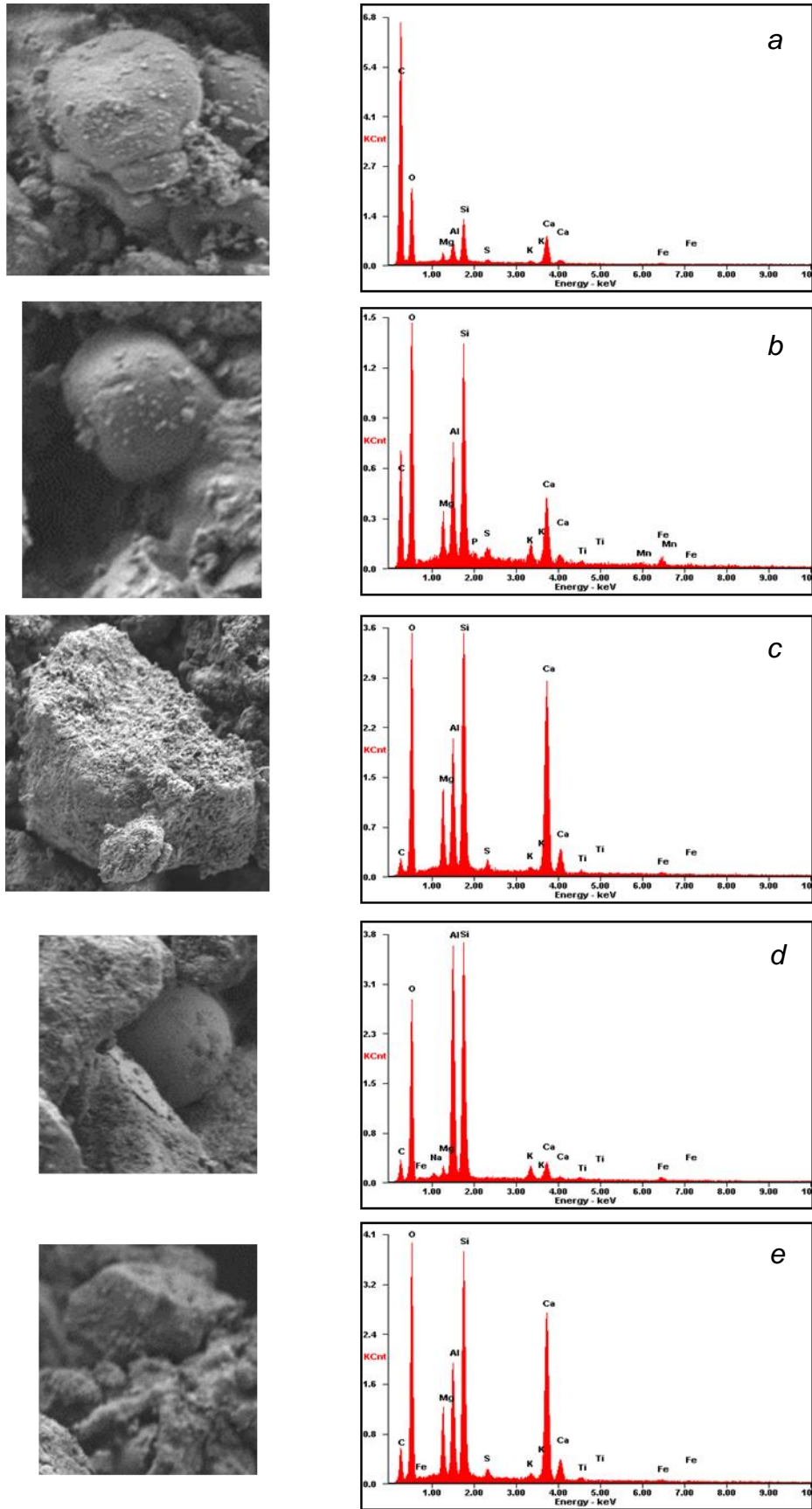
Figure 6.18a: SEM images of Individual taxiway dust particles (*a* to *e*) and associated EDX spectra.

142
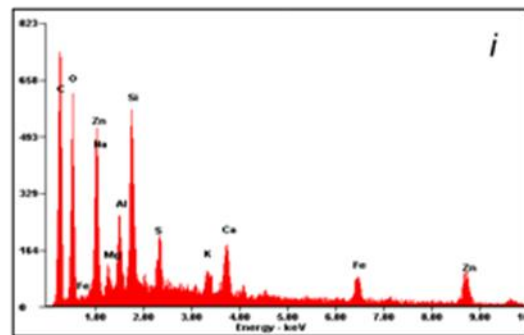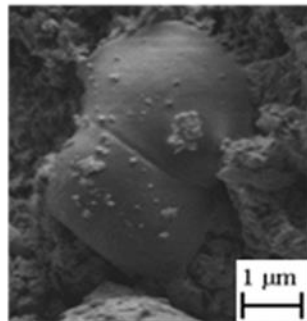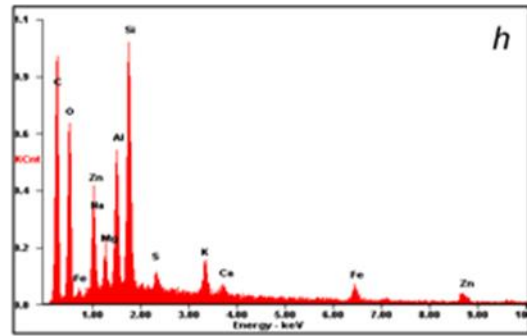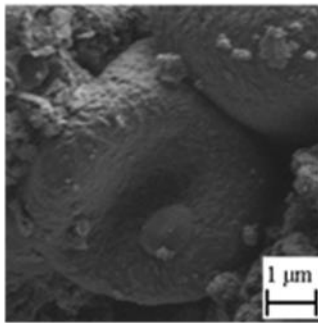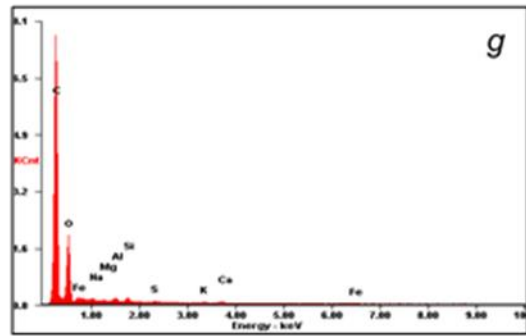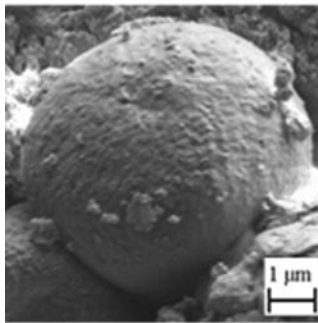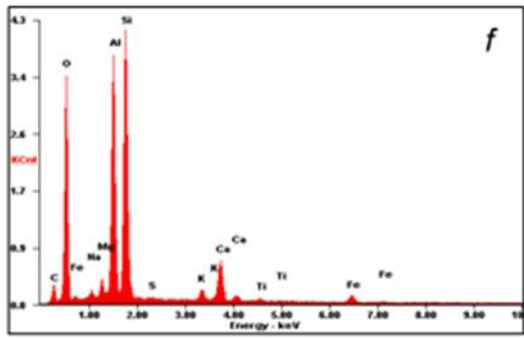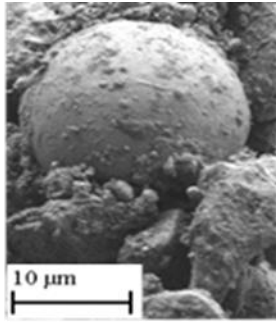
Figure 6.18b: SEM images of Individual taxiway
dust particles (*f* to *i*) and associated EDX spectra.
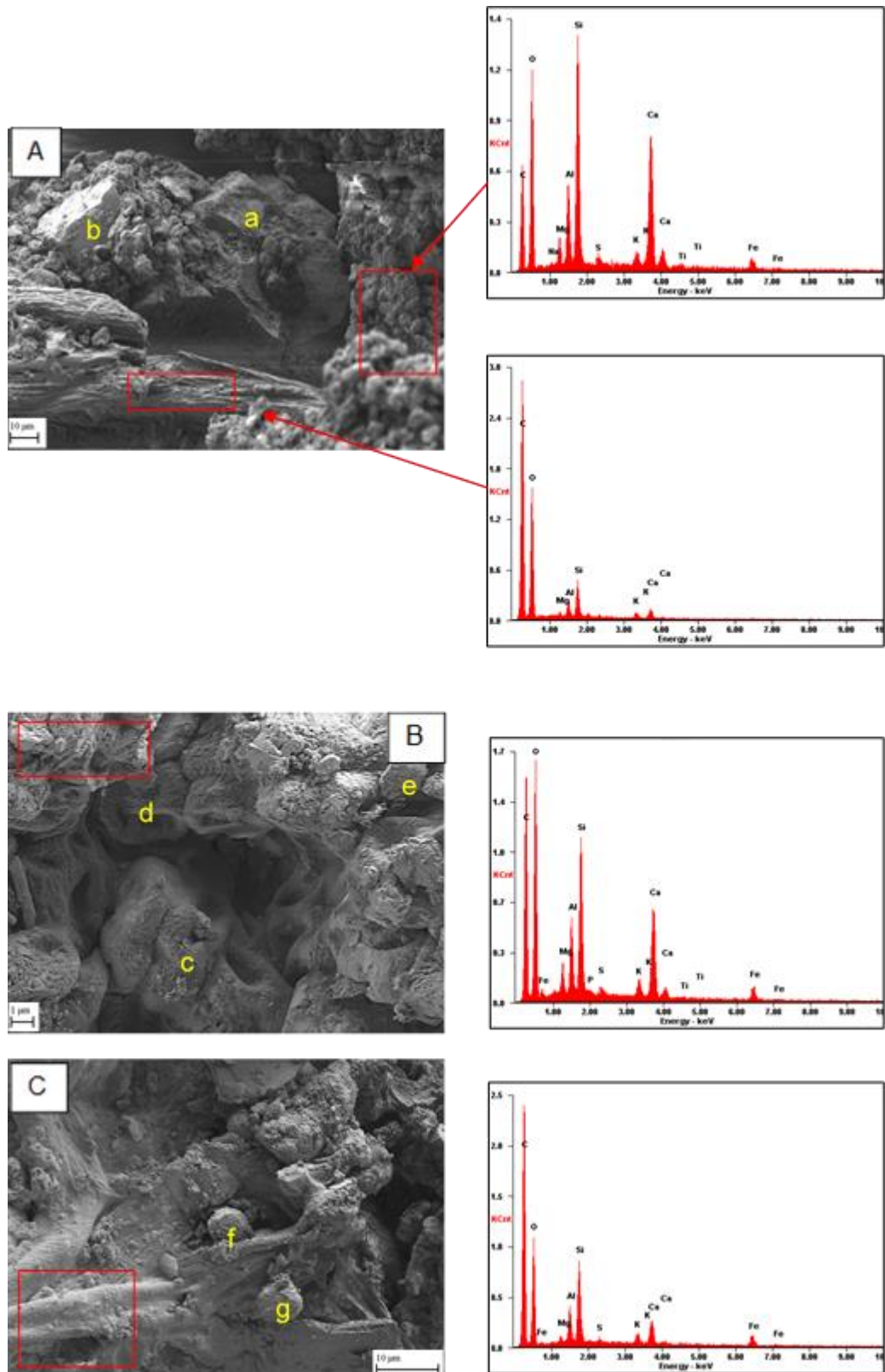
Figure 6.19: SEM images (A-C) showing the general morphological composition of the apron dust samples and individual particles (*a - g*).   The EDX spectra for each image relates to the area within the red box. The EDX spectra of the individual particles are shown in Figures 6.20a and 6.20b.
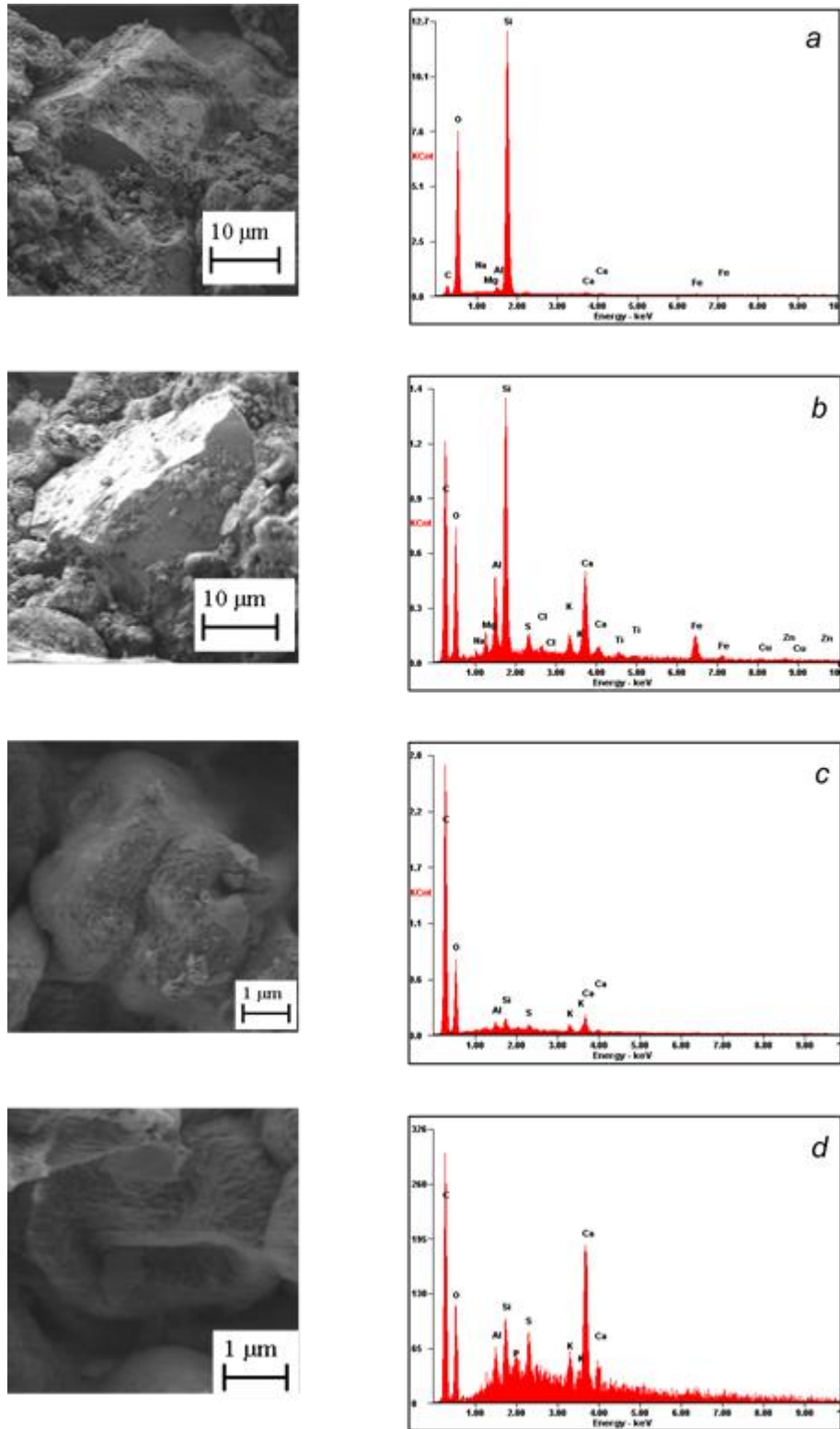
Figure 6.20a: SEM images of Individual apron dust particles *(a* to *d*) and associated EDX spectra.
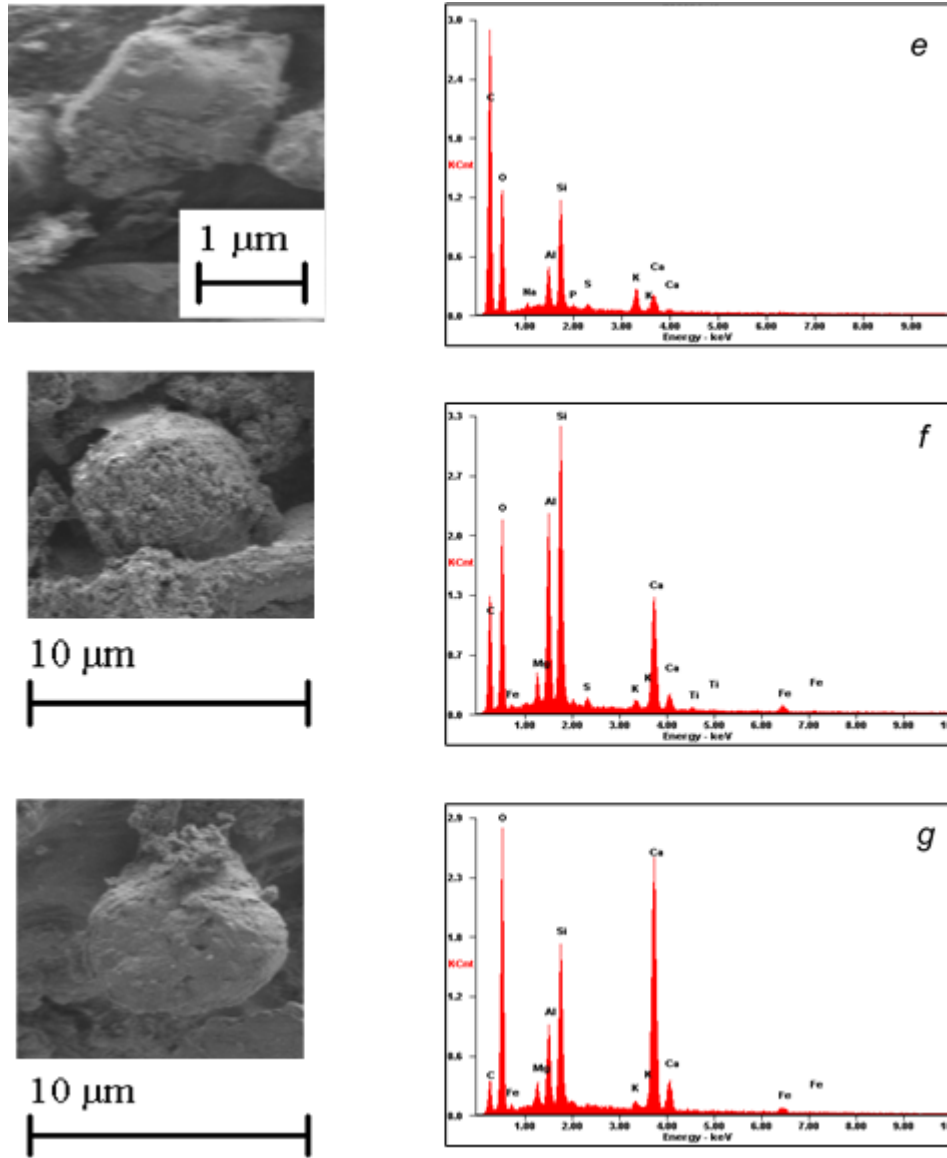
Figure 6.20b: SEM images of Individual apron dust particles *(e* to *g)* and associated EDX spectra.

Chapter 7

Results: Electron Spin Resonance (ESR)

Chapter 7 (Sections 7.1 to 7.2) comprises a description of the ESR analysis which constitutes the supplementary study that was completed on a small number of aircraft source and environmental samples. The ESR spectra for all samples was recorded at room temperature at X-band frequency (§ 3.8.1).

7.1 Aircraft Source Samples

7.1.1 Engine, Brake and Tyre Dusts

The ESR spectra for each of the aircraft source samples (i.e. engines; brakes and tyres) is shown in Figures 7.1 to 7.3. Distinct variations are displayed between each of the aircraft sources. The ESR spectra of each of the engine dusts is very similar although some inter-sample variability, mainly due to the amount of material present, does exist (Figure 7.1). A broad single line peak is clearly identifiable within each of the samples. The greatest spectrum intensity of this peak is evidenced in Engine 1 extending from a maxima of 118.30 to a minima of -178.63. The broad engine dust spectra displays a full width half height maximum (FWHM) of ~130mT.
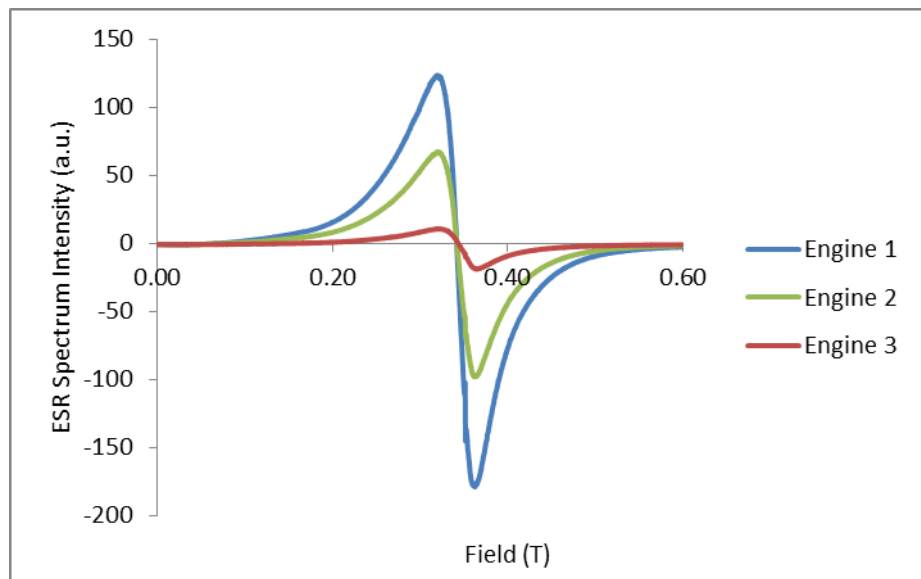
Figure 7.1: ESR Spectra of the Engine dust samples.

The brake dust samples display very similar ESR spectrum characteristics. A very distinctive narrow single line peak is clearly identifiable within each of the samples (Figures 7.2a and 7.2b). The spectrum intensity of this peak is greatest in Brake 1 reaching a maximum of 69.81 and a minimum of -85.84. The FWHM of the brake spectra is very narrow, ~2mT.
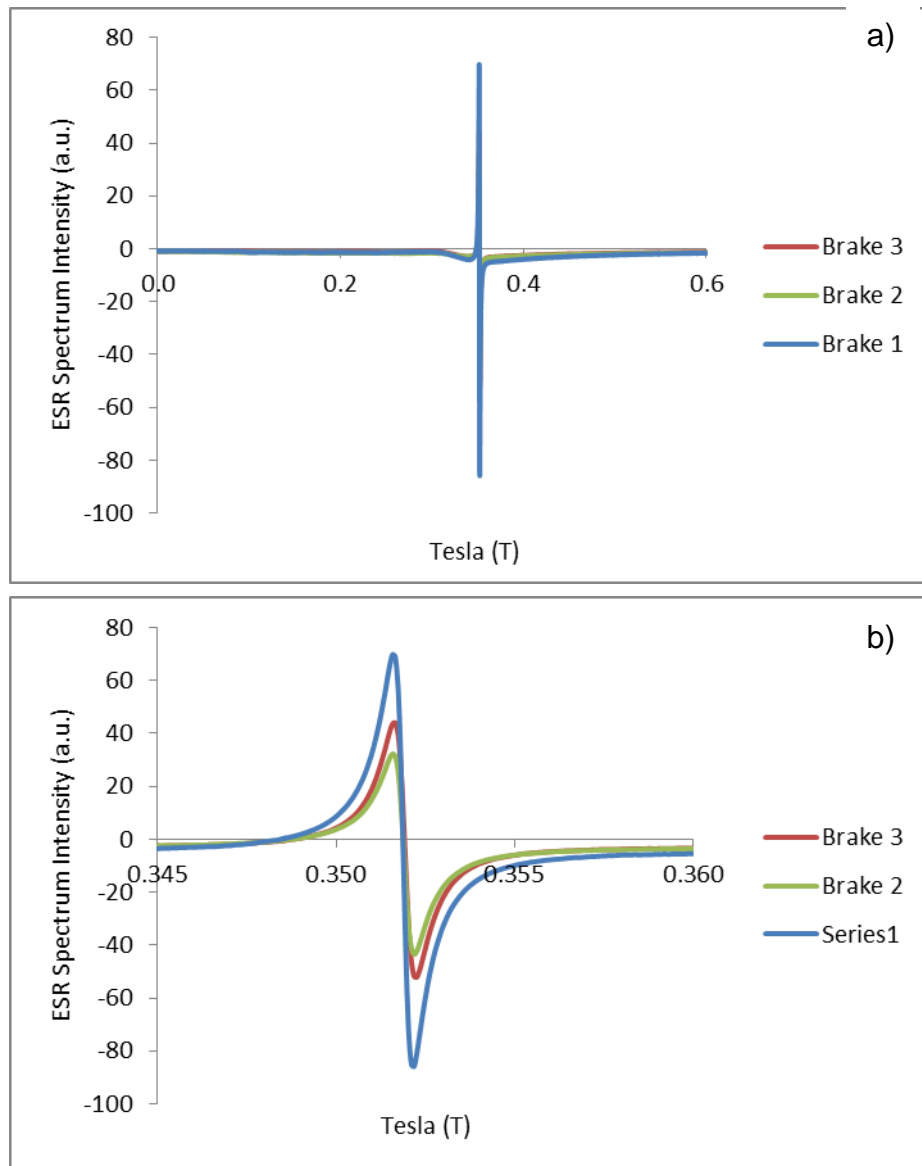
Figure 7.2: Figure (a) displays the ESR spectra of the brake dust samples; Figure (b) shows an expanded central section view of the ESR trace.

In contrast to the single line spectra of the engine and brake dusts, the tyre dusts feature a multi-line spectra which is indicative of a greater number of components (Figure 7.3). Whilst there is obvious variability between the individual samples, similar trends are observed. In tyre dust 1, three spectrum intensity peaks are clearly identifiable with values of 18.95, 35.72 and 35.06 respectively. Similar, though less intense peaks can also be seen within Tyre 2 and to a much weaker extent in Tyre dust 3. The greatest spectrum intensity is displayed within the central peak in Tyre 1 which extends from a maximum of 35.06 to a minimum of -110.45. From the central peak, the spectrum line extends into negative values after which point the spectral characteristics of the individual tyre dusts correspond very closely with each other.
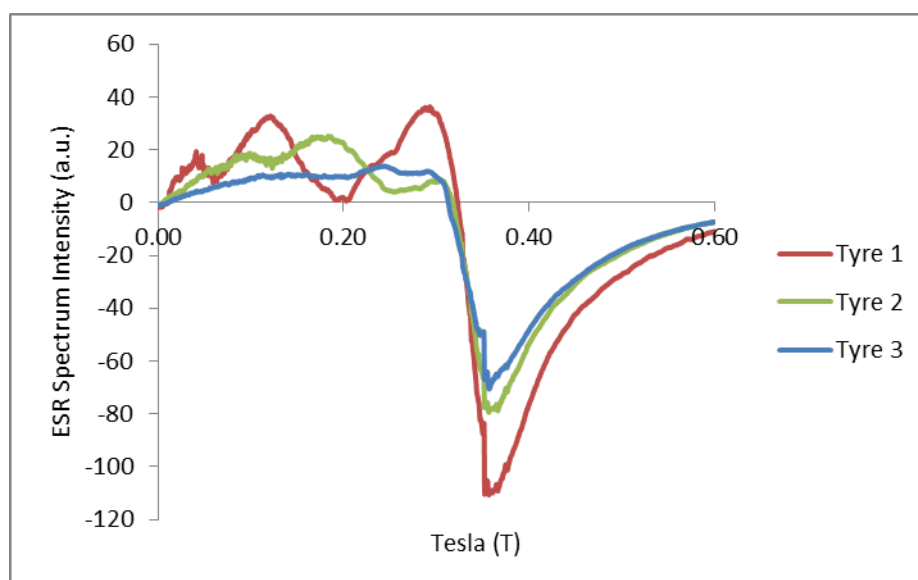
Figure 7.3: ESR Spectra of the Tyre dust samples.

7.2 Environmental Samples

The ESR spectra of the environmental samples (i.e. runway dust; taxiway dust; grass; soil and runway marking debris is displayed in Figures 7.4 to 7.8. Distinct variability is shown in the spectra of the samples from each of the different environments.

149

7.2.1 Runway marking debris

During the collection of dusts from hard surfaces, paint debris was noted to be present in several samples. The ESR spectrum of the runway marking debris (yellow paint) fragment is displayed in Figures 7.4a and 7.4b. The presence of a very distinctive six line hyperfine spectrum is clearly evidenced between ~0.32 and ~0.38T. It is so distinctive that it can be immediately identified as being due to the presence of Mn^{2+} ions.
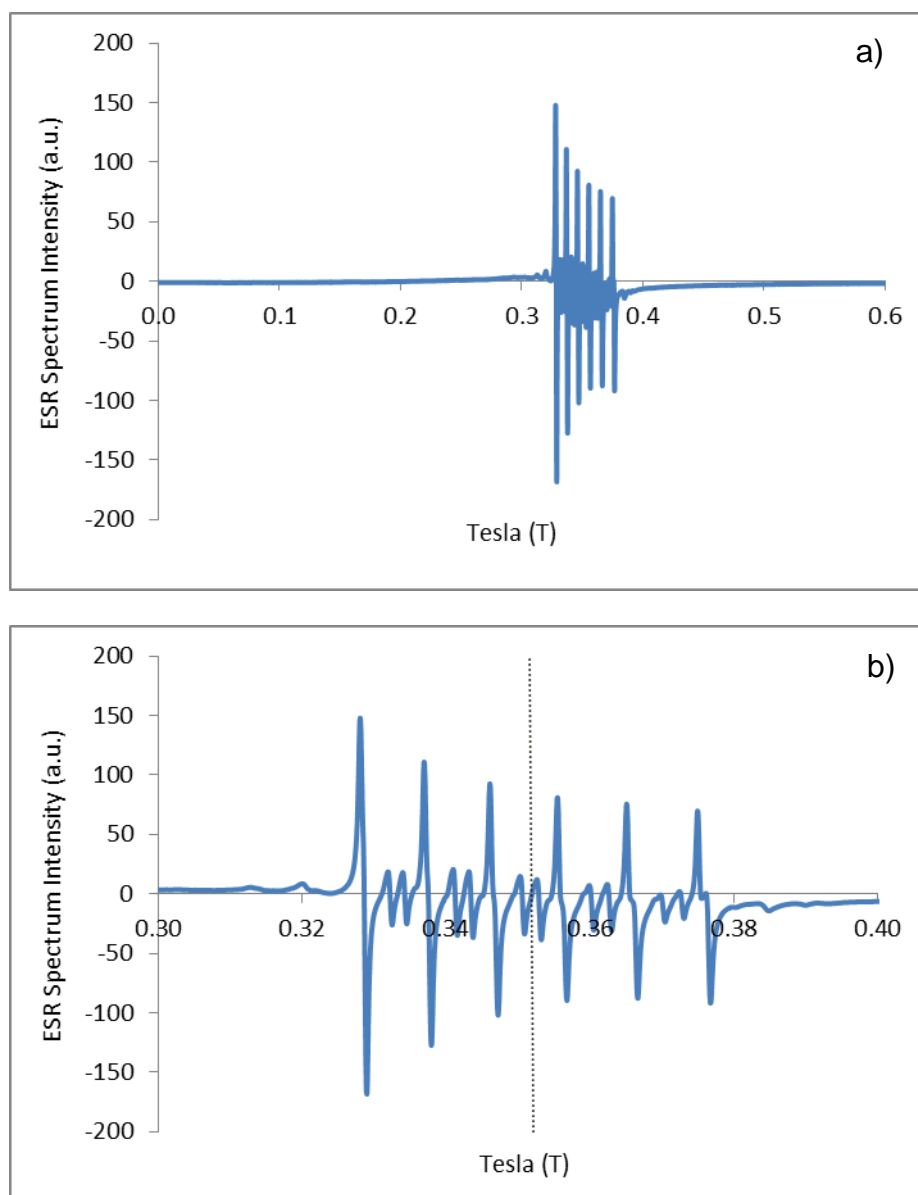
Figure 7.4: Figure (a) displays the ESR Spectra of the runway marking debris; Figure (b) shows an expanded view of the six line hyperfine feature.

7.2.2 Runway Dusts

The runway dusts (Figure 7.5) comprise a multi-line spectra indicative of several components. A weak yet distinctive six line hyperfine spectrum is clearly visible in the RD1 sample and to a much lesser extent in RD2 between ~0.32T and ~0.38T. The presence of a distinctive narrow line peak is also evident within both samples at 0.35T.
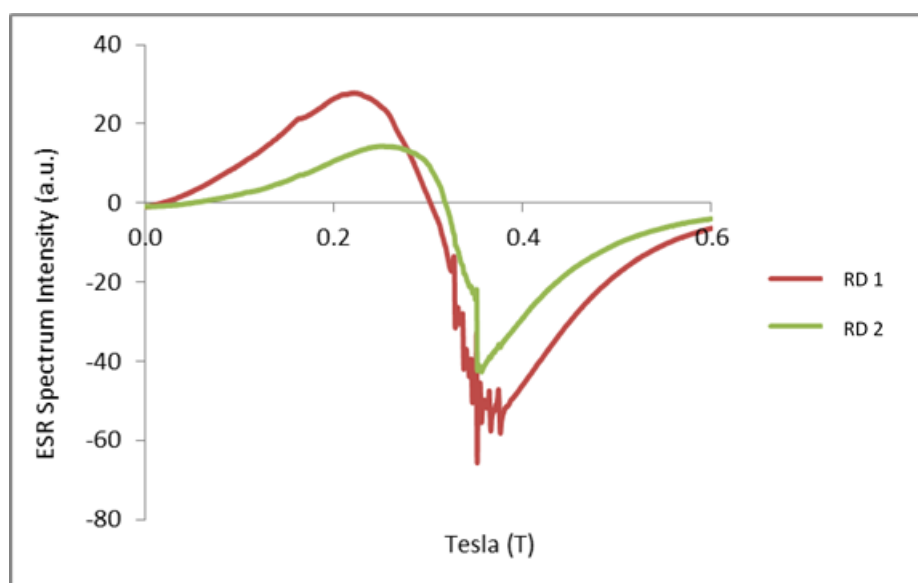
Figure 7.5: ESR Spectra of the Runway dust samples.

7.2.3 Taxiway Dust

A multicomponent spectra is clearly visible within the taxiway dust sample (Figure 7.6). Three spectrum intensity peaks can be seen at 24.83, 40.33 and 50.46 respectively. Of these, the central peak displays the greatest spectrum intensity which extends from a maxima of 50.46 to a minima of -102.21. A very narrow single line peak with a FWHM of ~2mT is also evident at a field of ~0.36T.

151
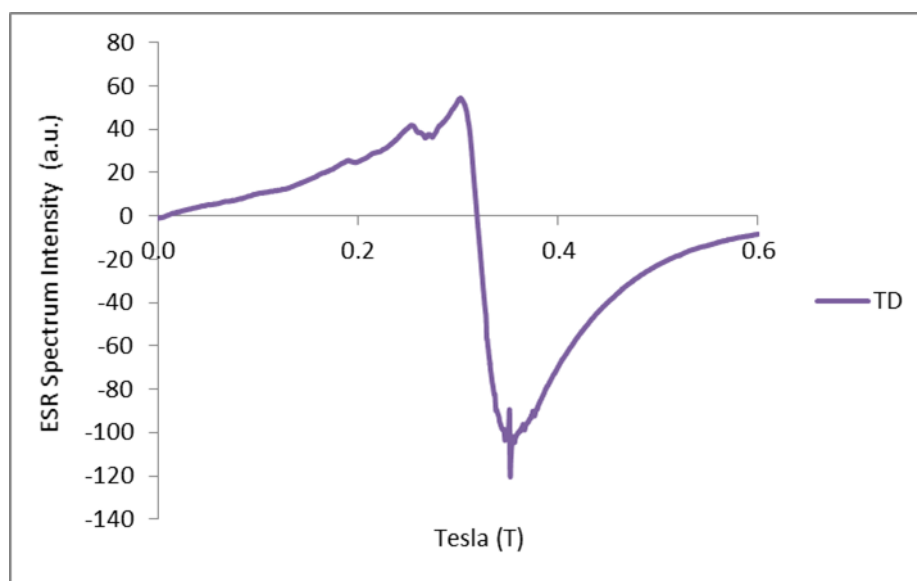
Figure 7.6: ESR Spectra of the Taxiway dust samples.

7.2.4 Grass

The ESR spectra of the grass samples (Figures 7.7a and 7.7b) is extremely weak. The very weak signal results in a base line shift and therefore the true 0 on this scale is below -1. The grasses display a number of weak yet distinctive components within the general background noise. Both samples feature a broad resonance peak at a field of ~0.12T, and a very distinctive narrow single line peak at ~0.35T. The presence of a hyperfine spectrum is clearly identifiable in Grass sample 1 between a field of ~0.33T and ~0.38T.

7.2.5 Soil

Figures 7.8a and 7.8b display the ESR spectra of the soil samples. The soils display very similar characteristics to those of the taxiway dust §7.2.2. Three clearly identifiable spectra peaks are displayed in Soil 1 at 6.3, 14.15 and 22.39 respectively. These peaks, though much weaker are also evident within Soil 2. The greatest spectrum intensity can be seen within the central peak of Soil 1 which extends from a maximum value of 22.39 to a minima of -37.73. Once again a narrow single line peak is also clearly visible in both the soil samples at 0.35T with a FWHM of ~2mT.
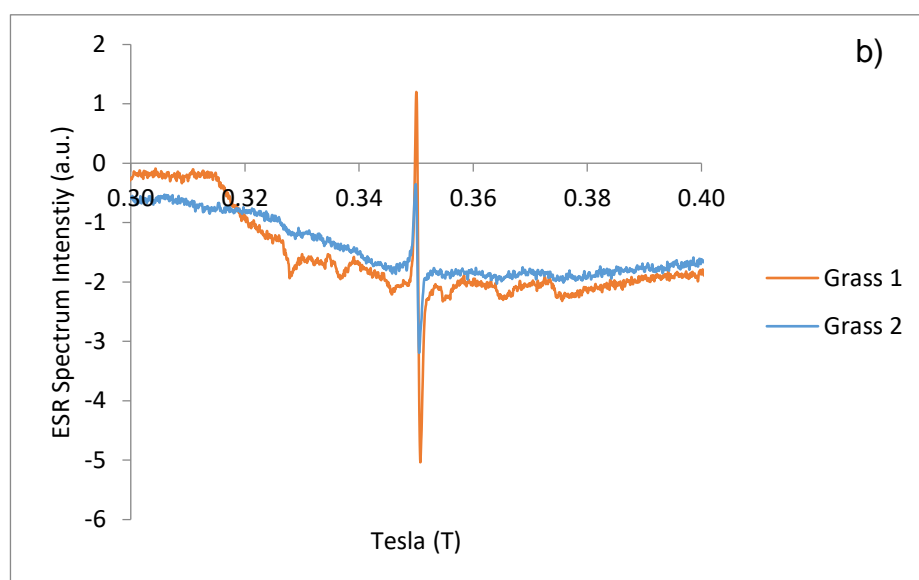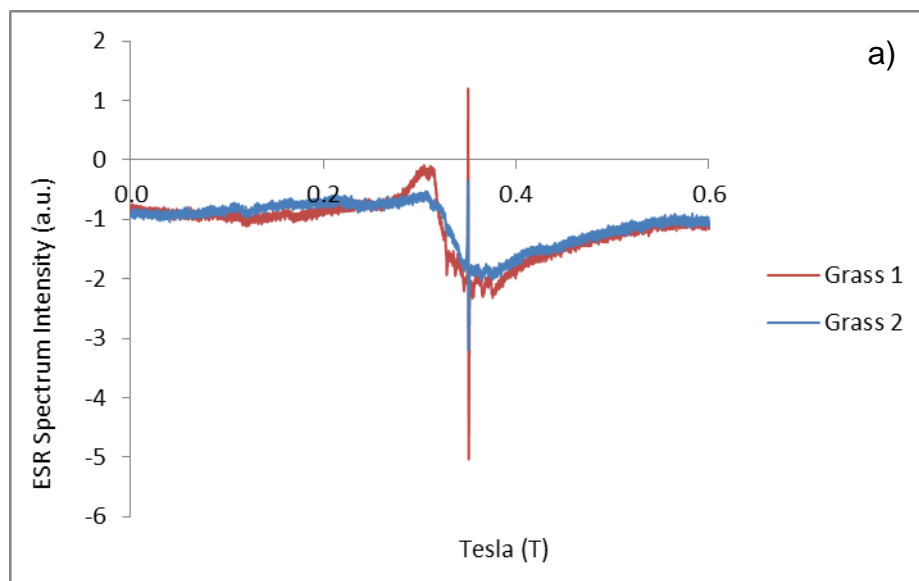
Figure 7.7: Figure (a) displays the ESR Spectra of the grass samples; Figure (b) shows an expanded central section view of the ESR trace.
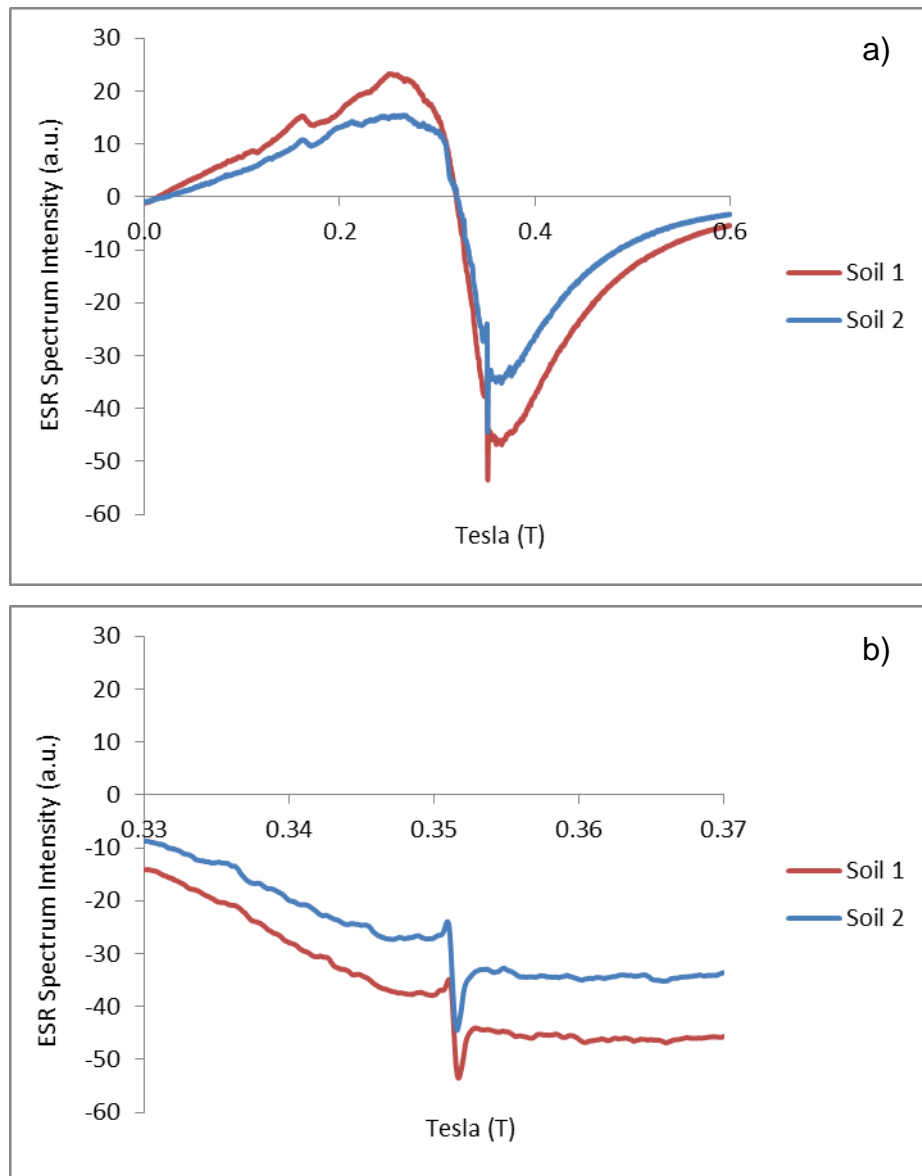
Figure 7.8: Figure (a) displays the ESR Spectra of the soil samples; Figure (b) shows an expanded central section view of the ESR trace.

Chapter 8

Discussion

Chapter 8, Sections 8.1 to 8.5 comprises a discussion and synthesis of the magnetic measurements, chemical analysis, SEM/EDX and ESR results which are presented in Chapters 4 to 7.

8.1 Magnetic measurements

The magnetics results along with an initial interpretation of this data have previously been outlined in Chapter 4 (§ 4.1 – 4.4). Interparametric ratios ($\chi ARM/\chi$ and $\chi ARM/SIRM$) were unavailable for the runway dusts and grass samples due to low sample masses (runway dusts) and low magnetic mineral concentrations (runway dusts and grass samples) preventing the accurate measurement of χ and ARM. Therefore, within sections 8.1.1.1; 8.1.1.3 and 8.1.1.4 references made with regard to ferrimagnetic grain size are based entirely on the $IRM_{-20mT}/SIRM$ ratio.

8.1.1 Aircraft Source Samples

The magnetic mineral composition and grain size characteristics of each of the aircraft source dust samples (i.e. aircraft engine, brake and tyre) has been investigated in (Chapter 4.1). The results show that there is a clear distinction between the magnetic mineral characteristics (grain size and magnetic mineral type(s)) within each of the three dust groups. The magnetic assemblages within the engine dusts are comprised predominantly of finer ferrimagnetic minerals with a significant antiferromagnetic component. The current analysis has provided no strong evidence of differences in the magnetic assemblages between the samples collected from different engine types but would be an appropriate element of a follow-on-study. In contrast to the engine dust samples, the brake and tyre dusts are characterised by coarser grained ferrimagnetic minerals. Further confirmation of the difference in the magnetic mineral characteristics of

the source samples has been achieved through the use of cluster analysis and cross plots.
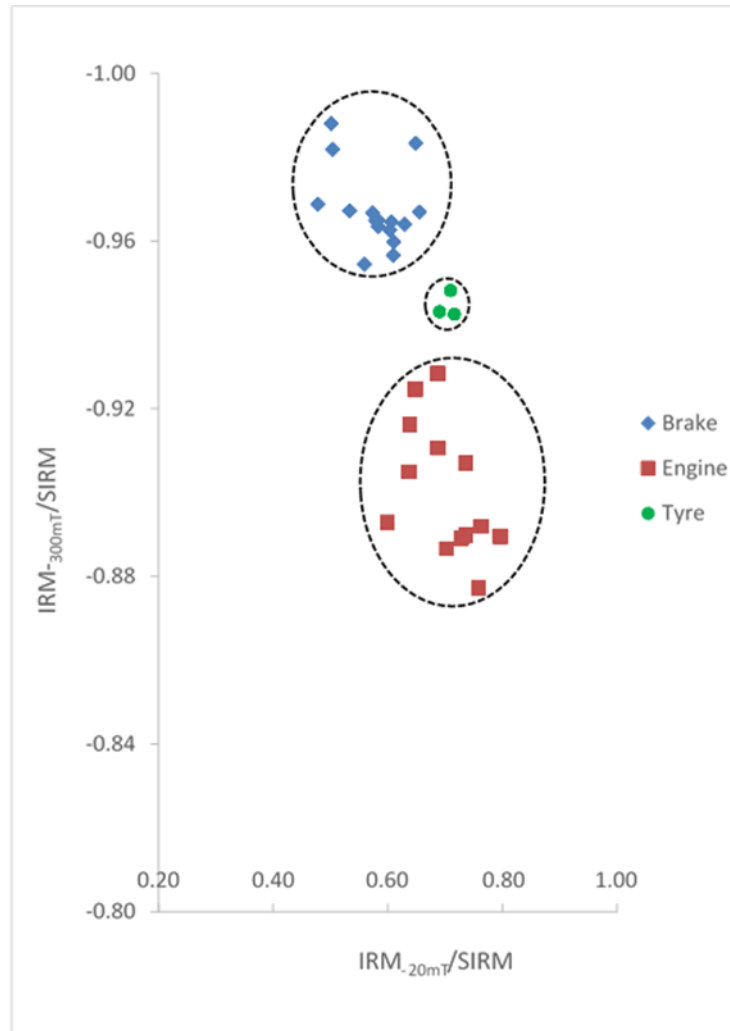
Figure 8.1: IRM$_{-20mT}$/SIRM versus IRM$_{-300mT}$/SIRM for the aircraft engine ($n = 13$), brake ($n = 16$) and tyre dusts ($n = 4$).

Cluster analysis based on the data from the four magnetic parameters (i.e. χARM/χ; χARM/SIRM; IRM$_{-20mT}$/SIRM; IRM$_{-300mT}$/SIRM) was used to assess whether each of the aircraft source samples (i.e. engine; brake and tyre dusts) could be classified into distinctive groups. An agglomerative method was applied to all the data and normalised to eliminate differences in magnitude between the variables. The analysis revealed that there were three major groups, one of which contained all of the engine dust samples, another containing the brake dusts and a third containing all of the tyre dust samples (Appendix 5).

156

Figure 8.1 plots IRM$_{-20mT}$/SIRM versus IRM$_{-300mT}$/SIRM for each sample set and illustrates the contrast in the magnetic mineral characteristics of the engine; brake and tyre-derived particulates. The range of variation in the lower reverse field ratio (IRM$_{-20mT}$/SIRM) is only slight and therefore it does not clearly differentiate between each sample set, however, the higher reverse field ratio (IRM$_{-300mT}$/SIRM) discriminates between the three sample sets very effectively. The more positive IRM$_{-300mT}$/SIRM ratios displayed by the engine dusts indicate that these samples contain a more significant antiferromagnetic component than the brake dusts which display less positive higher reverse field ratios and the tyre dusts which display ratios that are intermediate between the engine and brake dusts.

The variations in magnetic characteristics that are displayed between the individual sources, must result from differences in the nature of the iron content within aviation fuel (Jet A-1), Carbon-Carbon (C/C) brakes and aircraft tyres, and the combustion processes and conditions at the point of conversion of non-magnetic or weakly magnetic forms of iron into magnetic iron oxides.

The incomplete combustion of jet fuel, within the combustion section of the jet engine, generally results in the formation of ultrafine particulates which are a key component of aircraft exhaust emissions (Starik, 2008; Webb et al., 2008). The primary particulates are predominately carbonaceous material (or soot) and are composed of organic compounds and elemental or black carbon (§ 8.4.1) (Petzold et al., 2005; Herndon *et al.*, 2008; Dodson *et al.*, 2009). Metal particles derived from engine erosion and iron impurities within the Jet A-1 fuel used by commercial aircraft (Penner *et al.*, 1999; Jones, 2008; Abegglen *et al.*, 2016) (Table 8.1), may also be a component of the ultrafine particulate matter emitted by aircraft engine emissions (Starik, 2008; Mazaheri *et al.*, 2013). Iron impurities are converted into magnetic iron oxides during high temperature combustion which then contribute to the primary, non-volatile particulate matter. The specific nature of the iron impurities in the Jet A-1 fuel and/or the chemical processes which take place during the fuel combustion stage may relate to the significant antiferromagnetic mineral (haematite-like) content of these particulates (Flanders, 1994).

Table 8.1: Concentrations [g/kg^{-1}] of the most abundant metallic elements in sampled Jet A-1 fuel detected using ICP-MS (Adapted from Abegglen *et al.*, 2016).

Element	Jet A-1 fuel
Calcium	0.11315
Vanadium	0.00359
Aluminium	0.00308
Lead	0.00198
Iron	0.00169
Magnesium	0.00146
Titanium	0.00145
Sodium	0.00105
Copper	0.00196
Antimony	>0.0001
Chromium	(−)
Others	0.00491

The operation of aircraft braking systems occurs during routine aircraft manoeuvres including taxiing, landing and during undercarriage retraction upon take-off. These operations result in the production of brake dust or wear debris, largely resulting from the mechanical and/or chemical reactions which take place on sliding surfaces (Hutton *et al.*, 1999; Rietsch *et al.*, 2009). Modern aircraft brakes are comprised of C/C combinations owing to the stable behavioural characteristics which they feature at high temperatures (Wu *et al.*, 2016). C/C brakes contain additives, which may include iron oxides such as magnetite. Such additives act as antioxidants and are also used to modify the temperature characteristics and the mechanical and friction properties which occur during braking operations (Blau, 2001).

The operation of aircraft brakes during taxing and landing results in frictional heat generation. This process, which is most prevalent during the landing stage, results in brake lining wear. The resultant particles, form a friction film of abraded wear debris, which often becomes adhered to the wear surfaces of the C/C composite brakes and which is subsequently released as airborne particulate matter (Hutton *et* al., 1999; Curran, 2006).

Coarse grained ferrimagnetic minerals are likely to result from the conversion of iron additives or impurities within the matrix of the C/C brake, as a result of the elevated temperatures and chemical reactions which occur at the sliding/rubbing interface. This may be anticipated due to the oxidising environment and the extremely high operating temperatures (300 – 400 °C (BA Engineering, pers. comm.)) which occur within the braking mechanism area. The resultant ferrimagnetic (i.e. magnetite/maghemite-like) minerals are a component of the particulate matter that forms the brake wear debris which is ejected during braking.

The coarse grained ferrimagnetic minerals which are a feature of the tyre dusts, are a component of the PM, which is formed during retraction of the undercarriage as the nose wheel tyre rubs against the 'snubber pads'. During this short term phase, the temperatures resulting from frictional heat generation must be high enough to convert any iron impurities within the composition of the tyre into magnetic forms of iron oxides. Detailed information relating to the composition of aircraft tyres is unavailable due to the commercially sensitive nature of the data (BA Engineering, pers. comm.). However, aircraft tyres are known to contain metals amongst a variety of other materials (Lobo *et al.*, 2013).

8.1.2 Environmental Samples

The magnetics results for each of the environmental samples are outlined in Chapter 4, Sections 4.2 – 4.4.

8.1.2.1 Runway Dusts

The magnetics results for the runway dust samples are detailed in § 4.2.1. The results indicate a clear differentiation between the magnetic mineralogy and grain size of the magnetic mineral assemblages within Zone A (0 – 725 m) and Zone B (2300 – 3000 m). The dusts from Zone A display a significant antiferromagnetic component in contrast to Zone B which display a predominantly ferrimagnetic assemblage. The differences in the magnetic mineral characteristics of the runway dusts are further evidenced in Figure 8.2 which displays a cross plot of IRM$_{-20mT}$/SIRM versus IRM$_{-300mT}$/SIRM for the runway dust samples and in which two distinctive clusters are evident. The samples are not differentiated strongly

on the lower reverse field ratio (IRM$_{-20mT}$/SIRM) but do separate clearly on the higher reverse field ratio. The less negative higher reverse field ratios within the runway dusts in Zone A indicate that these samples contain a significant antiferromagnetic component in contrast to the Zone B dusts which display more negative higher reverse field ratios and are indicative of a predominantly ferrimagnetic assemblage (Walden *et al.*, 1999).

Figure 8.3 includes the runway dust samples plotted on a cross plot of IRM$_{-20mT}$/SIRM versus IRM$_{-300mT}$/SIRM including the aircraft source samples. The Zone A runway dusts display similar magnetic characteristics to the aircraft engine dusts both being dominated by ferrimagnetic minerals with a significant antiferromagnetic component. Zone A (Figure 3.9) represents an area of runway 23L, which incorporates the initial stages of the take-off roll. The findings point to the release and subsequent accumulation onto the runway surface of magnetic particulates from aircraft engine exhausts within the initial stages of take-off during which stage, high thrust levels have been initiated but the aircraft is still moving relatively slowly (Mazaheri et al. 2013). These findings correspond closely to those of Zhu *et al.* (2011) who observed significant concentrations immediately downwind of the take-off zone at Los Angeles International Airport.

The magnetic mineral characteristics of the runway dust samples collected from Zone B (Figure 3.9) are predominantly coarse-grained ferrimagnetic minerals which correspond closely to those of the brake and tyre dusts. Zone B incorporates the primary landing Zone for aircraft landing on runway 05R. The results indicate that there is an accumulation of magnetic particulates on the runway surface within Zone B resulting from landing operations during which brake and tyre smoke particulates are released and subsequently deposited onto the runway surface.

It is also important to note that tyre material was clearly visible within some of the runway dust samples collected from Zone B. The friction of aircraft tyres on the runway surface during landing results in the polymerisation and hardening of rubber which subsequently leads to the accumulation of rubber deposits on runway surfaces. The physical characteristics of this tyre material was very similar to the tyre dusts collected from the nose landing gear wheel well and

therefore, it is probable that this coarse material dominates the 'tyre' magnetic characteristics of both the nose landing gear wheel well deposit and the runway dust rather than the much finer particulate matter derived from tyre smoke.
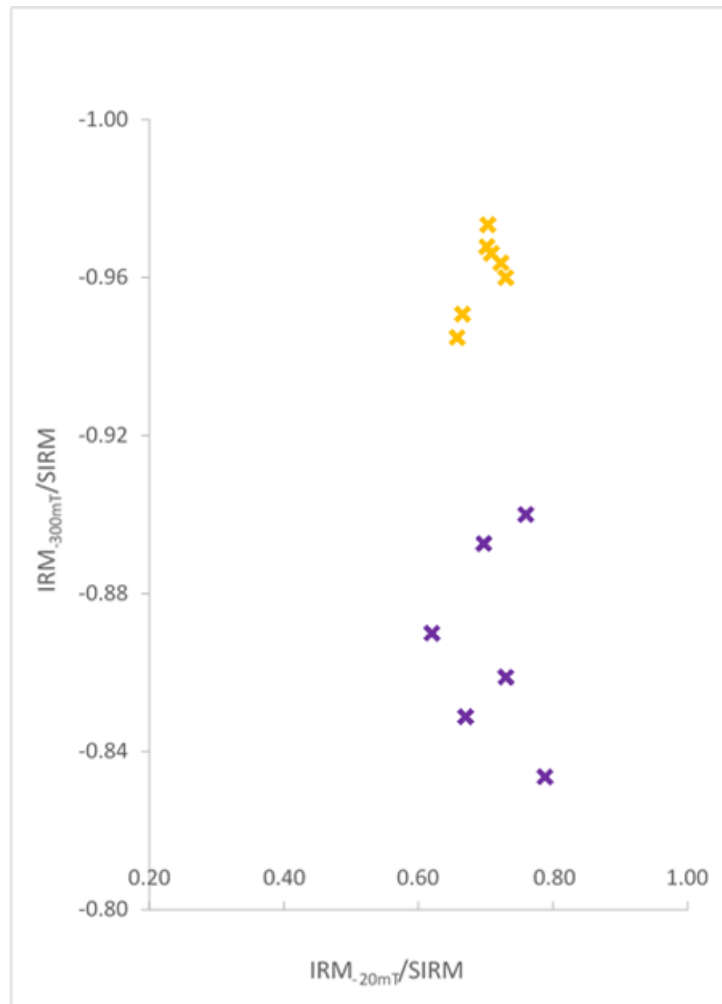
Figure 8.2: IRM$_{-20mT}$/SIRM versus IRM$_{-300mT}$/SIRM for the runway dust samples (Zone A = 0 – 725 m; Zone B = 2300 – 3000 m).
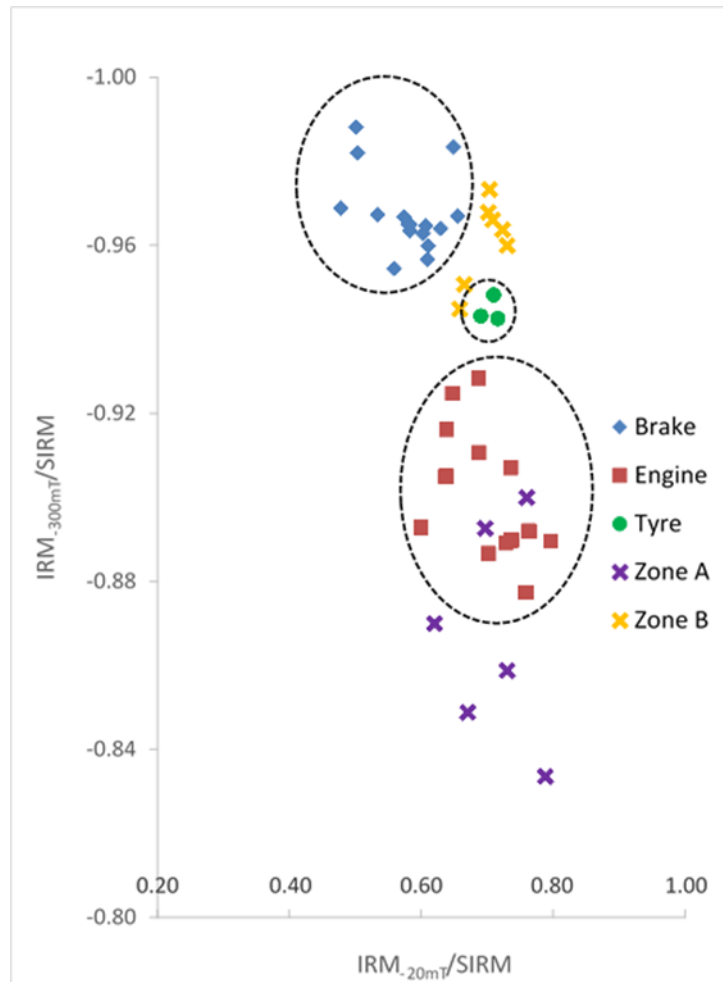
Figure 8.3: IRM$_{-20mT}$/SIRM versus IRM$_{-300mT}$/SIRM for the runway dusts along with the aircraft source samples (Zone A = 0 – 725 m; Zone B = 2300 – 3000 m).

Differences in the concentration of magnetic minerals § 4.2.1, were also observed between the two runway Zones, with much higher concentrations being evident within Zone B. It is possible that the higher concentrations are associated with the visible accumulation of coarse, rubber material on the runway surface deposited during landing rather than from tyre smoke. Such findings are consistent with those of Bennett *et al.* (2011), who state that a significant loss of rubber occurs during the landing phase of the LTO cycle.

8.1.2.2 Taxiway and Apron Dusts

The magnetics results for the taxiway and apron dusts are described in § 4.2.2. The results clearly show that the taxiway and apron dusts are comprised of mixed magnetic assemblages containing both antiferromagnetic and ferrimagnetic minerals. Whilst there is no obvious distinction between the magnetic mineral characteristics displayed by each sample set, there is some variability between individual samples.

Magnetic mineral concentrations throughout the taxiway and apron areas are high with the exception of a lower magnetic mineral concentration which is observed within the taxiway dusts at T1.2. The $IRM_{-20mT}/SIRM$ versus $IRM_{-300mT}/SIRM$ cross plot for the taxiway and apron dusts (Figure 8.4) further illustrates the variation in magnetic mineral characteristics between each sample. Overall there is a clear predominance of coarser ferrimagnetic mineral grain sizes throughout the taxiway and apron dust samples, however, there is also a presence of finer ferrimagnetic mineral grain sizes in some samples. The higher reverse field ratio ($IRM_{-300mT}/SIRM$) clearly demonstrates the variation in magnetic mineral assemblages between the samples. The more positive ratios, which are evident within both sample sets but are particularly prevalent within the taxiway dusts indicate a significant antiferromagnetic component in contrast to the less positive ratios which are once again a feature of both sample sets but are particularly predominant within the apron dusts and are indicative of a predominantly ferrimagnetic assemblage.
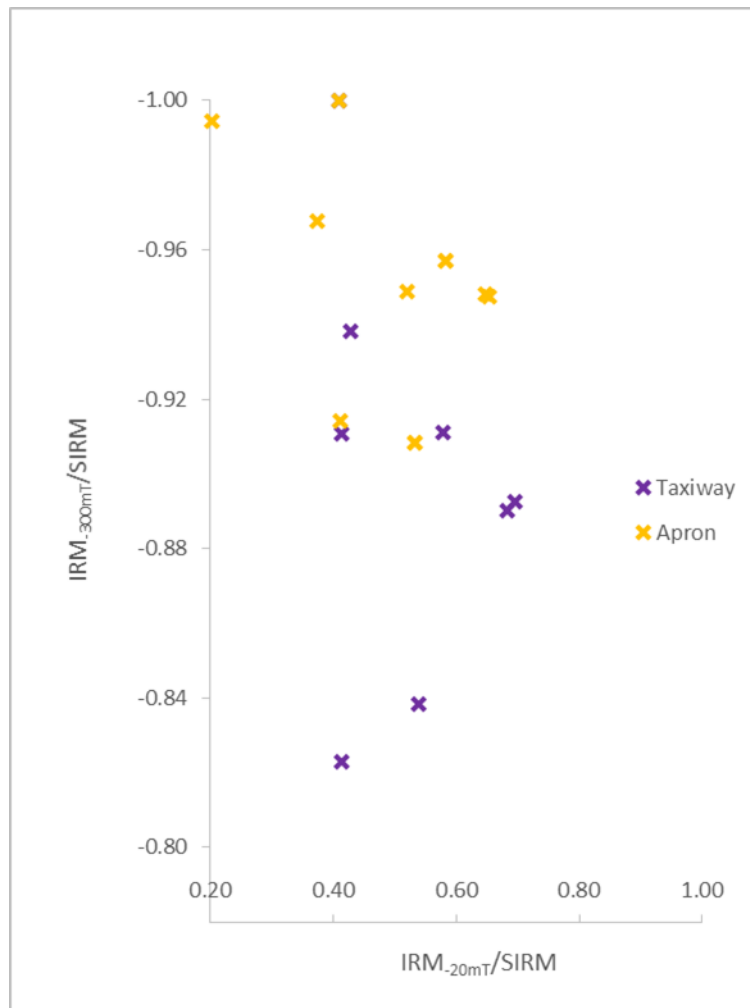
Figure 8.4: IRM$_{-20mT}$/SIRM versus IRM$_{-300mT}$/SIRM
for the taxiway and apron dusts.

Figure 8.5 displays the taxiway and apron dust samples incorporated onto a cross-plot of IRM$_{-20mT}$/SIRM versus IRM$_{-300mT}$/SIRM alongside the aircraft source samples. Whilst the variation in magnetic mineral characteristics between each sample set is clear, the taxiway dust samples are, in general, more antiferromagnetic than the brake and the majority of the apron dust samples.

The wide variation in magnetic characteristics that are evidenced throughout the taxiway and apron dusts results are indicative of the various routine aircraft operations which take place throughout these areas. The significant antiferromagnetic component within both the taxiway and apron dusts is

indicative of aircraft engine emissions. Aircraft engine emissions are released during initial engine start-up and also as a result of aircraft taxiing manoeuvres. In addition to the main engines, emissions are also generated by APU units. These small gas turbine engines housed within the tail cone of the aircraft produce similar emissions to those of the main aircraft engines which are released during the provision of power to the aircraft whilst on the ground (Lobo *et al.*, 2013) and also through the production of compressed air during main engine start up (Schafer *et al.*, 2003). The antiferromagnetic component is particularly prevalent within the taxiway dusts, which reflects the significant increase in engine emissions as the aircraft transitions from 'ground idle' to 'taxiway acceleration' as it moves towards the departure runway or terminal apron area (Wood *et al.*, 2008). Taxiway congestion further contributes to increased engine emissions through the intermittent acceleration and deceleration of the engines during stop and start modes (Masiol and Harrison, 2014).

Ferrimagnetic minerals are evident within both sample sets, with coarse grained ferrimagnetic mineral grain sizes being particularly prevalent in the apron areas. This partially reflects an accumulation of magnetic particulates within the brake dust and tyre wear debris which is accumulated as a result of the routine aircraft movements which take place within these areas. In addition to aircraft, a large number of ground support equipment and airside vehicles operate within the perimeter of the airfield. Vehicle derived emissions will comprise both exhaust and non-exhaust particulates. Coarse grained ferrimagnetic minerals, which are particularly prominent in the apron areas where vehicle activity is most concentrated, may be derived from non-exhaust emissions including those resulting from tyre, brake and clutch wear (Grigoratos and Martini, 2015) and abraded metal particles (Sagnotti *et al.*, 2006). The presence of fine ferrimagnetic minerals, which are characteristic of vehicle exhaust emissions (Hunt *et al.*, 1984; Sagnotti *et al.*, 2006) are evident within both areas.
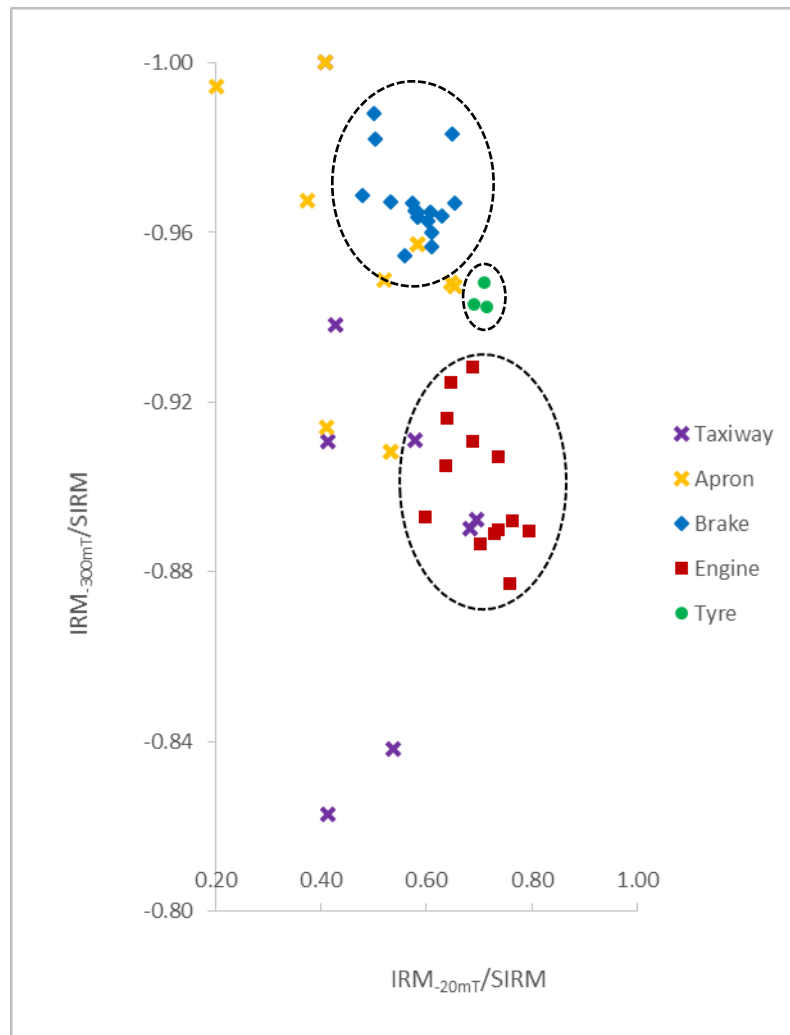
Figure 8.5: IRM$_{-20mT}$/SIRM versus IRM$_{-300mT}$/SIRM for the taxiway and apron dusts along with the aircraft source samples.

8.1.2.3 Runway 23L/05R Grass Samples

The magnetics results for grass samples collected from the transect alongside runway 23L/05R are described in § 4.3.1. The results indicate that these samples contain magnetic mineral assemblages dominated by ferrimagnetic minerals. A number of slight shifts in magnetic grain size are also evident throughout the transect.
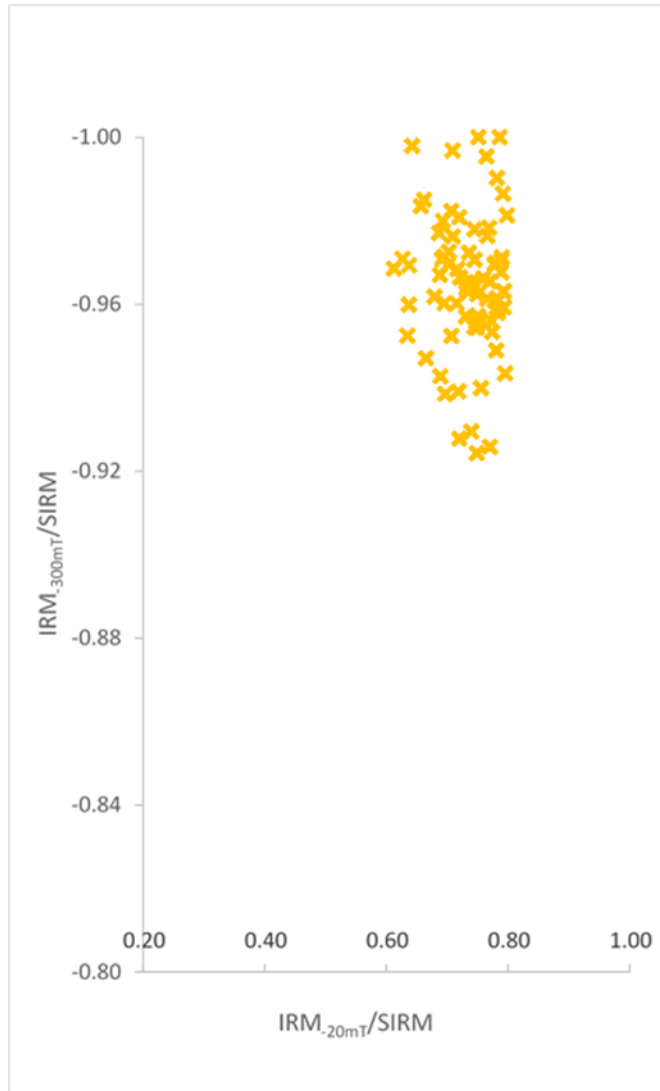
Figure 8.6: IRM$_{-20mT}$/SIRM versus IRM$_{-300mT}$/SIRM for the grass samples collected alongside runway 23L/05R.

The IRM$_{-20mT}$/SIRM versus IRM$_{-300mT}$/SIRM plot for the runway grass samples (Figure 8.6) further illustrates the magnetic mineral characteristics within these samples. Whilst there is little variation in the lower reverse field ratio (IRM$_{-20mT}$/SIRM), the higher reverse field ratio (IRM$_{-300mT}$/SIRM) further illustrates the dominance of ferrimagnetic mineral assemblages throughout the transect.

Figure 8.7 displays the runway grass samples incorporated onto a cross-plot of IRM$_{-20mT}$/SIRM versus IRM$_{-300mT}$/SIRM along with the aircraft source samples.
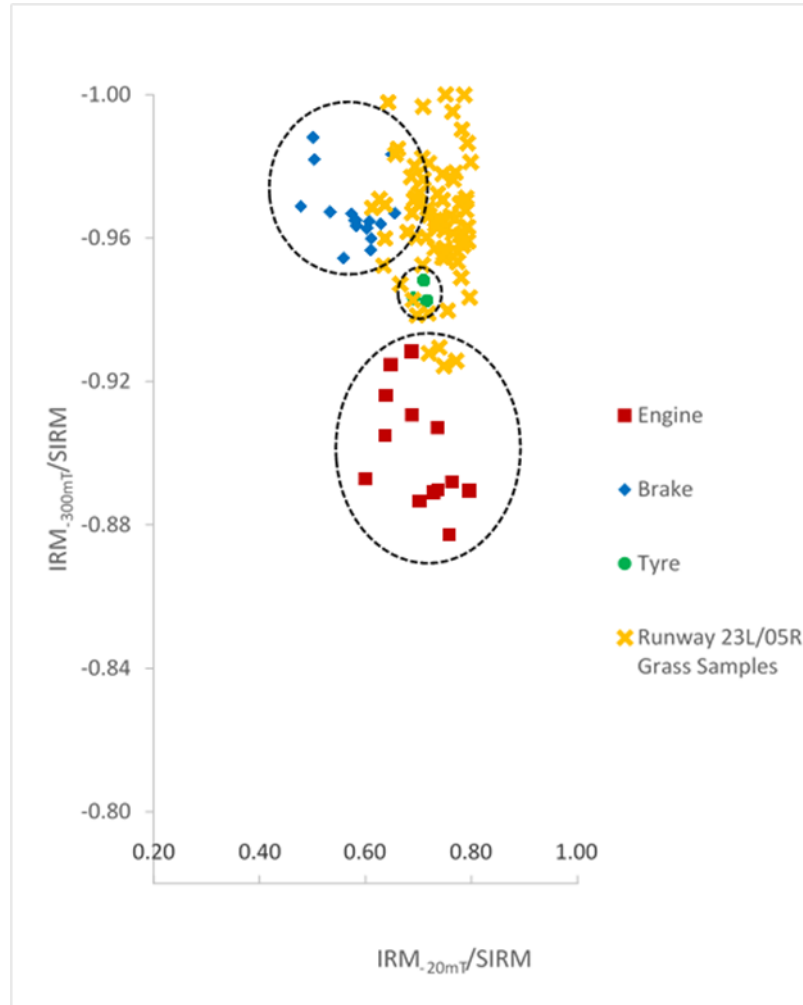
Figure 8.7: IRM$_{-20mT}$/SIRM versus IRM$_{-300mT}$/SIRM
for the grass samples collected alongside runway
23L/05R along with the aircraft source samples.

In terms of magnetic mineralogy, the grass samples appear to correspond more closely with the brake and tyre dusts which have a predominantly ferrimagnetic mineral composition. Such findings would suggest the deposition of magnetic particulates resulting from aircraft brake and tyre wear debris during aircraft landing and taxiing manoeuvres.

The grass data exhibits higher concentrations of magnetic minerals close to the threshold of runway 23L through to 475 m along the runway. This zone of high magnetic mineral concentrations may reflect the accumulation on vegetation surfaces of magnetic particulates released from aircraft engines during the

initiation of take-off and subsequent increase in engine thrust as the aircraft moves down the runway when departing on runway 23L. Such findings are consistent with those of a research study at Los Angeles International Airport in which very high concentrations of ultrafine particulates were measured immediately downwind of the take-off zone (Zhu *et al.* 2011).

It is important to note that the variable concentration of magnetic minerals on leaf surfaces may relate to different length time periods of deposition. During this research project, grass sampling was undertaken after a minimum 5 day period of dry weather. It is assumed that the preceding rainfall would have washed off significant amounts of particulate matter from leaf surfaces, and therefore it must be assumed that the results reflect a 5-day period of particle accumulation. Additionally the deposition of particulate matter on leaf surfaces depends on leaf surface area and leaf surface characteristics such as the presence of trichomes and other surface roughness elements (Gautam *et al.*, 2005; Kardel *et al.*, 2011; Sant'Ovaia *et al.*, 2012). This study focused on the leaves of grass species only. The grass mixture on the airfield at Manchester Airport consists of four different narrow leaved species (A. Clarke pers. comm.) all of which have similar leaf surface characteristics.

8.1.2.4 Taxiway and Apron Grass Samples

The magnetics results for the taxiway and apron grass samples are outlined in § 4.3.2.   Taxiway and apron grass samples are comprised of mixed magnetic mineral assemblages containing both ferrimagnetic and antiferromagnetic minerals.   Whilst there is no obvious distinction in the magnetic mineral characteristics displayed by each sample set, there is some variability between individual samples and a much greater antiferromagnetic component is apparent within the taxiway grass samples.

The $IRM_{-20mT}/SIRM$ versus $IRM_{-300mT}/SIRM$ cross plot for the taxiway and apron grass samples (Figure 8.8) illustrates the variation in magnetic mineral characteristics between samples. The higher reverse field ratio ($IRM_{-300mT}/SIRM$)

shows that both sample sets contain a predominantly ferrimagnetic mineral assemblage but also emphasises the significant antiferromagnetic component, which is particularly evident within the taxiway grass samples.
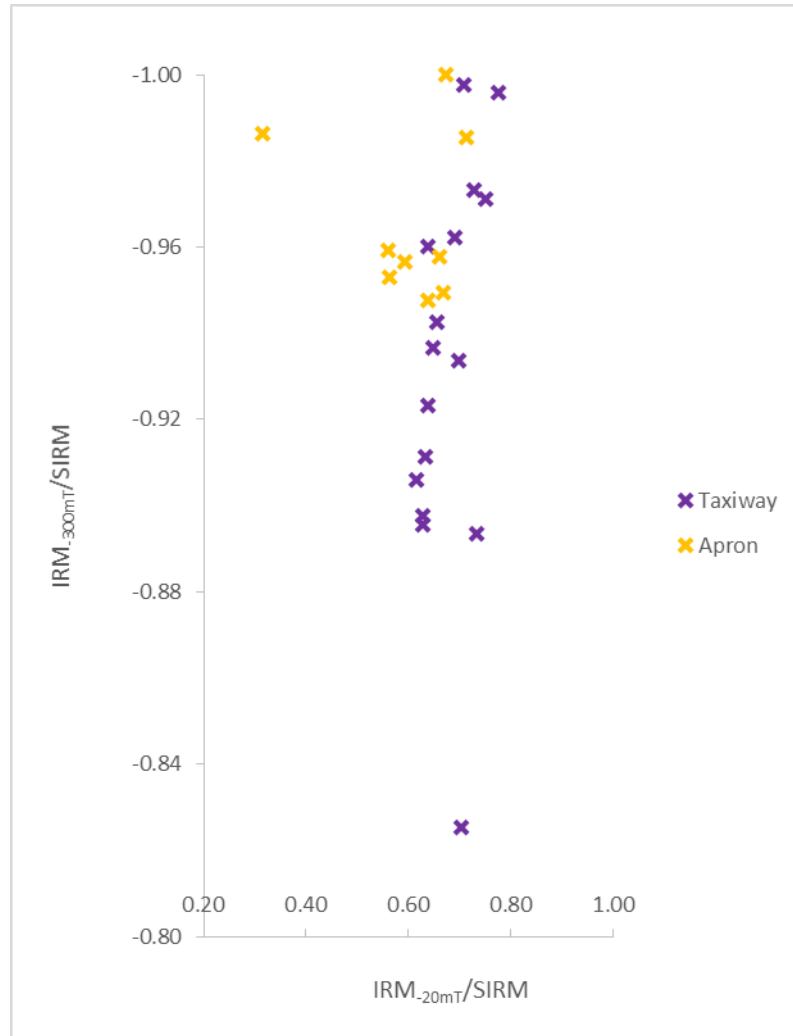
Figure 8.8: IRM$_{-20mT}$/SIRM versus IRM$_{-300mT}$/SIRM for the taxiway and apron grass samples.

Figure 8.9 displays a cross-plot of IRM$_{-20mT}$/SIRM versus IRM$_{-300mT}$/SIRM for the taxiway and apron grass samples alongside the aircraft engine, brake and tyre dusts. All of the apron grass samples align closely with the brake and tyre dust samples, however, the taxiway samples display much greater variability. Whilst some taxiway samples show similar magnetic characteristics to the brake and tyre dusts, a number of samples correspond more closely with those of the engine dust samples.
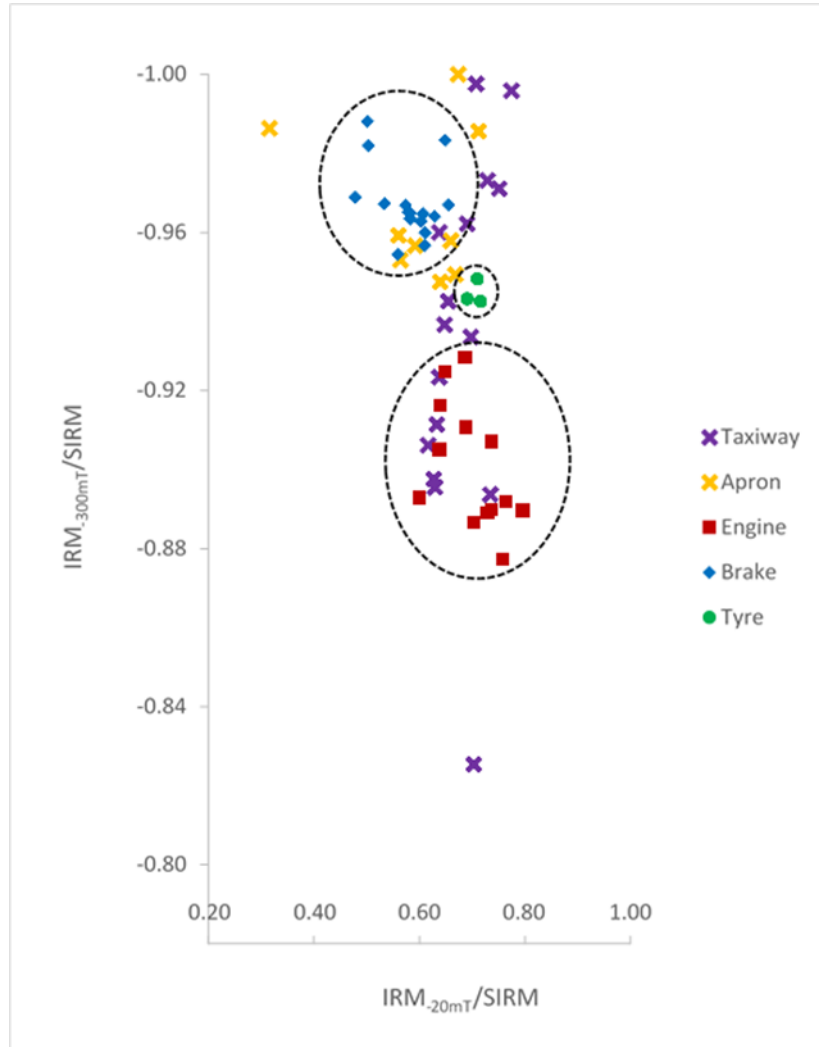
Figure 8.9: $IRM_{-20mT}/SIRM$ versus $IRM_{-300mT}/SIRM$ for the taxiway and apron grass samples along with the aircraft source samples.

Magnetic mineral concentration is low throughout both the taxiway and apron grass samples (§5.3.2), although overall the taxiway samples display higher concentrations.

The taxiway and apron grass data is consistent with that of the dusts and reflects the variety of aircraft manoeuvres and ground operations that take place within these areas (§ 8.1.1.2).
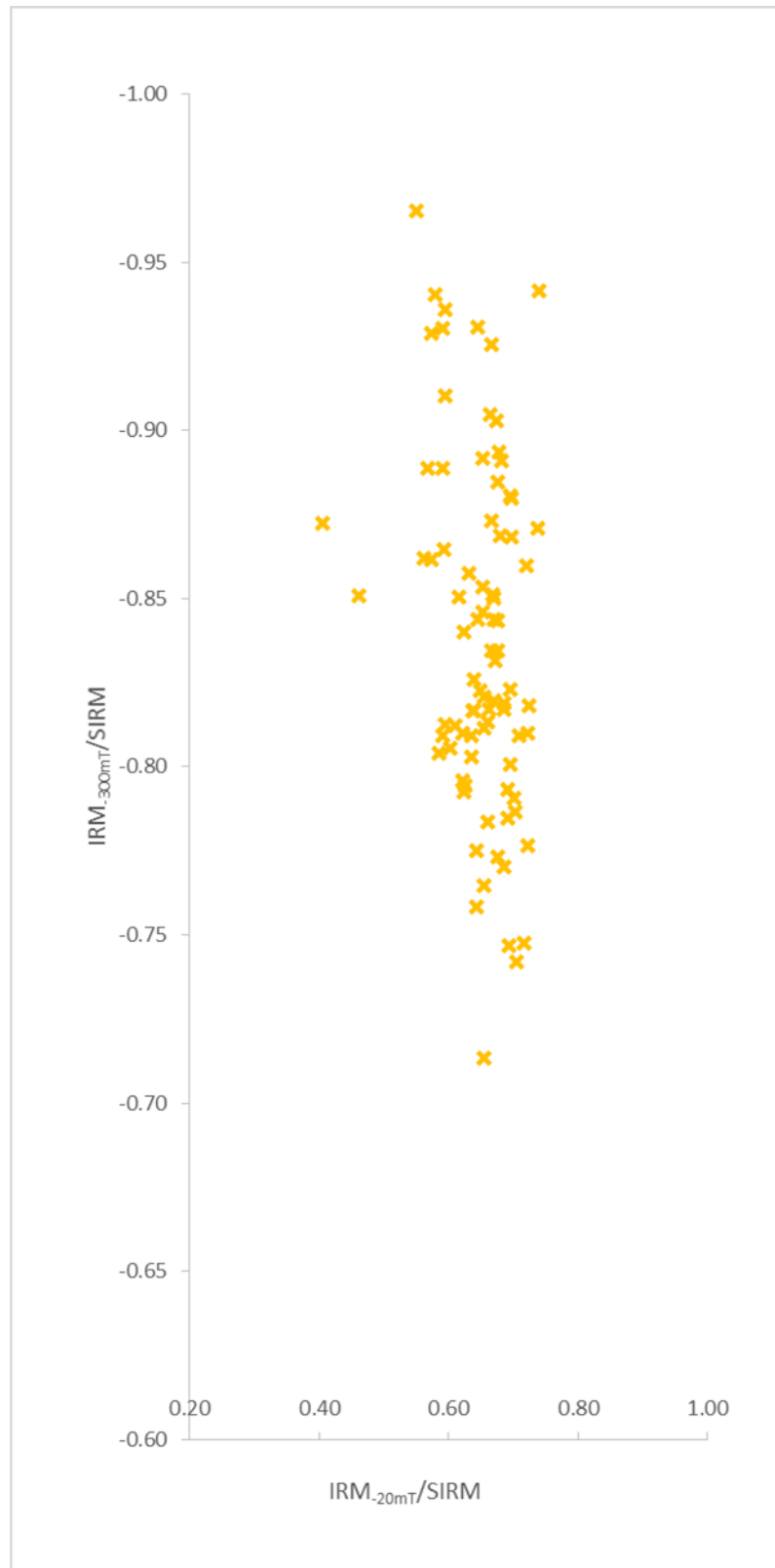
Figure 8.10: IRM$_{-20mT}$/SIRM versus IRM$_{-300mT}$/SIRM for the soil samples collected alongside runway 23L/05R.
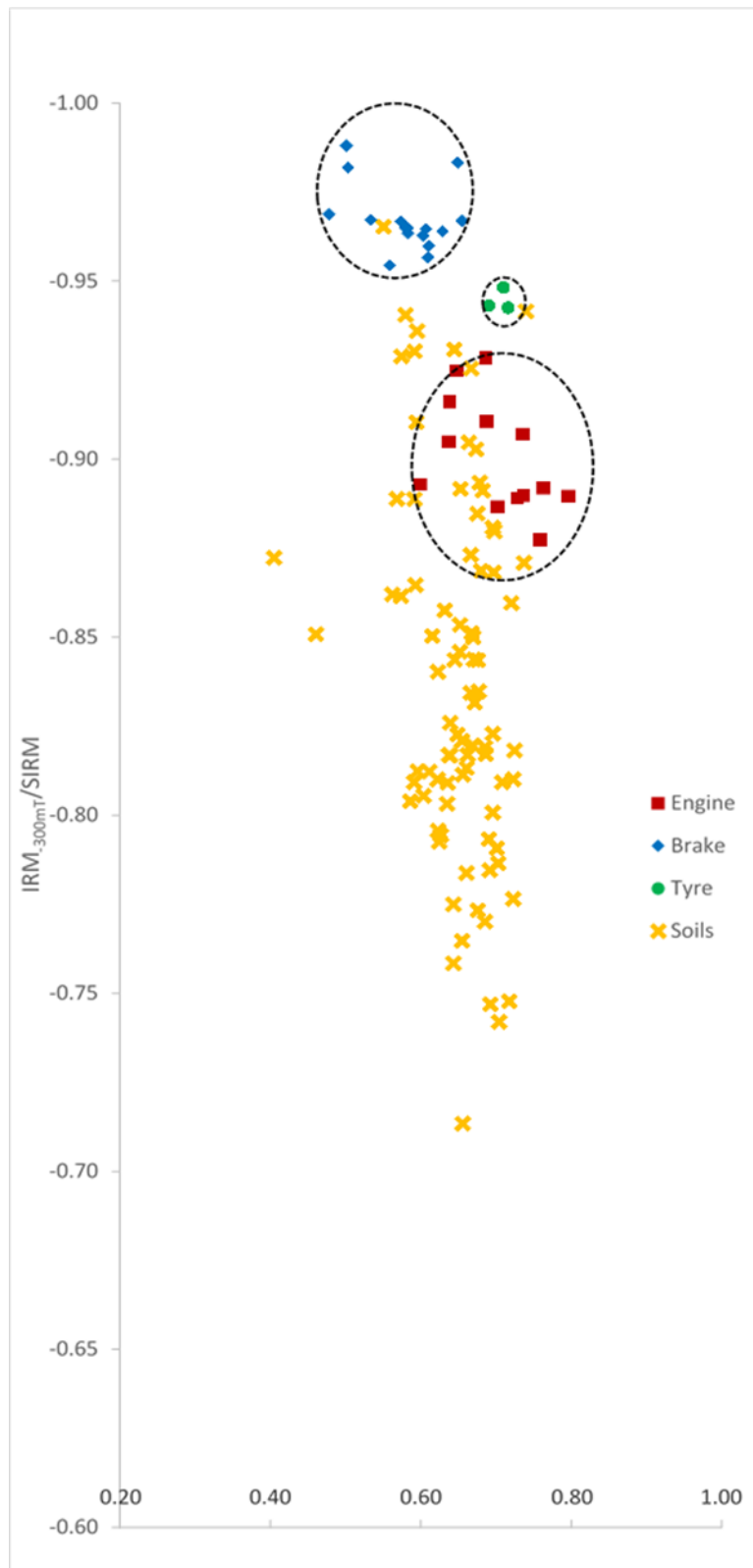
Figure 8.11: $IRM_{-20mT}/SIRM$ versus $IRM_{-300mT}/SIRM$ for the soil samples collected alongside runway 23L/05R along with the aircraft source samples.

8.1.2.5 Runway 23L/05R Soil Samples

The magnetics results for the runway 23L/05R soil samples are described in §
4.4.1. The soil samples have a ferrimagnetic content with a significant
antiferromagnetic component, with the exception of an absence of
antiferromagnetic minerals between 275 m and 575 m. There is, however, much
greater variation in ferrimagnetic mineral grain size along the transect with shifts
between finer and coarser ferrimagnetic mineral grains sizes being evident and
whilst several distinctive zones are identifiable, the presence of finer
ferrimagnetic mineral grain sizes are particularly prevalent within the critical area.

The $IRM_{-20mT}/SIRM$ versus $IRM_{-300mT}/SIRM$ cross plot (Figure 8.10) shows the
magnetic mineral composition and grain size characteristics of the soil samples
collected along the runway transect. The range of variation within the higher
reverse field ratio ($IRM_{-300mT}/SIRM$) highlights the prominence of a significant
antiferromagnetic component within the sample set. The lower reverse field ratio
($IRM_{-20mT}/SIRM$) illustrates some variability between finer and coarser
ferrimagnetic mineral grains sizes between the individual samples.

Figure 8.11 shows the runway soil samples plotted alongside the engine, brake
and tyre dust samples. Whilst the variation in magnetic mineral characteristics
between each sample set is clear, approximately two thirds of the soil samples
are more antiferromagnetic than all of the engine, brake and tyre dust samples.

Magnetic mineral concentrations vary between high and low values throughout
most of the runway transect. There is less variation, however, in magnetic
mineral concentration extending throughout the critical area to 275 m along the
runway. Within this zone, high magnetic mineral concentrations are evident.

The variability in the concentration and type/grain size of magnetic minerals in
the soils is most probably due to inputs from a number of sources, in addition to
atmospheric deposition. Primary magnetic minerals can be present from the
weathering of the soil parent material. The underlying geology of the area is Bollin
Mudstone, which is composed mainly of red and occasionally green and grey
dolomitic mudstones. Where the rock is red the Fe (III) content is usually

haematite which may contribute to the observed antiferromagnetic component which is evident throughout most of the runway transect (Hobbs *et al.*, 2002). Enhancement of the near-surface concentration of magnetic minerals may arise from fermentation processes possibly involving bacterially-mediated production of magnetic iron oxides, as well as iron oxide transformations in the oxidising and reducing conditions associated with organic matter. Ferrimagnetic minerals produced by these processes are typically of a fine grain size (Maher, 1986).

In relation to the varying concentration of magnetic minerals, soils accumulate particulate matter over long periods of time. Whilst there was consistency in the depth of soil sampled at each point, the accumulation period integrated in this depth will be variable from sample to sample, which will have a direct impact on the magnetic mineral content accumulated from the atmosphere.

One area of the transect where there is some consistency in the magnetic mineral concentration and type/grain size is in the critical area extending to 275 m. The higher concentration of magnetic minerals and finer ferrimagnetic mineral grain sizes within this zone may reflect the release of particulates during the initial thrust stage prior to take off.

Thus surface soils are essentially very noisy substrates. Therefore, if they are to be used in particulate monitoring and characterisation studies, it is necessary that any anthropogenic signal can be discriminated from the natural background sources.

8.1.2.6 Taxiway and Apron Soil Samples

The magnetics results for the taxiway and apron soil samples are described in § 4.4.2. The results indicate that the taxiway and apron soil samples comprise mixed magnetic mineral assemblages of antiferromagnetic and ferrimagnetic minerals. The individual sample sets do not display any obvious distinctive magnetic mineral characteristics although some inter-site variability is apparent. The IRM$_{-20mT}$/SIRM versus IRM$_{-300mT}$/SIRM cross plot for the taxiway and apron

soils (Figure 8.12) further illustrates the variation in magnetic mineral assemblages between the individual samples.
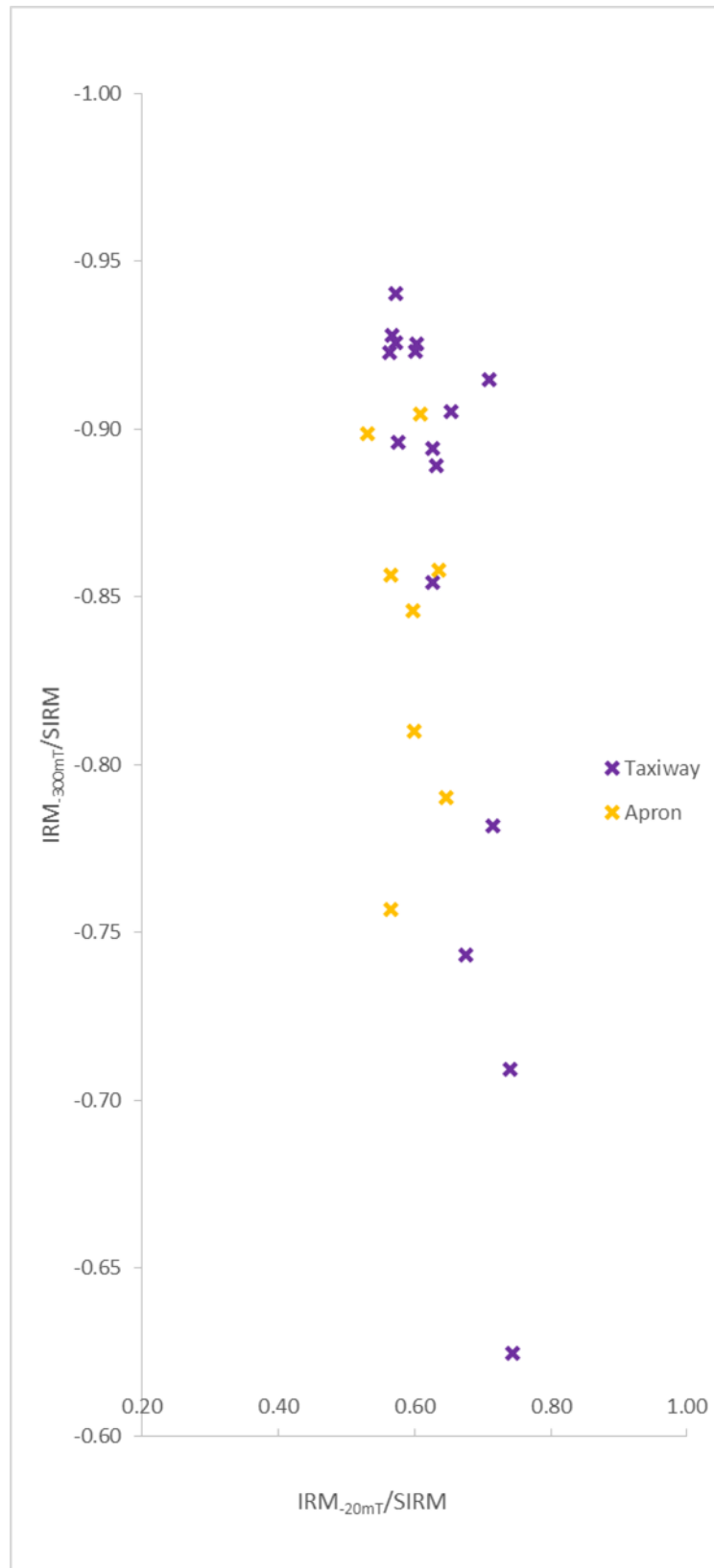
Figure 8.12: IRM$_{-20mT}$/SIRM versus IRM$_{-300mT}$/SIRM for the taxiway and apron soil samples.
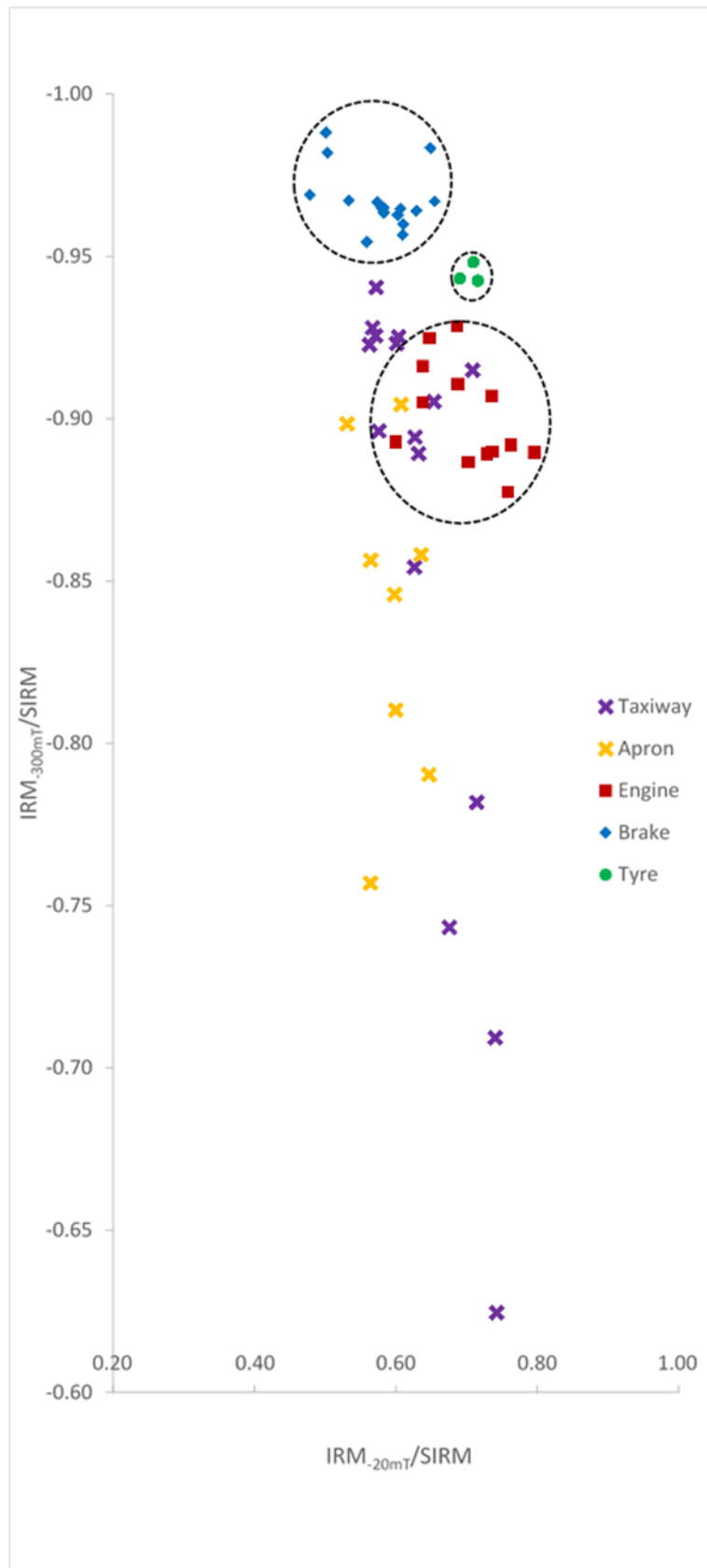
Figure 8.13: IRM$_{-20mT}$/SIRM versus IRM$_{-300mT}$/SIRM for the taxiway and apron soil samples along with the aircraft source samples.

The higher reverse field ratio (IRM$_{-300mT}$/SIRM) confirms the presence of ferrimagnetic mineral assemblages but also highlights the significant antiferromagnetic component that exists within each sample set. The lower reverse field ratio (IRM$_{-20mT}$/SIRM) further demonstrates the variation between coarser and finer ferrimagnetic mineral grain sizes of the individual samples within each area although finer ferrimagnetic mineral grain sizes are the most prominent within the taxiway soil samples.

Figure 8.13 presents the IRM$_{-20mT}$/SIRM versus IRM$_{-300mT}$/SIRM soil data alongside that for the aircraft engine, brake and tyre dusts. The behaviour of the taxiway and apron soils is very similar to that of the runway soils (§ 8.1.2.5). Magnetic mineral concentrations are highly variable. Concentrations within the taxiway areas, however, are generally lower than those within the apron areas. The wide variation in magnetic characteristics that are displayed probably reflects a combination of natural sources of magnetic minerals and particulates derived from the wide variety of aircraft manoeuvres that take place throughout these areas (§ 8.1.1.2).

8.2 Chemical Analysis

The principal aim of this research is to identify distinctive and characteristic 'fingerprints' of primary particulates within the airport environment to facilitate investigation of the spatial distribution of the deposited PM from different emission sources within the airport environment . Therefore, this section focuses on the key elements (i.e. Ni; Cr; Ti; Cu and Zn), which were identified within each of the aircraft source samples (i.e. aircraft engines, brakes and tyres) and furthermore which could be used as distinctive chemical 'fingerprints' to characterise the individual sources.

8.2.1 Aircraft Source Samples

The main elemental metallic composition of each of the aircraft source samples (i.e. aircraft engines, brakes and tyres) is presented in Chapter 5 (§ 5.1). The results indicate that there are some clear distinctions between the elemental characteristics of each of the three dust groups. Those metals that show a difference in content between the sources are focused on here.   High

concentrations of Fe were found within all of the aircraft source and environmental samples, consistent with the ubiquitous nature and abundance of Fe within the environment. Fe will not therefore be used in 'fingerprinting'. Similarly, high concentrations of Al were also found throughout the samples, whilst Pb was present in all samples in low concentrations.

Ni and Cr were found to be the most significant metals within the engine dust samples. The significant presence of both of these metals is likely to reflect their existence within aviation fuel (Jet A-1) and also within aircraft engine exhaust components. Ni and Cr are both present in trace amounts in Jet A-1 fuel (Abegglen *et al.*, 2016; Environment Canada, n.d.) and have been identified as a component of the soot which is produced during incomplete combustion of the jet fuel within the combustion section of the engine (Abegglen *et al.*, 2016). The subsequent particulates are emitted during aircraft engine operations including engine start-up; taxing; take-off and landing procedures. Ni and Cr alloys are also commonly used in the construction of aircraft engine exhaust systems due to their high tensile strength and hardness and resistance to high temperature oxidation and corrosion (FAA, 2013; Abegglen *et al.*, 2016). Following combustion, gas temperatures are very high as they enter the high-pressure turbine which houses the turbine blades. Ni and Cr super alloys, which are able to withstand the high temperatures (1400 – 1500 °C) and stresses are used in the construction of the components within these areas (Schreiber and Gerendas, 2014; Pollock, 2016). The mechanical wear and erosion of these engine components may further contribute to the presence of Ni and Cr within the engine dust (Masiol and Harrison, 2014).

The most significant metals within the brake dusts were found to be Ti, Cu and Zn. The existence of these metals in the dusts probably relates to their presence in various brake and brake-related aircraft components. Literature relating specifically to aircraft brakes is limited due to the commercially sensitive nature of the data (Lobo *et al.*, 2013). However, aircraft brakes comprise the same key components as vehicular brakes i.e. binders, fillers, fibres, frictional additives or lubricants and abrasives (Grigoratos and Martini, 2015) and whilst the

composition and relative proportions will differ (Whitefield *et al.*, 2008), the abundance of literature relating to vehicular brake may be used for comparison.

Ti has light-weight, strong, corrosion resistant properties and as such it is used widely in aircraft construction and repair (FAA, 2013). Ti containing compounds are routinely used within the manufacture and repair of aircraft brake disks and pads (Wahlström *et al.*, 2010; Bruno, 2016). In C/C brake discs, such compounds are used as a component of the carbonised fibre coating which serves to extend the lifetime wear of the discs by limiting friction, and the tendency for oxidation under the high temperature conditions which are present during braking operations (Bruno, 2016). Cu possesses high thermal and electrical conductivity properties, and as such, it is used predominantly as a wiring component within the aircraft electrical system (Adachi and Tainosho., 2004; FAA, 2013; Saha *et al.*, 2017). However, within aircraft brake pads, Cu is a constituent of the amorphous fibres, which are used to enhance mechanical strength and durability (Langhof *et al.*, 2016). Zn is a component of the liquid coating used to treat C/C composites to inhibit catalysed oxidation (Stover, 2003). Brake disc components, such as pistons, may also be electroplated with Zn for corrosion protection (Rike, 1998). Zn is also added to tyre rubber during the vulcanisation process (Bennett *et al.*, 2011) and may also be a component of the brake dust.

The presence of the metals in the brake dust is probably produced through the activation of aircraft brakes during landing and taxiing operations. Such debris may include the abraded brake lining material from discs and pads (Masiol and Harrison, 2014) and that associated with the friction layer of C/C composite brakes (Wu *et al.*, 2016). The resultant particles will ultimately become released as airborne PM and may subsequently be deposited within the airport environment. Cu is reported to be a key indicator of brake wear (Whitefield *et al.*, 2011; Amato *et al.*, 2009; Hagino *et al.*, 2016). High concentrations of Ti and Zn, however, have also been identified as being present within brake wear debris (Adachi and Tainosho., 2004; Amato *et al.*, 2010; Grigoratos and Martini., 2015).

Zn, Cu and Ti were found to be the most prominent metallic elements within the tyre dust samples, with particularly high concentrations of Zn. The dominance of

Zn within these samples probably reflects the use of Zn during rubber vulcanisation (Amari *et al.*, 1999; Kreider *et al.*, 2010; Bennett *et al.*, 2011). During this process ZnO is used as an activator to speed up the rate of vulcanisation (Wik *et al.*, 2009; Lobo *et al.*, 2013; Grigoratos and Martini, 2015).

The presence of Cu, may be related to the composition of the beads, which along with the body, sidewall and tread are a main component of aircraft tyres. The beads, whose function it is to support the rim of the tyre, are high tensile steel loops which are embedded within the two inner edges of the tyre (Kongo Kondé *et al.*, 2013). Cu is a component of the bronze or brass alloys which are used to protect the steel beads from corrosion (McAfee *et al.*, 2016). No literature was available to support the presence of Ti within aircraft tyre components. As previously mentioned, Ti is commonly used within the fabrication and repair of aircraft brake discs and pads. Therefore, it must be assumed that the Ti concentrations within the tyre dusts reflect some contamination of brake wear particles within these samples.

The occurrence of the metals within the tyre dusts is likely to result from the chemical (e.g. volatilisation) and mechanical processes (shear forces) during landing which result in the production of tyre wear particles which form the tyre smoke (Grigoratos and Martini, 2015). Particles may also be generated through the action of the nose wheel tyre rubbing against the 'snubber pads' during undercarriage retraction. Consistent with the findings here, Zn, Cu and Ti have each been acknowledged as being components of tyre wear (Grigoratos and Martini, 2015). Moreover, tyre wear particles have been identified as being a significant source of Zn in the environment (Adachi and Tainosho, 2004; Grigoratos and Martini, 2015).

Further confirmation of the differences in the elemental characteristics of the aircraft source samples has been achieved through the use of principal components analysis (Figure 8.14). The PC1 and PC2 data for each element is presented in Appendix 5. PCA axis1 explains 68.87% of the variance in the dataset. Zn has the most influence on the dataset with an eigen value of -0.66647 and is highly correlated to the tyre dust samples.

181
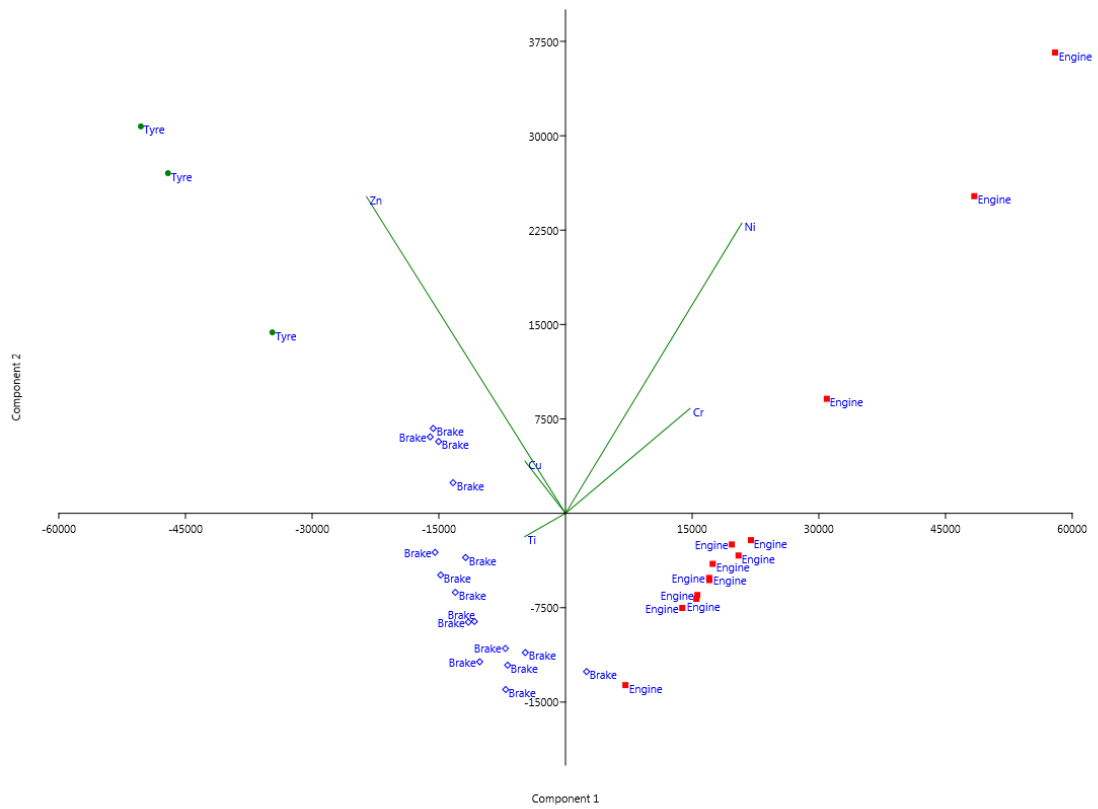
Figure 8.14: PCA analysis of the main metallic elements in the aircraft source dust samples (i.e. aircraft engine, brake and tyre dusts).

8.2.2 Environmental Samples

The main elemental metallic composition of each of the environmental samples is outlined in Chapter 5 (§ 5.2 – 5.4).

8.2.2.1 Runway Dusts

The main elemental metallic composition of the runway dusts is detailed in (§ 5.2.1). The results show that there is no clear distinction in the concentration of Cr and Ni between Zones A and B, and with little variation being shown throughout. There is, however, a significant difference in the concentrations of Zn, Cu and Ti between each of the Zones with Zone B displaying much greater concentrations than Zone A.

The much higher concentrations of Zn, Cu and Ti within the runway dusts in Zone B must relate to the accumulation of particulates associated with the landing operations that are predominant within this area. Ti, Cu and Zn have been identified as the most significant metals within the aircraft brake and tyre dust samples (§ 8.2.1). The presence of each of these metals within the Zone B runway dusts is likely to result from the production and subsequent release of brake wear and tyre smoke particulates during landing. Cu and Zn have been found to be key components of tyre wear debris (Grigoratos and Martini, 2015). Zn resulting from the vulcanisation process (Amari *et al.*, 1999; Kreider *et al.*, 2010; Bennett *et al.*, 2011) and Cu as a component of the bronze or brass alloys used within the manufacture of tyre beads (McAfee *et al.*, 2016). Tyre smoke particulates are released during touchdown as the aircraft wheels meet the runway surface (Masiol and Harrison, 2014) during which time a significant loss of rubber occurs (Bennett *et al.*, 2011). Cu and Zn are probably present in the tyre smoke particulates.

Zn, Cu and Ti, are used within the manufacture of aircraft brake discs and pads (Wahlström *et al.*, 2010; Bennett *et al.*, 2011; Bruno, 2016; Langhof *et al.*, 2016; Wu *et al.*, 2016) and have each been found to be components of brake dust debris (Grigoratos and Martini, 2015). The presence of these metals within the Zone B

runway dusts probably relates to the production and subsequent release of particulates resulting from the abrasion of the lining material from brake discs and pads as the aircraft slows down and is brought to a halt (Masiol and Harrison, 2014).

The differences in the elemental composition of the runway dust samples have been investigated using principal components analysis (Figure 8.15). The PC1 and PC2 data for each element is presented in Appendix 5. PCA axis 1 explains 99.8% of the variance in the dataset. Zn displays the most influence on the dataset with an eigen value of 0.99915 and is highly correlated with the runway dusts in Zone B. A slight influence from Cu and Ti is also apparent with eigen values of 0.03201 and 0.02599 respectively. These results confirm the significance of Zn, Cu and Ti as being major components of the runway dusts.
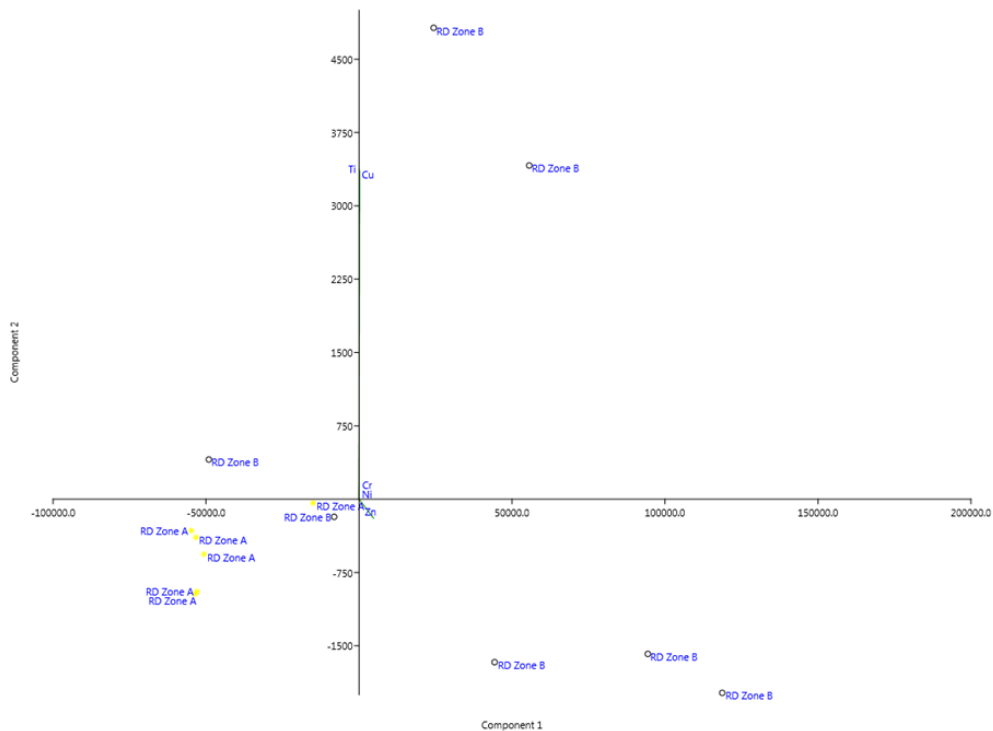
Figure 8.15: PCA analysis of the main metallic elements in the runway dust samples (Zone A = 0 – 725 m; Zone B = 2300 – 3000 m).

8.2.2.2 Taxiway and Apron Dusts

The main elemental metallic composition of the taxiway and apron dusts is detailed in (§ 5.2.2). Extremely variable concentrations of the main elements identified within each of the aircraft source samples (i.e. Ni; Cr; Zn; Cu and Ti) are evident throughout the taxiway and apron dust samples. The varied concentrations of these elements is representative of the diversity of aircraft operations and manoeuvres that occur within these areas. The presence of Ni and Cr is indicative of emissions from aircraft engine exhausts (Abegglen *et al.*, 2016) which are released during main engine start-up and taxiing manouevres and also from the erosion/mechanical wear of engine exhaust components (Vander Wal *et al.*, 2014). The concentration of Ni and Cr is generally much higher within the apron dust samples which may reflect the greater intensity of aircraft activity within this area. Additional contributions to the engine exhaust particulates within the apron area may result from APU emissions used for the provision of ground power whilst the aircraft is parked at the stand (Lobo *et al.*, 2013) and engine check starts following maintenance work (Masiol and Harrison, 2014). The increases in Cr concentration within individual taxiway dust samples possibly reflects the intermittent acceleration and deceleration of the engines during the stop and start modes due to taxiway congestion (Masiol and Harrison, 2014). The presence of Zn, Ti and Cu is indicative of the contribution of emissions from aircraft brake and tyre wear. Varied concentrations of each element were displayed throughout the taxiway and apron dusts although once again, the highest concentrations were observed within the apron dusts. The variation in concentrations is likely to result from the assimilation of the metals within the brake and tyre wear debris which is produced through the abrasion of the brake lining material from discs and pads (Masiol and Harrison, 2014) and the friction layer of C/C composite brakes (Wu *et al.*, 2016) and tyre wear during the intensive aircraft manoeuvres which take place within the taxiway and apron areas. A further contribution to the Cr content within the taxiway and apron dusts may also result from the erosion and subsequent accumulation of emissions from the yellow paint used for taxiway and apron markings (Adachi and Tainosho, 2004) and the corrosion of spray paints used during aircraft maintenance (Touri *et al.*, 2013).
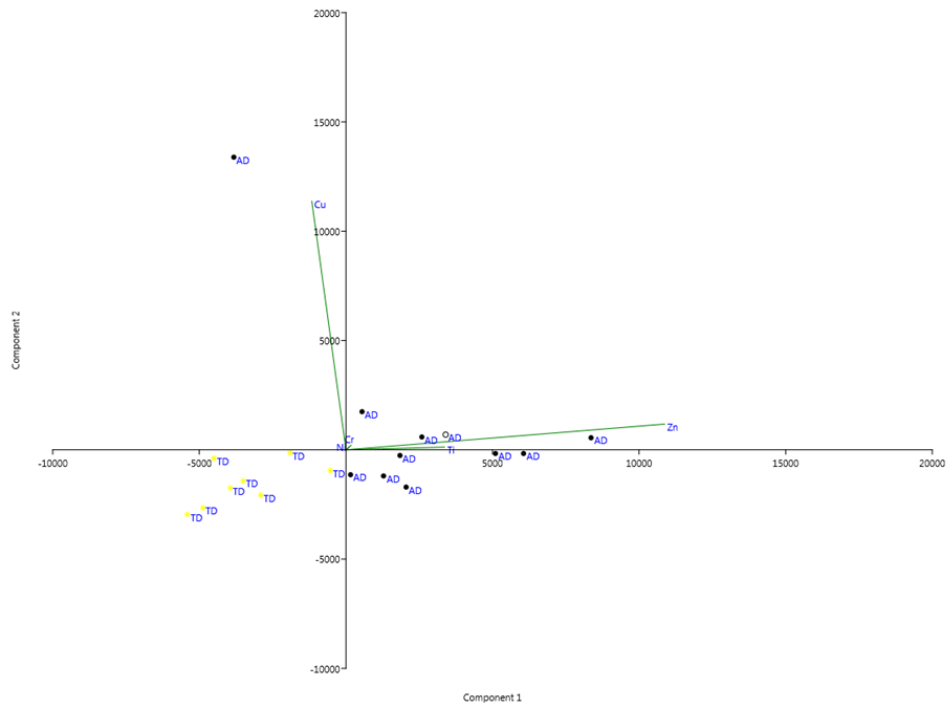
Figure 8.16: PCA analysis of the main metallic elements in the taxiway and apron dust samples.

In addition to aircraft movements, the large number of airside vehicles and ground support equipment which operate within the perimeter of the airfield will provide a further contribution to the emission loads within these areas including Cr from the corrosion of vehicle parts (Lu *et al*., 2006) and Cu, Zn and Ti resulting from brake and tyre wear debris (Al-Fatlawi and Al-Alwani, 2012; Grigoratos and Martini, 2015) and clutch wear (Grigoratos and Martini, 2015). The varied concentrations of the key elements throughout the taxiway and apron dusts may also result from the resuspension of materials due to the turbulence from the numerous aircraft and vehicle activities which take place within these areas (Curran, 2006).

Principal components analysis has further been used to investigate the differences in the elemental composition of the taxiway and apron dusts (Figure 8.16). The PC1 and PC2 data for each element is presented in Appendix 5. PCA axis 1 explains 56% of the variance in the dataset and PCA axis 2, 41.79%. The

lack of a significant signal from the PCA probably reflects the different and varied inputs from a wider range of sources within these areas. PCA analyses revealed Zn, Ti and Cu to be the most important elements within the dataset with eigen values of 0.95022; 0.29391 and -0.10177 respectively. PCA axis 1 shows a strong correlation between Zn and the apron dusts and a weaker correlation with the taxiway dusts. These results reflect the different concentration levels with higher concentration levels of Zn being found in the apron dusts as described above.

8.2.2.3 Runway 23L/05R Grass Samples

The principal metallic composition of grass samples collected from runway 23L/05R is detailed in (§ 5.3.1). The results do not identify a definitive pattern in terms of elemental concentration. Cu and Zn were found to be the dominant metals which may relate to deposition from aircraft brake and tyre wear. Prior to sampling it was expected that concentrations would be much higher within the samples collected within the landing zone (Zone B) as for the runway dust samples. However, there is no clear zonation within the samples.

8.2.2.4 Taxiway and Apron Grass Samples

The elemental characteristics of the taxiway and apron grass samples are very similar. Therefore, this section focuses only on the metals that show a difference in content between the two areas. Very little variation is observed in the concentration of Cu and Zn throughout the taxiway and apron grass samples (§ 5.3.2).

The taxiway and apron grass data are consistent with those of the surface dusts and are representative of the variety of aircraft manoeuvres that take place within these areas. However, the absence of Ni and Cr within these samples provides no evidence of the engine inputs which were identified within the dust samples within these areas (§ 8.2.2.2).

8.2.2.5 Runway 23L/05R Soil Samples

There is very little variation in Ni and Cr concentrations throughout the transect (§ 5.4.1). Concentrations of Ti, Zn and Cu are relatively high throughout the runway transect with several peaks in concentration being evident. Notable increases in the concentration of each of these metals can be seen within the Critical Area. Further increases in the concentration of Cu occur at 225 m and 2125m and in Zn and Ti at 2125 m and 2625 m respectively.

The variability in the concentration of each of the elements is likely to be related to the inputs from various sources. There is no clear pattern in the concentration of Ni and Cr, both of which are thought to be indicative of inputs from aircraft engine emissions and the mechanical wear/erosion of engine components. However, the higher concentrations of Ti, Zn and Cu, which are particularly evident within the samples collected within the area of the landing zone (Fig 3.9), are probably associated with emissions from brake and tyre wear.

In addition to deposition from local, aircraft-related sources, the metals may also be present as a component of regionally derived particulates from urban and industrial sources. Furthermore, weathering of the soil parent material may also contribute to the presence of metals within the soils. Published work on background soil levels for the Manchester area are limited. However, data from the BGS (2017) indicates that the background levels for Ni and Cr within the MAN airport area are much lower that the levels identified within the runway soil samples. Ni values range from 0.016 – 0.024 (g kg^{-1}) and Cr values from 0.021 – 0.035 (g kg^{-1}) in comparison to those of the runway soil samples which for Ni range from 0.24 - 0.27 (g kg^{-1}) and for Cr from 2.16 – 2.38 (g kg^{-1}) which suggests an input from airport related activities.

8.2.2.6 Taxiway and Apron Soil Samples

The results of the chemical analysis for the taxiway and apron soil samples are described in § 5.4.2.

There is very little variation in Ni and Cr concentration between these sample sets. In contrast to this, the concentrations of Ti, Zn and Cu within the taxiway

and apron soil samples are extremely variable, with notably higher concentrations of Ti and Cu and some peaks in Zn being clearly identifiable within the apron soils.

Once again, the Ti, Zn and Cu results are consistent with those of the taxiway and apron dusts which reflects the wide variety of aircraft manoeuvres and associated airport operations that take place within these areas (§ 8.2.2.2). The more significant presence of Ti, Cu and Zn within the apron soils does, however, suggest that there is a greater input of brake and tyre wear emissions within this area.

As for the runway soils samples inputs from various other sources may provide a further contribution to the metal content of the soils within these areas (§ 8.2.2.5). However, the Ni and Cr values which range from 0.24 – 0.27 (g kg^{-1}) and 2.17 – 2.25 (g kg^{-1}) respectively are much higher than those identified within background levels (§ 8.2.2.5) which further suggests a contribution from airport related activities.

8.3 SEM/EDX

The SEM/EDX results are presented in Chapter 6 (§ 6.1 - 6.2).

8.3.1 Aircraft Source Samples

The SEM/EDX results for the aircraft source samples (i.e. aircraft engines, brakes and tyres) (§ 6.1) suggest that there are clear distinctions in the morphological and chemical characteristics of the particles within each of the three dust groups.

Analysis of the individual engine dust particles identifies the predominance of angular and sub-angular particles. Rounded and sub-rounded particles, though less prevalent, are also clearly identifiable within the dusts. The engine dusts were found to be dominated by small particles predominantly within the 0 – 5 μm size range which were found to be C and O rich. However, the elemental composition of the individual particles was found to be quite varied and contained a range of other elements including Si; S; Na; Al; Ni; Cr; Fe; P; K; Mg and Ca. These findings are consistent with those of other researchers who have also

identified a wide range of other elements as being components of PM samples derived from aircraft engines (Kinsey *et al.*, 2011; Mazaheri et al., 2013). Kinsey *et al.* (2011), found S, as a component of secondary particulates, to be the most dominant element within such emissions.

The morphological and elemental composition of the rounded engine dust particulates are typical of aircraft engine exhaust emissions. Following combustion, gas temperatures within the engine exhaust system are very high ~1400 - 1500 °C. The small rounded 'spherical' particles which are evident within the engine dusts are associated with particulates resulting from high temperature combustion processes (Blaha *et al.*, 2008; Kim *et al.*, 2009) and moreover, those derived from aircraft engine emissions (Mazaheri *et al.*, 2013). The cenosphere (hollow) which is clearly visible in Figure 6.4c provides further confirmation of the high temperature combustion processes which are involved in the formation of these particles (Lu *et al.*, 2008; Bourliva and Papadopoulou., 2015).

The combustion of Jet A-1 aviation fuel results in the production of CO_2 and H_2O. Trace amounts of other elements including metals such as Fe; Al; Ni and Cr may also be present within the soot and by-products resulting from aircraft engine combustion processes (Masiol and Harrison, 2014; Abegglen *et al.*, 2016). The resultant particles may be released during routine aircraft engine operations such as start-up; taxiing; take-off and landing. The variability in the chemical composition of such particles is likely to be related to the different engine types (Table 3.1) (Agrawal *et al.*, 2008) and differences in the elemental composition of the Jet A-1 fuels (Schäfer *et al.*, 2006).

The mechanical wear and erosion of the engine components may further contribute to the engine dust particles (Masiol and Harrison 2014). The more irregular shaped particles (i.e. angular and sub-angular) are more likely to be associated with particles derived through the erosion and mechanical wear of engine components (Masiol and Harrison, 2014). The presence of metals including Al and Cr within these particles probably relates to their use within the

manufacture and construction of the aircraft engine parts (FAA, 2013; Abegglen *et al.*, 2016).

The brake dust samples are dominated by sub-angular particles although some rounded particles are also evident. The brake dust particles displayed minimal size variation with the majority being within the 0 – 10 µm size range which is also consistent with the findings of Mazaheri *et al.* (2013). The particles were found to be dominated by C and O although trace amounts of other elements including Si; Fe; Ca; Ti; Zn; Al and S were also identified within the individual particles. The presence of various other elements within brake wear particles have also been identified by other researchers (Adachi and Tainosho 2004; Wahlström *et al.*, 2010). The presence of Al is indicative of the phosphate coating used to improve the friction performance of C/C composite brakes (Fan *et al.*, 2017).

Brake dust particles are a component of the brake wear debris which results from the abrasion of the lining material on brake discs and pads (Masiol and Harrison 2014) and the friction layer of C/C composite brakes (Hutton *et al.*, 1999; Wu *et al.*, 2016; Fan *et al.*, 2017). The brake dust samples were found to be C and O rich. Most modern aircraft are fitted with C/C composite brakes. Carbon is susceptible to oxidation particularly as a result of the high operating temperatures ~300 - 400°C (BA Engineering pers.comm.) that occur within the braking mechanism during landing and taxiing operations (Masiol and Harrison 2014; Yee, 2016). The differences in the chemical composition of the brake dust particles probably relates to the thermal and/or chemical generation processes (Wahlström *et al.*, 2010) that occur at the sliding/rubbing interface during the heavy braking demands and intermittent use of brakes during landing and taxiing operations (Masiol and Harrison 2014). Differences in the elemental composition of the additives used to reduce friction and brake wear (Österle and Dmitriev 2016; Fan *et al.*, 2017) may further contribute to the varied elemental composition of the brake wear particles.

The tyre dust particles fall predominantly within the rounded category and display an extremely varied particle size range (≤ 60 µm) although the highest percentage

are observed to be within the ≤ 20 µm size categories.   The tyre dust particles are dominated by C and O, though Si and trace amounts of other elements were also observed within individual particles. The presence of Al, Ca, S, Ti, Cu and Zn within the composition of these particles is indicative of their originating from tyre tread (Adachi and Tainosho, 2004; Grigoratos and Martini, 2015). Furthermore the presence of S and Zn are indicative of particles generated through the vulcanisation process of which they are by-products (Bennett *et al.*, 2011).   Individual particles were found to have distinctive morphological and microstructural characteristics i.e. 'spherical' and 'molten drop' with 'smooth' and 'orange-peel' textures which are indicative of high temperature combustion processes (Xue and Lu, 2008; Bourliva and Papadopoulou., 2015).

Tyre dust particles are a component of the tyre wear debris and smoke which is produced through the chemical and mechanical processes which occur during landing and taxiing operations (Grigoratos and Martini 2015). Particles may also result from nose wheel tyre abrasion during undercarriage retraction following take-off. The chemical composition of the particles is likely to be reflective of the composition of the main aircraft tyre components (i.e. body, sidewall, tread and beads) (Kongo Kondé *et al.*, 2013) and the elements used within the vulcanisation process (Lobo *et al.*, 2013; Wik *et al.*, 2009; Grigoratos and Martini, 2015).

8.3.2 Environmental Samples

The main elemental metallic composition of each of the environmental samples is outlined in Chapter 6, (§ 6.2).

8.3.2.1 Runway Dusts

The SEM/EDX results for the runway dusts (§ 6.2.1) identify differences between the morphological and chemical characteristics between the samples collected within Zones A and B.

The Zone A runway dust particles were found to predominate within the ≤10 µm size range. C and O rich angular, rounded and sub-rounded particles were identified within the dusts in this Zone.   These particles display similar

morphological and chemical characteristics to those of the aircraft engine dust particles. The varied elemental composition of the particles within the Zone A runway dusts probably reflects the differences in the composition of Jet A-1 aviation fuel (Schäfer *et al.*, 2006) and the differences in aircraft engine type and the associated combustion process. Variations may also result from the differences in the elemental composition of the particles derived from the mechanical wear and erosion of aircraft engine parts and airframe corrosion (Amato *et al.*, 2010; Mazaheri *et al.*, 2013).

The results are indicative of the release and subsequent accumulation of engine dust particles resulting from the high temperature combustion processes which occur within the aircraft engine exhaust system during the initial stages of take-off (Mazaheri *et al.*, 2013).

The Zone B runway dusts were found to be extremely varied with particles being evenly distributed across each of the roundness categories although the particle size was predominantly within the ≤10 µm size fraction. SEM/EDX analysis of the particles within this Zone shows similarities to the brake and tyre dust particles. Zone B is the predominant landing Zone for runway 23L/05R. The morphological and chemical characteristics of the particles within this area indicate that they are predominantly associated with the production and subsequent release of brake wear and tyre smoke particulates during landing. The variations in chemistry probably relate to the varied composition of brake pads, discs and tyres.

8.3.2.2 Taxiway and Apron Dusts

The main elemental metallic composition of the taxiway and apron dusts is detailed in (§ 6.2.2).

Analysis of the particles within the taxiway and apron dust samples shows a wide range of morphological and chemical characteristics. The variation in the particles within the samples collected within these areas reflects the wide variation in aircraft manoeuvres and airport operations that take place within these areas. The presence of aircraft engine related particles are clearly

evidenced within both the taxiway and apron dust samples. Such particles are indicative of the aircraft engine emissions released during APU operations; engine check starts; initial start-up and taxiing (Masiol and Harrison, 2014).

Brake and tyre derived particles are also widespread throughout both the sample sets. The presence of these particles partly reflects the intensity of the routine aircraft movements and operations that take place throughout these areas. A further contribution to the emissions within these areas may result from the vehicular derived exhaust and non-exhaust particles that may also be generated through the operation of the extensive number of vehicles and ground support equipment that operate within the airfield perimeter.

The presence of Al, Si and Ca within both samples sets may also be reflective of the particles associated with the asphalt runway; taxiway and apron material and soil minerals (Adachi and Tainosho 2004).

Furthermore, the wide variation in the morphological and chemical characteristics of the particles within the taxiway and apron dusts may also be attributable to the resuspension of materials from various sources owing to the turbulence created by the intensive aircraft and vehicle activities that take place within these areas (Curran, 2006).

8.4 ESR

The ESR results for the aircraft source and environmental samples are presented in Chapter 7 (§7.1 to 7.2). To enable comparison between the individual samples and for the purposes of ESR modelling, the ESR spectra for each of the aircraft source and environmental samples has been averaged into eight plots (spectra) Figure 8.17).

8.4.1 Aircraft Source Samples

The ESR results for the aircraft source samples (i.e. engines, brakes and tyres) is presented in Chapter 7 (§ 7.1). The results highlight distinct differences between the ESR spectral characteristics of each of the three dust groups.

The engine dust spectra are all very similar each displaying a very distinctive broad line resonance peak. Spectra characteristics of this type have previously been identified in carbon based materials such as soots and carbon blacks (Peña *et al.*, 2001). The similarities between the ESR spectra of the carbon based materials and the engine dusts are likely to relate to the predominance of carbonaceous material (i.e. soot) within the primary particulates that are produced within the combustion section of the jet engine through the incomplete combustion of the Jet A-1 fuel (Petzold *et al.*, 2005; Herndon *et al.*, 2008; Dodson *et al.*, 2009). In the samples here, however, the peak widths are about a factor of 10 larger. This indicates a much greater variability in the engine dusts when compared to the pure carbon blacks. This is probably caused by the heating that the engine dust has undergone as well as lower chemical purity.
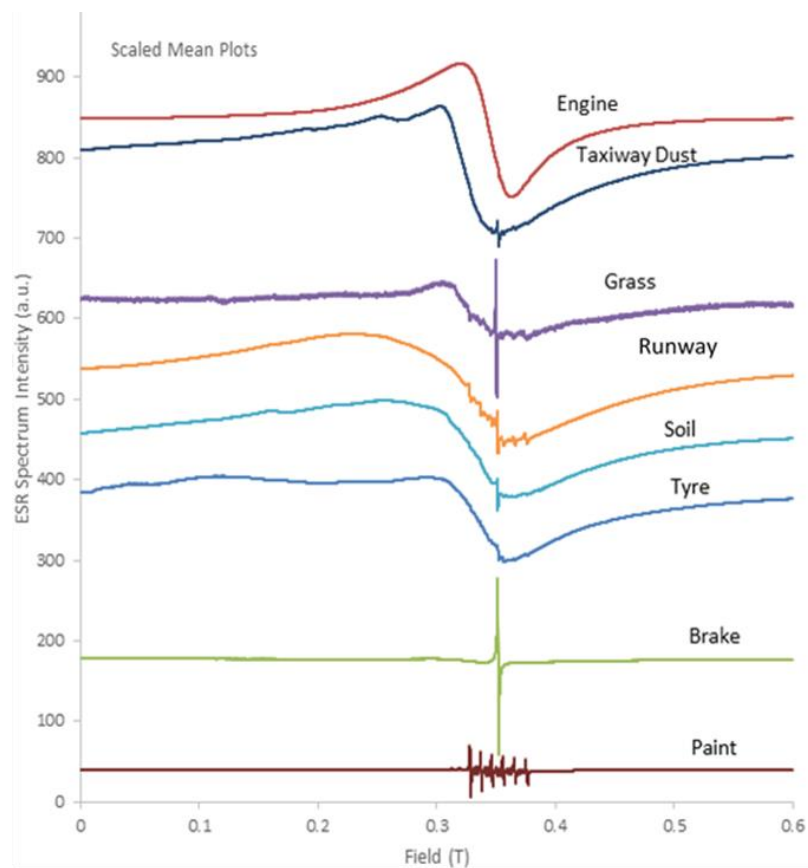
Figure 8.17: Scaled mean plots displaying the ESR spectra of the individual aircraft source (i.e. engine, brake and tyre) and environmental samples (i.e. runway dust; taxiway dust; grass; soil and runway marking debris). The spectra have been offset (by between 180 and 850ESR absorption arbitrary units (a.u.) and scaled by a factor of (x1, x2, x40) (Appendix 4).

The brake dusts display a classic g = 2 narrow line spectrum which results from paramagnetic free electron spins in carbon like materials (Peña *et al.*, 2001; Alagarsamy and Hoon 2017). Whilst the resonance frequency differs owing to spectrometer differences, the shape of the absorption line of the brake spectra is seen to be similar to those identified in certain carbon black grades after being subjected to different heat treatments (Figure 8.18) (Peña *et al.*, 2001). Modern aircraft feature C/C composite brakes. It is possible, therefore, that the occurrence of this spectra within the brake dust samples, relates to changes in the morphology and chemical structure of the C/C composite brakes that are caused during the high temperature conditions that occur during routine braking operations.
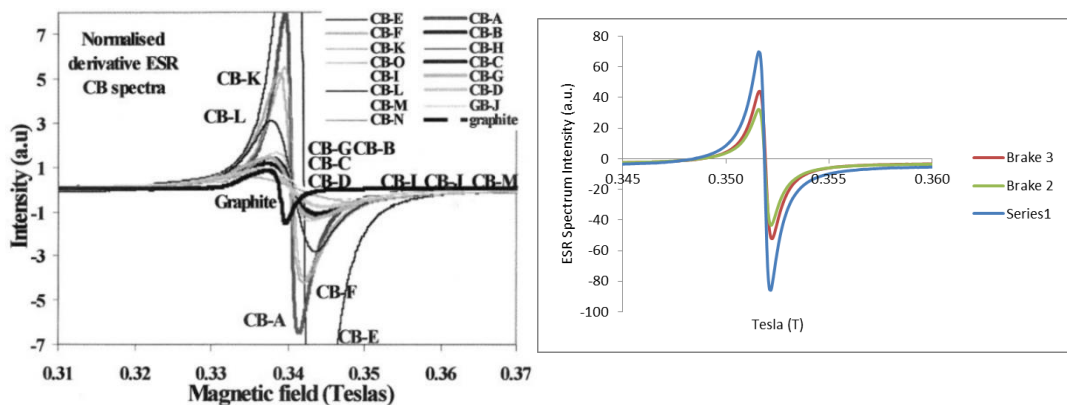
Figure 8.18: The graph on the left shows the normalised derivative ESR spectra of different Carbon Black grades (Peña *et al.*, 2001:161). The line width corresponds closely with that of the brake dust spectra which is displayed to the right.

The multi-line ESR spectra of the tyre dusts (Figure 7.3) indicate the presence of several inputs including Fe. These dusts display a relatively small amount of g = 2 absorption overlying a broad resonance ferri- of multiple para-magnetic resonance peak with three lower field (high g-value) features. These spectra are consistent with the multiple materials employed in the fabrication of tyres during manufacture (Amari *et al.*, 1999; Bennett *et al.*, 2011; Grigoratos and Martini, 2015). Aircraft tyres are composed of various materials (Lobo *et al.*, 2013) including a range of carbon polymeric and trace compounds which are used

during manufacture of aircraft tyres. Data relating to the specific composition of aircraft tyres are, however, currently unavailable (§ 8.1.1) although it is known to vary depending on the manufacturer.

Tyre wear particles are a component of the tyre wear debris which is produced through the abrasion caused by the nose wheel tyre rubbing against the 'snubber pads' during take-off and the tyre smoke particulates produced through frictional heat generation generated during landing and taxing operations.

8.4.2 Environmental Samples

The ESR results for each of the environmental samples are outlined in Chapter 7 (§7.2.1 to 7.2.5).

8.4.2.1 Runway Marking Debris

The ESR spectra of the runway marking debris (yellow paint) clearly displays a classic six line paramagnetic Mn^{2+} ion spectrum. Mn^{2+} impurities are prevalent in the environment as well as many industrial materials, and are also found in chalk and limestone and are therefore likely to be a component of the concrete runway surfaces. Most importantly, however, the presence of this component within the runway marking debris (yellow paint) sample establishes Mn^{2+} as a marker material within the airport environment.

8.4.2.2 Runway Dusts

The runway dust (§7.2.1) spectra are comprised of multiple components, indicative of inputs from different sources or sources that themselves comprised of more than one magnetic material. The presence of the g = 2 and Mn^{2+} components together with the very broad humped spectra is consistent with the presence of many different para- and ferri- magnetic components. The narrow g = 2 component, which was also evident within the brake and tyre dusts (§8.4.1), in the airport environment, is indicative of the presence of carbon based materials (Peña *et al.*, 2001).

Such materials are found within the brake and tyre wear particulates and tyre smoke which may be deposited on the runway during aircraft landing and taxiing operations. Mn^{2+} impurities may be indicative of inputs from various sources (§8.4.2.1). However, the Mn^{2+} component has been established as a marker for runway marking debris within the airport environment and therefore its presence within the runway dust spectra may indicate the accumulation of particulates derived from the erosion of runway markings (Adachi and Tainosho, 2004) and furthermore may also reflect inputs resulting from the resuspension of materials due to the turbulence from aircraft activities (Adachi and Tainosho, 2004; Curran, 2006).

8.4.2.3 Taxiway Dust

The taxiway dust (§7.2.2) comprises a multicomponent ESR spectrum. The presence of a g = 2, component and the multiple para-magnetic resonance peak comprising three lower field (high g-value) features is indicative of the presence of inputs of brake and tyre derived materials. Such inputs reflect the accumulation of brake and tyre wear emissions from aircraft and ground support equipment and vehicles during the intensive aircraft manoeuvres and operations that take place within these areas (§8.1.1.2 and 8.2.2.2). The resuspension of previously deposited material due to the turbulence created by moving traffic may provide a further contribution (Curran, 2006).

8.4.2.4 Grass

The multicomponent features seen clearly in the ESR spectra of the grass samples (Figure 7.7) and in the ESR spectrum of the mean grass data (Figure 8.17) include a broad resonance (ferri- or multiple para- magnetic resonance) peak with one low field (high g-value) feature, a narrow single line peak at ~0.35T and a Mn^{2+} component. Vegetation has been shown to be an effective receptor and biomonitor of PM (Matzka and Maher, 1999; Szonyi *et al.,* 2008; Hansard *et al.,* 2011; Sadeghian, 2012; Muñoz *et al.,* 2017) and therefore the presence of these components within the grass samples may reflect the inputs from aircraft and local airport derived sources.

The broad resonance feature which occurs at a field of ~0.12T (and thus g-value) is consistent with Fe^{3+} paramagnetic ions and is also featured within the engine dust spectra. The presence of this component within the runway grass samples may, therefore, reflect the deposition of particulates released from aircraft engines. However, the presence of this component may also be representative of soil inputs related to the growth process. The presence of the narrow $g = 2$ component at ~0.35T, also present within the aircraft brake and tyre dusts suggests the presence of carbon based materials (Peña *et al.*, 2001) which is indicative of the presence of aircraft brake and tyre wear. The Mn^{2+} component as discussed in (§ 8.4.2.2) may be representative of inputs from various sources.

8.4.2.5 Soil

The ESR spectrum of the soil is very similar to the one seen within the taxiway dust samples and therefore the presence of these components within the soil samples is likely to reflect the varied inputs from brake and tyre derived materials as discussed in § 8.4.2.3.

8.5 Synthesis

8.5.1 Aircraft Source Samples

Significant differences have been observed between the magnetic mineral, geochemical, morphological and ESR spectra characteristics of each of the aircraft source samples (i.e. aircraft engine, brake and tyre dusts). The differences in the characteristics which are displayed between each of the three dust groups are thought to relate to differences in the iron content and chemical composition of Jet A-1 aviation fuel; aircraft engine exhaust components; Carbon-Carbon (C/C) brakes and tyres and the associated particle generation processes.

8.5.1.1 Engine Dusts

The engine dusts are characterised by finer ferrimagnetic sizes with a significant antiferromagnetic component and a unique presence of Ni and Cr. SEM/EDX analyses of the individual particles shows that the engine dusts are dominated by

small <5 µm, C and O rich particles. The morphology of these particles is varied and includes rounded and sub rounded particles although angular and sub-angular particles are seen to predominate. The ESR spectra of these dusts are dominated by a single, broad line resonance peak.

The ESR spectra of the engine dusts indicate that they are composed of carbon based materials (Peña *et al.*, 2001) which are produced during the high temperature combustion processes that take place within the combustion section of the engines. During this stage, carbonaceous primary particulates (soot) composed of organic compounds and elemental or black carbon are formed through the incomplete combustion of Jet A-1 aviation fuel (Petzold et al., 2005; Herndon *et al.*, 2008; Dodson *et al.*, 2009). These particulates and also magnetic particulates formed through these processes are commonly associated with heavy metals (e.g. Xie *et al.,* 2001; Zhu *et al.,* 2013). The morphological and microstructural characteristics of the small rounded 'spherical' particles identified within the engine dusts are typical of those originating from high temperature combustion processes (Blaha *et al.*, 2008; Lu *et al.*, 2008; Kim *et al.*, 2009; Bourliva and Papadopoulou., 2015) and have been found to be a constituent of aircraft engine emissions (Mazaheri *et al.*, 2013). Metal particles and trace amounts of other elements have also been identified as being a component of aircraft engine emissions (Starik, 2008; Masiol and Harrison *et al.*, 2014; Mazaheri *et al.*, 2013; Abegglen *et al.*, 2016). Iron impurities are converted into magnetic iron oxides during high temperature combustion. The specific nature of the iron impurities in the Jet A-1 fuel and/or the chemical procesees that take place during the fuel combustion stage may relate to the significant antiferromagnetic mineral (haematite-like) content of these particulates, as is further evidenced in the ESR spectra by the presence of the Fe^{3+} component and the broadline nature of the general dust spectra.

The more angular and sub-angular particles are characteristic of those derived through the erosion and mechanical wear of engine components (Masiol and Harrison *et al.*, 2014). The unique presence of Ni and Cr within the engine dusts and associated particles reflects the presence of these elements within the

composition of Jet A-1 aviation fuel (Schafer *et al.*, 2006) and in aircraft engine exhaust components.

8.5.1.2 Brake and Tyre Dusts

In contrast to the engine dusts, the brake and tyre dusts are comprised of coarser grained ferrimagnetic minerals and are enriched with Ti, Cu and Zn. Whilst the brake and tyre dusts display very similar magnetic and chemical characteristics, significant differences are observed in the morphological and chemical characteristics of the individual particles and the ESR spectra of each dust.

8.5.1.3 Brake Dusts

The brake dust particles, which are largely within the <10 µm size range, are dominated by C and O rich sub-angular particles. Though less abundant, the presence of 'rounded' particles are also clearly evident within these samples. The ESR spectra of these dusts are dominated by a very distinctive narrow, single line resonance peak. The ESR spectra of the brake dust samples are indicative of the predominance of carbon based materials within these dusts (Peña *et al.*, 2001; Algarsamy *et al.*, 2017). Such materials reflect the C/C composition of modern aircraft brakes which is a component of the brake dust and wear debris produced as a result of the mechanical and/or chemical reactions that take place on sliding surfaces during operation of the aircraft brakes. The coarser grained ferrimagnetic characteristics and the presence of Ti, Cu and Zn within the brake dusts is thought to be associated with the composition of the additives used to modify the friction properties, temperature characteristics and mechanical properties of aircraft brake components or to act as antioxidants during braking operations (Blau, 2001; Wahlström *et al.*, 2010; Bruno, 2016). The individual brake dust particles were found to be in the small size range <10 µm and dominated by C and O. Significant differences were, however, observed in the morphological characteristics of the individual particles. The small 'rounded' particles are indicative of those being formed under high temperature conditions (Blaha *et al.*, 2008; Kim *et al.*, 2009) and are indicative of the very high operating temperatures ~300 - 400°C (BA Engineering pers.comm.) that occur within the

braking mechanism area through the function of the aircraft brakes during landing and taxiing operations. In contrast to this, the sub-angular particulates which predominate the brake dusts are thought to be representative of particles associated with the abraded lining material from discs and brake pads and that associated with the friction layer of C/C composite brakes.

8.5.1.4 Tyre Dusts

The tyre dusts display a multi-line ESR spectra in contrast to the single line spectra evident for the engine and brake dusts. There is also much greater variation in relation to the size of the individual tyre dust particles, although particles within the ≤ 20 µm size range are seen to predominate. The tyre dusts are dominated by rounded 'spherical' C and O rich particles with a unique presence of Zn and display distinctive 'smooth' and 'orange-peel' textures.

The ESR spectra of the tyre dusts indicate that they are comprised of several components including carbon based materials and Fe. Whilst carbon is known to be a key component in the manufacture of tyres, data relating to the specific composition of aircraft tyres is commercially sensitive although they are known to contain a wide range of materials including metals (Lobo *et al.*, 2013).

Tyre dusts are a component of the PM that is formed through the spin brake function as the nose wheel tyre rubs against the 'snubber' pads during undercarriage retraction following take-off. The distinctive morphological and structural characteristics of the 'rounded' tyre dusts particles are indicative of the high temperature processes involved within this short-term stage. The frictional temperatures that are generated during this phase must also be sufficient to convert any iron impurities into magnetic forms of iron oxides. The occurrence of Cu and Zn within the tyre dusts reflects the chemical composition and manufacturing processes involved in the manufacture of tyres.   Cu is a component of the tyre beads (McAfee *et al.*, 2016) whilst the presence of Zn is undoubtedly related to the use of Zn during the tyre rubber vulcanisation process (Adachi and Tainosho, 2004; Bennett *et al.*, 2011; Grigoratos and Martini, 2015). Such metals are a component of the tyre smoke particulates produced through the chemical (e.g. volatilisation) and mechanical (shear forces) which occur during landing.

8.5.2 Environmental Samples

8.5.2.1 Runway Dusts

Significant variations have been identified in the magnetic; chemical; morphological and ESR spectra characteristics of the runway dusts collected within Zone A and Zone B.

The Zone A dusts display a predominantly fine-grained ferrimagnetic mineral assemblage with a significant antiferromagnetic component. The individual C and O rich particles within this zone are comprised of angular, rounded and sub-rounded particles in the ≤10 µm size range. The magnetic characteristics of the dusts and morphological features of the runway dust particles in this zone display a close correspondence to those of the engine dusts and reflect the chemical composition of Jet A-1 aviation fuel and aircraft engine exhaust components and the associated combustion processes and mechanical wear and erosion (Schäfer *et al.*, 2006; Amato *et al.*, 2010; Mazaheri *et al.*, 2013). Zone A incorporates the initial stages of the take-off roll for aircraft departing on Runway 23L. The results suggest an accumulation of aircraft engine exhaust particulates released during the initiation of take-off when the aircraft is still moving relatively slowly. These findings are consistent with those of Zhu *et al.* (2011) who observed very high concentrations of ultrafine particulates immediately downwind of the take-off zone at Los Angeles International Airport.

The Zone B dusts are dominated by coarse-grained ferrimagnetic minerals and display high concentrations of Zn, Cu and Ti. SEM/EDX analyses identifies the presence of C and O rich particles across each of the roundness categories but predominantly within the ≤10 µm size range. The Zone B runway dusts display similar magnetic and chemical characteristics to those of the brake and tyre derived dusts. Such findings point to the production and release of brake wear and tyre smoke particulates and subsequent deposition onto the runway surface during landing and taxiing operations. (Lobo *et al.*, 2013).

Furthermore, the multicomponent ESR spectra of the runway dusts further confirm the presence of brake and tyre wear particles and tyre smoke within these dusts. The Mn^{2+} component has, however, been identified as a marker for

runway marking debris and, therefore, the presence of this component within these samples may reflect the accumulation of particles derived from the erosion of runway markings (Adachi and Tainosho, 2004). However, Mn^{2+} impuriries are also present in other environmental and industrial materials including marine carbonates which are used in the manufacture of concrete. Therefore, the presence of this component may also be reflective of inputs from other sources such as concrete dust derived through weathering of the runway surface. The subsequent resuspension of such materials may occur through the turbulence created by aircraft manouevres during taxiing, take-off and landing (Adachi and Tainosho, 2004; Curran, 2006).

8.5.2.2 Taxiway and Apron Dusts

The taxiway and apron dusts display wide variation in terms of magnetic, chemical, and morphological characteristics, as is further evidenced by the multicomponent ESR spectra of the taxiway dust sample. There is no obvious unique distinction between the two areas although some inter-site variability is apparent. Both areas comprise a mixed magnetic assemblage containing both ferrimagnetic and antiferromagnetic mineral assemblages. Whilst there is a clear predominance of ferrimagnetic mineral grain sizes throughout the areas, finer ferrimagnetic mineral grain sizes are also evident. The morphological and chemical characteristics of the samples are also extremely varied. The wide variability in the characteristics of the dusts in these areas is representative of the presence of particulates from a wide range of sources. Such variability is indicative of the nature and intensity of the aircraft manoeuvres and airport operations that take place throughout the apron and taxiway areas. The results indicate that inputs within these areas are derived from a number of different sources including aircraft engine emissions, APU emissions, brakes and tyres, as well as exhaust and non-exhaust emissions from the extensive number of vehicles and ground support equipment that operate within the airfield perimeter. The results also suggest that these areas contain inputs from other sources including the asphalt runway; taxiway and apron material and soil minerals as well as inputs from other sources resulting from the resuspension of materials as

a result of the intensive airport operations that take place throughout the taxiway and apron areas (Curran, 2006).

8.5.2.3 Runway Grass Samples

The runway grass samples do not show any clear variability and zonation in terms of magnetic mineralogy and chemical composition, and there is an absence of the distinctive magnetic and chemical characterisics that have been identified within each of the aircraft source samples, and which are clearly evidenced within the runway dust samples.

However, higher concentrations of magnetic minerals were observed in the samples collected close to the runway threshold and up to 475 m along the runway. This zone of high magnetic mineral concentrations corresponds closely to findings of the Zone A runway dusts and is thought to reflect the accumulation on the vegetation surfaces of magnetic particulates released from aircraft engines during the early stages of the take-off cycle. These findings are consistent with those of the Zone A runway dusts and of those of a research study at Los Angeles International Airport in which very high concentrations of ultrafine particulates were measured immediately downwind of the take-off zone (Zhu *et al.* 2011). The presence of Cu and Zn within the runway grass samples is indicative of the deposition of particulates relating to aircraft brake and tyre wear, although there is no clear spatial pattern in terms of the distribution of these metals.

The magnetic and chemical data for the runway grass samples have been shown to be very limited and inconclusive. Previous researchers have identified significant variability between the leaves of different vegetation species in relation to their ability for capturing PM (Cao *et al.,* 2015; Munoz *et al.,* 2017). Therefore, the absence of a significant antiferromagnetic component within these samples is likely to be reflective of the inefficiency of grass leaves as an effective biomonitor rather than being attributable to an absence of aircraft engine emissions along the runway transect. The ESR spectra of the grass samples does however indicate the presence of an Fe^{3+} component which is consistent with those featured within the engine dust spectra and therefore indicative of the

presence of aircraft engine exhaust emissions within these samples. A Mn^{2+} component is also evident within these samples. The presence of this component, which is also evident within the runway dust samples, indicates the presence of runway marking debris resulting from the erosion of runway markings (Adachi and Tainosho, 2004). However, Mn^{2+} impurities are endemic in the environment and also in many industrial materials including civil engineering (marine carbonate sediment based) concrete. Therefore, the incidence of this component within the runway grass samples may reflect the inputs from other sources including soil as well as inputs from other materials which may become resuspended through the intensive aircraft manouevres that take place throughout the runway and adjacent areas (Curran, 2006).

8.5.2.4 Taxiway and apron grass samples

The taxiway and apron grass area data are very limited and shows no obvious distinction between the magnetic and chemical characteristics of the samples collected within each of the areas. The magnetics data are, however, consistent with those of the taxiway and apron dusts which suggests that these areas include inputs from various sources relating to the varied and intensive aircraft manoeuvres and ground operations associated with these environments (§ 8.5.2.2).

There is an absence of Cr and Ni within the taxiway and apron grass. These have been shown to be indicative of aircraft engine exhaust emissions. Very little variation is observed in the concentration of Cu and Zn throughout these areas which is also indicative of the deposition of particulates resulting from aircraft and vehicle brake and tyre wear. The absence of the chemical engine dust 'fingerprint' within the runway grass samples reinforces the unsuitability of grass as an efficient medium for the deposition of PM.

8.5.2.5 Runway soil samples

The runway soil samples display high concentrations of magnetic minerals throughout the transect with very high concentrations being particularly prominent

within the critical area and up to 275 m along the runway. The runway soil samples display little variation in terms of magnetic mineralogy, which is shown to be ferrimagnetic with a significant antiferromagnetic component throughout the transect. There is, however, considerable variation in ferrimagnetic grain size, with shifts between finer and coarser ferrimagnetic grain sizes being evident throughout. The finer ferrimagnetic mineral assemblages and the significant antiferromagnetic component which are seen throughout the critical area and up to 275 m along the runway are consistent with the findings of the runway dust samples. This area also corresponds with a zone of higher magnetic mineral concentrations which is also evident in the runway dusts and grass samples. Such findings support those of Zhu *et al.* (2011) and are indicative of an accumulation of aircraft engine exhaust emissions during the initial stages of the take-off roll.

Whilst little variability is shown in the concentration of Ni and Cr along the runway transect, higher concentrations of Ti, Zn and Cu are observed throughout with particularly high concentrations being evident between 2125 m and 2625 m. This area of the runway corresponds with that of Zone B in the runway dusts and is representative of the predominant landing area for aircraft arriving on Runway 05R. Increased concentrations of these metals within the runway soil samples within this area suggests an accumulation of brake and tyre particulates during landing and taxiing operations (Lobo *et al.*, 2013). Such findings are further supported by the presence of the multiple paramagnetic resonance peak within the soil ESR spectra, this being indicative of inputs from brake and tyre derived materials.

The interpretation of the soil magnetic and chemical data has probably been complicated by inputs from various natural and anthropogenic sources (Hanesch *et al.,* 2007). Such sources include atmospheric deposition from local, aircraft-related activities as well as regionally derived anthropogenic particulates. Further inputs may include primary magnetic minerals which are present through weathering of the soil parent material. The underlying geology is a Bollin Mudstone. The Iron (III) component within this rock type is usually haematite (Hobbs *et al.*, 2002) which may account for the antiferromagnetic content which

is prevalent throughout a significant part of the runway transect. Enhancement of the near-surface concentration of magnetic minerals may also be associated with various pedogenic processes involving the fermentation and decomposition of organic matter. Such processes typically produce fine grained ferrimagnetic minerals (Maher, 1986) which may also account for the presence of this component within the runway soil samples.

8.5.2.6 Taxiway and Apron Soil Samples

The taxiway and apron soil samples display wide variability in relation to magnetic mineralogy with no obvious distinction between the two areas. Whilst little variation is shown in the concentration of Ni and Cr throughout the sample sets there is, significant variability shown in relation to Ti, Cu and Zn concentrations with the highest concentrations being evident within the apron soils. The variation in the magnetic and chemical characteristics of the taxiway and apron samples is indicative of inputs from the different aircraft manoeuvres and ground support operations that take place throughout these areas. However, the more significant presence of Ti, Cu and Zn identified within the apron soils suggests that there is a greater input of brake and tyre wear emissions within this area. It must also be noted, as for the runway soil samples, that inputs from various other sources may provide a further contribution to the magnetic mineral and chemical composition of the soils within these areas (§ 8.5.2.5).

Chapter 9

Research Findings and Conclusions

9.1 Research Findings

The main aim of this research project has been to develop a methodology to enable the identification of distinctive and characteristic 'fingerprints' of primary particulates from different airport derived sources (aircraft engines, brakes and tyres) and furthermore, to use these 'fingerprints' to investigate source attribution and assess the relative contribution of different emission sources within the 'airside' airport environment. A mixed analytical approach incorporating magnetic measurements, geochemical analysis, scanning electronic microscopy (SEM); energy dispersive x-ray (EDX) and electron spin resonance (ESR) has been used to identify distinctive and characteristic 'fingerprints' of primary particulates derived from different commercial aircraft sources. The characteristics of dust samples collected from aircraft engines, brakes and tyres have been shown to differ significantly.

A magnetically 'harder' magnetic mineral component related to the presence of antiferromagnetic minerals, together with finer ferrimagnetic mineral grain sizes and the unique presence of Ni and Cr distinguishes the engine dusts from aircraft brake and tyre derived PM deposits which are characterised by the predominance of coarser ferrimagnetic mineral assemblages and the presence of Ti, Cu and Zn.

Distinctive differences have also been observed between the morphological and chemical composition of the individual particles in each of the aircraft derived dust sources. The engine dusts are characterised by smaller, respirable and thus potentially toxic, <5 µm sub-angular and angular particles and a less abundant presence of rounded particles. The brake dusts are characterised by the dominance of sub-angular particles which are largely in the ≤ 10 µm size range. The tyre dusts comprise mostly rounded particles. The size of these particles is more variable than those of the engine and brake dusts although they are largely

within the ≤ 20 µm size range. EDX analysis of the individual particles enables further differentiation between the different sources. Engine dust particles display a unique presence of Ni and Cr and the tyre dusts Zn, whilst the brake dust particles have an absence of the characteristic elemental 'fingerprints' which are evidenced within the engine and tyre dusts.

The contrasting characteristics of these dusts are thought to relate to differences in the chemical compositions of aviation fuel (Jet A-1) combined with engine lubrication oil and mechanical wear; C/C brakes and tyres used on commercial aircraft and the associated combustion processes and temperatures under which the associated particulates are formed. These results demonstrate the potential of a multi analytical approach for the identification and differentiation of particles from three different aviation sources within an airport environment.

Similar techniques have been applied in this study to various atmospheric dusts, grass and surface soil samples, as opposed to point sources, collected from within the airport environment in an attempt to investigate the spatial distribution of deposited particulate matter and the potential for identifying the emission sources. The runway data suggests that there is wide variation in the magnetic mineral assemblage; chemical composition and morphology of the dusts collected within the predominant take-off zone (Zone A) and those from the landing zone (Zone B). The samples collected within the take-off zone show a close resemblance (in terms of their magnetic, chemical and morphological characteristics) to those of the engine dusts. In contrast the samples collected within the landing zone display similar characteristics to those of the brake and tyre dusts.

The runway grass and soil data is less conclusive. No obvious zonation is apparent along the runway transects, as evidenced within the runway dust samples. However, the results do suggest that there is an accumulation of aircraft engine derived particulate matter emissions close to the runway threshold and which extends to ~ 450m along the runway. Such emissions are thought to represent an accumulation of engine dust particulates released during the initial stages of the take-off cycle. Overall, however, the results for the samples collected alongside the runway are largely inconclusive and probably reflect the

limited efficiency of grass as an effective biomonitor and the complexity of the various anthropogenic and natural inputs in surface soils originating from atmospheric deposition and natural pedogenic processes.

The techniques have also been applied to taxiway and apron dusts, soil and grass samples. The results reflect the complexity of inputs of PM from various sources within these areas including manoeuvring aircraft, ground support vehicles and equipment, buildings and the resuspension of previously deposited materials.

In a supplementary study, the application of ESR has demonstrated the potential use of this technique to assist in the characterisation of airport derived sources. ESR analysis has enabled the identification of unique and distinctive spectral 'fingerprints' which characterise each of the aircraft sources i.e. aircraft engine, brake and tyre dusts. Whilst Mn^{2+} impurities are endemic in the environment, the presence of this distinctive component within a sample of eroded runway marking debris establishes Mn^{2+} as a potential marker for materials derived from the erosion of runway, taxiway and apron markings. The identification of such 'fingerprints' highlights the potential use of ESR as a technique to assist in source apportionment particularly in areas which feature a complexity of inputs from various sources e.g. taxiway and apron areas.

9.2 Concluding Remarks

In conclusion, the results of this research project demonstrate that a multiple analytical approach incorporating the use of magnetic measurements, geochemical analysis, SEM/EDX and ESR can be used for the identification of PM sources in the airport environment. Furthermore, the potential application of such distinctive 'fingerprints' to investigate source attribution within the airport environment and to assist in the assessment of the potential impact of airport derived PM on airport employees, passengers and the surrounding communities.

9.3 Suggestions for Further Work

The complex nature of PM in the airport environment requires further investigation. Mounting concerns have been raised regarding the potential health issues for airport employees and those living and working in close proximity to

airports which may be associated with increased exposure to airport derived PM emissions (Press-Kristensen, 2012). Therefore, further investigations into PM within the airport environment should include:

i)   SEM/EDX analysis of magnetic extracts: Previous studies have focused on SEM/EDX analysis of magnetic particles to characterise and distinguish those derived from various anthropogenic and natural sources (e.g. Kim et al. 2007; Blaha et al. 2008; Bucko 2012; Górka-Kostrubiec 2015). However, within this study the extraction of magnetic particulates proved unsuccessful due to the low sample masses of the individual samples. Further work may therefore include the collection of additional aircraft source and environmental dust samples which may be bulked together to provide a larger sample mass in preparation for magnetic extraction techniques. The use of such techniques may contribute to the identification of distinctive aircraft and airport derived magnetic 'fingerprints' which could further assist in the investigation of PM pollution within the airport environment.

ii)   In this study SEM has been used to investigate the particle size and morphology of the aircraft source and environmental dust samples. Particle size is critical as PM_{10} and $PM_{2.5}$ have been identified as posing a serious threat to human health due to the potential for entering into the human respiratory system (Spassov *et al.*, 2004; Nelin et al., 2012). Therefore, further work may involve the use of particle size analysis to provide more detailed investigations into the size of particles derived from aircraft and airport related sources.

iii)   Within this study aircraft source sampling has been focused on different jet aircraft types and engines. Further research may extend the sampling to include other aircraft and engine types such as turboprop and turboshaft.

iv)   The supplementary ESR study which was conducted as part of this research demonstrates the potential for using ESR as a technique for the investigation of PM within the airport environment. Different aircraft and airport related sources have been found to display distinctive spectra 'fingerprints' which could be usefully applied to areas in which there appears to be a greater

complexity of inputs from various sources. The ESR spectra 'fingerprint' associated with different aircraft and environmental sources highlights the potential for using ESR within areas which feature a complexity of inputs from various sources e.g. taxiway and apron areas.

v)   In the present research study the environmental sampling at MAN was restricted to the available environmental mediums i.e. taxiway, apron and runway dusts, grass and soil. It would be interesting, therefore, to investigate the possibility of positioning high volume air samplers or artificial passive air samplers such as those used by Cao *et al.* (2015) (§ 2.4.2) at locations around the airport such as adjacent to the apron or taxiways. Furthermore, the use of a cascade impactor in conjunction with a high volume air sampler would also facilitate particle size analysis of the collected samples

References

Abegglen, M., Brem, B.T., Ellenrieder, M., Durdina, L., Rindlisbacher, T., Wang, J., Lohmann, U., Sierau, B. (2016). 'Chemical characterization of freshly emitted particulate matter from aircraft exhaust using single particle mass spectrometry'. *Atmospheric Environment*, 134, pp. 181-197.

Abdel-Shafy, H., Mansour, M.S.M., (2016). 'A review on polycyclic aromatic hydrocarbons: Source, environmental impact, effect on human health and remediation'. *Egyptian Journal of Petroleum*, 25 (1), 1pp. 107-123.

Abu-Allaban, M., Gillies, J.A., Gertler, A.W., Clayton, R., Proffitt, D., (2003). 'Tailpipe, resuspended road dust, and brake-wear emission factors from on-road vehicles'. *Atmospheric Environment*, 37 (37), pp. 5283-5293.

Adamo, P., Crisafulli, P., Giordano, S., Minganti, V., Modenesi, P., Monaci, F., Pittao, E., Tretiach, M., Bargagli, R., (2007). 'Lichen and moss bags as monitoring devices in urban areas. Part II: Trace element content in living and dead biomonitors and comparison with synthetic materials. *Environmental Pollution*, 146 (2), pp. 392-399.

Adachi, K., Tainosho, Y., (2004). 'Characterization of heavy metal particles embedded in tire dust'. *Environment International*, 30 (8), pp. 1009-1017.

Agrawal, H., Sawant, A.A., Jansen, K., Miller, J.W., Cocker III, D.R., (2008). 'Characterization of chemical and particulate emissions from aircraft engines'. *Atmospheric Environment*, 42, pp. 4380-4392.

Alagarsamy, R., Hoon, S.R. (2015). 'Use of EPR spectroscopy for the determination of concentration and chemical form of paramagnetic metals in coastal sediments', International Symposium on "Dynamics of Indian Ocean: Perspective and Retrospective", Goa, India, 30 November - 4 December.

Alagarsamy, R., Hoon, S.R. (2017). 'Metal pollutants in Indian continental coastal marine sediment along a 3,700 km transect: An Electron Paramagnetic Resonance spectroscopic study'. *Science of the Total Environment*, 'accepted August 7th 2017'.

Al-Fatlawi, S.M.G., Al-Alwani, M., (2012). 'Heavy metal pollution of roadside dust samples with different traffic volumes at Hilla City'. *The Iraqi Journal for Mechanical and Material Engineering*, 12 (4), pp. 660-672.

Amari, T., Themelis, N.J., Wernick, I.K., (1999). 'Resource recovery from used rubber tires'. *Resources Policy*, pp. 179-188.

Amato, F., Pandolfi, M., Viana, M., Querol, X., Alastuey, A., Moreno, T., (2009). 'Spatial and chemical patterns of PM10 in road dust deposited in urban environment. *Atmospheric Environment*, 43 (9), pp. 1650-1659.

Amato, F., Moreno, T., Pandolfi, M., Querol, X., Alastuey, A., Delgado, A., Pedrero, M., Cots, N., (2010). 'Concentrations, sources and geochemistry of airborne particulate matter at a major European airport'. *Journal of Environmental Monitoring*, 12, pp. 854-862.

Andreau, K., Leroux, M., Bouharrour, A., (2012). 'Health and Cellular Impacts of Air Pollutants: From Cytoprotection to Cytotoxicity'. *Biochemistry Research International,* Vol. 2012, Article ID 493894.

Angino, E.E., Hathaway, R., Worman, J., (1971). 'Identification of manganese in water solutions by electron spin resonance', *in* Nonequilibrium systems in natural water chemistry: *Advances in Chemistry*, Ser. No. 106, pp. 299-308.

Aničić, M., Tomaševića, M., Tasić, M., Rajšić, S., Popović, A., Frontasyeva, M.V., Lierhagen, S., Steinnes, E., (2009). 'Monitoring of trace element atmospheric deposition using dry and wet moss bags: Accumulation capacity versus exposure time. *Journal of Hazardous Materials*, 171 (1-3), pp. 182-188.

Arteaga, V.E., Mitchell, D.C., Matt, G.E., Quintana, P.J.E., Schaeffer, J., Reynolds, S.J., Schenker, M.B., Mitloehne, F.M., (2015). 'Occupational Exposure to Endotoxin in PM 2.5 and Pre-and Post-Shift Lung Function in California Dairy Workers. *Journal of Environmental Protection*, 6 (6), pp. 552-565.

Barrett, S.R.H., Britter, R.E., Waitz, I.A., (2010). 'Global mortality attributable to aircraft cruise emissions'. *Environmental Science and Technology*, 44 (19) pp.7736-7742.

Bennett, M., Christie, S., Graham, A., Thomas, B., Vishnyakov, V., Morris, K., Peters, D., Jones, R., Ansell, C., (2011). 'Composition of smoke generated by landing aircraft'.
Environmental Science & Technology, 45 (8), pp.3533-3538.

Bell, M.L., (2012). 'Assessment of the health impacts of particulate matter characteristics'. *Research report (Health Effects Institute)*, 161, pp. 5-38.

British Geological Survey (BGS), (2017). '*Contaminant distribution in soil*' http://mapapps2.bgs.ac.uk/bccs/home.html [accessed 04 December 2017].

Billon, G., Ouddane, B., Laureyns, J., Boughriet, A., (2003). 'Analytical and Thermodynamic Approaches to the Mineralogical and Compositional Studies on Anoxic Sediments'. *Journal of Soils and Sediments*, 3, pp. 180-187.

Blaha, U., Sapkota, B., Appel, E., Stanjek, H., Rösler, W., (2008). 'Micro-scale grain-size analysis and magnetic properties of coal-fired power plant fly ash and its relevance for environmental magnetic pollution studies. *Atmospheric Environment*, 42 (36), pp. 2878-2890.

Blau, P.J., (2001). '*Compositions, functions, and testing of friction brake materials and their additives*'. Report ORNL/TM-2001/64, Oak Ridge National Laboratory.

Blundell, A., Hannam, J., Dearing, J., Boyle, J., (2009). 'Detecting atmospheric pollution in surface soils using magnetic measurements: A reappraisal using an England and Wales database'. *Environmental Pollution*, 157, pp. 2878-2890.

Boughriet, A., Ouddane, B., Wartel, M., (1992). 'Electron spin resonance investigations of Mn compounds and free radicals in particles from the Seine river and its estuary'. *Marine Chemistry*, 37, pp. 149-169.

Bourliva, A., Papadopoulou, L., (2015). 'Microstructural characteristics of magnetic particles in urban and industrial dusts from Thessaloniki Area, Greece'. *Proceedings of the 14th International Conference on Environmental Science and Technology*, Rhodes, 3 – 5 September.

Boyer, R.R., (1995). 'Titanium for aerospace: Rationale and applications'. *Advanced Performance Materials*, 2 (4), pp. 349-368.

Boyle, J.F., Sayer, C.D., Hoare, D., Bennion, H., Heppel, K., Lambert, S.J., Appleby, P.G., Rose, N.L., Davy, A.J., (2016). 'Toxic metal enrichment and boating intensity: sediment records of antifoulant copper in shallow lakes of eastern England'. *Journal of Paleolimnology*, 55, pp. 195-208.

Bruno, C. (2016). '*Aircraft brake disc materials and methods*'. US Patent 20160281268.

Bućko, M., (2012). 'Application of magnetic, geochemical and micro-morphological methods in environmental studies of urban pollution generated by road traffic'. *Report Series in Geophysics*, 69, pp. 1-65.

Buggiano, V., Petrillo, E., Alló, M., Lafaille, C., Redal, M.A., Alghamdi., M.A., Khoder, M.I., Shamy, M., Muñoz, M.J., (2015). 'Effects of airborne particulate matter on alternative pre-mRNA splicing in colon cancer cells'. *Environmental Research*, 140, pp. 185-190.

Burnett, R.T., Pope III, C.A., Ezzati, M., Olives, C., Lim, S.S., Mehta, S., Shin, H.H., Singh, G., Hubbell, B., Brauer, M., Anderson., H.R., Smith, K.R., Balmes, J.R., Bruce, N.G., Kan, H., Laden, F., Prüss-Ustün, A., Turner, M.C., Gapstur, S.M., Diver, W.R., Cohen, A., (2014). 'An integrated risk function for estimating the global burden of disease attributable to ambient fine particulate matter exposure'. *Environmental Health Perspectives*, 122 (4), pp. 397-403.

Buzcu, B., Yue, Z.W., Fraser, M.P., Nopmongcol, U., Allen, D.T., (2006). 'Secondary particle formation and evidence of heterogeneous chemistry during a wood smoke episode in Texas'. *Journal of Geophysical Research*, 111 (10), D10S13, *doi:10.1029/2005JD006143*.

Cao, L., Apperl, E., Hu, S., Ma, M., (2015). 'An economic passive sampling method to detect particulate pollutants using magnetic measurements'. *Environmental Pollution*, 205, pp. 97-102.

Carugno, M., Consonni, D., Randi, G., Catelan, D., Grisotto, L., Bertazzi, A., Biggeri, A., Baccini, M., (2016). 'Air pollution exposure, cause-specific deaths and hospitalizations in a highly polluted Italian region'. *Environmental Research*, 147, pp. 415-424.

Correia, A.W., Pope III, C.A., Dockery, D.W., Wang, Y., Ezzati, M., Dominici, F., (2013). 'The effect of air pollution on life expectancy in the United States: an analysis of 545 US counties for the period 2000 to 2007'. *Epidemiology*, 24 (1), pp. 22-31.

Crook, N.P., Hoon, S.R., Taylor, K.G., Perry, C.T. (2002). 'Electron Spin Resonance as a high sensitivity technique for environmental magnetism: determination of contamination in carbonate sediments'. *Geophysical Journal International*, 149, pp. 328-337.

Crosby, C.J., Fullen, M.A., Booth, C.A., Searle, D.E., (2014). 'A dynamic approach to urban road deposited sediment pollution monitoring (Marylebone Road, London, UK)'. *Journal of Applied Geophysics*, 105, pp. 10-20.

Curran, R., (2006). '*Method for estimating particulate emissions from aircraft brakes and tyres*'. Technical Report, QineriQ/05/01827, QinetiQ Ltd, Farnborough, UK.

Daley, B., (2010). *Air transport and the environment.* London: Routledge

DEFRA (Department for Environment, Food & Rural Affairs) (2005). '*Particulate Matter in the United Kingdom.*'
https://uk-air.defra.gov.uk/assets/documents/reports/aqeg/pm-summary.pdf
[accessed 23 June 2016].

Deschamps, E., Weidler, P.G., Friedrich, F., Weiss, C., Diabaté, S., (2014). 'Characterization of indoor dust from Brazil and evaluation of the cytotoxicity in A549 lung cells'. *Environmental Geochemistry and Health*, 36 (2), pp. 225-233.

Dodson, R., (2009). 'An analysis of continuous black carbon concentrations in proximity to an airport and major roadways'. *Atmospheric Environment*, 43 (24), pp. 3764–3773.

Eberhard, W.L., Brewer, W.A., Wayson, R.L., (2005). 'Lidar observation of jet engine exhaust for air quality'. *Second Symposium on Lidar Atmospheric Applications,* San Diego, CA, American Meteorological Society, 3 (4), https://ams.confex.com/ams/pdfpapers/83405.pdf [accessed 23 June 2016].

Edina Digimap (2017). Data Download. '*Backdrop Mapping*'.
http://digimap.edina.ac.uk/datadownload/osdownload [accessed 20 May 2017].

EEA (European Environment Agency) (2016). '*Air quality in Europe – 2016 report*'
https://www.eea.europa.eu/publications/air-quality-in-europe-2016 [accessed 08 May 2016].

Elbir, T., (2008). 'Estimation of engine emissions from commercial aircraft at a midsized Turkish airport'. *Journal of Environmental Engineering*, 134 (3), pp. 210-215.

Environment Canada (n.d.), '*Jet A/Jet A-1*'.

http://www.etc-cte.ec.gc.ca/databases/Oilproperties/pdf/WEB_Jet_A-Jet_A-1.pdf [accessed 19 July 2017].

EPA (United States Environment Protection Agency) (2016).'*Health and environmental effects of particulate matter (PM)*'. https://www.epa.gov/pm-pollution/health-and-environmental-effects-particulate-matter-pm [accessed 08 June 2016].

FAA (Federal Aviation Administration) (2013). '*Aircraft Metals Chapter 5: Aircraft materials, processes and hardware*'. https://www.faa.gov/regulations_policies/.../aircraft/amt.../FAA-8083-30_Ch05.pdf [accessed 13 July 17].

Fan, S., Yang, C., He, L., Deng, J., Zhang, L., Cheng, L. (2017). 'The effects of phosphate coating on friction performance of C/C and C/SiC brake materials'. *Tribology International*, 114, pp. 337-348.

Flanders, P.J. (1994). 'Collection, measurement, and analysis of airborne magnetic particulates from pollution in the environment (invited)'. *Journal of Applied Physics*, 75, pp. 5931.

Fuzzi, S., Baltensperger. U., Carslaw, K., Decesari, S., Denier van der Gon, H., Facchini, M.C., Fowler, D., Koren, I., Langford, B., Lohmann, U., Nemitz, E., Pandis, S.,Riipinen, I., Rudich, Y., Schaap, M., Slowik, J.G., Spracklen, D.V., Vignati, E., Wild, M., Williams, M., Gilardoni, S., (2015). 'Particulate matter, air quality and climate: lessons learned and future needs'. *Atmospheric Chemistry and Physics,* 15, pp. 8217-8299.

Gautam, P., Blaha, U., Appel, E., (2005). 'Integration of magnetism and heavy metal chemistry of soils to quantify the environmental pollution in Kathmandu, Nepal'. *Island Arc*, 14 (4), pp. 424-435.

Google Earth 7.1.8.3036 (2017). *Manchester International Airport* 37 25.818' N, 122 05.36' W. Places and Road Layers. https://www.google.com/earth/index.html [accessed 01 July 2017].

Google Maps (2014). *Manchester Airport* https://www.google.co.uk/maps/ [accessed 01 August 2014].

Górka-Kostrubiec, B., (2015). 'The magnetic properties of indoor dust fractions as markers of air pollution inside buildings. *Building and Environment*, 90, pp. 186-195.

Grigoratos, T., Martini, G., (2015). 'Brake wear particle emissions: a review'. *Environmental Science and Pollution Research*, 22 (4), pp. 2491-2504.

Hagino, H., Oyama, M., Sasaki, S., (2016). 'Laboratory testing of airborne brake wear particle emissions using a dynamometer system under urban driving cycles'. *Atmospheric Environment*, 131, pp. 269-278.

Hanesch, M., Rantitsch, G., Hemetsberger, S., Scholger, R., (2007). 'Lithological and pedological influences on the magnetic susceptibility of soil: Their consideration in magnetic pollution mapping'. *Science of the Total Environment*, 382 (2-3), pp. 351-363.

Hansard, R., Maher, B.A., Kinnersley, R., (2011). 'Biomagnetic monitoring of industry-derived particulate pollution'. *Environmental Pollution*, 159 (6), pp. 1673-1681.

Hansell, A.L., Blangiardo, M., Fortunato, L., Floud, S., de Hoogh, K., Fecht, D., Ghosh, R.E., Laszio, H.E., Pearson, C., Beale, L., Beevers, S., Gulliver, J., Best, N., Richardson, S., Elliott, P., (2013). 'Aircraft noise and cardiovascular disease near Heathrow airport in London: small area study'. *British Medical Journal*, 348, pp. 3504.

Hay, K.L., Dearing, J.A., Baban, S.M.J., Loveland, P., (1997). 'A preliminary attempt to identify atmospherically-derived pollution particles in English topsoils from magnetic susceptibility measurements. *Physics and Chemistry of the Earth*, 22(1), 207-210.

Heathrow Airport (2016). Heathrow: Aircraft noise. '*Working towards a quieter Heathrow*'. http://www.heathrow.com/noise [accessed 27 June 2016].

Herndon , S.C., Onasch, T.B., Frank, B.P., Marr, L.C., Jayne, J.T., Canagaratna, M.R., (2005). 'Particulate emissions from in-use commercial aircraft'. *Aerosol Science and Technology*, 39 (8), pp. 799-809.

Herndon, S.C., Jayne, J.T., Lobo, P., Onasch, T.B., Fleming, G., Hagen, D.E., Whitefield, P.D., Miake-Lye, R.C., (2008). 'Commerical aircraft engine emissions characterization of in-use aircraft at Hartsfield-Jackson Atlanta International Airport'. *Environmental Science & Technology*, 42 (6), pp. 1877-1883.

Hobbs, P.R.N., Hallam, J.R., Forster, A., Entwisle, C., Jones, L.D., Cripps, A.C., Northmore, K.J., Self, S.J., Meakin, J.L. (2002). Engineering geology of British rocks and soils - Mudstones of the Mercia Mudstone Group. British Geological Survey Research Report, RR/01/02. 106 pp.

Hsu, H.H., Adamkiewicz, G., Houseman, E.A., Vallarino, J., Melly, S.J., Wayson, R.L., Spengler, J.D., Levy, J.I., (2012). 'The relationship between aviation activities and ultrafine particulate matter concentrations near a mid-sized airport'. *Atmospheric Environment*, 50, pp. 328-337.

Hsu, H.H., Adamkiewicz, G., Houseman, E.A., Zarubiak, D., Spengler, J.D., Levy, J.I., (2013). 'Contributions of aircraft arrivals and departures to ultrafine particle counts near Los Angeles International Airport'. *Science of the Total Environment*, 44 (1), pp. 347-355.

Hu, X., Su, Y., Ye, R., Li, X., Zhang, G., (2007). 'Magnetic properties of the urban soils in Shanghai and their environmental applications'. *Catena*, 70, pp. 428-436.

Hu, S., Fruin, S., Kozawa, K., Mara, S., Winer, A.M., Paulson, S.E., (2009). 'Aircraft emission impacts in a neighbourhood adjacent to a general aviation airport in Southern California'. *Environmental Science and Technology*, 43, pp. 8039-8045.

Hudda, N., Gould, T., Hartin, K., Larson, T.V., Fruin, S.A., (2014). 'Emissions from an international airport increase particle number concentrations 4-fold at 10 km downwind'. *Environmental Science & Technology*, 48 (12), pp. 6628-6635.

Hunt, A., Jones, J., Oldfield, F., (1984). 'Magnetic measurements and heavy metals in atmospheric particulates of anthropogenic origin'. *Science of the Total Environment*, 33, pp. 129-139.

Hunt, A., (1986). 'The application of mineral magnetic methods to atmospheric aerosol discrimination'. *Physics of the Earth and Planetary Interiors*, 42, pp. 10-21.

Hutton, T.J., McEnaney, B., Crelling, J.C., (1999). 'Structural studies of wear debris from carbon-carbon composite aircraft brakes'. *Carbon*, 37, pp. 907-1916.

IATA, (2015) '*IATA Air Passenger Forecast Shows Dip in Long-Term Demand*'. http://www.iata.org/pressroom/pr/Pages/2015-11-26-01.aspx [accessed 27 June, 2016]

ICAO (International Civil Aviation Organization), (2011). 'Airport Air Quality Manual', first ed. International Civil Aviation Organization, Montreal.

ICAO, (2014). Capacity and Efficiency. '*Air Navigation Report*'. https://www.icao.int/airnavigation/Documents/ICAO_AN%20Report_EN_final_30042014.pdf [accessed 08 May 2016].

IPCC (Intergovernmental Panel on Climate Change), (1999). 'Aviation and the global atmosphere'. Summary for Policymakers. IPCC Working Groups I and III.

Johnson, G.R., Mazaheri, M., Ristovski, Z.D., Morawska, L.A., (2008). 'Plume capture technique for the remote characterization of aircraft engine emissions'. *Environmental Science and Technology*, 42, pp. 4850-4856.

Jones, M., (2008). *Engine Fuel Filter Contamination*. Boeing Commercial Aero Magazine QTR_03. (http://www.boeing.com/commercial/aeromagazine/articles/qtr_3_08/pdfs/AERO_Q308_article3.pdf) (accessed 8 June 2013).

Jordanova, D., Jordanova, N., Lanos, P., Petrov, P., Tsacheva, T., (2012). 'Magnetism of outdoor and indoor settled dust and its utilization as a tool for revealing the effect of elevated particulate air pollution on cardiovascular mortality'. *Geochemistry, Geophysics,Geosystems*,13(8), http://onlinelibrary.wiley.com/doi/10.1029/2012GC004160/full [accessed 18 January 2017].

Kardel, F., Wuyts, K., Maher, B.A., Hansard, R., Samson, R., (2011). 'Leaf saturation isothermal remanent magnetization (SIRM) as a proxy for particulate matter monitoring: Inter-species differences and in-season variation'. *Atmospheric Environment*, 45 (29), pp. 5164-5171.

Keuken, M.P., Moerman, M., Zandveld, P., Henzing, J.S., Hoek, G. (2015). 'Total and size-resolved particle number and black carbon concentrations in urban areas near Schiphol airport (the Netherlands)'. *Atmospheric Environment*, 104, pp. 132–142.

Kim, W., Doh, S.J., Park, Y.H., Yun, S.T., (2007). 'Two-year magnetic monitoring in conjunction with geochemical and electron microscopic data of roadside dust in Seoul, Korea'. *Atmospheric Environment*, 41 (35), pp. 7627-7641.

Kim, W., Doh, S.J., Yu, Y., (2009). 'Anthropogenic contribution of magnetic particulates in urban roadside dust'. *Atmospheric Environment*, 43 (19), pp.3137-3144.

Kim, K.H., Kabir, E., Kabir, A. (2015). 'A review on the human health impact of airborne particulate matter'. *Environment International*, 74, pp. 136-143.

Kinsey, J.S., Dong, Y., Williams, D.C., Logan, R., (2010). 'Physical characterization of the fine particle emissions from commercial aircraft engines during the Aircraft Particle Emissions eXperiment (APEX) 1-3'. *Atmospheric Environment*, 44 (17), pp. 2147-2156.

Kinsey, J.S., Hays, M.D., Dong., Y., Williams, D.C., Logan, R., (2011). 'Chemical Characterization of the Fine Particle Emissions from Commercial Aircraft Engines during the Aircraft Particle Emissions eXperiment (APEX) 1 to 3'. *Environmental Science and Technology*, 45 (8), pp. 3415-3421.

Kongo Kondé, A., Rosu, I., Lebon, F., Brardo, O., Devésa, B. (2013). 'On the modeling of aircraft tire'. *Aerospace Science and Technology*, 27, pp. 67-75.

Kreider, M.L., Panko, J.M., McAtee, B.L., Sweet, L.I., Finley, B.L., (2010). 'Physical and chemical characterization of tire-related particles: Comparison of particles generated using different methodologies'. *Science of the Total Environment*, 408, pp. 652-659.

Lai, S., Zhao, Y., Ding, A., Zhang, Y., Song, T., Zheng, J., Ho, K.F., Lee, S.C., Zhong, L., (2016). 'Characterization of PM2.5 and the major chemical components during a 1-year campaign in rural Guangzhou, Southern China'. *Atmospheric Research*, 167, pp. 208-215.

Langhof, N., Rabenstein, M., Rosenlöcher, J., Hackenschmidt, R., Krenkel, W., Rieg, F., (2016). 'Full-ceramic brake systems for high performance friction applications'. *Journal of the European Ceramic Society*, 36 (15), pp. 3823-3832.

Lecoanet, H., Lévêque, F., Ambrosi, J.P., (2001). 'Magnetic properties of salt-marsh soils contaminated by iron industry emissions (Southeast France)'. *Journal of Applied Geophysics*, 48 (2), pp. 67-81.

Lecoanet, H., Leveque, F., Ambrosi, J.P., (2003). 'Combination of magnetic parameters: an efficient way to discriminate soil-contamination sources (south France)'. *Environmental Pollution*, 122, pp. 229-234.

Lee, D., (2004). 'The impact of aviation on climate' in Harrison, R., Hester, R. (eds), *Transport and the Environment, Issues in Environmental Science and Technology*, 20, The Royal Society of Chemistry pp. 1-23.

Lee, D.S., Fahey, D.W., Forster, P.M., Newton, P.J., Wit, R.C.N., Lim, L.L., Owen, B., Sausen, R., (2009). 'Aviation and global climate change in the 21st century'. *Atmospheric Environment*, 43 (22-23), pp. 3520-3537.

Lee, D.S., Pitari, G., Grewe, V., Gierens, K., Penner., J.E., Petzold, A., Prather, M.J., Schumann, U., Bais, A., Berntsen, T., Iachetti, D., Lim, L.L., Sausen, R., (2010). 'Transport impacts on atmosphere and climate: aviation'. *Atmospheric Environment*, 44, pp. 4678-4734.

Lehndorff, E., Urbat, M., Schwark, L., (2006). 'Accumulation histories of magnetic particles on pine needles as function of air quality. *Atmospheric Environment*, 40 (36), pp. 7082-7096.

Liati, A., Brem, B.T., Durdina, L., Vogtli, M., Dasilva, Y.A.R., Eggenschwiler, P.D., Wang, J., (2014). 'Electron microscopic study of soot particulate matter emissions from aircraft turbine engines'. *Environmental Science and Technology*, 48, pp. 10975-10983.

Lin, H., Tao, J., Du, Y., Liu, T., Qian, Z., Tian, L., Di, Q., Zeng, W., Xiao, J., Guo, L., Li, X., Xu, Y., Ma, W., (2016). 'Differentiating the effects of characteristics of PM pollution on mortality from ischemic and hemorrhagic strokes'. *International Journal of Hygiene and Environmental Health*, 219 92), pp. 204-211.

Liou, K.N., Takano, Y., Yue, Q., Yang, P., (2013). 'On the radiative forcing of contrail contaminated by black carbon'. *Geophysical Research Letters*, 40, pp. 778-784.

Lobo, P., Hagen, D.E, Whitefield, P.D., (2012). 'Measurement and analysis of aircraft engine PM emissions downwind of an active runway at the Oakland International Airport'. *Atmospheric Environment*, 61, pp. 114–123.

Lobo, P., Whitelfield, P.D. Hagen, D.E., (2013). '*ACRP Report 97: Measuring PM Emissions from Aircraft Auxiliary Power Units, Tires, and Brakes*. The National Academies Press: Washington, D.C.

Lobo, P., Hagen, D.E., Whitefield, P.D., Raper. D., (2015). 'PM emissions measurements of in-service commercial aircraft engines during the Delta-Atlanta Hartsfield Study'. *Atmospheric Environment*, 104, pp. 237-245.

Lu, S.G., Bai, S.Q., Cai, J.B., Xu, C., (2005). 'Magnetic properties and heavy metal contents of automobile emission particulates'. *Journal of Zhejiang University Science B*, 6 (8), pp. 731-735.

Lu, S.G., Bai, S.Q., (2006). 'Study on the correlation of magnetic properties and heavy metals content in urban soils of Hangzhou City, China'. *Journal of Applied Geophysics*, 60 (1), pp. 1-12.

Lu, S.G., Bai, S.Q., Xue, Q.F., (2007). 'Magnetic properties as indicators of heavy metals pollution in urban topsoils: A case study from the city of Luoyang, China'. *Geophysical Journal International*, 171 (2), pp. 568-580.
Lu, X., Wang, L., Li, L.Y., Lei, K., Huang, L., Kang, D., (2010). Multivariate statistical analysis of heavy metals in street dust of Baoji, NW China'. *Journal of Hazardous Materials*, 173, pp. 744-749.

Lyons, R., Oldfield, F., Williams, E., (2012). 'The possible role of magnetic measurements in the discrimination of Sahara/Sahel dust sources'. *Earth Surface Processes and Landforms*, 37 (6), pp. 594-606.

Maher, B.A. (1986). '*Characterisation of soils by mineral magnetic measurements*'. *Physics of the Earth and Planetary Interiors*, 42 (1-2), pp. 76-92.

Maher, B.A., Moore, C., Matzka, J., (2008). 'Spatial variation in vehicle-derived metal pollution identified by magnetic and elemental analysis of roadside tree leaves'. *Atmospheric Environment*, 42 (2), 364-373.

Malig, B.J., Green, S., Basu, R., Broadwin, R., (2013). 'Coarse particles and respiratory emergency department visits in California'. *American Journal of Epidemiology*, 178 (1), pp.58–69.

Manchester Airport (2016). Airspace & operations. *Living near the airport.* http://www.manchesterairport.co.uk/community/living-near-the-airport/airspace-and-operations/ [accessed 27 June 2016].

Manchester Airport (2017). Manchester Airport Press Releases. *Manchester Airport hits new heights as MAG announces its 2016/17 results.* http://www.manchesterairport.co.uk/about-us/media-centre/press-releases/ [accessed 14 July 2017].

Masiol, M. and Harrison, R.M., (2014). 'Aircraft engine exhaust emissions and other airport-related contributions to ambient air pollution: A review'. *Atmospheric Environment*, 95, pp. 409-455.

Matzka, J., Maher, B., (1999). 'Magnetic biomonitoring of roadside tree leaves: identification of spatial and temporal variations in vehicle-derived particulates' *Atmospheric Environment*, 33, pp. 4565-4569.

Mazaheri, M., Johnson, G.R., Morawska, L. (2011). 'An inventory of particle and gaseous emissions from large aircraft thrust engine operations at an airport'. *Atmospheric Environment*, 45 (20), pp. 3500-3507.

Mazaheri, M., Bostron, T.E., Johnson, G.R., Morawska, L., (2013). 'Composition and morphology of particle emissions from in-use aircraft during takeoff and landing'. *Environmental Science and Technology*, 47 (10), pp. 5235 – 5242.

McAffee, C., Whidden, J.A., Dulisse, M.L. (2016). '*Materials and methods for enhancing physical properties and dispersion in carbon black and mixtures containing carbon black*'. US Patent 20160604697.

Meng, J., Liu, J., Fan, S., Kang, C., Yi, K., Cheng, Y., Shen, X., Tao, S., (2016). 'Potential health benefits of controlling dust emissions in Beijing'. *Environmental Pollution*, 213, pp. 850-859.
Mense, A., Kholodilin, K.A., (2014). 'Noise expectations and house prices: the reaction of property prices to an airport expansion'. *The Annals of Regional Science*, 52 (3), pp. 763-797.

Metrolink (2016). Future Metrolink. *Services on the Airport line opened to passengers on Monday 3 November.* http://www.metrolink.co.uk/futuremetrolink/Pages/airport-line.aspx. [accessed 10 June 2016].

Mitchell, R. & Maher, B.A., (2009). 'Evaluation and application of biomagnetic monitoring of traffic-derived particulate pollution'. *Atmospheric Environment*, 43 (13), pp. 2095-2103.

Mitchell, D.C., Armitage, T.L., Schenker, M.B., Bennett, D.H., Tancredi, D.J., Langer, C.E., Reynolds, S.J., Dooley, G., Mehaffy, J.D., Mitloehner, F.M., (2015). 'Particulate matter, endotoxin, and worker respiratory health on large Californian dairies'. *Journal of Occupational and Environmental Medicine*, 57 (1), pp. 79-87.

Morris, K., (2006). *An estimation of the tyre material erosion from measurements of aircraft tyre wear.* British Airways Environmental Affairs, ENV/KMM/1131/14.18; 2006 http://britishairways.it/cms/global/pdfs/csr/PSDH_Technical_Reports.pdf [accessed 27 June 2016].

Muñoz, D., Aguilar, B., Fuentealba, R., Préndez, M., (2017). 'Environmental studies in two communes of Santiago de Chile by the analysis of magnetic properties of particulate matter deposited on leaves of roadside trees. *Atmospheric Environment*, 152, pp. 617-627.

Muxworthy, A.R., Matzka, J., Fernández Davila, A. Petersen, N., (2003). 'Magnetic signature of daily sampled urban atmospheric particles'. *Atmospheric Environment*, 37 (29), pp. 4163-4169.

Nelin, T.D., Joseph, A.M., Gorr, M.W., Wold, L.E., (2012). 'Direct and indirect effects of particulate matter on the cardiovascular system'. *Toxicology Letters*, 208 (3), pp. 293-299.

Norouzi, S., Khademi, H., Cano, A. F., Acosta, J.A., (2016). ' Biomagnetic monitoring of heavy metals contamination in deposited atmospheric dust, a case study from Isfahan, Iran'. *Journal of Environmental Management*, 173, pp. 55-64.

Oldfield, F., Hunt., A., Jones, M.D.H., Chester, R., Dearing, J.A., Olsson, L., Prospero, J.M., (1985). 'Magnetic differentiation of atmospheric dusts'. *Nature*, 317, pp. 516-518.

Oldfield, F., (1999). *Environmental Magnetism: the range of applications* in Environmental Magnetism: A Practical Guide (Eds. Walden, J; Oldfield, F & Smith, J) London: Quaternary Research Association.

Onat, B., Sahin, U.A., Akyuz, T., (2013). 'Elemental characterization of PM2.5 and PM1 in dense traffic area in Istanbul, Turkey'. *Atmospheric Pollution Research*, 4 (1), pp. 101-105.

Onder, S., Dursun, S., Gezgin, S., Demirbas, A., (2007). 'Determination of Heavy Metal Pollution in Grass and Soil of City Centre Green Areas (Konya, Turkey)'. *Polish Journal of Environmental Studies*, 16 (1), pp. 145-154.

Österle, W., Dmitriev, A.I., (2016). 'The role of solid lubricants for brake friction materials'. *Lubricants*, 4 (1), p. 5.

Ouddane, B., Boust, D., Martin, E., Fischer, J.C., Wartel, M., (2001). 'The Post-Depositional Reactivity of Iron and Manganese in the Sediments of a Macrotidal Estuarine System'. *Estuaries*, 24, pp. 1015-1028.

Pascal, M., Falq, G., Wagner, V., Chatignoux, E., Corso, M., Blanchard, M., Host, S., Pascal, L., Larrieu, S., (2014). 'Short-term impacts of particulate matter (PM_{10}, $PM_{10-2.5}$, $PM_{2.5}$) on mortality in nine French cities'. *Atmospheric Environment*, 95, pp. 175-184.

Peña, J.M., Allen, N.S., Edge, M., Liauw,C.M., Hoon, S.R., Valange, B., Cherry, R.I., (2001). 'Analysis of radical content on carbon black pigments by electron spin resonance: influence of functionality, thermal treatment and adsorption of acidic and basic probes'. *Polymer Degradation and Stability*, 71, pp. 153-170.

Penner, J.E., Lister, D.H., Griggs, D.J., Dokken, D.J., McFarland, M. (Eds.) (1999). *Aviation and the Global Atmosphere*. Cambridge University Press.

Perrino, C., (2010). 'Atmospheric particulate matter'. *Proceedings of a C.I.S.B. Minisymposium*, pp. 35-43.

Pettijohn, F.J., Potter, P.E., Siever, R., (1987). '*Sand and sandstone*', 2nd ed. New York: Springer-Verlag.

Petzold, A., Fiebig, M., Fritzsche, L., Stein, C., Schumann, U., Wilson, C.W., Hurley, C.D., Arnold, F., Katragkou, E., Baltensperger, U., Gysel, M., Nyeki, S., Hitzenberger, R., Giebl, H., Hughes, K.J., Wiesen, P., Madden, P., Puxbaum, H., Vrchoticky, S., Wahl, C., (2005). 'Particle emissions from aircraft engines – a survey of the European Project PartEmis'. *Meteorologische Zeitschrift* 44, pp. 465-476.

Pollock, T.M. (2016). 'Alloy design for aircraft engines'. *Nature Materials*, 15, pp. 809-815.

Pope, C.A.III., Burnett, R.T., Thurston, G.D., Thun, M.J., Calle, E.E., Krewski, D., Godleski, J.J., (2004). 'Cardiovascular mortality and long-term exposure to particulate air pollution: epidemiological evidence of general pathophysiological pathways of disease' *Circulation* 109, pp.71–77.

Pope, J.C., (2008). 'Buyer information and the hedonic: The impact of a seller disclosure on the implicit price for airport noise'. *Journal of Urban Economics*, 63 (2), pp. 498-516.

Popovitcheva, O.B., Persiantseva, N.M., Trukhin, M.E., Rulev, G.B., Shonija, N.K., Buriko, Y.Y., Starik, A.M., Demirdjian, B., Ferry, D., Suzann, J., (2000). 'Experimental characterization of aircraft combustor soot: Microstructure, surface area, porosity and water adsorption'. *Physical Chemistry Chemical Physics*, 2 (19), pp. 4421-4426.

Press-Kristensen, K., (2012). '*Air Pollution in Airports: Ultrafine particles, solutions and successful cooperation'* The Danish Ecocouncil.

Raaschou-Nielsen, O., Andersen, Z.J., Beelen, R., Samoli, E., Stafoggia, M., Weinmayr, G., Hoffmann, B., (2013). 'Air pollution and lung cancer incidence in 17 European cohorts: prospective analyses from the European study of cohorts for air pollution effects (ESCAPE)'. *The Lancet Oncology*, 14 (9), pp. 813-822.

Rengarajan, T., Rajendran, P., Nandakumar, N., Lokeshkumar, B., Rajendran, P., Nishigaki, I., (2015). ' Exposure to polycyclic aromatic hydrocarbons with special focus on cancer'. *Asian Pacific Journal of Tropical Biomedicine*, 5 (3), pp. 182-189.

Revuelta, M.A., McIntosh, G., Pey, J., Pérez, N., Querol, X., Alastuey, A., (2014). 'Partitioning of magnetic particles in PM10, PM2.5 and PM1 aerosols in the urban atmosphere of Barcelona (Spain)'. *Environmental Pollution*, 188, pp. 109-117.

Rietsch, J.C., Dentzer, J., Dufour, A., Schnell, F., Vidal, L., Jacquemard, P., Gadiou, R., Vix-Guterl, C., (2009). 'Characterizations of carbon composites and wear debris after heavy braking demands'. *Carbon*, 47 (1), pp. 85–93.

Rike, R.E. (1998). '*Piston with moisture protective outer cover for use in disc brake assembly*', US Patent 5826686A.

Robertson, D. J., Taylor, K.G., Hoon, S.R., (2003). 'Geochemical and mineral magnetic characterisation of urban sediment'. *Applied Geochemistry*, 18, pp.269-282.

Robinson, A.L., Grieshop, A.P., Donahue, N.M., Hunt, S.W., (2010). 'Updating the Conceptual Model for Fine Particle Mass Emissions from Combustion Systems. *Journal of the Air and Waste Management Association*, 60 (10), pp. 1204-1222.

Rogers, F., Arnott, P., Zielinska, B., Sagebiel, J., Kelly, K.E., Wagner, D., Lighty, J.S., Sarofim, A.F., (2005). 'Real-time measurements of jet aircraft engine exhaust'. *Journal of the Air and Waste Management Association*, 55 (5), pp/ 583-593.

Sadeghian, M.M., (2012). 'Biomonitoring of vehicles derived particulate matter using magnetic properties of Ulmus carpinifolia leaves'. *International Journal of Agriculture and Crop Sciences*, 4 (16), pp. 1180-1183.

Sagnotti, L., Macrì, P., Egli, R., (2006). 'Magnetic properties of atmospheric particulate matter from automatic air sampler stations in Latium (Italy): Toward a definition of magnetic fingerprints for natural and anthropogenic PM10 sources. *Journal of Geophysical Research: Solid Earth*, 111 (12).

Saha, B., Nimbalkar, V., Anant Sagar, D.B., Sagar, Sai Krishna Rao, M., Deshmukh, V.P., (2017). 'Bronzes for Aerospace Applications'. *Aerospace Materials and Material Technologies*, pp. 247-266. https://link.springer.com/chapter/10.1007/978-981-10-2134-3_11 [accessed 03 June 2017].

Sant'Ovaia, H., Lacerda, M.J., Gomes, C., (2012). 'Particle pollution - An environmental magnetism study using biocollectors located in northern Portugal'. *Atmospheric Environment*, 61, pp. 340-349.

Schäfer, K., Jahn, C., Sturm, P., Lechner, B., Bacher, M., (2003). 'Aircraft emission measurements by remote sensing methodologies at airports'. *Atmospheric Environment*, 37, pp.5261–5271.

Schäfer, L.M., Striebich, R.C., Gomach, J., Edwards, T. (2006). 'Chemical class composition of commercial jet fuels and other specialty kerosene fuels', *14th AIAA/AHI Space Planes and Hypersonic Systems and Technologies Conference,* Canberra, 06 – 09 November.

Sharma, A., Tripathi, B., (2008). 'Magnetic mapping of fly-ash pollution and heavy metals from soil samples around a point source in a dry tropical environment'. *Environmental Monitoring and Assessment*, 138 (1-3), pp. 31-39.

Shaughnessy, W.J., Venigalla, M.M., Trump, D., (2015). 'Health effects of ambient levels of respirable particulate matter (PM) on healthy, young-adult population'. *Atmospheric Environment*, 123 (Part A), pp. 102-111.

Schreiber, K., Gerendas, M. (2014). '*Segment component in high temperature casting material for an annular combustion chamber, annular combustion chamber for an aircraft engine, aircraft engine and method for the manufacture of an annular combustion chamber*'. US Patent 8646279.

Shu, J., Dearing, J., Morse, A., Yu, L., Yuan, N., (2001). 'Determining the sources of atmospheric particles in Shanghai, China, from magnetic and geochemical properties.' *Atmospheric Environment*, 35, pp. 2615-2625.

Spassov, S., Egli, R., Heller, F., Nourgaliev, K., Hannam, J., (2004). 'Magnetic quantification of urban pollution sources in atmospheric particulate matter'. *Geophysical Journal International*, 159 (2), pp. 555-564.

Spicer, C.W., Holdren, M.W., Smith, D.L., Hughes, D.P., Smith, M.D., (1992). 'Chemical composition of exhaust from aircraft turbine engines'. *Journal of Engineering for Gas Turbines and Power*, 114 (1), pp. 111-117.

Stansfield, S.A., Matheson, P., (2003). 'Noise pollution: non-auditory effects on health'. *British Medical Bulletin*, 68, pp. 243-257.

Starik, A.M. (2008). 'Gaseous and particulate emissions with jet engine exhaust and atmospheric pollution. *Advances on Propulsion Technology for High-Speed Aircraft*, 15, pp. 1-22.

Stettler, M.E.J., Eastham, S., Barrett, S.R.H., (2011). 'Air quality and public health impacts of UK airports. Part i: Emissions'. *Atmospheric Environment*, 45 (31), pp.5415-5424.

Stover, E.R. (2003). '*Methods of inhibiting catalyzed oxidation of carbon-carbon composites using phosphoric acid, a zinc salt, and an aluminum salt and articles made there from*'. US Patent US6551709.

Szczepaniak-Wnuk, I., Górka-Kostrubiec, B., (2016). 'Magnetic particles in indoor dust as marker of pollution emitted by different outside sources'. *Studia Geophysica et Geodaetica*, 60, pp. 297-315.

Szonyi, M., Sagnotti, L., Hirt, A., (2008). 'A refined biomonitoring study of airborne particulate matter pollution in Rome, with magnetic measurements on *Quercus Ilex* tree leaves.' *Geophysical Journal International*, 173, pp. 127-14.

Sun, S.Q., Wang, Dy, He, M., Zhang, C., (2009). 'Monitoring of atmospheric heavy metal deposition in Chongqing, China – based on moss bag technique'. *Environmental Monitoring and Assessment*, 148 (1), pp. 1-9.

Tchounwou, P.B., Yedjou, C.G., Patlolla, A.K., Sutton, D.J., (2012). 'Heavy metal toxicity and the environment'. *Molecular, Clinical and Environmental Toxicology*, 101, pp. 133-164.

Tesche, M., Achtert, P., Glantz, P., Noone, K.J., (2016). 'Aviation effects on already-existing cirrus clouds'. *Nature Communications*, 7, (Article number: 12016)

Tesseraux, I., (2004). 'Risk factors of jet fuel combustion products'. *Toxicology Letters*, 149 (1-3), pp. 295-300.

Touri, L., Marchetti, H., Sari-Minodier, I., Molinari, N., Chanez, P., (2013). 'The airport atmospheric environment: respiratory health at work'. *European Respiratory Review*, 128, pp. 124-130.

Tsiouri, V., Kakosimos, K.E., Kumar, P., (2015). 'Concentrations, sources and exposure risks associated with particulate matter in the Middle East Area – a review'. *Air Quality, Atmosphere and Health*, 8 (1), pp. 67-80.

Urbat, M., Lehndorff, E., Schwark, L., (2004). 'Biomonitoring of air quality in the Cologne conurbation using pine needles as a passive sampler – Part I: magnetic properties'. *Atmospheric Environment*, 38 (23), pp. 3781-3792.

UK Data Service (2017). Census Support. '*Easy Download*'. https://borders.ukdataservice.ac.uk/easy_download.html [accessed 20 May 2017].

USDA (United States Department of Agriculture), (2017). '*Soil survey manual*'. https://www.nrcs.usda.gov/wps/portal/nrcs/detailfull/soils/ref/?cid=nrcs142p2_054262 [accessed 01 June 2017].

Van Loon, G.W; Duffy, S.J., (2011). '*Environmental chemistry: a global perspective*'. 3rd ed. Oxford: Oxford University Press.
Vander Wal, R.L., Bryg, V.M., Huang, C.H., (2014). 'Aircraft engine particulate matter: Macro- micro- and nanostructure by HRTEM and chemistry by XPS'. *Combustion and Flame*, 161 (2), pp. 602-611.

Virmani, Y.P., Zeller, E.J., (1974). 'Analysis of background copper concentrations in sea water by electron spin resonance'. *Analytical Chemistry*, 46, pp. 324-325.

Wahlström, J., Olander, L., Olofsson, U., (2010). 'Size, shape and elemental composition of airborne particles from disc brake materials'. *Tribology Letters*, 38, pp. 15-24.

Wakeman, S., Carpenter, R., (1974). 'Electron spin resonance spectra of marine and fresh-water manganese nodules'. *Chemical Geology*, 13, pp. 39-47.

Walden, J., Whittaker, R.J., Hill, J., (1991). 'The use of mineral magnetic analyses as an aid in investigating the recent volcanic disturbance history of the Krakatau Islands, Indonesia'. *The Holocene,* 1, pp. 64–67.

Walden J., Oldfield, F., Smith, J., (1999). *Environmental Magnetism A Practical Guide* London: Quaternary Research Association.

Wang, G., Oldfield, F., Xia, D., Chen, F., Liu, X., Zhang, W., (2012). 'Magnetic properties and correlation with heavy metals in urban street dust: A case study from the city of Lanzhou, China. *Atmospheric Environment*, 46, pp. 289-298.

Wang, J., Geng, N.B., Xu, Y.F., Zhang, W.D., Tang, X.Y., Zhang, R.Q., (2014). 'PAHs in $PM_{2.5}$ in Zhengzhou: concentration, carcinogenic risk analysis, and source apportionment'. *Environmental Monitoring and Assessment*, 186 (11), pp. 7461-7473.

Wang, B., Xia, D., Yu, Y., Jia, J., Xu, S., (2014). 'Detection and differentiation of pollution in urban surface soils using magnetic properties in arid and semi-arid regions of northwestern China. *Environmental pollution,* 184, pp. 335-346.

Wang, B., Dunsheng, X., Yu, Y., Jia, J., Nie, Y., Wang X., (2015). 'Detecting the sensitivity of magnetic response on different pollution sources - A case study from typical mining cities in northwestern China'. *Environmental Pollution*, 207, pp. 288-298.

Wayson, R.L., Fleming, G.G., Lovinelli, R., (2009). 'Methodology to estimate particulate matter emissions from certified commercial aircraft engines'. *Journal of the Air & Waste Management Association*, 59 (1), pp. 91-100.

Webb, S., Whitefield, P.D., Miake-Lye, R.C., Timko, M.T.,Thrasher, T.G., (2008). '*ACRP Report 6: Research needs associated with particulate emissions at airports'.* Transportation Research Board'. The National Academies Press: Washington, D.C.

Westerdahl, D., Fruin, S.A., Fine, P.L., Sioutas, C., (2008). 'The Los Angeles International Airport as a source of ultrafine particles and other pollutants to nearby communities'. *Atmospheric Environment*, 42 (13), pp. 3143-3155.

Whitefield, P., Lobo, P., Hagen, D., (2008). 'Aircraft-generated PM Emissions', *Cambridge Particle Meeting*, Univeristy of Cambridge, UK, 13 May 2011.

Whitefield, P.D., Lobo, P., Hagen, D.E., Timko, M.T., Miake-Lye, R.C., Taylor, C., Ratliff, G., Lukachko, S., Sequeria, C., Hileman, J., Waitz, I., Webb, S., Thrasher, T.G., Ohsfeldt, M., Kaing, H.K., Essama, S.C. (2008). *'ACRP Report 9: Summarizing and Interpreting Aircraft Gaseous and Particulate Emissions Data*'. Transportation Research Board'. The National Academies Press: Washington, D.C.

Wik, A., Dave, G. (2009). 'Occurrence and effects of tire wear particles in the environment – A critical review and an initial risk assessment'. *Environmental Pollution*, 157, pp. 1-11.

Winther, M., Kousgaard, U., Ellermann, T., Massling, A., Klenø Nøjgaard J., Ketzel, M. (2015). 'Emissions of NO_x particle mass and particle numbers from aircraft engines, APU's and handling equipment at Copenhagen Airport'. *Atmospheric Environment*, 100, pp. 218-229.

Wong, C.M., Tsang, H.K.L., Thomas, G.N., Lam, K.B., Chan, K.P., Zheng, Q., Ayres, J.G., Lee, S.Y., Lam, T.H., Thach, T.Q., (2016). 'Cancer mortality risks from long-term exposure to ambient fine particle'. *Cancer Epidemiology, Biomarkers & Prevention*, 25 (5), DOI: 10.1158/1055-9965.EPI-15-0626.

Wood, E., Herndon, S., Miake-Lye, R., Nelson, D., Seeley, M., (2008). *ACRP Report 7: Aircraft and Airport-Related Hazardous Pollutants: Research Needs and Analysis*, Transportation Research Board.

World Health Organization, (2016). *WHO releases country estimates on air pollution exposure and health impact*. http://www.who.int/mediacentre/news/releases/2016/air-pollution-estimates/en/. [accessed 27 June 2016].

Wu, S., Liu, Y., Ge, Y., Ran, L., Peng, K., Yi, M. (2016). 'Structural transformation of carbon/carbon composites for aircraft brake pairs in the braking process'. *Tribology International*, 102, pp. 497-506.

Xia, D., Wang, B., Yu, Y., Jia, J., Nie, Y., Wang, X., Xu, S., (2014). 'Combination of magnetic parameters and heavy metals to discriminate soil-contamination sources in Yinchuan - A typical oasis city of Northwestern China'. *Science of the Total Environment*, 485-486 (1), pp. 83-92.

Xie, S., Dearing, J.A., Bloemendal, J., Boyle, J.F., (1999). 'Association between the organic matter content and magnetic properties in street dust, Liverpool, UK. *Science of the Total Environment*, 241 (1-3), pp. 205-214.

Xie, S., Dearing, J.A., Boyle, J.F., Bloemendal, J., Morse, A.P., (2001). 'Association between magnetic properties and element concentrations of Liverpool street dust and its implications'. *Journal of Applied Geophysics*, 48 (2), pp. 83-92.

Xu, Q,F., Lu, S.G., (2008). 'Microstructure of ferrospheres in fly ashes: SEM, EDX and ESEM analysis'. *Journal of Zhejiang University-SCIENCE A,* 9 (11), pp. 1595 – 1600.

Yacovitch, T.I., Yu, Z., Herndon, S.C., Miake-Lye, R., Liscinsky, D., Knighton, W.B., Kenney, M., Schoonard, C., Pringle, P., (2016). '*ACRP Report 164: Exhaust emissions from in-use general aviation aircraft*'. The National Academies Press: Washington, DC.

Yang, T., Liu, Q., Li, H., Zeng, Q., Chan, L., (2010). 'Anthropogenic magnetic particles and heavy metals in the road dust: Magnetic identification and its implications'. *Atmospheric Environment*, 44, pp. 1175-1185.

Yee, W (2016). 'Oxidation of Carbon-Carbon Composite'. MSc. thesis, Southern Illinois University Carbondale.

Yim, D.H., Lee, G.L., Lee, I.H., Allroggen, F., Ashok, A., Caiazzo, F., Eastham, S.D., Malina, R., Barrett, S.R.H. (2015). 'Global, regional and local health impacts of civil aviation emissions'. *Environmental Research Letters*, 10, http://iopscience.iop.org/article/10.1088/1748-9326/10/3/034001/pdf [accessed 17 June 2016].

Yu, K.N., Cheung, Y.P., Cheung, T., Henry, R.C., (2004). 'Identifying the impact of large urban airports on local air quality by nonparametric regression'. *Atmospheric Environment*, 38, pp. 4501-4507.

Yu, Z., Herndon, S.C., Ziemba, L.D., Timko, M.T., Liscinsky, D.S., Anderson, B.E., Miake-Lye, R.C., (2012). 'Identification of lubrication oil in the particulate matter emissions from engine exhaust of in-service commercial aircraft'. *Environmental Science and Technology*, 46, pp. 9630-9637.

Yu, Z., Liscinsky, D.S., Fortner, E.C., Yacovitch, T.T., Croteau, P., Herndon, S.C., Miake-Lye, R.C. (2017). 'Evaluation of PM emissions from two in-service gas turbine general aviation aircraft engines'. *Atmospheric Environment*, 160, pp. 9-18.

Yun, Y., Gao, R., Yue, H., Li, G., Zhu, N., San, N., (2015). 'Synergistic effects of particulate matter (PM_{10}) and SO_2 on human non-small cell lung cancer A549 *via* ROS-mediated NF-κB activation'. *Journal of Environmental Sciences*, 31, pp. 146-153.

Zanobetti, A., Bind, M.C., Schwartz, J., (2008). 'Particulate air pollution and survival in a COPD cohort'. *Environmental Health*, 7, pp. 48.

Zhu, Y., Fanning, E., Yu, R.C., Zhang, Q., Froines, J.R., (2011). 'Aircraft emissions and local air quality impacts from takeoff activities at a large International Airport'. *Atmospheric Environment*, 45(36), pp. 6526-6533.

Zhu, Z., Li, Z., Bi, X., Han, Z., Yu, G., (2013). 'Response of magnetic properties to heavy metal pollution in dust from three industrial cities in China'. *Journal of Hazardous Materials*, 246-247, pp. 189-198.

Zong, Y., Xiao, Q., Lu, S., (2017). 'Magnetic signature and source identification of heavy metal contamination in urban soils of steel industrial city, Northeast China. *Journal of Soils and Sediments*, 17(1), pp. 190-203.

The characterisation of particulate pollution in an airport environment: Manchester International Airport, UK, a case study
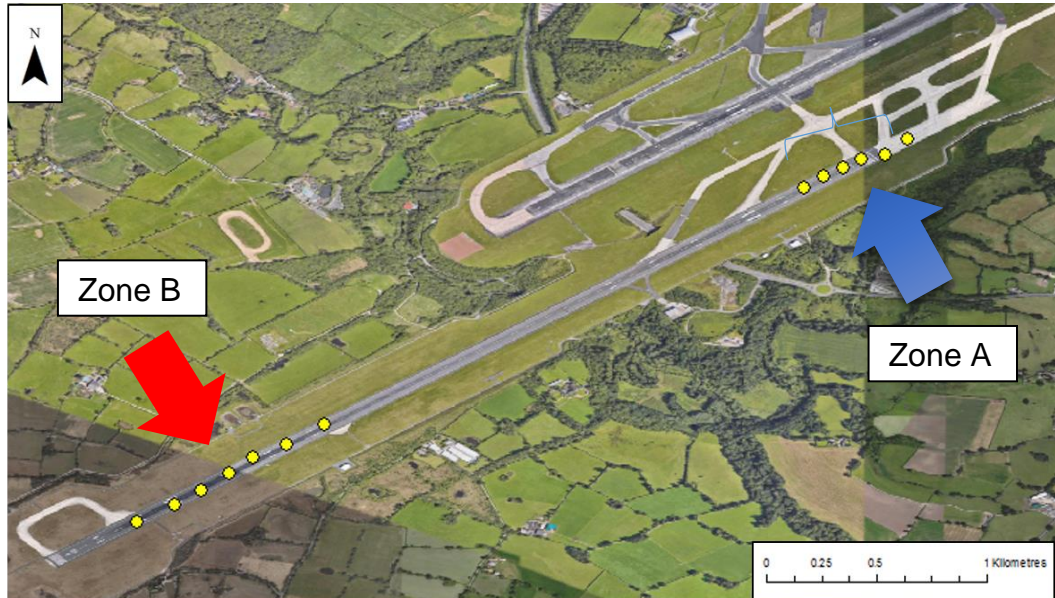
APPENDICES

Appendix 1

Sampling Locations

Runway Dust Sampling Locations
○

Figure A1.1: Satellite image of MAN displaying the runway dust sampling locations on runway 23L/05R. Zone A = 0 – 725 m, Zone B: 2300 – 3000 m (Google Earth, 2017). Final map created in ArcGIS (v.10.4.1).

Figure A1.2: Satellite image of MAN displaying the specific site locations of the Taxiway and Apron dust sampling areas (Google Earth, 2017). Final map created in ArcGIS (v. 10.4.1).

Appendix 2

Types of Magnetic Behaviour

The following explanations of magnetic behaviour and magnetic grain size have been compiled from Thompson and Oldfield (1986) and Walden *et al.* (1999).

Ferrimagnetism

Ferrimagnetic minerals include the 'cubic', spinel-type oxides such as magnetite and maghemite. They possess two oppositely aligned, but unequal, spin lattices. When placed in a magnetic field, ferrimagnetic minerals acquire a strong positively aligned magnetic moment. Once removed from the magnetic field they retain part of the magnetic moment indicating that they are able to hold a remanence. Low concentrations of ferrimagnetic minerals often dominate the magnetic properties of environmental samples.

Antiferromagnetism

Antiferromagnetic minerals, have equal and opposite magnetic moments on magnetic sub-lattices. Like ferrimagnetic minerals, however, they acquire a positively aligned magnetic moment, when placed in a magnetic field that is perpendicular to the spin directions, or if the material exhibits canted antiferromagnetic behaviour. This magnetic moment is partially retained as a magnetic remanence on removal from the magnetic field. However, the magnetic moment is much weaker than in ferrimagnetic minerals and is likely to result from defects in the crystal lattice of the minerals. Examples of antiferromagnetic minerals include haematite and goethite.

Paramagnetism

Paramagnetic minerals include most other minerals containing iron, nickel and cobalt. In such minerals, the magnetic moments align parallel to the direction of the applied field. The paramagnetic moment is relatively weak and is subsequently lost on removal from the magnetic field. Thus, paramagnetic

minerals do not retain a remanence. Although paramagnetism is often masked by stronger ferrimagnetic and antiferromagnetic behaviour it may be significant in situations where high concentrations of non-ferrimagnetic or antiferromagnetic forms of iron and/or manganese compounds occur or where ferrimagnetic materials are present as small single domain particles. Under these circumstances the material may be said to display super-paramagnetic behaviour.

Diamagnetism

Diamagnetism is the weakest of the four main types of magnetic behaviour. When placed in a magnetic field diamagnetic minerals acquire a net magnetic moment which is aligned in the opposite direction to the field. As the diamagnetic moment is lost on removal from the field no magnetic remanence is retained. Diamagnetism is often masked by other forms of magnetic behaviour as discussed above. As water, carbon, silica and calcium carbonate are all diamagnetic the diamagnetic effects on magnetic susceptibility may be significant in wet samples, sediments rich in biogenic silica or calcium carbonate and peat or organic mud. Diamagnetic effects may also result from the use of plastic sample holders.

Appendix 3a

**Table A3.1**: Certified reference materials used for calibration and quality control for XRF measurements.

|	
CRM 7002	Light sandy soil
GBW7309	Stream sediment
GBW7602	Bush, branches and leaves
GBW7603	Bush, branches and leaves
GBW7604	Poplar leaves
GBW7605	Tea
LGC6139	River clay sediment
NCSDC70302	Carbonate rock
NCSDC70309	Carbonate rock
NCSDC70314	Tibet sediment
NCSDC70317	Tibet sediment
NCSDC70319	Tibet sediment
NCSDC73301	Rock
NCSDC73302	Rock
NCSDC73303	Rock
NCSDC73309	Stream sediment
NCSDC73373	Stream sediment
NIST2709	San Joaquin Soil

From: 'Toxic enrichment and boating intensity. Sediment records of antifoulant copper in shallow lakes of eastern England' (Boyle *et al.*, 2016, p. 202.)

Appendix 3b
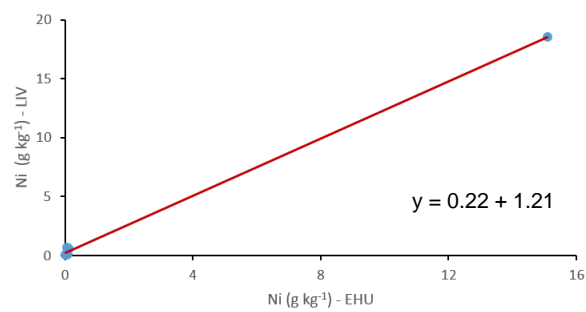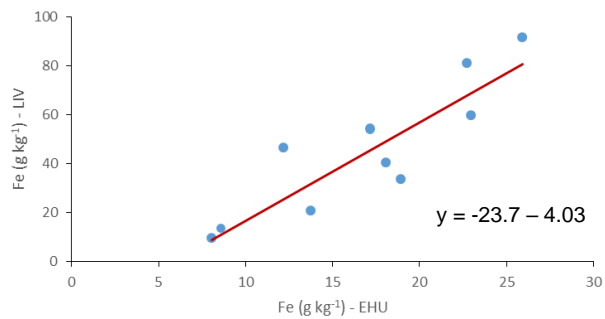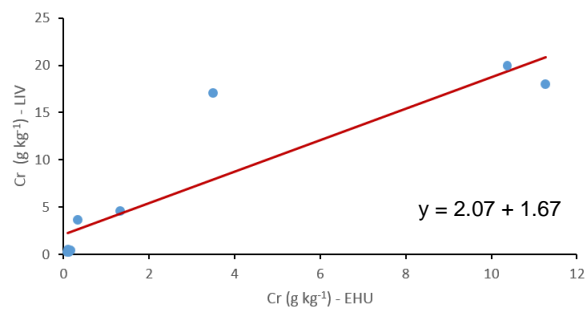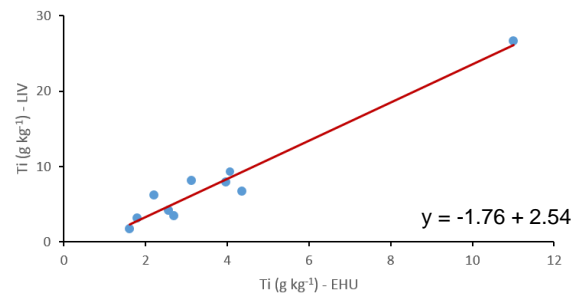
Figure A3.1a: Linear regression for Ti, Cr, Fe and Ni concentrations (g kg^{-1}) for XRF analysis completed on the Oxford Instruments X-MET 7500 Series portable XRF analyser at Edge Hill University (EHU) and the Bruker S$_2$ Ranger at Liverpool University (LIV).
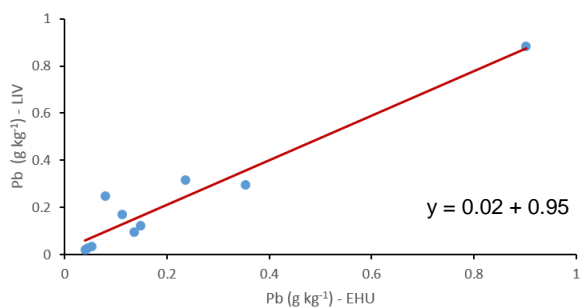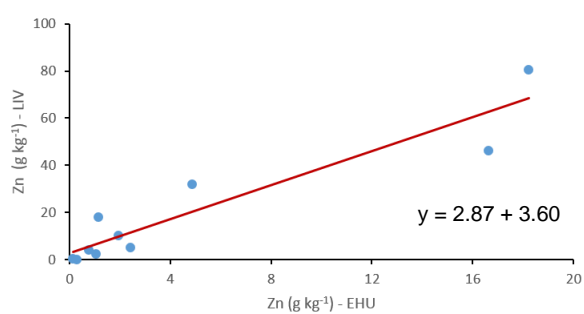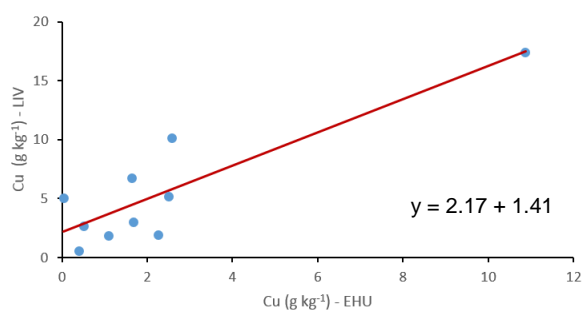
Figure A3.1b: Linear regression for Cu, Zn and Pb concentrations (g kg^{-1}) for XRF analysis completed on the Oxford Instruments X-MET 7500 Series portable XRF analyser at Edge Hill University (EHU) and the Bruker S$_2$ Ranger at Liverpool University (LIV).

Appendix 4

i)   **ESR electromagnetic modelling package** (After Hoon, 2017).

Here the application of an ESR electromagnetic modelling package, outlined elsewhere (Alagarsamy and Hoon 2017, Crook et al 2002), is demonstrated in outline form. ESR is an electromagnetic quantum mechanical effect making its detailed description complex and beyond the scope of the current study. However, it enables modelling of (identifiable) components that comprise the ESR absorption spectrum. The ability to do this helps in source apportionment, sediment unmixing and fingerprinting of environmental sediments. ESR is sensitive to the magnetic moment associated with unpaired electrons, be they uncorrelated as in a paramagnetic material, or correlated by a quantum mechanical exchange field as in ferri-, ferro-, antiferro, or canted antiferro-magnetic domains. Furthermore, diagmagnetic materials are 'ESR silent'. Thus ESR 'sees through' any diamagnetic matrix or components in a sediment detecting the para- or single domain or domain ordered ferri-, magnetic components. As ESR is a magnetic resonance phenomenon, it follows that is only the magnetic components that contribute to a spectrum. The parameters used in the model to generate the components of the ESR spectrum are then also descriptive of the sediment. ESR is then complimentary to environmental magnetism techniques. Its very high sensitivity enables spectra to be obtained from a few 10's of milligrams of material rather than 10 or more grams or so as required for conventional environmental methods (e.g. IRM, SIRM, etc.).

Parameters that affect the magnitude of the ESR absorption include, for example, the high (microwave) frequency magnetic susceptibility and magnetic volume fraction. Absorption increases non-linearly with microwave RF field, rfh, thus this is kept low, typically to 1mW. If ferrimagnetic spins have a low damping constant, $\square$, or paramagnetic spins have a long spin-lattice relaxation time, t_2, absorption lines are very narrow. The field at which a simple ESR (differential) absorption peak crosses the zero absorption baseline is known as the resonance field. It depends upon the microwave frequency as well as the g value of the spins. For free electrons and simple dilute $s = \frac{1}{2}$ paramagnetic moments, g is very close to

2.000. Departures from g ~ 2 are themselves measures of the local environment of the spin, and thus a 'fingerprint' parameter or of other paramagnetic ions.

Examples of applying the SER modelling package developed by Hoon to a selection of the mean ESR spectra are displayed and described in outline below as exemplars and an indication of future work that may follow on from the current study.

Figure A1 displays the spectrum of runway marking debris fragment. It is dominated by the Mn^{2+} six line hyperfine spectrum. Mn^{2+} ions pervade the environment, natural marine carbonate sediments, concrete, and many plastics, pigments and rubbers. It us seen in the majority of airport ESR sediment spectra to some degree. Note the characteristic relatively narrow overall width of < 100mT.
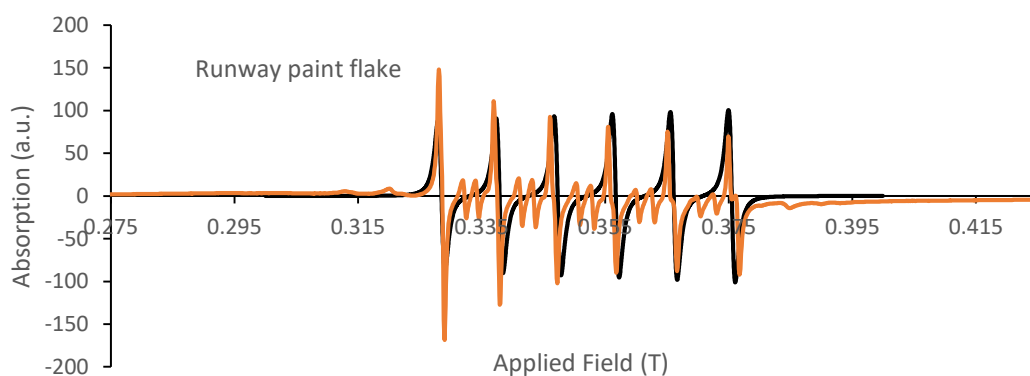

Figure A4.1: Runway marking debris flake displaying the Mn^{2+} six line hyperfine spectrum. Model spectrum (black line) fits the 6 principal lines only, not the inter-peak hyperfine detail, sediment spectrum brown curve.

Table A4.1: Primary model parameters, a single paramagnetic component p1.

Paint	p1
g	2.00000
V x Sus	9.00E-03
n	6
t2 (ms)	6.00
Bfs	-
f(GHz)	9.8637
rfh (mT)	0.005

Figure A4.2 shows the mean brake spectrum and model curve (black line). As noted earlier in the thesis, the ESR spectrum from the brake material is very simple. It exhibits a very narrow (~ 1.4 mT wide) g ~ 2 spectrum. Similar ESR components are seen throughout all airport sediments. Pure carbon and graphitic particles can also behave in this manner.
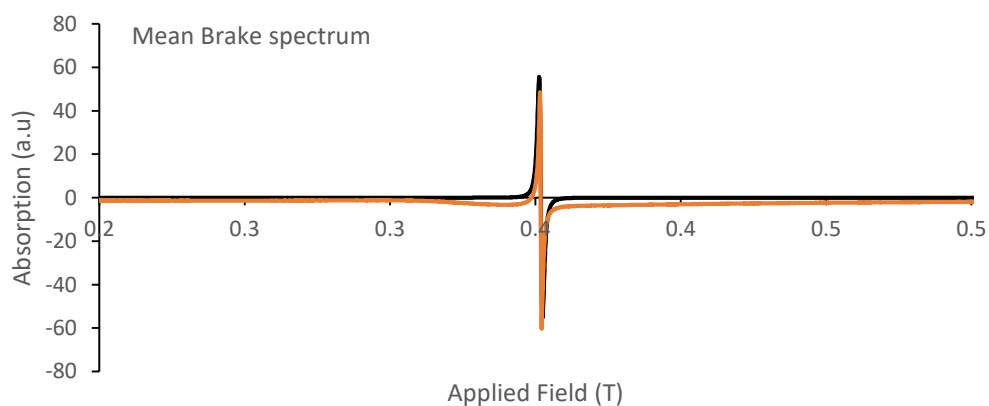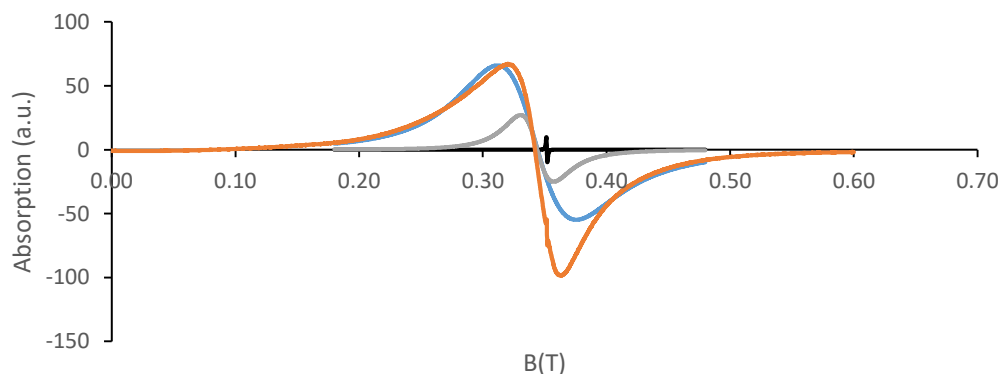

Figure A4.2:

Table A4.2: Primary model parameters, a single paramagnetic component p1.

Brakes	p1
g	1.99680
V x Sus	4.40E-04
n	1
t2 (ms)	8.400
f(GHz)	9.8637
rfh (mT)	0.005

Figure A4.3 displays the mean engine spectrum. This is considerably broader than the brake spectrum requiring several components to model the general features including a series of similar absorption curves modelled using multiple overlapping peaks (n > 1, see table A3) similar in concept to the Mn^{2+} hyperfine spectrum, figure A1, but for which the line width is larger (rather than smaller) than the peak separation. Physically this corresponds to a spread in the local environment experienced by a paramagnetic species.


Figure A4.3: displays the mean engine spectrum. Three paramagnetic components employed to partially model the sediment spectrum (brown curve), p1 blue, p2 grey, p3 black lines.

Table A4.3: Table A4.3 Primary model parameters, a multi-mode paramagnetic peak, p1, two single paramagnetic components, p2, p3.

Engines	p1 (Blue Line)	p2 (Grey Line)	p3 (Black Line)
g	2.0000	2.0500	2.0000
V x Sus	9.00E-03	3.30E+00	8.00E-05
n	6	1	1
t2 (ms)	6.0000	0.1000	8.4000
Bfs	0.0094	-	-
f(GHz)	9.8637		
rfh (mT)	0.005		

Figure A4.4 displays the mean soil spectrum. Four components have been used to partially model the sediment spectrum (brown curve). A strong g =2 peak is seen surrounded by a weak Mn^{2+} component (not modelled) in the centre of the spectrum. Note the low field peak at ~ 0.17T, consistent with paramagnetic Fe^{3+} ions. The broad peak is modelled using a ferrimagnetic component (black line) as well as a broad paramagnetic one (grey line). The inclusion of a ferrimagnetic term necessitates use of its saturation magnetisation, M_s, uniaxial magnetic anisotropy, K_u, ferrimagnetic damping parameter, $\square$, (rather than the spin-lattice relaxation time) and the Langevin superparamagnetic modelling factor, X_m. The latter is higher the larger the initial magnetic susceptibility of the material.
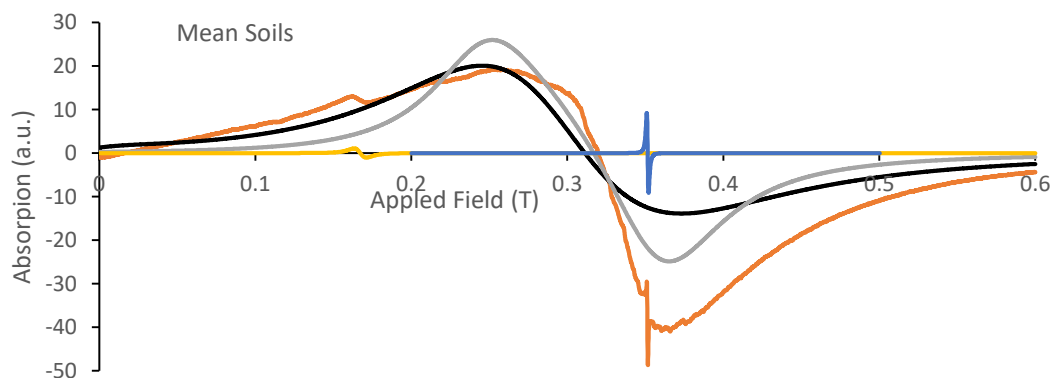
Figure A4.4: Mean soil spectrum.

Table A4.5: Modelling components for the mean soils spectrum. Note the inclusion of a ferrimagnetic term and thus additional magnetic parameters (K_u, M_s, $\square$, X_m) as a consequence.
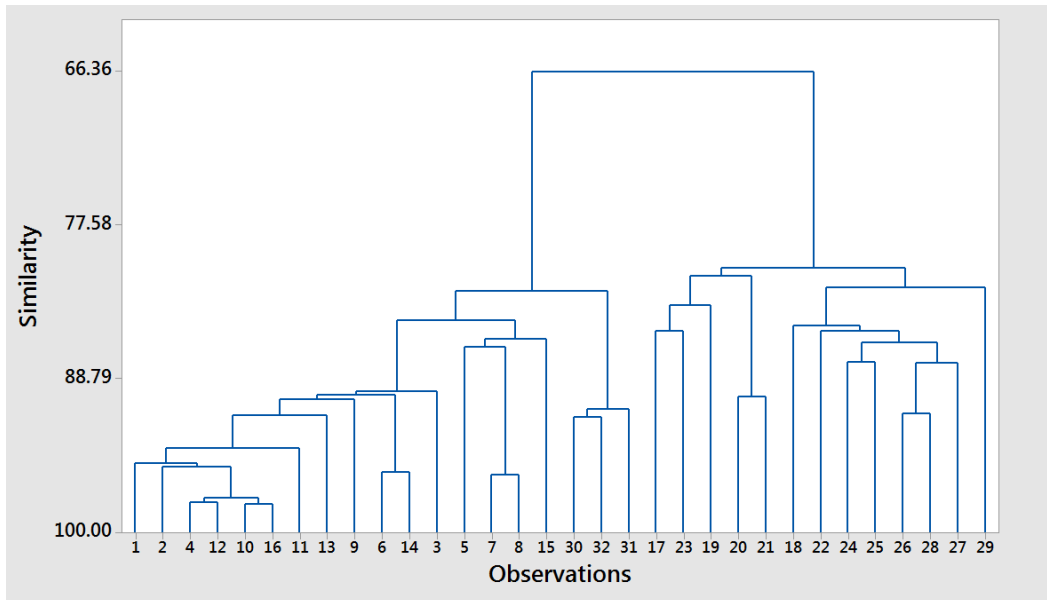
Soil	Ferri	p1	p2	p3
g	-	1.99900	2.32000	4.20000
V x Sus	-	7.920E-05	2.10E+00	1.80E-03
n	-	1	5	1
t2 (s)	-	-	0.1	0.4
Bfs	-	-	0.022	-
Vol Frac (ferri)	0.3			
K_u (kJ/m^3)	6			
M_s (kA/m)	480			
X_m	40			
$\square$	0.3			
f(GHz)	9.8495			
rfh (mT)	0.005			

Table A4.6: Scaling factor and offset used in the scaled mean plots (§8.4.1).

Sample	1. Scaling Factor	Offset
Mean_T	1	385
Mean_E	1	850
Mean_B	2	180
Mean_G	40	660
Mean_S	2	460
Mean_R	2	540

Appendix 5

Cluster analysis diagram:

Figure A5.1: Custer analysis based on magnetic parameter data (i.e. $\chi ARM/\chi$; $\chi ARM/SIRM$; $IRM_{-20mT}/SIRM$; $IRM_{-300mT}/SIRM$) for the aircraft source dust samples (i.e. engines, brakes and tyres). Three distinctive groups are shown. Samples 1 – 16: Brake dusts; 17 – 29: Engine dusts and 30 – 32: Tyre dusts.

Table A5.2: Principal components analysis (PCA) of the main metallic elements in the aircraft source dusts (i.e. aircraft engines, brakes and tyres.

Metal	PC1	PC2
Ti (Eigen value)	-0.13596	-0.05219
Cr (Eigen value)	0.41643	0.23543
Ni (Eigen value)	0.58911	0.65078
Zn (Eigen value)	-0.66540	0.71040
Cu (Eigen value)	-0.13527	0.11692

Summary:

Eigen value	5.71278	1.80510
% Variance	69.886	22.082

Table A5.3: Principal components analysis (PCA) of the main metallic elements in the runway dusts.

Metal	PC1	PC2
Ti (Eigen value)	0.02599	0.70879
Cr (Eigen value)	0.00198	0.00198
Ni (Eigen value)	0.00094	0.01707
Zn (Eigen value)	0.99915	-0.04104
Cu (Eigen value)	0.03201	0.70338
Summary:		
Eigen value	3.78617	3.89202
% Variance	99.89200	0.10268

Table A5.4: Principal components analysis (PCA) of the main metallic elements in the taxiway and apron dusts.

Metal	PC1	PC2
Ti (Eigen value)	0.29391	0.01071
Cr (Eigen value)	0.05149	0.01841
Ni (Eigen value)	0.01012	0.01085
Zn (Eigen value)	0.95022	0.10278
Cu (Eigen value)	-0.10177	0.99442
Summary:		
Eigen value	1.60287	1.19631
% Variance	55.989	41.788